ON THE INTERACTION OF POLYSTYRENE LATICES AND POLY(L-LYSINE)

by

William Dean Corry, B.S.

A THESIS
Presented to the Department of Biochemistry
and the Graduate Division of the
University of Oregon Health Sciences Center
in partial fulfillment of
the requirements for the degree of
Doctor of Philosophy

November 1975

ACKNOWLEDGMENTS

The following are some of the people to whom I am indebted for their help in the past few years; Dr. G.V.F. Seaman for his embodiment of the standards which scientific excellence demands, an example which has greatly aided my education; Dr. D.A. Rigas for his concern and encouragement; Drs. R.T. Jones and H.S. Mason for timely advise and the generous loan of equipment; Janet Cowan for many hours of diligent effort in the preparation of this thesis; Mrs. D.A. Rigas for technical assistance and Dr. J.H. Fellman for initial insights into the nature of science.

TABLE OF CONTENTS

Chapter

LIST OF TABLES

LIST OF FIGURES

A LIST OF SYMBOLS

Symbol	Dimensions*	Definition
A	ML^2T^{-2}	Hamaker's constant for two materials suspended in a third.
$\overline{A}$	L^2T^{-2}	First calibration constant for the Ubbelohde viscometer.
$\mathring{A}$	L	Angstrom unit.
A_1	-	The first virial coefficient of a polymer.
A_2	L^3M^{-1}	The second virial coefficient of a polymer.
A_3	L^6M^{-2}	The third virial coefficient of a polymer.
A_{11}	ML^2T^{-2}	Hamaker's constant for two spheres of material 1 in a vacuum.
A_{22}	ML^2T^{-2}	Hamaker's constant for two spheres of material 2 in a vacuum.
A_{12}	ML^2T^{-2}	Hamaker's constant for two spheres of equal size; one of material 1, the other of material 2, when suspended in a vacuum.
a	L	Radius of a cylindrical or spherical object.
a_b	-	The thermodynamic activity of molecules of the b^{th} species.
α	-	The relative degree of expansion of a polymer over its unperturbed dimensions.
$\overline{\alpha}$	-	The Mark-Houwink parameter.
$\overline{B}$	L^2	The second calibration constant for the Ubbelohde viscometer.
C_a	ML^{-3}	The concentration of the a^{th} species.

* M = Mass; L = Length; T = Time; Q = charge.

Symbol	Dimensions	Definition
C_c	ML^{-3}	The critical coagulation concentration of a suspension of colloidal particles.
χ	-	Flory's term for characterizing the extent of polymer-solvent interactions.
D	L^2T^{-1}	The diffusion coefficient of a single particle.
$D_r(u)$	L^2T^{-1}	The relative diffusion coefficient between two particles, when separated by a distance characterized by the dimensionless variable u.
$D_r(\infty)$	L^2T^{-1}	The relative diffusion coefficient between two particles, when separated by an infinite distance.
dl	L^3	Deciliter
δ	L	Thickness of an adsorbed polymer layer.
E_v	L^3	The elution volume of a polymer or protein on a column.
e	Q	The fundamental charge on an electron.
ϵ	-	The dielectric constant of a material.
η	$ML^{-1}T^{-1}$	The dynamic viscosity of a fluid.
(η)	-	The limiting viscosity number of a polymer based on its volume fraction.
$[\eta]$	L^3M^{-1}	The limiting viscosity number of a polymer based on its concentration.
η_{sp}	L^3M^{-1}	The reduced viscosity number of a polymer based on its concentration.
ΔG_m	ML^2T^{-2}	The free energy of mixing--the polymer layers adsorbed to the surfaces of two colliding particles.

Symbol	Dimensions	Definition
$\Delta G'_m$	ML^2T^{-2}	The entropic contribution to the free energy of mixing the polymer layers adsorbed to the surfaces of two colliding particles.
g	MT^{-2}	A unit expressing an acceleration equivalent that of gravity.
g	-	A dimensionless number characterizing the ability of two polymer chains to approach one another's center of gravity.
Γ	-	The angle characterizing the extent by which the rotational freedom of a polymer segment about its axis has been diminished.
$\gamma_{\pm}$	L^3M^{-1}	The mean ionic activity coefficient of salt ions.
H	L	The distance between the surface of two spheres.
ΔH_a	ML^2T^{-2}	The heat of adsorption for a polymer.
ΔH_m	ML^2T^{-2}	The heat of mixing two polymer layers which are adsorbed to the surfaces of two particles.
H	L	The distance between the surfaces of two spheres.
H_o	L	The distance between the surfaces of two spheres when a stable aggregate is formed.
I	QT^{-1}	Electric current.
J	-	Absolute fringe number.
K	ML^3T^{-1}	The observed rate constant or rate constant which is calculated when the potential energy of interaction between two particles is taken into account.
K_o	ML^3T^{-1}	The theoretical rate constant for rapid coagulation, when every collision produces an aggregate.

Symbol	Dimensions	Definition
k	ML^2T^{-2}	Boltzmann's constant.
κ	L^{-1}	The Debye-Hückel parameter.
Λ_i	$M^{-1}L^{-3}TQ^2$	The specific conductance of the i^{th} species.
λ	L	The wavelength of light or of the intrinsic electronic frequency of a material.
M	-	Molar.
M_n	-	The number average molecular weight of a polymer.
M_v	-	The viscosity average molecular weight of a polymer.
M_w	-	The weight average molecular weight of a polymer.
m_b	ML^{-3}	Molality of the i^{th} component.
μ_i	L^2T^{-2}	The chemical potential of the i^{th} species.
N	-	Avogadro's Number.
$N(0)$	ML^{-3}	The concentration of particles in a suspension before aggregation has started.
$N(t)$	ML^{-3}	The concentration of particles in a suspension at time t.
n	$M^{-1}L^3$	The specific refractive increment of the solute.
ng	M	Nanogram.
$n_i(\infty)$	ML^{-3}	The concentration of ions of type i in bulk solution.
$n_i(x)$	ML^{-3}	The number of ions of type i at a distance x from the charged surface.
ν	L^2T^{-1}	The kinematic viscosity of a fluid.

Symbol	Dimensions	Definition
$\bar{\nu}$	L^3M^{-1}	Partial specific volume of a polymer.
ω	T^{-1}	Angular velocity.
ω_{ab}	ML^2T^{-2}	The energy associated with a contact between molecules a and b.
$\Delta\omega_{ab}$	ML^2T^{-2}	The net change of energy associated with the formation of one ab contact from aa and bb contacts.
P(x)	$ML^{-1}T^{-2}$	The pressure tending to separate two plates.
P	-	The probability of an event.
pH_b	-	The pH of the bulk suspending medium.
pH_s	-	The pH of a solution at a surface.
Φ	M^{-1}	Flory's universal constant.
$\Phi(x)$	-	The normalized distribution of perpendicular extensions of a polymer adsorbed to an interface.
ϕ_a	-	The volume fraction of component a.
Π	$ML^{-1}T^{-2}$	Osmotic pressure.
$\psi(0)$	$ML^2T^{-2}Q^{-1}$	The surface potential of an interface.
$\psi(d)$	$ML^2T^{-2}Q^{-1}$	The potential at the point midway between two charged surfaces.
$\psi(x)$	$ML^2T^{-2}Q^{-1}$	The potential of an interface at a distance x away from its surface.
q	ML^{-3}	The number of atoms contained in a cubic centimeter of a pure material.
R	ML^2T^{-2}	The universal gas constant; equivalent to Nk.
R	$ML^2T^{-1}Q^{-2}$	Electrical resistance.

Symbol	Dimensions	Definition
R	L	The distance between the centers of two particles.
R_e	-	The Reynold's number of a fluid.
R_o	L	The distance between the centers of two particles when a stable aggregate is formed.
$[r^2]^{1/2}$	L	The root mean square end to end distance of a polymer.
$[r_g^2]^{1/2}$	L	The radius of gyration of a polymer.
$[r_o^2]^{1/2}$	-	The unperturbed root mean square end to end distance of a polymer.
$\rho(x)$	ML^{-3}	The charge density of a solution a distance x away from an interface.
$\bar{\rho}$	ML^{-3}	The density of a solution.
ΔS_m	ML^2T^{-2}	The entropy of mixing the polymer layers adsorbed to the surface of two colliding particles.
s	-	The standard deviation of a set of experimental data.
s	-	A measure of the distance between two spherical particles = $R/a = u + 2$.
$\sum_i^q x_i$	-	The sum of all x_i; $x_i + x_j + \ldots + x_q$.
σ	QL^{-2}	The surface charge density at an interface.
σ	-	The true standard deviation of a distribution.
T	-	Absolute temperature.
t	T	Time.
U_i	L^3	The excluded volume of the i^{th} species.

Symbol	Dimensions	Definition
u_e	$ML^3T^{-3}Q^{-1}$	The electrophoretic mobility of a particle.
μm	L	Micron
T	-	A measure of the dielectric susceptibility of an atom.
$\upsilon(x)$	-	The normalized distribution of segment densities of a polymer about an interface.
V	L^3	The volume of a substance.
V	$ML^2T^{-2}Q^{-1}$	Voltage.
V_A	ML^2T^{-2}	The potential energy of attraction between two particles.
V_R	ML^2T^{-2}	The potential energy of repulsion between two particles.
V_T	ML^2T^{-2}	The potential energy of interaction between two particles.
$\bar{V}_i$	L^3M^{-1}	The partial molar volume of the i^{th} component.
v_e	LT^{-1}	The electrophoretic velocity of a particle.
v_f	LT^{-1}	The velocity of a fluid through a pipe.
W	-	A correction factor used to correct the theoretical maximum rated constant K_o for the effect of V_T and viscous interactions.
X_i	-	The mole fraction of the i^{th} component.
x	L	Distance.
$\overline{x^2}$	L^2	The mean square displacement of a particle, due to Brownian motion.
z	-	The valence of an ion.
ζ	$ML^2T^{-2}Q^{-1}$	The zeta potential of a particle.

CONVENTIONS

Symbols

The definitions of the symbols used in this thesis are tabulated in the preceding list. With some exceptions, a given symbol will have only one meaning throughout the thesis. These exceptions refer to universally accepted symbols which have several meanings, which have also achieved general acceptance. Rather than change the commonly accepted symbols of these parameters, all of the relevant original definitions were retained. This was done on the assumption that the ambiguity associated with a symbol having several meanings would be less confusing than the reassignment of new symbols. In most cases this is of little consequence as the meaning of a symbol is apparent from its context and when it is not, the definition of the symbol is included in the text.

Subscripts

Single numerical subscripts indicate that the parameter subscripted refers to a particular component of a system. The subscript 1 always refers to the solvent or suspending medium. In a two component system, the subscript 2 refers to the solute or suspended material. In a polyelectrolyte-salt solution the subscript 2 refers to the polymer and the subscript 3 refers to the salt. Thus, in a salt-polyelectrolyte system the terms X_1, X_2 and X_3 refer to the

mole fraction of the solvent, polyelectrolyte and salt respectively. Exceptions to this convention are the terms A_1, A_2, and A_3 which refer to the first, second, and third virial coefficients of a polymer and the terms b_0, b_1, and b_2 which refer to the coefficients of a power series.

Double subscripts are used to show that the parameter subscripted is a measure of the interaction between the two materials denoted by the subscript.

Alphabetical subscripts are used to increase the number of available symbols. However, they are usually used to differentiate subtypes of a parameter. Thus pH_b and pH_s are both used to denote pH, but the former is the pH of the bulk solution, while the latter is the pH of the solution at the surface of a particle.

Superscripts

All numbers, except the number one, refer to the power by which a quantity is raised.

The superscript ^{o} indicates that the value of the term superscripted is to be taken at the reference state of the material referred to. Thus, μ_1^o, refers to the chemical potential of the solvent in its reference state.

The prime superscript is used to designate the first derivative of the term so marked. Similarly, two primes indicate the second derivative of the term superscripted and so forth.

Parentheses

Parentheses and brackets are used as clarifiers in algebraic expressions to indicate that the quantities enclosed by them are to be evaluated together.

They are also used to show that the value of the term immediately preceding them is a function of the quantity or the quantities enclosed by the parentheses. Thus, $V_T(u, T, C_3)$ indicates that V_T is a function of u, T and C_3.

The symbols Φ and N, which are used to denote constants, are at variance with the aforementioned usage of parentheses, as the meanings of the symbols completely change when they are followed by parentheses. However, after the meaning of the symbols has changed, the parentheses still indicate that the new quantities referred to by the symbols $\Phi(x)$ and $N(t)$ are still functions of the quantities enclosed by the parentheses.

When the term preceding a quantity in parentheses is an operator, such as a log or exp, the parentheses are used to delimit the term on which the operator functions.

Unspecified Symbols

The symbols b, c, d, f, $\bar{b}$, $\bar{c}$, $\bar{d}$, $\bar{f}$, and γ are used to denote a constant or independent variables whose dimensions are determined by the context of the situation in which it is used and whose magnitude is usually unspecified.

The symbols ξ, θ, and Z are used to indicate a variety of dependent variables. The meaning of the symbol will be defined as it is used. The form of the functions that the symbol represents may or may not be specified and any independent variables will be enclosed in parentheses following the symbol.

1. INTRODUCTION

This thesis documents the application of the D. L. V. O. (Derjaguin, Landau, Verwey and Overbeek) theory of the stability of lyophobic colloids to establishing the mechanisms by which a low molecular weight polyelectrolyte aggregates colloidal particles. Although this study lies at the interface between colloid and polymer chemistry its relevance to biochemistry and the biological sciences is clear, in view of the important role played by polymers at the liquid solid interface in these fields. In fact, the impetus for this study was derived from the observations of Katchalsky and coworkers (1, 2) who found that red cells could be aggregated by a poly(l-lysine) of molecular weight 4600. The size of the polymer seemingly precluded the possibility of aggregation by a bridging type of mechanism. However, Gregory (3) showed that a low molecular weight polycation could aggregate polystyrene latices at appreciably faster rates than could be obtained with high concentrations of salt and concluded that neither a bridging mechanism nor a mechanism due solely to a reduction in electrostatic repulsion would account for his observations.

Polystyrene latices were chosen as a model particle for the present investigation, as a meaningful interpretation of the vast majority of studies involving polyelectrolytes and biological surfaces have been hindered by a lack of knowledge of the interfacial properties

of biological membranes. While it is convenient to envisage an interface as a mathematically defined boundary past which the molecules of each phase do not pass, this picture is naive. The interfacial region between two phases is in actuality an ill defined zone where the composition of matter at any fixed point in the interface fluctuates randomly from moment to moment. However, the time average concentration of a non-surface active component of either phase will continuously change across the interface from its concentration in one phase to its concentration in the other phase. Conversely, the concentration of surface active compounds increase sharply from their concentration in bulk solution to their maximal concentration in the interfacial region. In that the difficulty of ascertaining the properties of any material located at the interface is directly related to the complexity of the interface, it was advantageous to work with as simple an interface as possible. However, as the complexity of the interface declines, semblances to a biological system also vanish. Thus, the polystyrene-water interface was chosen as a compromise between the simpler metal-liquid interfaces and the exceedingly complex biological membranes.

The traditional methods for assessing the mechanism by which a polymer induces particles to aggregate are based on the properties of the aggregated particles. In particular, the flow rate of solvent through beds of packed flocs and the volume of the sedimented particle mass

constitute the most frequently used criteria. While these criteria certainly indicate something of the properties of the adsorbed polymer layer, an irrefutable relationship between a polymer's mechanism of aggregation and the properties of the resultant aggregate has yet to be demonstrated. Thus, new standards for determining the mechanism of polymer induced aggregation were needed. The futility of examining the aggregated particles was evident. While the absence of interparticle polymeric bridges was proof of coagulation, their presence does not prove flocculation as bridging may have occurred after the particles had coagulated. The search for an appropriate criterion finally culminated with the realization that the distinguishing feature of polymeric flocculents is their ability to aggregate particles in the presence of electrostatic repulsive forces which would greatly diminish the rate of coagulation of the particles in the absence of the polymer. The D. L. V. O theory of colloidal stability provided a means of predicting the rate at which lyophobic colloids would coagulate and had been used with a moderate success in the past. However, few if any investigators have used it as a means of comparing the rate at which a polymer aggregated a particle suspension and the rate at which the suspension would be coagulated if the polymer had no effect other than to reduce the electrostatic potential of the particles.

This investigation is therefore concerned with establishing the mechanism by which low molecular weight polyelectrolytes destabilize

colloidal suspensions and in characterizing some of the properties of the polyelectrolyte at the polystyrene-water interface. It is further hoped that studies of this rather simple model system will contribute toward the understanding of more complex biological systems. However, in a larger sense this thesis marks the first time the theories of classical colloid chemistry have been used to determine the mechanism by which low molecular weight polyelectrolytes aggregate lyophobic colloids.

1:1. Theory of Colloidal Stability

Colloidal dispersions are suspensions of particles in which at least one dimension of the particle lies between 10 Å and 10,000 Å. These suspensions can be considered stable when there is no change in the total number of particles with time. Thus, a measure of colloidal instability is the rate at which the total particle concentration or number decreases.

In unstirred systems Brownian motion supplies the driving force that aggregates the particles. Einstein showed, theoretically, that the average square displacement $\overline{x^2}$ of a particle in any direction, in time, t, is given by:

$$\overline{x^2} = 2Dt \qquad 1\text{-}1$$

where D is the diffusion coefficient of the particle. From this theory it is possible to predict the average or minimum time required

for two particles to collide when Brownian motion is the only force effecting their approach.

The first attempt to predict the rate of coagulation of a particle suspension was proposed by Smoluchowski (4). Assuming a suspension of monodisperse particles, with no repulsive forces between them, he showed that if the relative diffusion coefficient of two particles, D_r, is simply the sum of their individual coefficients and every collision resulted in permanent contact between the particles, the total number of particles, $N(t)$, (singlets, doublets, triplets, etc.) that are present at time, t, is given by:

$$\frac{1}{N(t)} = K_o t + \frac{1}{N(0)} \qquad 1\text{-}2$$

where $N(0)$ is the particle concentration before the particles begin to aggregate (at $t = 0$), and K_o is the rate constant for the process. For spherical particles the aforementioned rate constant is related to the relative diffusion coefficient, D_r, of two particles by the equation:

$$K_o = 4\pi R_o D_r \qquad 1\text{-}3$$

where D_r is the sum of the diffusion coefficients of the two single particles and R_o is the distance between particle centers when a stable aggregate has formed.

The diffusion coefficient of a single spherical particle of radius a in a suspending medium of viscosity η is given by:

$$D = \frac{kT}{6\pi\eta a} \qquad 1\text{-}4$$

where T is the absolute temperature of the medium and k is Boltzmann's constant.

If stable aggregates are formed when $R_o = 2a$, equation 1-3 predicts a rate constant of $\sim 5.4 \times 10^{-12}$ particles^{-1} cm^3 sec^{-1} for aqueous dispersions undergoing rapid coagulation at room temperature. Direct measurement of K_o (5, 6) has usually yielded experimental values considerably lower than the predicted value. The work of Spielman (7) and Honig et al. (8) suggests that this discrepancy is due to an incorrect assumption about the nature of the particle's relative diffusion coefficient. Spielman argued that as particles approach one another, their viscous motions through the suspending medium affect one another, and the relative diffusion coefficient of the particles will therefore be a function of their distance of separation. Solving the appropriate hydrodynamic expression he published curves of the manner in which the relative diffusion coefficient $D_r(u)$ varies with distance between the particles. Honig et al (8) corroborated Spielman's work and expressed the particles' relative diffusion coefficient as a function of u, where u is defined for two equal spheres as the ratio of the distance between their surfaces to their radius. For these spheres the relationship between the relative diffusion coefficient at infinite separation, $D_r(\infty)$, and a separation, u, is given by (8):

$$D_r(u) = D_r(\infty)\left[\frac{6u^2+4u}{6u^2+13u+2}\right] \qquad 1\text{-}5$$

When this expression is used with equations 1-7 and 1-6 to predict the rate at which rapidly coagulating systems aggregate, the result agrees well with experimental results.

The usefulness of equation 1-2, even when corrected for diffusion effects, is rather limited as it does not account for the interparticle attractive and repulsive forces which determine the percentage of collisions that will result in the lasting contact of the particles. For these systems Smoluchowski's equation must be modified by the inclusion of a correction factor, W:

$$\frac{1}{N(t)} = \frac{K_o t}{W} + \frac{1}{N(0)} \qquad 1\text{-}6$$

Working with aerosols, Fuchs (9) showed that W is related to the potential energy of interaction, $V_T(u)$, of two particles. In 1940 Derjaguin (10) applied Fuchs' (9) theory to solutions. The relationship between W, and $V_T(u)$, when corrected for the Spielman effect is:

$$W = 2\int_{R_o}^{\infty} \frac{D_r(\infty)}{D_r(u)} \exp\left[\frac{V_T(u)}{kT}\right] \frac{du}{(u+2)^2} \qquad 1\text{-}7$$

The potential energy of interaction for the particles is the sum of the attractive, V_A, and repulsive, V_R, potential energy of the particles. The relationship between V_R, V_A, and the predominant

forces between lyophobic colloids was formulated by Derjaguin and Landau (11) and Verwey and Overbeek (12) in terms of the well known D.L.V.O. theory. The original D.L.V.O. theory of colloidal stability regarded coulombic repulsion between the particles as the main stabilizing factor in dispersions of lyophobic colloids. Since then a variety of repulsive forces between colloidal particles have been detected. A partial list of the more important repulsive forces includes:

1) Electrostatic interactions: Ionic groups on the surface of lyophobic colloids establish an electrostatic field about the particle that is often large enough to prevent the particle from making permanent contact with other particles. Electrostatic forces operate over large distances in terms of molecular dimensions and are the primary means of suspension stabilization. The role of electrostatic forces has been dealt with in depth by the D.L.V.O. theory and will be considered later.

2) Adsorbed layers: van der Waal's attractive forces frequently cause a monolayer of solvent molecules to bind to the solid phase of a liquid-solid interface. This increases the distance of closest approach of two particles and thereby diminishes the extent of the attractive forces which may be attained. If the particles are very small ($a < 100$ Å) adsorbed layers

may keep the particles far enough apart that van der Waal's attractive forces cannot bind them together (13). Vold (14) has also demonstrated that layers of adsorbed material may alter the van der Waal's attractive forces between two materials. Layers of adsorbed polymer or surfactant can generate large repulsive forces when the layers of two coated particles overlap. These repulsive forces are due to the heat of mixing the polymer layers and the decrease in the entropy of the adsorbed layer, which will be discussed in section 1:2.

3) van der Waal's repulsive forces: At very short distances between particle surfaces the repulsive forces between the particles rise sharply. This rise occurs when the electron clouds of the various atoms on the two particles begin to overlap. These forces are usually not considered in calculations of colloidal stability as they are not measurable until the particles are permanently bound.

The foundations for calculating the electrostatic forces between two particles were laid by Gouy (15) and Chapman (16). They defined the relationship between surface charge, on an infinite plane, and surface potential by assuming:

1) The surface of the plane is flat and all charges are considered to be uniformly smeared.

2) The dielectric constant of the suspending medium, ϵ, is not affected by the potential gradient and is equal to that of the bulk liquid at all points.

3) The ions are point charges whose distribution, with respect to the charged surface, is given by a Boltzmann distribution.

4) The surface charge is small enough that the potential $\psi(x)$ obeys $[\frac{ze\psi(x)}{kT}] \ll 1$ at all points.

The charge density, $\rho(x)$, at a distance x away from the surface of an infinite plane is related to the potential, $\psi(x)$, at that point by the Poisson equation in one dimension:

$$\frac{d^2\psi(x)}{dx^2} = -\frac{4\pi}{\epsilon}\rho(x) \qquad 1\text{-}8$$

Since, the charge density equals the sum of the dissolved ion types:

$$\rho(x) = e\sum_i z_i n_i(x) \qquad 1\text{-}9$$

where,

z_i = the valence of the i^{th} ion type

$n_i(x)$ = the number of the i^{th} ion type per cm^3 at x

According to assumption three, the number of ions at x is given by a Boltzmann distribution:

$$n_i(x) = n_i(\infty)\exp[\frac{-z_i e\psi(x)}{kT}] \qquad 1\text{-}10$$

where $n_i(\infty)$ is the number of i^{th} type ions per cm^3 in the bulk solution. From equations 1-8, 1-9, and 1-10, the Poisson-Boltzmann equation can be constructed:

$$\frac{d^2\psi(x)}{dx^2} = -\frac{4\pi e}{\epsilon} \sum_i z_i n_i(\infty) \exp\left[\frac{-z_i e\psi(x)}{kT}\right] \qquad 1\text{-}11$$

For the present system in which only a single symmetrical electrolyte is present, the Poisson-Boltzmann equation may be rewritten as:

$$\frac{d^2\psi(x)}{dx^2} = \frac{8\pi z e n_i(\infty)}{\epsilon} \sinh\left[\frac{ze\psi(x)}{kT}\right] \qquad 1\text{-}12$$

For low surface potentials where $\left[\frac{z\epsilon\psi(0)}{kT}\right] \ll 1$, the sinh term may be approximated by the first term of its infinite series:

$$\sinh x = x + \frac{x^3}{3!} + \frac{x^5}{5!} + \ldots + \frac{x^{2n+1}}{(2n+1)!} \qquad 1\text{-}13$$

to give:

$$\frac{d^2\psi(x)}{dx^2} = \frac{8\pi z^2 e^2 n_i(\infty)}{\epsilon kT} \psi(x) = \kappa^2 \psi(x) \qquad 1\text{-}14$$

where κ is the Debye-Hückel parameter and

$$\kappa = \left[\frac{8\pi z^2 e^2 n_i(\infty)}{\epsilon kT}\right]^{1/2}$$

This type of equation is a linear, homogeneous differential equation of the second order with a general solution:

$$\psi(x) = b \exp(\kappa x) + c \exp(-\kappa x) \qquad 1\text{-}15$$

where b and c are constants whose values are determined by the boundary conditions of the equation.

The boundary condition which determines the value of b is, $\psi(x) \rightarrow 0$ as $x \rightarrow \infty$. This condition requires that b be set to zero. Substituting $x = 0$ into the equation, the value of c must be equal to the surface potential of the infinite sheet $\psi(0)$. The relationship between distance from the surface of the plane, x, and the potential at that point is:

$$\psi(x) = \psi(0)\exp(-\kappa x) \qquad 1\text{-}16$$

The relationship between surface charge density, σ, and surface potential, $\psi(0)$, can be derived from the requirement of electrical neutrality throughout the system. This can be expressed as:

$$\sigma = -\int_0^\infty \rho(x)dx \qquad 1\text{-}17$$

This is an expression of the fact that the total net space charge density must be equal to but of opposite sign to the total surface charge. Thus, substituting from equation 1-8, changing the limits of integration to those of $\frac{d\psi(x)}{dx}$ at ∞ and 0 from equation 1-16 yields:

$$\sigma = \frac{\kappa\epsilon\psi(0)}{4\pi} \qquad 1\text{-}18$$

For systems where the surface potential is not small and $[\frac{z\epsilon\psi(x)}{kT}] \sim 1$, the Poisson-Boltzmann equation may be integrated exactly, for symmetrical electrolytes, to give:

$$\psi(x) = \frac{2kT}{ze} \ln\left[\frac{1+\gamma \exp(-\kappa x)}{1-\gamma \exp(-\kappa x)}\right] \qquad 1\text{-}19$$

where

$$\gamma = \frac{\exp\left[\frac{ze\psi(0)}{2kT}\right]-1}{\exp\left[\frac{ze\psi(0)}{2kT}\right]+1}$$

The charge density under these circumstances is given by:

$$\sigma = \left[\frac{2\epsilon kT n_i(\infty)}{\pi}\right]^{1/2} \sinh\left[\frac{ze\psi(0)}{2kT}\right] \qquad 1\text{-}20$$

No exact solution of the Poisson equation is possible for spherical particles. However, for particles whose radius is large in comparison with κ, the flat plate model adequately approximates $\psi(x)$.

One method of calculating the repulsive potential between two flat plates separated by a distance $2d$ is to consider the osmotic force generated by the excess ion concentration between the plates, when the diffuse double layers of each plate overlap one another. Since the ion distribution between the plates is governed by the distribution of $\psi(x)$ it is necessary to solve the Poisson-Boltzmann equation with the boundary conditions $\psi(x) = \psi(0)$ when $x = 0$ and $x = 2d$ and $d\psi(x)/dx = 0$ when $x = d$. The latter boundary condition is a consequence of the symmetrical distribution of potential about the plate's midpoint. This solution involves an elliptical integral which cannot be solved analytically. However, if the interaction between the plates is

not too great, the potential at the midpoint between the two points, $\psi(d)$, may be approximated by the sum of two single double layer potentials at a distance d from their surface (12):

$$\psi(d) \sim 2\psi(0)\exp[-\kappa d] \qquad 1\text{-}21$$

The ion concentration and distribution of the electrolyte within the two plates is governed by a Boltzmann distribution. Hence, at the midpoint between the plates, the concentration of ions, $\rho(d)$, is:

$$\rho(d) = n_i(\infty)\exp[\frac{-ze\psi(d)}{kT}] + n_i(\infty)\exp[\frac{ze\psi(d)}{kT}] \qquad 1\text{-}22$$

and the osmotic pressure, $\Pi(s)$, at this point is:

$$\Pi(d) = kT\ \rho(d) = 2KTn_i(\infty)\cosh[\frac{ze\psi(d)}{kT}] \qquad 1\text{-}23$$

The osmotic pressure, $\Pi(\infty)$, of the ions in bulk solution, where $\psi(x) = 0$ is:

$$\Pi(\infty) = 2kTn_i(\infty) \qquad 1\text{-}24$$

The pressure, $P(x)$, tending to separate the two plates is, therefore, the difference between the bulk solution osmotic pressure and the osmotic pressure midway between the plates where:

$$P(x) = \Pi(d) - \Pi(\infty) = 2n_i(\infty)kT[\cosh[\frac{ze\psi(d)}{kT}]-1] \qquad 1\text{-}25$$

The potential energy of repulsion between these two plates equals twice the amount of work required to bring one plate from a distance of ∞ to a distance $2d$ away from the other plate:

$$V_R = -2\int_{\infty}^{d} P(x)dx = -2\int_{0}^{d} 2n_i(\infty)kT[\cosh[\frac{ze\psi(d)}{kT}]-1]dx \qquad 1-26$$

The exact solution of this integral cannot be readily evaluated because of the complex relationship between $\psi(d)$ and x. However, this difficulty can be partially circumvented by approximating the cosh term by its equivalent infinite series and using the terms in the series up to the second order. Thus:

$$V_R = \frac{4n_i(\infty)[ze\psi(0)]^2}{kT}\int_{\infty}^{d} \exp[-2\kappa x]dx$$

$$= \frac{4n_i(\infty)[ze\psi(0)]^2}{\kappa kT}\exp[-2\kappa d] \qquad 1-27$$

Exact solutions for the potential energy of interaction between parallel plates have been published by Devereaux and de Bruyn (17) while Honig and Mul (18) have tabulated numerical calculations of V_R for spherical particles.

Derjaguin (19) has developed an approximate method for calculating the potential energy of repulsion between spheres by treating their surfaces as a series of infinitely thin concentric cylinders. The ends of the cylinders are treated as flat plates and the flat plate equation is applied to each pair of cylinder-cylinder interactions. V_R is obtained by integration over the surface of the spheres.

This approach was used by Verwey and Overbeek (12) for spheres where $\psi(0)$ was small, $\kappa a \gg 1$ and the distance between the

surface of the spheres is large in comparison to $1/\kappa$. For suspensions where $\frac{ze\psi(0)}{kT} \not> 2$ and $\kappa a \not< 10$, the potential energy of repulsion can be approximated within five percent by:

$$V_R = \frac{\epsilon a \psi^2(0)}{2} \ln[1+\exp(-\kappa a u)] \qquad 1\text{-}28$$

At all distances of separation, this approximation tends to overestimate V_R, but it asymptotically approaches the correct value as the distance between the spheres increases.

In the D. L. V. O. theory of colloidal stability, the only source of attractive forces between particles which are dealt with are London-van der Waal's forces. However, several other types of attractive forces between chemically similar particles are also known to exist.

1) Ion bridging: Multivalent cations can act as bridging agents between anionic surfaces.

2) Charge fluctuations: When the charge groups on two surfaces are partially ionized, random fluctuations in the pattern of charge groups on one surface will induce fluctuations in the pattern of charge groups on the other surface. This results in a net attraction between the surfaces (20). Since these forces are of an electrostatic nature they are screened by electrolytes and decay at a rate that is proportional to the factor $\exp[-\kappa H]$. Thus, they are ineffective in solutions with a high ionic strength or with particles whose surfaces are

fully ionized. Pethica (21), however, has speculated that fully ionized surfaces may still exhibit charge fluctuations due to the transient formation of ion pairs between the charge groups on the surface and their counterions in solution.

3) Electrostatic forces: Bierman (22) and Parsegian and Gingell (23) have considered the nature of the electrostatic interactions between two different types of particles; those which maintain a constant surface potential by the adsorption or desorption of ions and those which have a constant surface charge density. They demonstrated that if two particles of the first type approach one another, their electrostatic interaction will always be of a repulsive nature when their surface potentials are of the same sign and magnitude. Similarly, two particles will always repel one another when their surface charge densities are fixed and of the same sign. Conversely, two particles which maintain constant surface potentials of the same sign but of different magnitudes will repel one another only part of the time. Depending on the particular particles, their electrostatic interaction will be of a repulsive nature at all interparticle separations greater than a given distance, H, and attractive at all distances less than H. However, particles of this type probably do not occur naturally as Frens and coworkers (24) have shown that the

time required to establish equilibrium with respect to ion adsorption is much greater than the time of an interparticle collision. Thus, most particle-particle collisions occur between two particles with an effective constant surface charge density. The nature of their interaction will therefore depend only on the sign of their surface charge.

4) Image forces: Ions which are located between two unchanged walls of a material with a low dielectric constant have a higher free energy than an ion which is completely surrounded by a material with a high dielectric constant (25). Thus, ions tend to leave the region between two spheres with a low dielectric constant and thereby create a region with an osmotic pressure that is lower than the osmotic pressure of the bulk solution. This results in a force that acts as if there were an attraction between the particles. The magnitude of this effect is dependent on the extent of screening by other electrolytes and diminishes exponentially with increasing ionic strength.

The role these forces play in determining the stability of colloidal systems is not well understood and has not been vigorously researched. However, it is reasonably certain that in the present system the extent of attractive forces due to ion bridging or electrostatic attractive forces is negligible. The extent of charge fluctuations on the surface of the polystyrene latices are not known and are very difficult to

calculate in the absence of information on the solution properties of the SO_4^--H^+ and SO_4^--Na^+ bonds. Similarly little is known about the role of image forces.

The basis of the van der Waal's forces between two atoms is the result of the mutual attraction between two dipoles. Debye (26, 27) showed that molecules with permanent dipole moments influence the spatial orientation of other molecules with dipole moments in a manner that results in their mutual attraction. Molecules with dipole moments can also induce dipole moments in other molecules, which also results in an attraction between them (28). The attraction between non-polar molecules was explained by London (29) on a quantum-mechanical basis. He showed that on a statistical basis the distribution of electrons about an atom will be temporarily asymmetrical. This results in a transient dipole moment which will induce a similar dipole moment in other atoms. The net result is an attractive force between the neutral atoms. According to London's theory, these forces between atoms will be proportional to the inverse seventh power of the distance between the atoms. Thus, the attractive potential, V_A, between atoms will vary with the inverse sixth power of the distance between them. Thus

$$V_A = -\frac{T}{R^6} \qquad 1\text{-}29$$

where T is a constant whose value is a function of the atoms dielectric

susceptibility. Attempts to relate T to the properties of various atoms have been made by London (29), Slater and Kirkwood (30) and Moelwyn-Hughes (31).

Hamaker (32) calculated the attractive potential between two spherical particles in a vacuum by summing the interatomic attractive forces between all pairs of atoms to give:

$$V_A = \frac{A_{22}}{6}\left[\frac{2}{(2+u)^2-4} + \frac{2}{(u+2)^2} + \ln\left[\frac{(u+2)^2-4}{(u+2)^2}\right]\right] \qquad 1\text{-}30$$

where A_{22} is Hamaker's constant which is related to the attraction between individual atoms in a vacuum by:

$$A_{22} = q^2\pi^2\lambda \qquad 1\text{-}31$$

q is the number of atoms cm^{-3} in the sphere and λ is the wavelength of the intrinsic electronic frequency of the material (material 2) in the sphere. When the spheres are suspended in a liquid the dielectric properties of the suspending medium (material 1) invariably alter the magnitude of the attractive forces. If A_{11}, A_{22} and $A_{12} = (A_{11}A_{22})^{1/2}$ are the Hamaker constants for the attractive forces between two equal spheres of material 1, material 2 and material 1 and material 2 respectively, the Hamaker constant, A, for two spheres of material 2 suspended in material 1 is (32):

$$A = A_{11} + A_{22} - 2A_{12} \qquad 1\text{-}32$$

Estimates of A for polystyrene in water have varied over a wide range of values. Schenkel and Kitchener (33) have calculated a value of 10^{-12} erg, Ottewill and Walker (34) 5×10^{-14} erg, and Smith, Mitchell and Ninham (35) 1.2×10^{-13} erg. The discrepancy between these values is probably attributable to the differences in methods of estimating A and more importantly, to evolving viewpoints on the nature of the Hamaker constant.

In 1948 Casimir and Polder (36) showed that the London-van der Waal's forces between particles decay more rapidly than predicted by equation 1-30. The increased rate of decay is due to the finite speed of light and is a function of λ. These reduced forces are said to be retarded. At a distance, H, between the spheres where $H \geq \frac{10\lambda}{2\pi}$ the London-van der Waal's forces are fully retarded when $H \ll a$ and the potential energy of attraction between the two spheres (33) is given by:

$$V_A \simeq \frac{2.45\lambda Aa}{120\pi H^2} \qquad 1\text{-}33$$

For sphere separations where $R < 0.1\lambda$, retardation effects are small enough that equation 1-30 can be used directly. At sphere separations where $0.1\lambda < R < \frac{10\lambda}{2\pi}$ no analytic correction factor for estimating retardation effects is available. However, this presents no problem as λ has been estimated at 1000 Å for polystyrene (33) and

at distances where retardation effects become significant, V_A is negligible.

The theory of the nature of the London-van der Waal's forces was revolutionized in 1955 when Lifshitz (37) published a quantum mechanical theory of the atomic and molecular forces in condensed media. Since then Parsegian and coworkers (35, 38) have extended his theory to include the interaction of particles in colloidal suspension. Their work indicates that the bulk of the attractive forces between colloidal particles consist mainly of electromagnetic fluctuations of low frequency. Thus, the traditional assumption that London forces, or electromagnetic fluctuations in the ultraviolet region, constitute the majority of the attractive forces is frequently incorrect. In aqueous systems London forces often constitute less than 50% of the total attractive force. Furthermore, they have noted that forces between particles are not necessarily additive. The concept of additivity requires the total attractive force between two particles to be the sum of the individual interactions of each individual unit of constituent matter with every other unit of constituent matter in the other particle. The principle of additivity is a basic assumption in Hamaker's theory which predicts a distance dependence of V_A that decays more rapidly than the Lifshitz theory. In the Lifshitz theory the rate of decay is a function of particle geometry, distance, temperature, λ, and the dielectric susceptibilities of the particles and the suspending media. Finally, Parsegian and

Ninham (38) have developed method for calculating the attractive forces between a variety of particles from a limited knowledge of the dielectric properties of the material and the suspending medium.

Calculations of V_A by the Lifshitz method are cumbersome and require extensive computer facilities. However, equation 1-30 frequently provides a good estimate of V_A. Smith, Mitchell and Ninham (35) have shown that for polystyrene spheres in water an expression equivalent to equation 1-30 predicts V_A with an accuracy of 5% or better at particle separations of $u \leq 10^{-2}$. At separations where $u > 10^{-2}$, V_A is negligible and the increasing error in V_A is of no consequence. The fortuitous agreement between expression 1-30 and the non-retarded Lifshitz expression is the result of errors in the microwave region balancing those in the ultraviolet and infrared regions. Retardation effects are not significant when $u < 10^{-2}$ and need not be considered.

Equations 1-7, 1-28, and 1-30 provide the basis for quantitative predictions of the stability of a suspension when the experimentally measurable quantities $\psi(0)$, κ, a, ϵ and A are known. Qualitative predictions of suspension behavior can be made on the basis of the shape of the potential energy of interaction curve V_T. When $\kappa a \gg 1$, the total energy of interaction between two spheres, V_T is:

$$V_T = \frac{\epsilon a \psi^2(0)}{2} \ln[1+\exp(-\kappa a u)] - \frac{A}{6}\left[\frac{2}{(2+u)^2-4} + \frac{2}{(2+u)^2} + \ln\left[\frac{(u+2)^2-4}{(2+u)^2}\right]\right] \qquad 1\text{-}34$$

For varying values of A, κa, and $\psi(0)$, three types of potential energy of interaction curves can be observed. These correspond to three different types of behavior for a particle suspension.

In suspensions where the particles have large surface potentials or the ionic strength of the suspending medium is low, the potential energy of interaction between two particles can be represented by the diagram given in figure 1-1. The sizable electrostatic forces between the particles of the suspension create large potential energy barriers that can prevent Brownian motion from coagulating the particles. In practice a potential energy barrier that is greater than about 10 kT is sufficient to stabilize a colloidal suspension.

Slow coagulation of particle suspensions may be brought about by a reduction of the potential energy barrier to a height of several kT. The addition of moderate amounts of salt, to a particle suspension, can produce this reduction, as is demonstrated by the potential energy diagram in figure 1-2. The added salt increases the magnitude of κ and thereby the rate at which V_R decreases with distance between the particles. When the energy barrier is only a few kT in height, a small fraction of the collisions between the particles will have enough energy to surmount the potential energy barrier and form a stable aggregate. Another type of slow coagulation may be obtained when the addition of salt to a stable suspension creates a secondary minimum, as in figure 1-3. In this situation, the existence of large surface

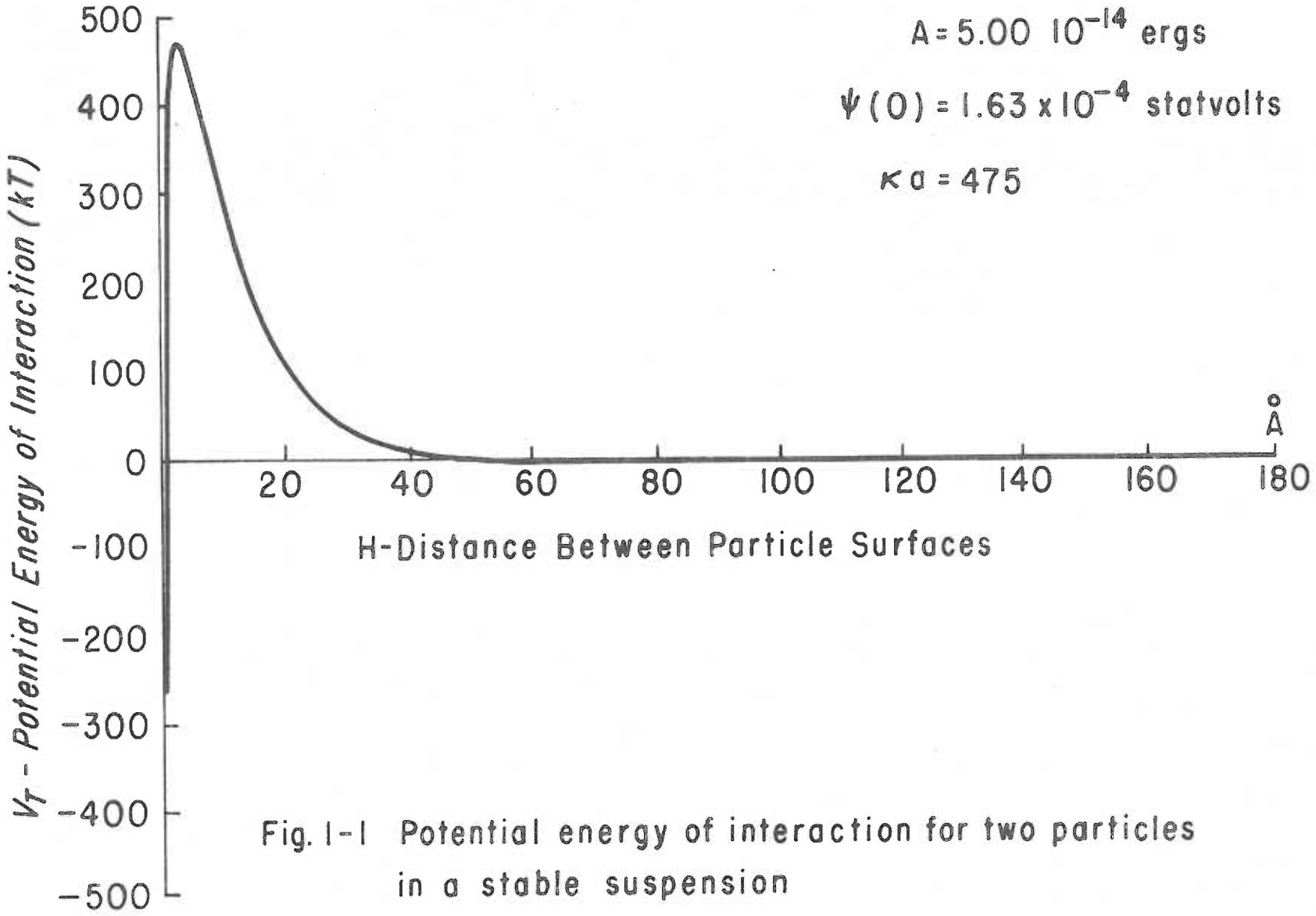

Fig. 1-1 Potential energy of interaction for two particles in a stable suspension

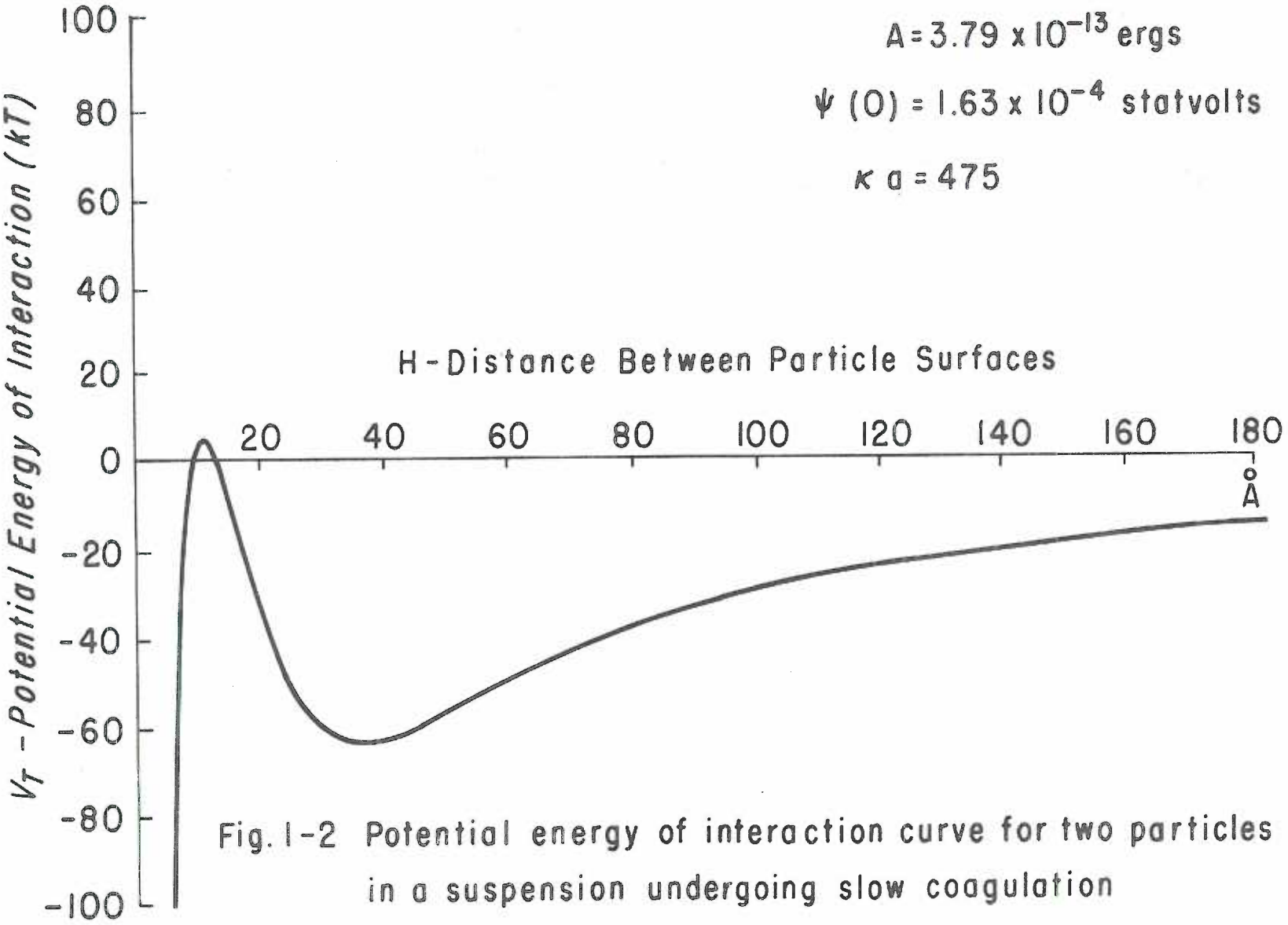

Fig. I-2 Potential energy of interaction curve for two particles in a suspension undergoing slow coagulation

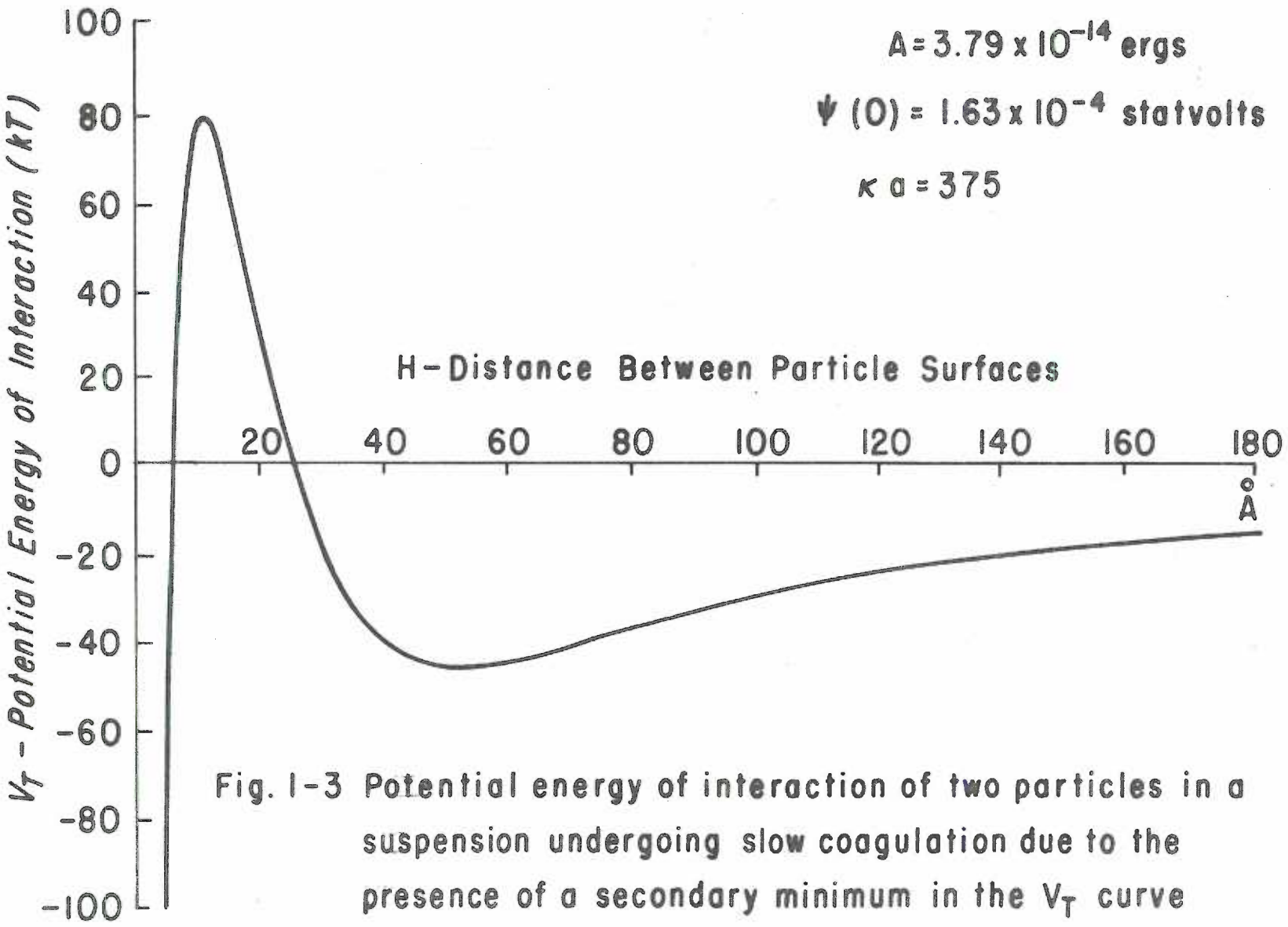

Fig. I-3 Potential energy of interaction of two particles in a suspension undergoing slow coagulation due to the presence of a secondary minimum in the V_T curve

potential creates a large potential energy barrier when the distance between the particles is small. However, the electrostatic repulsive forces decay more rapidly than do the attractive forces and an attractive potential energy well may occur when the particles are separated by distances of several hundred angstroms. The depth of this well is often only a few kT units and particle pairs present in it are often only quasistable. However, a portion of these aggregates will exist long enough to collide with a third particle and form stable aggregates. These stable aggregates are the nucleus of large aggregates.

When large amounts of salt are added to a stable suspension, the electrostatic forces are almost completely suppressed. In these cases, where the potential energy of attraction is larger at every point than the repulsive potential, as in figure 1-4, rapid coagulation results. In suspensions that are undergoing rapid coagulation every particle-particle collision produces an aggregate.

1:2. Polymer Adsorption and Colloidal Stability

When a polymer is added to a colloidal suspension the properties of the particle-solvent interface and the stability of the suspension will be altered. Changes in the stability of a suspension reflect changes in the manner in which the interparticle potential energy of interaction varies with distance. These alterations in the potential energy versus

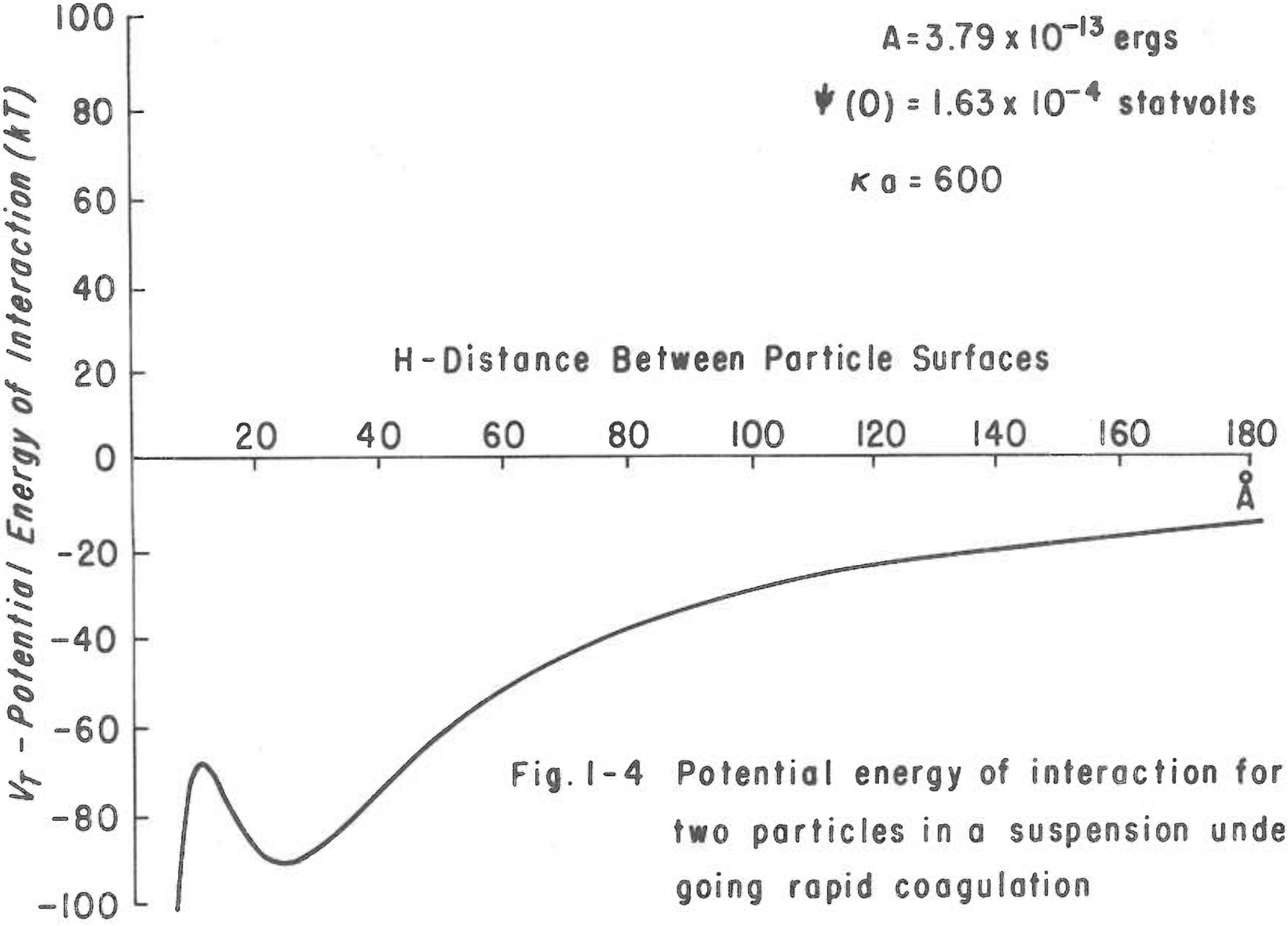

Fig. I-4 Potential energy of interaction for two particles in a suspension undergoing rapid coagulation

distance curves are readily visualized in terms of the effect of a polymer layer on the free energy of a two particle system.

The configuration of the adsorbed polymer, which is of paramount importance to calculations of the free energy of a polymer coated particle can, at present, only be described in general terms. The segments of an adsorbed polymer chain, the smallest repeating unit of the chain, are generally envisaged as an alternating series of loops and trains. A train is a sequence of segments, which are all adsorbed to the solid phase of an interface. A loop is a sequence of segments which are bound at both ends to the solid phase of the interface but otherwise lie in the liquid phase. When a sequence of segments extends into the liquid phase but is attached to the solid interface only at one end, it is termed a tail. Rubin (39), Hoeve (40), Roe (41), Silberberg (42, 43, 44, 45), Hesselink (46) and Motomura et al. (47, 48, 49, 50) have generated theories for predicting the configuration and properties of adsorbed neutral polymers.

The effect of an adsorbed polymer layer on the stability of a colloidal suspension is usually assessed by calculating the change in the free energy of a two particle system as a function of the distance between the particles. The first part of this calculation entails an evaluation of the effect of the polymer layer on the van der Waal's attractive forces and the electrostatic forces between the particles. The second part considers the interaction of the two polymer layers.

The effect of adsorbed layers of solvent and other materials was first treated by Vold (14). Extending Hamaker's approach, she showed that when the Hamaker constant of the adsorbed layer differed from that of the core particle, the potential energy of attraction between the core particles would be reduced. Initially, the work of Johnson and coworkers (51) appeared to support this concept. They measured the rate of aggregation of a suspension of polyvinylacetate particles with a diameter of 1.9 microns and found it to be much less than the theoretical rate predicted for rapid coagulation. N.M.R. spectroscopy confirmed the existence of a layer of bound water on the surface of the particles and it was suggested that the layer of bound solvent was responsible for the lowered rate of aggregation. In view of the subsequent findings of Spielman (7) and Honig et al. (8) the validity of this reasoning appears to be in doubt. However, Vincent and coworkers (52, 53) and Parfitt (13) have examined the phenomenon more closely and have suggested that the "Vold effect" is effective in stabilizing particles when the diameter of the particles is small (<100 Å) or the layer of adsorbed solvent very thick (> 20 Å). These suggestions have been corroborated recently by the work of Kiefer and his colleagues (54) who find that the thickness of the adsorbed layer must be 0.01 that of the particle radius to have an effect.

Adsorbed polymer layers also affect long range forces between colloidal particles by altering their repulsive potentials. Neutral

polymers can increase electrostatic repulsive forces (55), and polyelectrolytes may increase or decrease them. A number of studies (56, 57, 58) have related the amount of polyelectrolyte adsorbed to a particle with the electrostatic potential of the particle but no general theory for relating the two has yet been developed. This is due, in part, to the lack of a theory of adsorbed polyelectrolyte configuration. For practical purposes this does not pose a great difficulty as the repulsive potential of the particle can be estimated by measurements of a particle's zeta potential.

For small particle separations the overlap of polymer layers on the particles usually causes a noticeable change in the free energy of the system. This change is the sum of the free energy of mixing for the adsorbed polymer layers and the free energy of adsorption if the polymers bridge between the particles. The free energy of mixing, ΔG_m, of the adsorbed layers is composed of an enthalpy term, ΔH_m and an entropy term, ΔS_m.

$$\Delta G_m = \Delta H_m - T\Delta S_m \qquad 1\text{-}35$$

The entropic contribution to the free energy is primarily due to the reduction in configurational free energy the polymer experiences. The overlap of the polymer layers always reduces the total number of polymer configurations available to the adsorbed polymer chains. These volume restriction effects invariably result in a decrease in the

entropy of the chains and generate a repulsive force between the particles. For low degrees of polymer coverage this effect may be visualized by considering Bagchi and Vold's (59) model. Consider a single molecule adsorbed to a flat surface. Let $\Phi(x)$ be the polymer's normalized distribution of perpendicular extensions from the adsorbing surface, where x is the extension. $\Phi(x)$ has the property, $\int_0^\infty \Phi(x)dx = 1$. If an impenetrable non-adsorbing wall is placed a distance d away from the adsorbing surface, the fraction of the total possible configurations left to the polymer will be given by $\int_0^d \Phi(x)dx$. Therefore, the change in configurational entropy, ΔS_m, is:

$$\Delta S_m = k \ln \int_0^d \Phi(x)dx - k \ln \int_0^\infty \Phi(x)dx$$

$$= k \ln \int_0^d \Phi(x)dx \qquad 1\text{-}36$$

The change in free energy $\Delta G'_m$ per cm^2 due to entropic repulsion alone is given by:

$$\Delta G'_m = -kTb \ln \int_0^d \Phi(x)dx \qquad 1\text{-}37$$

where b is the number of polymer molecules per cm^2 of surface. When two polymers are adsorbed to opposing surfaces a distance d apart, the percentage of configurations available to each polymer will be even less than the figure listed in equation 1-36, and the free energy

of repulsion will be more than doubled.

Estimates of $\Delta G'_m$ for two flat polymer covered plates have been given by a number of investigators by two different approaches. Hesselink (60, 61) and most investigators (62, 63) derive analytical expressions for the segment density distributions for different types of adsorbed polymers and calculate the effect of decreasing the volume available to the polymer chains. These calculations usually show $\Delta G'_m$ to increase exponentially when plate separation distances become less than the polymer's root mean square end to end distance $[r^2]^{1/2}$. For small polymers, ($[r^2]^{1/2} \sim 10$ Å), $\Delta G'_m$ attained a value of ~3 kT per adsorbed polymer chain at distances of about 6 Å. However, these calculations did not treat the effects of the polymer's excluded volume. The other major method of calculating $\Delta G'_m$ uses a computer to simulate a self avoiding three dimensional random walk for an irreversibly adsorbed tail on a cubic latice. This approach has the advantage of being able to treat excluded volume effects in a relatively simple fashion. For a 100 unit polymer chain constrained between two plates approximately 6 Å apart, $\Delta G'_m$ approaches 50 kT per adsorbed chain. These results are in reasonable agreement with those of Hesselink and coworkers for adsorbed tails and probably provide a good estimate of $\Delta G'_m$ for most polymers.

The entropy of a two particle system can be further decreased by the simultaneous adsorption of a polymer loop onto both particles. This important phenomenon is the primary means by which neutral polymers aggregate particle suspensions and is termed bridging. The largest component of this decrease is the result of the entropic losses each polymer segment experiences on adsorption. This loss will be a function of each polymer segment's average number of neighbors and coordination number. Fleer (64) has estimated this loss at 0.3 kT per adsorbed segment. A secondary entropic loss is the result of the decrease in the total number of configurations available to the loop or tail which has bridged. This increases the free energy of a two particle system by about 5 kT per loop or chain that is adsorbed. This particular increase in free energy decreases as the distance between the plates diminishes (64).

The enthalpy of mixing the polymer layers, ΔH_m, is primarily controlled by the interaction of the solvent and the polymer. The quantitative treatment of ΔH_m which follows was given by Flory (65). ΔH_m is due to the interchange of contacts between molecules of the solvent and the solute, on mixing. If ω_{11}, ω_{22} and ω_{12} are the energies associated with solvent-solvent, solute-solute and solvent-solute contacts respectively, the change in energy for the formation of a solvent-solute contact, $\Delta\omega_{12}$, is:

$$\Delta\omega_{12} = \omega_{12} - \frac{\omega_{11}+\omega_{22}}{2} \qquad 1\text{-}38$$

For a given arrangement of molecules in a solution, where there are c contacts between solvent and solute molecules, the heat of formation of that solution, ΔH_m, from the pure components is:

$$\Delta H_m = c\Delta\omega_{12} \qquad 1\text{-}39$$

The average value of c is approximately equal to the product of the volume fraction of the solvent, ϕ_1, and the total number of polymeric contact sites. For polymers each monomeric unit will have $b-2$ contacts with its neighbors. Thus, for a polymer of d segments, the heat of mixing the polymer and the pure solvent is:

$$H_m \simeq (b-2)d\Delta\omega_{12}\phi_1 \qquad 1\text{-}40$$

This expression may be rewritten by creating the term, χ, to characterize the polymer-solvent interaction energy. For the general case where the solvent contains f segments χ is defined as:

$$\chi = \frac{fb\Delta\omega_{12}}{kT} \qquad 1\text{-}41$$

Thus the quantity $kT\chi$ represents the difference in energy of a solvent molecule immersed in the pure polymer compared to one in pure solvent. Using this definition expression 1-40 can be rewritten as:

$$\Delta H_m \simeq dkT\chi\phi_1 \qquad 1\text{-}42$$

In athermal solvents, χ is zero and therefore the solvent molecule does not change energy when forming polymer-solvent contacts. Thus, the enthalpy of mixing is zero in an athermal solvent. In other solvents it is difficult to calculate the enthalpy of mixing as χ is generally unknown. However, ΔH_m may be approximated from a knowledge of the polymer's second virial coefficient, A_2, and the surface concentration in gm cm^{-3} of the polymer, C_2. This approach was first proposed by Fischer (66) who suggested that much of the repulsive force between polymer coated particles was due to the excess osmotic pressure between the particles. This osmotic pressure, Π, is given by:

$$\Pi = A_2 N k T C_2^2 \qquad 1\text{-}43$$

where N is Avogadro's number. ΔH_m is obtained by integrating Π over the volume element where the polymer layers overlap. Thus for two spheres of radius a, with a polymer layer of thickness δ:

$$\begin{aligned}\Delta H_m &= 2\int_0^{\delta V} \Pi dV \\ &= \frac{4}{3}\pi A_2 N k T C_2^2 [\delta - (\frac{R-2a}{2})]^2 [3(a+\delta) - \delta + (\frac{R-2a}{2})] \\ &= \frac{4}{3}\pi A_2 N k T C_2^2 [\delta - (\frac{R-2a}{2})]^2 [2(a+\delta) - \frac{R}{2}] \qquad 1\text{-}44\end{aligned}$$

δV is the volume of the region where the polymer layers overlap and R is the distance between particle centers. In certain circumstances the heat of mixing the adsorbed polymer layers can decrease

the free energy of a two particle system as the particles collide. This happens when the particles are suspended in a poor solvent for the polymer and A_2 is negative. Adsorbed polymer layers in poor solvents are self attracting and therefore promote aggregation. When the polymers are dissolved in a good solvent A_2 is positive and the heat of mixing generates a repulsive force. Although the derivation given in equation 1-44 is a reasonable first approximation it overestimates ΔH_m by tacitly assuming that the bulk of the adsorbed polymer lies in the liquid portion of the interface and that the segments are uniformly distributed throughout the layer. However, several recent estimations of ΔH_m for neutral polymers have included the effects of polymer configuration (61, 64). Unfortunately, little work has been done on the osmotic pressures generated on the overlap of adsorbed layers of polyelectrolytes.

Polymeric bridging can also reduce the enthalpy of a two particle system. The extent of this decrement is a function of the heat of adsorption for the polymer segments and the number of segments adsorbed. Fleer (64) has suggested that the latter quantity may be calculated from the polymer's normalized distribution of segment densities, $\upsilon(x)$, where x is the distance normal to the adsorbing surface. Consider the case of two flat polymer coated plates a distance d apart. b segments from each plate will be able to adsorb onto the other plate.

$$b = \frac{NC_2}{M_n} \int_d^\infty \upsilon(x)dx \qquad 1\text{-}45$$

where C_2 is the molar surface concentration of adsorbed polymer and M_n the molecular weight of the polymer segments. If complete adsorption of all b segments is assumed and the heat of adsorption taken as $\Delta\omega_{23}$ kT per adsorbed segment, the heat of adsorption, ΔH_a, for two polymer covered plates a distance d apart is:

$$\Delta H_a = \frac{2NC_2\Delta\omega_{23}}{M_n} \int_d^\infty \upsilon(x)dx \qquad 1\text{-}46$$

Calculations of ΔH_a are again complicated by a lack of knowledge of $\upsilon(x)$. $\Delta\omega_{23}$ may be estimated from measurements of the heat of adsorption for a polymer's monomeric units onto the liquid-solid surface of interest if the extent of adsorption can be determined. Infrared spectroscopy has been used (67) to measure the percentage of polymeric segments that were in a train configuration. However, this technique is ill suited to aggregated aqueous dispersions.

1:3. Criterion for Flocculation

The preceding sections have shown that colloidal suspensions may be aggregated by a reduction of the electrostatic forces between the particles or by a bridging mechanism. In 1966 LaMer (68) suggested that the terms coagulation and flocculation be applied to these two mechanisms respectively. Unfortunately, certain polyelectrolytes

aggregate particles by both mechanisms and it is necessary to refine these definitions of flocculation and coagulation for these instances. Henceforth, the term coagulation will be used to denote any process which controls the rate at which a particle suspension aggregates solely by altering the electrostatic and van der Waal's forces between the particles. The term, flocculation, will be used to denote processes where polymeric bridging causes a suspension's rate of aggregation to be greater than or equal to the rate expected on the basis of van der Waal's and electrostatic forces alone. Three corollaries of these definitions provide the foundations of this work:

1) The measured rate constant correction factor, W (stability ratio), for coagulated suspensions must equal the value given by equation 1-30.
2) The measured rate constant correction factor for suspensions flocculated by polymers must be equal to or less than the value predicted by equation 1-30.
3) The measured rate constant correction factor for suspensions that are stabilized by adsorbed polymer must be greater than the value predicted by equation 1-30.

These definitions and their corollaries provide a kinetic basis for deciding the mechanism by which a polymer affects the stability of a particle suspension.

The work of this thesis is based on these three definitions which will be used to determine the mechanism by which a low molecular weight poly(l-lysine) aggregates a suspension of polystyrene latices. This is to be accomplished in two phases. Initially, the magnitude of Hamaker's constant for the polystyrene latices in 0.10 M NaCl will be determined from measurements of the size, surface potential and rate of coagulation of the particles in 0.10 M NaCl. The rate of aggregation of the polystyrene latex suspension will then be measured in the presence of varying amounts of poly(l-lysine) and correlated to the zeta potential of the particles. The mechanism by which poly(l-lysine) aggregates the polystyrene latices can then be determined by a comparison of the rate at which the polymer coated particles aggregate and the predicted rate for a suspension of uncoated particles with the same zeta potential.

2. GENERAL METHODOLOGY

This section lists the procedures and statistical methods which were used throughout this work. Specialized techniques for measuring a given parameter of the polystyrene latices or poly(l-lysine) molecules are given in the sections on their characterization.

2:1. Materials and Equipment

All salts used were reagent grade quality.

Chromerge: Chromerge, a concentrated chromium trioxide solution, was obtained from the Van Waters and Rogers Scientific Company of Seattle, Washington.

Ascarite: Ascarite, a sodium hydrate asbestos, was obtained from the A.H. Thomas Company of Philadelphia, Pennsylvania.

2:2. Preparation and Purity Criteria for Distilled Water

The purity of the water which is used in studying the behavior of colloidal suspensions is of paramount importance as minute quantities of certain contaminants can drastically affect the behavior of these suspensions. Nonsurface active electrolytes reduce the electrostatic forces between particles by diminishing the thickness of the double layer about the particles. This is of little importance as all work will be conducted at relatively high NaCl concentrations (>0.01 M).

However, ionic and nonionic surface active materials are of particular importance as they strongly absorb to lyophobic colloids (69, 70). At the polystyrene latex concentrations to be worked with (5×10^7 particles ml^{-1}), 10^{-7} M concentrations of typical cationic surfactants can significantly alter the electrophoretic mobility of the particles (69). Thus the following procedures were instituted to prepare and check the purity of the water.

2:2:1. Preparation

Twice distilled water was prepared from tap water that had been distilled in a two stage pyrex still. The upper stage was equipped with a glass bead spray trap to prevent contamination of the final distillate by entrainment of the contaminants in the second stage. The water was stored in a series of 20 gallon pyrex carboys. The carboys had been cleaned by the use of a concentrated nitric acid and 95% ethanol wash which was followed by many rinses of twice distilled water. All carboys and the still were interconnected by pyrex tubing with teflon joints. The storage jugs were connected to the atmosphere through a rubber tubing whose end was fitted with a drying tube filled with Ascarite to adsorb atmospheric carbon dioxide. Water was drawn off the storage jugs with a glass siphon tube fitted with a greaseless teflon stopcock. With the use of these precautions the water was maintained at a high standard of purity.

2:2:2. Purity

The purity of the distilled water was assessed by determining the level of the following contaminants:

Electrolytes: The level of dissolved ions was checked with a Radiometer conductivity meter and pH meter. The theoretical conductivity of water at 25° C has been calculated to be 5.48×10^{-8} ohm^{-1}cm^{-1} (71), while that of the distilled water was within the limits of $(1\text{-}2) \times 10^{-6}$ ohm^{-1}cm^{-1}. This corresponds to a solution which has a H^+-HCO_3^- concentration of ~ 2.5×10^{-6} M and a pH of ~ 5.9. The conductivity of the water increased on contact with the atmosphere in a manner which could be followed with a pH meter. This increase was attributed to the absorption of CO_2, as the pH of the water immediately after it had passed from the still, was very near 7.0 and after it had been stored in the storage carboys for several days, between 6.0 and 6.5.

Particulate Matter: The Electrozone-celloscope, whose operation is described in section 3:4:3, was used to determine the level of particulate contamination. Particulate matter whose volume exceeded 0.1 μm^3 was present at a concentration of less than 2×10^4 particles ml^{-1}.

Surfactants: The level of surfactants present in the distilled water was assessed initially by a determination of the surface tension

of the water with the dual capillary rise method of Kay and McClure (72). The surface tension of the water at 28.2 and 21.1°C was 71.59 and 72.53 dyne cm^{-1} respectively. These values agree with those of the literature (73) within 0.20%, which is within the limits of experimental error. For a typical ionic surfactant, S.D.S., this surface tension is indicative of a bulk surfactant concentration of less than 5×10^{-3} M (74), and for a typical nonionic surfactant a bulk concentration of less than 10^{-5} M (75). This method was therefore abandoned for an electrophoretic assay and the less precise but more rapid and sensitive foaming assay.

Kitchener and Cooper (76) noted that bubbles which reach the surface of very pure water burst in about 10^{-2} sec. Some surface films containing as little as 10^{-10} mole cm^{-2} of solute are able to retard the escape of bubbles from the surface of the water for several seconds. Thus, when a flask of distilled water is agitated the length of time required for the bubbles at its surface to burst serves an an index of the level of surfactants in the water. This test of the water purity was administered periodically with the result that the bubbles always burst within two seconds. For most surfactants, this is indicative of a bulk concentration of less than 10^{-6} M.

The most sensitive assay for ionic surfactants was a determination of the electrophortic mobility of the test polystyrene latices when suspended in 0.10 M NaCl to a concentration of

~ 5×10^7 particles ml^{-1}. The procedure used to measure the electrophoretic mobility of the particles is described in section 3:4:5. Electrophoretic mobilities of the polystyrene latices were always within the limits of 3.60-3.80 $\mu m\ sec^{-1} volt^{-1} cm$, which was within the limits of the 3% operational error associated with the technique. These measurements suggested that the bulk concentration of cationic surfactants was less than 10^{-7} M and that the bulk concentration of anionic surfactants was less than 10^{-6} M.

With the exception of the electrophoretic assay and the foam test, no checks on the purity of the water were made after the initial check as the system was closed to the usual sources of contamination (71, 77, 78).

2:3. Cleaning Procedures

All beakers, pipettes, stirbars and glassware which came into contact with the poly(l-lysine) solutions was cleaned by the use of an ethanolic-KOH or a sulfuric acid-Chromerge cleaning solution.

The sulfuric acid-Chromerge mixture was made by mixing 4 fluid ounces of Chromerge with eight pounds of concentrated sulfuric acid. Objects cleaned with the mixture were immersed in it for at least ten minutes and then filled with distilled water a minimum of ten times. All glassware that would come into contact with the polystyrene latices

was cleaned with an ethanolic-KOH cleaning solution rather than the sulfuric acid-Chromerge mixture.

The ethanolic-KOH cleaning solution consists of 120 grams of potassium hydroxide dissolved in a minimum of distilled water with enough absolute ethanol added to make a liter of solution. Glassware was usually immersed in it for a minimum of five minutes and rinsed copiously with twice distilled water.

During the cleaning procedures all glassware was handled on their exterior surfaces with tongs. After cleaning the glassware great care was taken to avoid touching any surfaces which would come into contact with the polymer or particles. Whenever possible, glassware was used immediately after cleaning, having been rinsed first with the solution it was to hold. All other glassware was air dried at room temperature.

2:4. Statistical Procedures

2:4:1. Least Squares Analysis

When it was necessary to fit a series of data points, to two or three terms of the power series:

$$y = b_0 + b_1 x + b_2 x^2 \qquad 2\text{-}1$$

a least squares estimator of the coefficients b_0, b_1 and b_2 was used to provide an unbiased, minimum variance estimate of the

coefficients (79). The procedures used for estimating only the first two coefficients, linear regression analysis, or all three coefficients have been described by Topping (80).

Estimates of the standard error of the mean for the random variables b_0, b_1 and b_2 were calculated by the method given by Topping (80).

2:4:2. Comparison of Means

Calculations of the probability that two sample means came from the same population were made with the Student t test. The results of the tests are reported in terms of the probability, p, that the two samples came from the same population.

2:4:3. Comparison of Standard Deviations

Estimates of the equivalents of the variance of two sample populations were performed by the F ratio test described by Freund (81).

2:4:4. Analysis of Errors

The error or uncertainty associated with any quantity θ was calculated by the principle of superposition of errors. Topping (82) has stated that if θ is a function of the independent variables $a, b, c, \ldots, f$, the error in θ, $\Delta\theta$, due to the uncertainty or errors $\Delta a, \Delta b, \Delta c, \ldots, \Delta f$ associated with $a, b, c, \ldots, f$ respectively is

given by:

$$\Delta\theta \simeq \frac{\partial\theta}{\partial a}\Delta a + \frac{\partial\theta}{\partial b}\Delta b + \frac{\partial\theta}{\partial c}\Delta c + \ldots + \frac{\partial\theta}{\partial f}\Delta f \qquad 2\text{-}2$$

Similarly, when $\Delta a, \Delta b, \Delta c, \ldots, \Delta f$ represent the standard error of the mean value of the quantities $a, b, c, \ldots, f$ respectively the most probable value for the standard error of θ, $\Delta\theta$, is:

$$(\Delta\theta)^2 = (\frac{\partial\theta}{\partial a}\Delta a)^2 + (\frac{\partial\theta}{\partial b}\Delta b)^2 + (\frac{\partial\theta}{\partial c}\Delta c)^2 + \ldots + (\frac{\partial\theta}{\partial f}\Delta f)^2 \qquad 2\text{-}3$$

Thus, the general procedure for calculating the standard error of a quantity θ began by expressing θ as a function of its independent variables. The quantity was then differentiated with respect to each of its independent variables and the square of each derivative multiplied by the square of the standard error of its respective independent variable. The square root of the sum of these terms was used as an estimate of the standard error of θ. When the uncertainty associated with a given independent variable was much larger than its measured standard error, the uncertainty term was used in calculations of the standard error of its dependent variable.

3. CHARACTERIZATION OF POLYSTYRENE LATICES

In order to calculate the potential energy of interaction between the polystyrene latices it was necessary to assess certain parameters of the particles which controlled the magnitude of this interaction. These parameters included the surface charge density, nature of the surface charge groups, mean size and Hamaker constant of the particles.

3:1. General Properties

The properties of polystyrene latex suspensions have been extensively investigated as their remarkable sphericity and uniformity of particle size make them ideal models for studies of a variety of colloidal phenomena. Some of the phenomena which have been investigated include studies on surface conductance (83, 84), electroviscous effects (85, 86, 87), light scattering (88, 89, 90), flocculation (3, 57, 91), coagulation (5, 92, 93, 94), the adsorption of surface active agents (69, 95, 96), and polymers (3, 57, 70, 97).

The first monodisperse polystyrene latices were produced by the Dow Chemical Company in 1947. Since that time many investigators have published similar methods of synthesizing polystyrene latices (98, 99). In these methods styrene which has been distilled under nitrogen is mixed with water and a surfactant under a nitrogen atmosphere.

Agitation of the styrene-water-surfactant system produces an emulsion of surfactant coated polystyrene micelles. The styrene in the micelles is polymerized by the addition of an initiator. The initiator is usually converted into a free radical in solution which then binds to one of the styrene molecules on the surface of a micelle to initiate the polymerization process. This sequence of events is pictured in the following reaction mechanism:

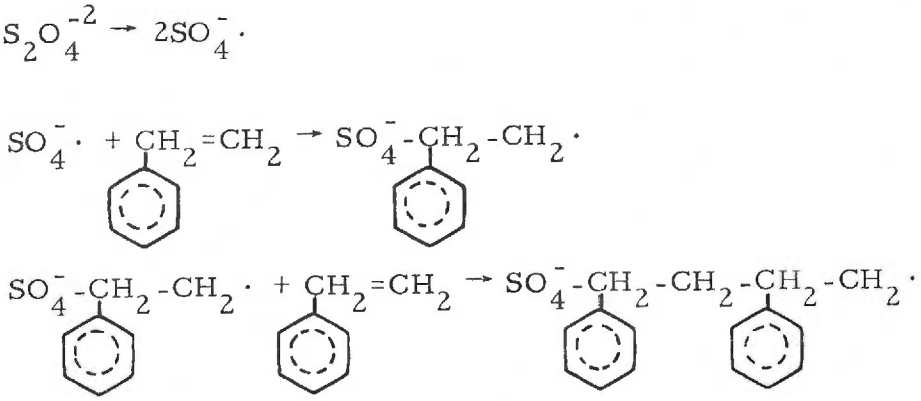

Alternatively, the initiator may bind to an isolated styrene molecule in bulk solution to produce a sulfated styrene radical. This radical will continue the polymerization process by binding to another styrene monomer in the bulk solution or on the surface of a micelle. Growth of the polymer chain continues, in solution or inside the micelles, by a free radical mechanism until the growing chain meets with another free radical or a terminating group. The resultant polystyrene chain usually has two ionic end groups which, in micelles, are predominantly located at the interface of the particle and the suspending medium. The size, surface charge density and the

monodispersity of a polystyrene latex suspension are determined by many variables including the amount of initiator and surfactant used, the temperature, rate of stirring and amount of oxygen present during the polymerization process. Although much of the surfactant can be removed by dialysis or ion exchange resins, Koteras and his colleagues (100) have developed a method of synthesizing monodisperse polystyrene latices in the absence of surfactants. Particles prepared by this method are also highly spherical, essentially monodisperse, of a low surface charge density and of course are free of surfactants.

Polystyrene latices prepared by these methods can be synthesized in a size range between 1,000 and 50,000 Å, with a coefficient of variation that frequently is less than 0.01. These particles consist of a spherical mass of intertwined polystyrene chains and unreacted styrene monomer. Pugh and Heller (101) have found the density of polystyrene spheres to be 1.057 gm ml^{-1}. Measurements of the number average molecular weight of the polystyrene chains in the particle show that they range from (0.5-2.0) x 10^5 Daltons (96, 102). Although the ends of the polymer chains often lie on the surface of the particles, up to 50 percent of the end groups cannot be detected by measurements of surface charge groups in some polystyrene samples (96). In the absence of surfactant, the specific surface area of charge groups varies between 300 $Å^2$ and 3000 $Å^2$ per charge group. The nature of the surface charge groups on the particles depends on the

surfactants and initiators used during the polymerization process. The most frequently used initiators, peroxides and persulfates result in carboxyl, sulfate and hydroxyl groups. However, the surface properties of the polystyrene latices can be changed, virtually without limit, as methods for covalently bonding antigens, proteins and a large variety of adducts to the surface of the polystyrene latices have been developed (103).

3:2. Theory and Selection of Methods

3:2:1. Particle Sizing

Light scattering, ultracentrifugation, electron microscopy and electronic particle sizing have been the most commonly used methods of determining the size distribution of a colloidal suspension. A more extensive list of available techniques has been given by Groves and Freshwater (104). For optically isotropic, monodisperse particle suspensions, light scattering combined with ultracentrifugation, is perhaps the most accurate method of measuring particle size distributions (90).. However, the equipment necessary to utilize this technique was not available.

Electron Microscopy: Although electron microscopy is a standard method of sizing colloidal suspensions, many investigators have noted that it is prone to certain types of artifactual errors. In 1955 Bradford and Vanderhoff (105) documented the swelling of polystyrene

latices in the electron beam. Heide (106) attributed these findings to the rapid accumulation of a layer of hydrocarbon contaminants. He investigated the effects of temperature on the rate of carbon deposition and removal from organic samples. With the use of a cooling chamber he was able to reduce the temperature of the region surrounding the sample to -190°C. When the region surrounding the sample was kept below -130°C little carbonaceous material was deposited or removed from samples when the sample was kept at room temperature. At temperatures between -130 and -160°C, carbon layers were removed from the sample at a rate that could approach 6 Å per second. At higher temperatures layers of contamination could increase particle size at a rate of up to 10 Å per second. A shrinkage of polystyrene latices at -30°C has been reported by Davidson and Haller (107) in an extensive analysis of the errors involved in the sizing of polystyrene latices by electron microscopy. For short exposures to the electron beam ($t < 1$ min) no shrinkage or swelling was observed. However, even under optimal conditions a 5 percent error is associated with electron microscopic sizing of suspensions of monodisperse polystyrene latices (107).

Electronic Particle Sizing: The theoretical basis of electronic particle sizing (108, 109) stems from an application of Ohm's law. When an electric current is passed through an orifice in a glass tube which is surrounded and filled with an electrolyte solution, the flow of

current, I, through the orifice is given by $V = IR$ where V is the applied potential across the orifice and R the resistance of the orifice. The resistance of the orifice is determined by its geometry and the conductivity of the electrolyte solution. When a particle enters into the orifice, R will be increased by an amount that will depend on the particle's volume, shape, electrical conductivity and pathway through the orifice. Thus, measurement of increments in orifice resistance, on the passage of a particle, provides an index of the size of the particle.

In the Electrozone-celloscope, the instrument to be used, changes in orifice resistance are measured with a constant current generator and a transducer. The constant current generator maintains the flow of current through the orifice at a level that is controlled by the current and fine current controls. The current switch is used to incrementally adjust the current flowing through the orifice, while the fine current control offers a continuous but more limited adjustment of that current. When a particle passes through the orifice the constant current generator increases V by an amount that is proportional to the increase in R. The increment in V is also proportional to I, as for a given increment in R, a current setting of two milliamps will cause the constant current generator to increment V by twice the amount as a current setting of one milliamp. The increase in V, the pulse amplitude of a particle, is measured by the transducer which generates

a signal that is proportional to the pulse amplitude. This signal is amplified, in succession, by a preamplifier, a linear amplifier and a logarithmic amplifier. The factor by which the linear amplifier magnifies the pulse amplitude of the particle is determined by the setting on the gain control. The behavior of the logarithmic amplifier is controlled by the lin-log switch, which determines the range of the particle sizes that will be sized. A given log setting approximates the number of doublings of particle volume between the largest and smallest particles that are sized by the instrument. At log settings of 4 and 10 the ratio of the volumes of the largest to the smallest particles which are sized are 2^4:1 and 2^{10}:1 respectively. After the pulse amplitude has been processed by the logarithmic amplifier it is passed through a discriminator which eliminates all signals which are within certain limits specified by the operator. The lower limit is set with the lower threshold discriminator control and the upper limit with the upper threshold discriminator control. The upper threshold discriminator may be disabled by placing the model selector switch in the Σ position. Signals which have passed through the discriminator are then counted as particles by the Electrozone-celloscope and sent to an interface between itself and the PDP-8M digital computer. The interface converts the output of the Electrozone-celloscope into a binary signal which is passed on to the computer. When the computer receives the signal it determines which of 128 consecutive size ranges the signal

belongs in and increments the register in its memory which represents that size range by one. At the start of a size distribution analysis, the contents of each of the 128 registers is zero. Sizing analyses are terminated when the number of counts in one of the registers equals a predetermined number. The distribution of particle sizes in a sample is readily assessed by examining the distribution of counts in the registers.

The relationship between particle size and pulse amplitude is usually complex. However, polystyrene particles are virtually non-conductive and spherical, an optimal shape for electronic particle sizing. Thus, their pulse amplitude is only dependent on their volume and pathway through the orifice. Analyses (109, 110) of the relationship between a particle's pathway through the orifice and its apparent size are quite complex. This has prompted the development of methods for standardizing particle pathways through the orifice. Two methods are currently in use. Hydrodynamic focussing procedures align all particles entering the orifice with the axis of the orifice and thereby standardize their pathway. Pulse width analyzers electronically screen out all pulse amplitude signals whose duration exceeds a given limit. This limit is usually set to equal the duration of a pulse amplitude generated by a particle traveling down the axis of the orifice. Since this pathway represents the fastest transit time through the orifice, pulse width analyzers also effectively standardize the pathway of

the particles which are sized. When the pathway of a particle through the orifice is standardized, the pulse amplitude of a particle is proportional only to its volume.

An additional advantage accruing from the use of pulse width analyzers is their ability to eliminate the majority of coincidence counts. Coincidence counts are pulse amplitudes generated by the simultaneous passage of two or more particles through the orifice that are counted as a single particle. The effect of coincidence counts on particle counting and sizing has been treated by Princen and Kwolek (111) and Edmundson (112).

3:2:2. Surface Charge Group Density and Identification

van den Hul and Vanderhoff (96, 102) have demonstrated that x-ray studies, chemical analysis, potentiometric and conductimetric titrations can be used to identify and quantitate the surface charge groups on polystyrene latices. Although these methods provide measurements of the surface charge density, they lack sensitivity and require large quantities of material. Conversely, measurement of a particle's electrophoretic mobility quantitates its repulsive potential, requires a minimal number of particles and indicates the nature of its surface charge groups. The surface charge density of the polystyrene latices can be calculated from these measurements with an accuracy that rivals the other methods. Thus, electrophoresis was deemed the

method of choice for determination of surface potential and hence charge density.

The relationship between the velocity, v_e of a particle in an applied electrical field of strength, X, was given by von Smoluchowski (113) as:

$$\frac{v_e}{X} = u_e = \frac{\epsilon \zeta}{4\pi\eta} \qquad 3-1$$

where u_e is the electrophoretic mobility of the particle, ζ is its zeta potential, and ϵ and η are the dielectric constant and viscosity of the bulk suspending medium, respectively. This relationship is precise only for values of $\kappa a > 300$. Deviations from this relationship at lower values of κa have been attributed to the effect of the applied field on the atmosphere of counterions surrounding the particle and the conductance of the particles themselves.

At intermediate values of κa, $0.1 < \kappa a < 300$, the electrophoretic movement of the particle causes a distortion in the layer of counterions surrounding it. The center of the ion atmosphere lags behind the particle. This asymmetry generates an electrical force on the particle which usually results in a decrease in the final velocity of the particle. This phenomenon, termed a relaxation effect, has been treated independently by Booth (114) and Overbeek (115).

If the particles are conductive their electrophoretic mobility will be less than predicted by equation 3-1. Henry (116) developed a

general solution for the electrophoretic mobility of conducting and nonconducting spheres which takes the form:

$$u_e = \frac{\zeta\epsilon}{6\pi\eta}[1+\Lambda Z(\kappa a)] \qquad 3\text{-}2$$

where $Z(\kappa a)$ assumes a value of zero for small values of κa and one for large values of κa. Λ is given by:

$$\Lambda = \frac{\Lambda_1 - \Lambda_2}{2\Lambda_1 - \Lambda_2} \qquad 3\text{-}3$$

where Λ_1 is the specific conductance of the bulk electrolyte solution and Λ_2 is the specific conductance of the particles. Equation 3-1 is recovered from equation 3-3 for nonconducting particles when the dual limits, $\Lambda_2 = 0$ and $\kappa a \rightarrow \infty$, apply.

The electrophoretic mobility of a particle is affected by the interaction of the applied electrical fields with the counterions surrounding each particle. The attractive force applied to the counterions is transferred to the solvent and results in a viscous drag on the particles. These forces are called retardation forces. Wiersema, Loeb and Overbeek (117) have treated relaxation and retardation effects by numerically solving the equations relating zeta potential and electrophoretic mobility for spherical nonconducting particles over a wide range of values for κa. For systems where $\kappa a = 500$, equation 3-1 underestimates the exact value by one percent, when the zeta potential is within the limits of 170 to 260 microstatvolts. As the

zeta potential approaches zero this discrepancy vanishes. In solving the exact electrophoretic equations, Wiersema et al. (117) assumed that:

1) All interactions between particles could be neglected.
2) The particles and the adjacent layer of fluid which remains stationary with respect to them are rigid spheres.
3) The dielectric constant of the particle is uniform throughout.
4) The particle is nonconductive.
5) The charge on the sphere is uniformly smeared over its surface.
6) The diffuse layer of counterions surrounding the particle is described by the classical Gouy-Chapman theory.
7) The dielectric constant and viscosity of the suspending medium does not change with proximity to the sphere.
8) Brownian motion does not affect the mobility of the particles.

Surface charge densities are often calculated from the Gouy-Chapman relationship (equation 1-20) and electrophoretic measurements of a particle's zeta potential. This procedure substitutes the surface potential, required by the Gouy-Chapman equation, for a zeta potential. This substitution is justified only when:

1) The particle's hydrodynamic plane of shear coincides with the plane which passes through the center of its surface charge groups. If the plane of shear is not congruent with the plane

which passes through the center of the iongenic groups on the particle, the potential at the plane of shear, the zeta potential, will usually be less than the surface potential.

2) The surface charge density is less than 3×10^4 statcoulombs cm^{-2}. Haydon (118) has shown that at charge densities exceeding this figure the zeta potential begins to diverge from the surface potential for emulsions of surfactant coated petroleum ether droplets.

3) The surface containing the charge groups must be impenetrable to mobile counterions. Haydon (119) considered the effect of counterion penetration on the relationship between surface charge density and surface potential.

4) The electrolyte concentration must be low enough that the effects of the finite size of the counterions can be ignored. Bell and Levine (120), Hurwitz et al. (121) and Sanfeld et al. (122) have considered the effect of ion volume on the relationship between surface potential and surface charge density. With the exception of very low surface potentials the assumption of point charge counterions causes the Gouy-Chapman equation to overestimate the surface charge density at ionic strengths above 10^{-3}.

Surface charge groups may be identified by the manner in which surface charge density or surface potential fluctuates with pH. Since

polystyrene latices frequently have only one type of surface charge group, the pK point of the surface charge group is often enough to identify it. Although the procedure is direct enough, it is necessary to account for differences in bulk pH, pH_b and the pH of the suspending medium at the surface of the particle, pH_s. Hartley and Roe (123) demonstrated that because all ions obey a Boltzmann distribution about a charged surface the bulk pH is related to the surface pH by:

$$pH_s = pH_b + \frac{e\zeta}{2.303kT} \qquad 3\text{-}4$$

Thus for particles having a negative surface charge, $pH_s < pH_b$.

3:3. Materials and Equipment

Particle sizing apparatus: The particle sizing apparatus was purchased from Particle Data Equipment, Inc., of Elmhurst, Illinois. The apparatus consisted of a Coulter type sizing apparatus, termed the Electrozone-celloscope, an accompanying PDP-8M computer with an interface to the Electrozone-celloscope, a Telequipment oscilloscope and a Teletype command terminal to the computer. The basic Electrozone-celloscope was modified by the inclusion of a factory installed pulse width discriminator and by the replacement of the original slide type valving system with a glass stopcock system. The latter modification was made when measurements of flow times for solutions indicated that the apparatus was assaying a varying volume of

fluid when making particle counts. The modified apparatus is pictured in figure 3-1.

Electrophoresis chamber: The all glass electrophoresis chamber was constructed by A. Ryall of the Oregon Graduate Center, Beaverton, Oregon, in accordance with the specifications given in figure 3-2. The remainder of the electrophoresis equipment used is described by G.V.F. Seaman (124).

Stopcocks: Interkey P.T.F.E. stopcock keys were purchased for the electrophoresis chambers from G. Springham and Company, Ltd. of Temple Fields, England.

Ultrasonicator: A Bronwill Biosonik II ultrasonicator was loaned by Dr. F. Bacon of the University of Oregon Health Sciences Center.

Counting supplies: Isoton diluting fluid and Accuvette counting vials were obtained from the Coulter Company of Hyaleah, Florida.

Polystyrene latices: The polystyrene latices used as calibration sizing standards were obtained from the Dow Chemical Company of Midland, Michigan. The smaller particles, lot number LS-1165-B, had a mean diameter of 0.81 μm and a standard deviation of 0.005 μm while the larger particles, lot number LS-1028-E, had a mean diameter of 1.099 μm and a standard deviation of 0.0059 μm. The polystyrene latices used as an experimental test particle were generously synthesized by Dr. J.W. Goodwin of the University of Bristol at Bristol, England.

Fig. 3-1. Electronic particle sizing apparatus

1) Teletype
2) PDP-8/M digital computer
3) Telequipment oscilloscope
4) Electrozone celloscope
5) Current control
6) Gain control
7) Lower threshold discriminator
8) Mode selector
9) Upper threshold discriminator
10) Lin-Log control
11) 50 microliter metering section
12) Orifice


3
2
4
1


4
5
6
7
8
9
10
11
12
NORMALIZE
ON
OFF

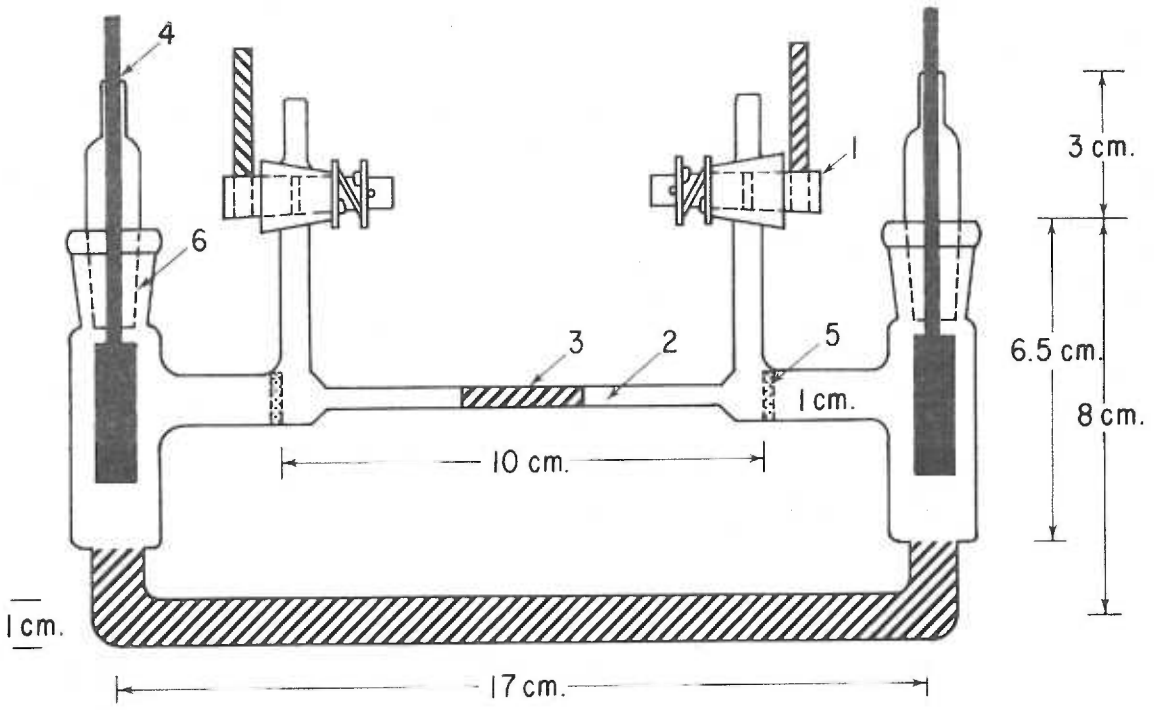

Fig. 3-2 All pyrex electrophoresis chamber

1 Glass impregnated P.T.F.E. (Fluon) stopcock key

2 Precision bore glass tubing: I.D. 2.000 ± 0.005 mm

3 Optical flat

4 Ag/AgCl Electrodes

5 Sintered glass disc

6 $\frac{14}{20}$ Ground glass joints

3:4. Methodology

3:4:1. Preparation of the Polystyrene Latices

The polystyrene latices were received in a suspension of 50 percent solids and diluted for experimentation by pouring an aliquot of the parent particle suspension into an ethanolic-KOH cleaned 20 ml Corex test tube. The particles were ultrasonicated for 20-30 seconds at maximum intensity by placing the bottom of the test tube on the tip of the ultrasonicator probe and irradiating the particles through the glass. This procedure was sufficient to disperse any weak aggregates, leaving only 1-2% of the particles in the form of doublets. The suspension was then diluted with twice distilled water to a desired concentration. The particles were dispersed and kept in suspension by continuous stirring with a magnetic stirbar. Continuous stirring was necessary to prevent settling of the particles over long periods of time.

3:4:2. Particle Sizing

The polystyrene latices were prepared for electron microscopy according to the method given in section 3:4:1 and given to Dr. Robert Brooks. He subsequently diluted the particles, added anough cytochrome oxidase to prevent the particles from aggregating and air dried them on a carbon stabilized Formvar coated 300 mesh copper grid. All sizing was done with a Philips model 200 electronmicroscope,

using an accelerator voltage of 60 kilovolts. The microscope was equipped with a horseshoe shaped anticontamination chamber that kept the temperature of the region surrounding the sample at -160°C. The sample was attached to a metal rod in connection with the outside air and was close to room temperature. Electron micrographs of the particles were enlarged and returned along with a calibration factor. This procedure was repeated on two separate occasions. The diameter of the particles in the electron micrographs were determined with a cathetometer calibrated to the nearest 0.01 mm. The average diameter of a particle in the photograph was ~ 12 mm.

Electronic Particle Sizing: The polystyrene latices were prepared for sizing by the method listed in section 3:4:1. When the particles had been dispersed in distilled water they were further diluted with Isoton to a concentration of approximately 1×10^6 particles ml^{-1}. Dow monodisperse polystyrene latices were prepared for use as calibration standards by diluting an aliquot of each sample with Isoton until a concentration of 1×10^6 particles ml^{-1} or less was obtained. The diameters of the two calibration standards were 1.099 ± 0.006 microns and 0.810 ± 0.006 microns. Diluted particle suspensions were placed on the sample platform of the Electrozone-celloscope so that the instrument's orifice was immersed in the sample. The head of pressure controlling the rate of flow of Isoton through the orifice, was then adjusted to approximately 12 cm of

mercury and particle sizing analysis initiated with the appropriate command to the PDP-8M digital computer.

The settings for the Electrozone-celloscope were chosen on a pragmatic basis. A 19 micron orifice was selected for sizing as the 12 micron orifice clogged too often to be of use. This choice produced less clogging but resulted in the production of more machine noise because of the higher current and gain settings which had to be used to detect the particles. The log setting of the Electrozone-celloscope was placed at 4 to obtain maximum resolving power from the instrument. The current and gain settings were increased until the particles with the modal diameter of the smaller calibration standard were well removed from the base line noise of the instrument. This corresponded to a current setting of 1 and a gain of 68. The fine current setting was placed on zero. The lower threshold setting was set at a minimum setting of 30 to eliminate base line noise and the mode selector was placed in the Σ position. The pulse width discriminator was not used in the sizing experiments.

After the settings of the machine had been established the instrument was calibrated by determining which registers of the computer's memory the modal diameter of each calibration sample was placed in. These registers, numbered 22 and 67, were then assigned the value for the modal diameter of each calibration standard, 0.81 and 1.10 microns respectively.

3:4:3. Measurement of Polystyrene Latex Particle Concentrations

A 30 micron orifice was used for the majority of counting procedures with one of the following Electrozone-celloscope settings: lin, current 1, fine current 0, gain 96, lower threshold 55, mode Σ; or log 6, fine current 0, gain 48, lower threshold 160, mode Σ. The 30 micron orifice was selected for its ability to detect the particles with a minimum amount of clogging. The settings of the Electrozone-celloscope were chosen on an empirical basis.

The initial step in determining the concentration of particles or aggregates in a suspension was to quantitatively dilute the suspension to a level of 2.8×10^5 particles ml^{-1} or less. At this particle concentration the level of coincidence counts was less than one percent of the total count. Most particle suspensions were diluted by placing 50.0 ± 0.02 microliter sample of the suspension in an Accuvette containing 10.05 ± 0.05 ml of Isoton. The use of Isoton and Accuvette counting vials reduced the amount of background particle contamination to ~ 8000 particles ml^{-1} or approximately five percent of the lowest particle concentration typically assessed. Samples were dispersed in the Accuvettes by rotating them end over end at 20 revolutions per hour for a minimum of one hour. When the polystrene latices had been dispersed, the Electrozone-celloscope was used to determine the number of particles in a 50 microliter sample of the suspension. The

particle concentration was taken from the average of five of these measurements. Under optimal conditions a stock solution of polystyrene latices could be reproducibly diluted and the particle concentration determined with a precision of three percent. This figure probably represents the limits of accuracy for this method.

The unusual procedure used to disperse suspensions in Isoton was developed because of the ease with which aggregates of salt coagulated polystyrene latices break up under high rates of shear. Shear rates large enough to break up large aggregates were generated when diluted particle suspensions were dispersed by violent shaking and at the orifice of the particle sizing apparatus. The first difficulty was circumvented by rotating diluted particle suspensions end over end for at least one hour at a rate of 20 revolutions per hour when they were to be dispersed. The rates of shear near the orifice of the sizing apparatus approach 10^6 sec^{-1} in the small orifice sizes. Birkner and Morgan (91) found that extensively aggregated suspensions were degraded by the high rates of shear at the orifice. However, Matthews and Rhodes (125) did not detect any change in the distribution of particle sizes with orifice diameter when particle suspensions were in the early stages of aggregation. The extent of aggregate fragmentation at the orifice was investigated by examining the pulse width distribution of an extensively aggregated suspension of 0.89 micron polystyrene latices. The pulse width discriminator was set to reject all pulse amplitudes

whose duration exceeded that of a particle traveling down the axis of the orifice. Aggregates which broke up near the orifice and had larger transit times than singlets would therefore not be counted. Under these conditions, particle size analysis of aggregated suspensions detected only singlets. No relationship between particle size and orifice transit time was found, as 2.02 micron particles were detected with the same pulse width discriminator settings used to detect 0.89 micron singlets. However, this experiment does not eliminate the possibility that non-spherical particles may have greater transit times than spherical particles of the same volume. If this possibility is discounted it seems that virtually all salt coagulated polystyrene aggregates undergo fragmentation on passage through the orifice. Fortunately, small aggregrates do not fragment until they have been detected and when the pulse width analyzer is not used they are counted as a single particle. This finding was further substantiated by experiments showing that during the early stages of aggregation the particle size distribution obtained with a 19 micron orifice is the same as that obtained with a 30 micron orifice.

3:4:4. Measurement of Coagulation Rates

Nonaggregated polystyrene latex suspensions were prepared by the procedure given in section 3:4:1 and diluted with twice distilled water to a concentration of 1×10^{8} particles ml^{-1}. The polystyrene

latex suspension was placed in a 12 ml plastic syringe and a NaCl solution placed in another 12 ml plastic syringe. At the start of the experiment the two fluids were mixed by simultaneously injecting both syringes into a polyethylene Y joint with an internal diameter of 0.2 cm. The mixed fluids were deposited into a vessel cleaned with ethanolic-KOH. This was usually a two ounce jar. The Reynold's number R_e, of the fluid on leaving the Y joint ($R_e \sim 500$) was not sufficient to produce turbulent flow ($R_e > 10^4$), but the swirling of the fluids on deposition in the aggregation vessel produced complete mixing of the fluids within 5 to 10 seconds. To maintain equal rates of flow from each syringe the two syringes were taped together and a bar fastened across the top of the two syringe plungers. The temperature of the fluids was maintained by the temperature of the room which was constant to ± 1°C during the course of an experiment. After the polystyrene latex-NaCl suspension had been mixed, 50 microliter aliquots were removed at 600-1000 second intervals until eight samples were taken. The sampling intervals were regularly spaced so that the total particle concentration would be roughly halved by the time eight samples were taken. The 50 microliter aliquots were placed in Accuvettes containing 10.10 ± 0.05 ml of Isoton. The aggregated suspension was dispersed throughout the Accuvette by tumbling it end over end for a minimum of one hour at 20 revolutions per hour. The particle concentration in each Accuvette was determined a minimum of five times with the Electrozone-celloscope to determine N(t).

After all eight samples had been counted, the rate constant for the coagulation process, K, and the particle concentration at the start of the experiment were determined by a linear regression analysis of the quantities of $1/N(t)$ vs t. The standard error of the correlation coefficients K and $1/N(0)$ were calculated by the method described in section 2:4:1. No corrections were made for the samples degree of polydispersity or initial concentration of doublets as these corrections were negligible in view of the errors involved in the assessment of $N(t)$. The initial concentration of polystyrene latices was always between the limits of $5\text{-}6 \times 10^{7}$ particles ml^{-1}. All coagulation experiments were run at this concentration as Hatton and coworkers (5) have shown that K is independent of $N(0)$ in this region but large increases in $N(0)$ produce a rapid rise in K.

3:4:5. Determination of Electrophoretic Mobility

The measurement of electrophoretic mobilities at low pH values required the use of an electrophoresis chamber of the type described by Seaman (124). The chamber was loaded through two stopcocks and the electrophoretic field established via Ag/AgCl electrodes immersed in 1.00 M or 0.10 M KCl.

The electrophoresis chamber was placed in a water bath, at $25.0 \pm 0.1°C$ to eliminate convection currents in the chamber caused by Joule heating. Particles placed in the chamber were observed

through a microscope equipped with a X40 water immersion objective and a 10X eyepiece in which a checkerboard graticule had been inserted. The chamber was mounted so the axis of the chamber bore was level and perpendicularly intersected the axis of the microscope. The focal plane of the microscope was adjusted to the stationary level of the chamber which lay at a distance 0.707a away from the axis of the chamber bore where a is the radius of the bore.

After the chamber was properly aligned, a test particle of known mobility was placed in the chamber and the stopcocks closed. The mobility of the particle was found by determining the length of time it took to traverse a fixed number of squares on the graticule. The mobility of a particle, as defined by equation 3-1 was usually determined at a field strength of 5 volts cm^{-1} by timing it over enough squares to give a total transit time of between 5 and 10 seconds. The usual test particles, freshly drawn and washed human red cells, have a mobility of 1.08 ± 0.03 $\mu m\ sec^{-1} volt^{-1} cm$ when suspended in 0.15 M NaCl buffered to a pH of 7.3 ± 0.2. Red cells were used as a test particle for the chamber whenever it was used.

3:5. Results

3:5:1. Particle Size Distribution

The mean, standard deviation and coefficient of variation of the particle size distribution, as determined by electron microscopy and

electronic particle sizing are presented in table 3-1. The particle size distributions as determined by electron microscopy and electronic particle sizing are presented in figures 3-3 and 3-4. The differences between the mean particle size as determined by the different methods are all significant at the $p < 0.0001$ level.

Table 3-1. Parameters of the polystyrene latex size distribution.

Sizing Method	Average Diameter (microns)	Standard Deviation (microns)	Number of Particles Sized	Coefficient of Variation
Electron microscopy (I)	0.850	0.009	9	0.011
Electron microscopy (II)	0.890	0.014	95	0.016
Electronic particle sizing	0.912	0.036	34,694	0.035

The first sizing experiment represented only a preliminary investigation of particle size and involved only one electron micrograph of nine particles. The cursory nature of the experiment does not warrant further consideration of the findings, which are presented only as evidence of the limitations of the technique. The second experiment was more extensive involving four electron micrographs. At least 20 particles were sized in each photograph. The mean diameter (microns), standard deviation and number of particles sized in each electron micrograph were 0.898 ± 0.010 (25), 0.895 ± 0.010 (24), 0.889 ± 0.012 (25) and 0.875 ± 0.015 (21) respectively. With the exception of

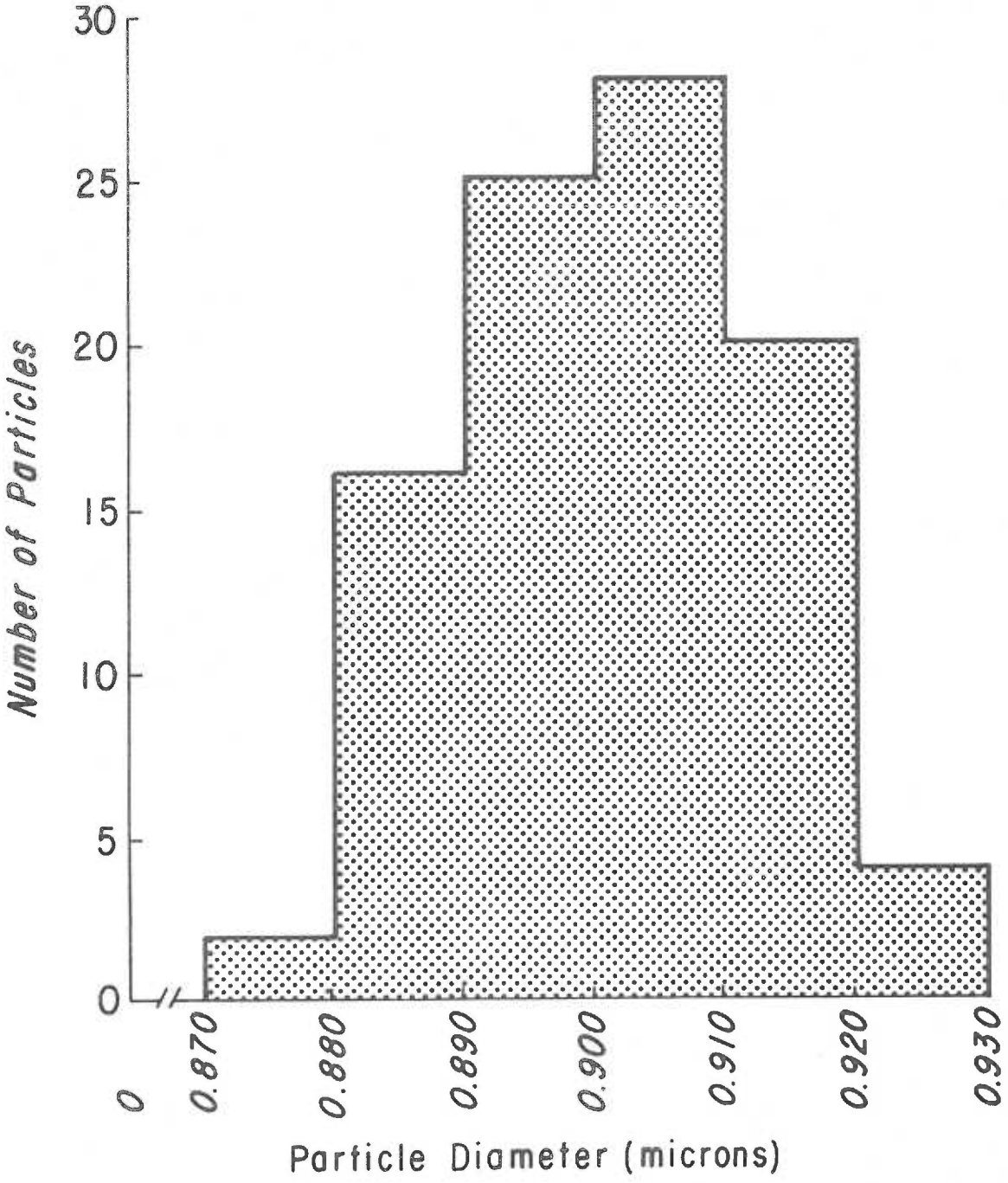

Fig. 3-3 Distribution of 0.90 micron polystyrene latex particle sizes as determined by electron microscopy

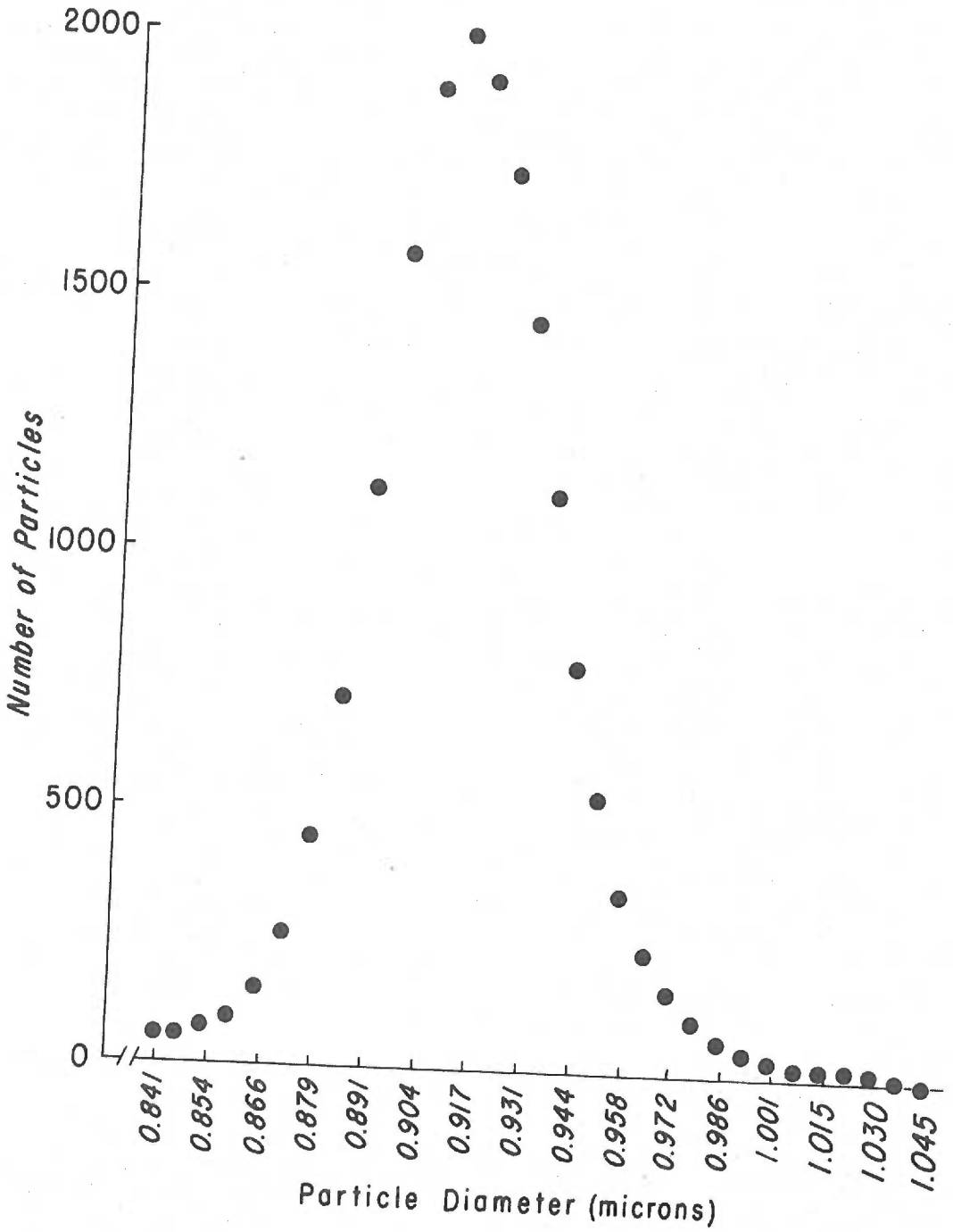

Fig. 3-4 Distribution of 0.90 micron polystyrene latex particle sizes as determined by electronic particle sizing

exposure time to the electron beam all particles were treated identically. Although the difference in the two larger average particle diameters and the smallest is significant, $p < 0.001$, shrinkage or swelling of the polystyrene latices in the electron beam is not necessarily indicated. Fluctuations in the magnification of the electron microscope may vary by one to two percent. Furthermore, under normal operating conditions non-uniform enlargement of the electron micrograph negatives may also contribute an equal amount of error to the calculation of the average particle diameter.

Aside from the inherent limitations of the Electrozone-celloscope's accuracy, which are caused by transient fluctuations in its circuitry, errors in electronic particle sizing procedures can be limited to those produced by partial orifice blockages, if calibration particles of an accurately known diameter are used. The instrument's manufacturers claim a 2 percent accuracy on a log 4 setting. Relative checks on the accuracy of the machine confirmed this claim. These tests involved sizing a single batch of polystyrene latices with three different current and gain settings so that the instrument sensed three different particle size distributions. Two of these phantom distributions were used to calibrate the machine and the third was used to check its accuracy. Absolute determination of the machine's accuracy were not possible as the best calibration particles available were Dow monodisperse polystyrene latices whose diameters had been determined by

electron microscopy. The accuracy with which the diameter of these particles is known is on the order of five percent according to Dow officials (105, 126). Thus, the error involved with assessments of particle size on the Electrozone-celloscope is approximated by the root of the sum of the squares of the errors associated with the diameter of each calibration particle and the accuracy of the instrument. This is on the order of $(5^2+5^2+2^2)^{1/2}$ or about seven percent. The mean diameter of the polystyrene latices was therefore assigned by weighting the results of the second and third experiments equally to yield a value of 0.90 ± 0.05 microns. The uncertainty associated with this term reflects the error associated with the determination rather than the standard deviation of the distribution.

The dispersity of the particle distribution is expressed by its standard deviations, s, and coefficient of variation, s/a. The differences in the standard deviations of the second and third sizing experiments, is significant at the $p < 0.01$ level. This type of discrepancy has been observed before by investigators (125, 127) who have noted that electronic particle sizing methods report larger standard deviations for particle size distributions than electron microscopy. This discrepancy is noticed when hydrodynamic focussing or pulse width analysis procedures are not employed and is attributable to the effects of a nonstandardized particle pathway through the orifice. The pulse width analyzer was not available for the sizing work done in

experiment three and as such that data collected by electron microscopy is probably more accurate. A five percent error is again associated with the standard deviation.

3:5:2. Characterization of Surface Charge Groups

The zeta potential of the polystyrene latices in 0.10 M NaCl is plotted as a function of bulk and surface pH in figures 3-5 and 3-6 respectively. The circular points were obtained by adding a concentrated NaOH solution to a suspension of polystyrene latices in 0.10 M HCl. The triangular points were obtained by adding concentrated HCl to the polystyrene latices suspended in 0.10 M NaCl. From the coincidence of the curves it is evident that the reduction in the electrophoretic mobility is not due to the cleavage of charge groups from the surface of the particles. However, the possibility that the alteration in mobility is due to a pH controlled adsorption of an ion cannot be eliminated from these data.

The surface charge density of the polystyrene latices at pH 7 was calculated from the Gouy-Chapman relationship and the tables of Wiersema, Loeb and Overbeek (117) to be 1.215×10^{4} statcoulombs cm^{-2}. This corresponds to a specific area of 395 $\mathring{A}^2$ per surface charge group, a figure which is well within the range of values listed by Vanderhoff and van den Hul (96). The standard deviation for the particle mobilities ranged from three to ten percent of the mean. This

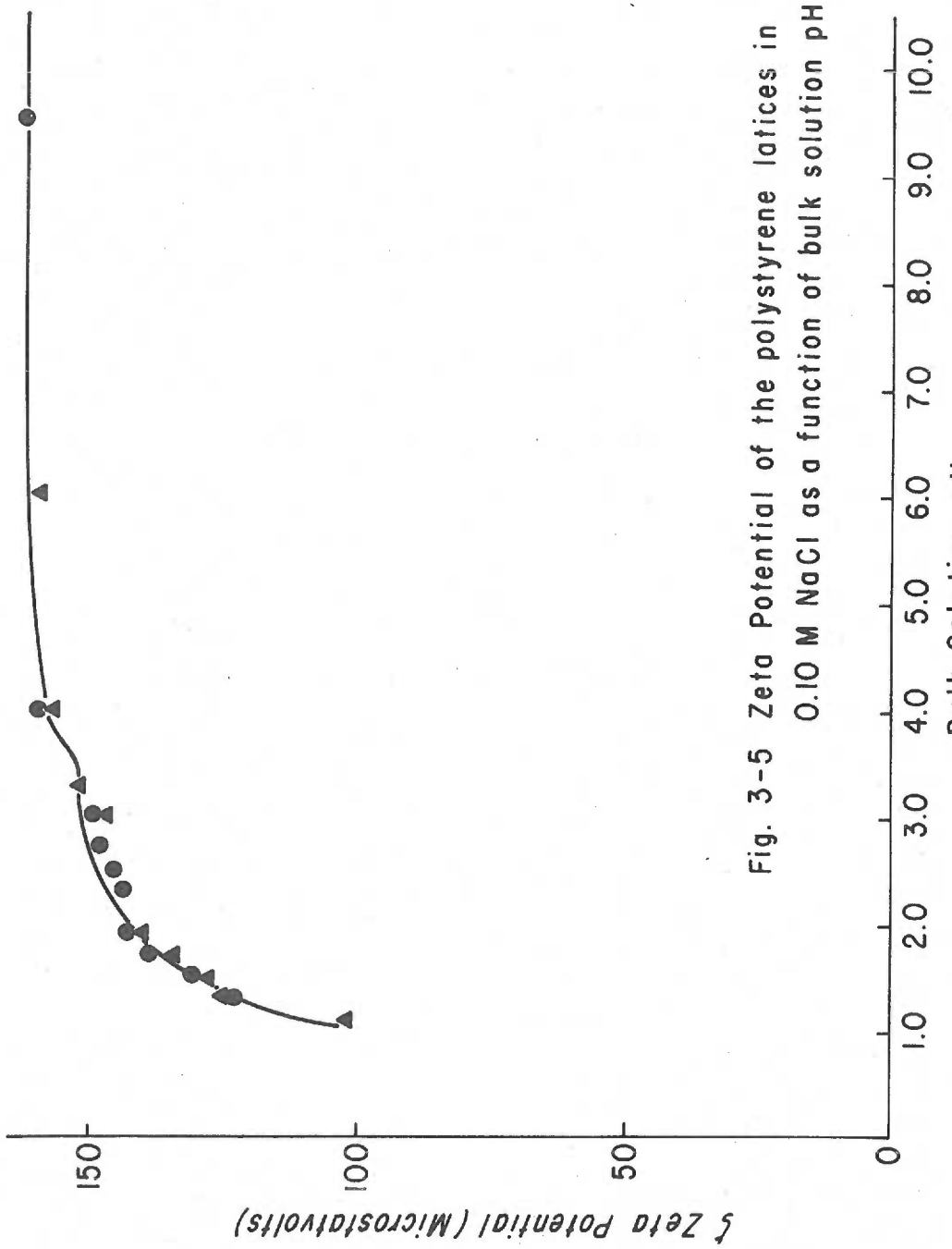

Fig. 3-5 Zeta Potential of the polystyrene latices in 0.10 M NaCl as a function of bulk solution pH

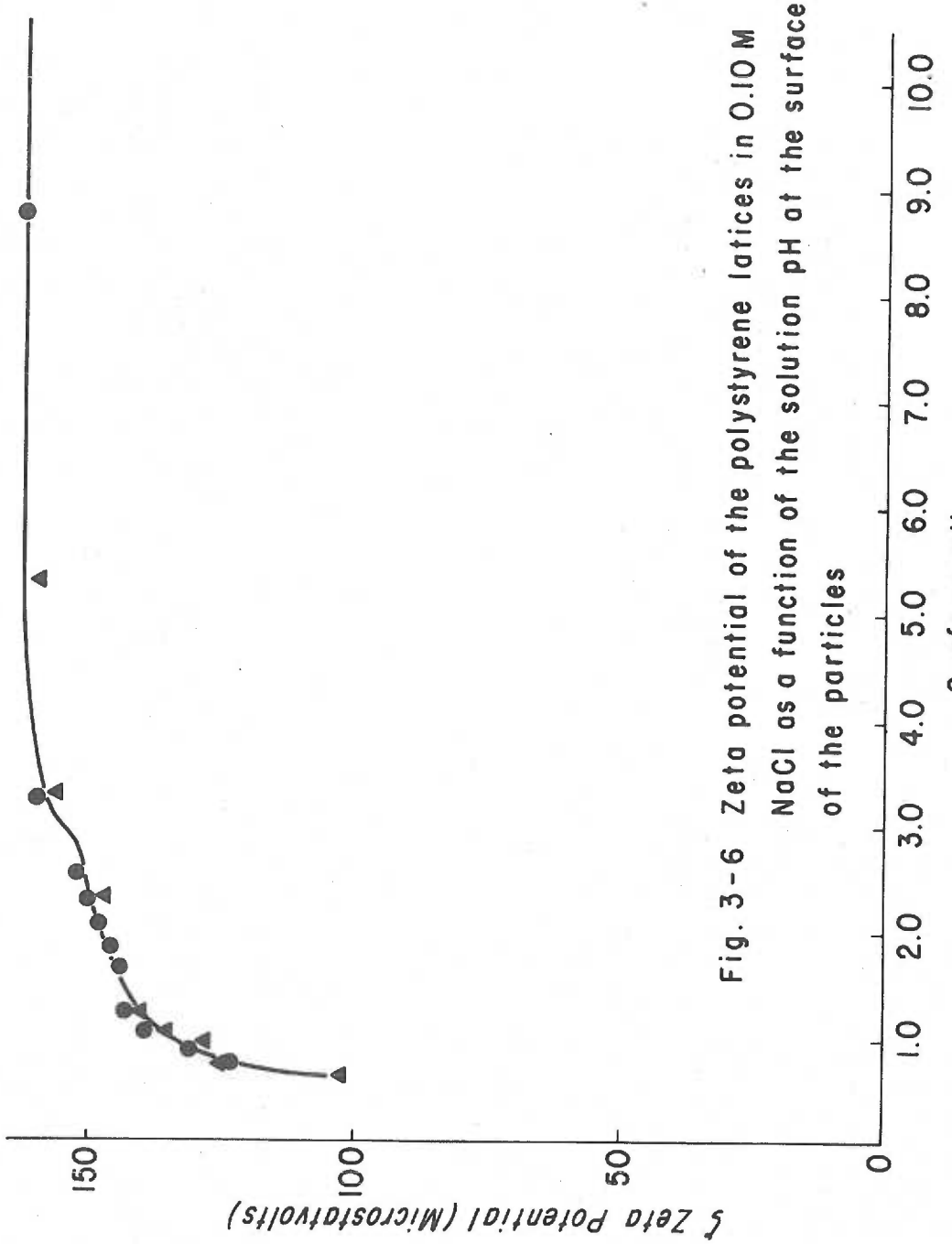

Fig. 3-6 Zeta potential of the polystyrene latices in 0.10 M NaCl as a function of the solution pH at the surface of the particles

dispersion represents the inherent variability of the particle distribution itself, the effects of Brownian motion and systematic errors involved in focussing the microscope on the particles at the stationary level of the electrophoresis chamber. The latter source of error was reduced to a level of one percent by using standard particles to check the proper functioning of the electrophoresis chamber.

The effect of Brownian motion was most noticeable when the mean square displacement of the particles due to Brownian motion was a significant fraction of the distance traveled by the particle under the influence of the electrophoretic field. The extent of this effect increased when the pH of the solution approached 1.0, as the zeta potential of the particles was reduced, and the high conductivity of the suspending medium required the use of low field strengths, ~ 2 volt cm^{-1}. Under these conditions the average distance traveled by a particle in one second was 5.6 microns. The mean square displacement of the particles in the same period of time was 3 microns. Thus, the random movement of the particles, due to Brownian motion, was easily responsible for the largest portion of the scatter in the electrophoretic mobility of the particles under these conditions.

The very low value of the pH of the surface charge group, $pK < 1$ and the shape of the pH vs mobility curve are those expected for polystyrene latices with sulfate charge groups (128). The presence of the sulfate groups is the result of using a persulfate initiator to

synthesize the polystyrene latices. A plot of surface charge density vs surface pH given in figure 3-7, shows an eleven percent increase in surface charge density in the pH range 2.5 to 4.5. This may be attributable to carboxyl groups which may have adsorbed onto the particles, as the electrophoretic mobility of polystyrene latices having only sulfate groups on their surface does not change above pH 2.5 (128). Hydroxyl groups may also be present on the surface of the particles since sulfate radicals, which are generated by a degration of the persulfate molecule, can react with water forming a hydroxyl radical. These radicals are also capable of initiating styrene polymerization (102). Thus, from figure 3-7, it is evident that approximately 90 percent of the surface charge groups are sulfates, which will be fully ionized when the pH of the suspending medium is greater than 2.5.

3:5:3. Polystyrene Latex Rate of Coagulation

The rates of polystyrene latex coagulation, K, at varying NaCl concentrations are presented in table 3-2. Each rate constant represents the mean of at least two experiments which have been corrected for viscosity and temperature effects to the value they would have at 20°C. The correction was made by assuming that K is directly proportional to the temperature of the system and inversely proportional to its viscosity. The variance associated with each mean rate constant represents the standard deviation of the mean rate

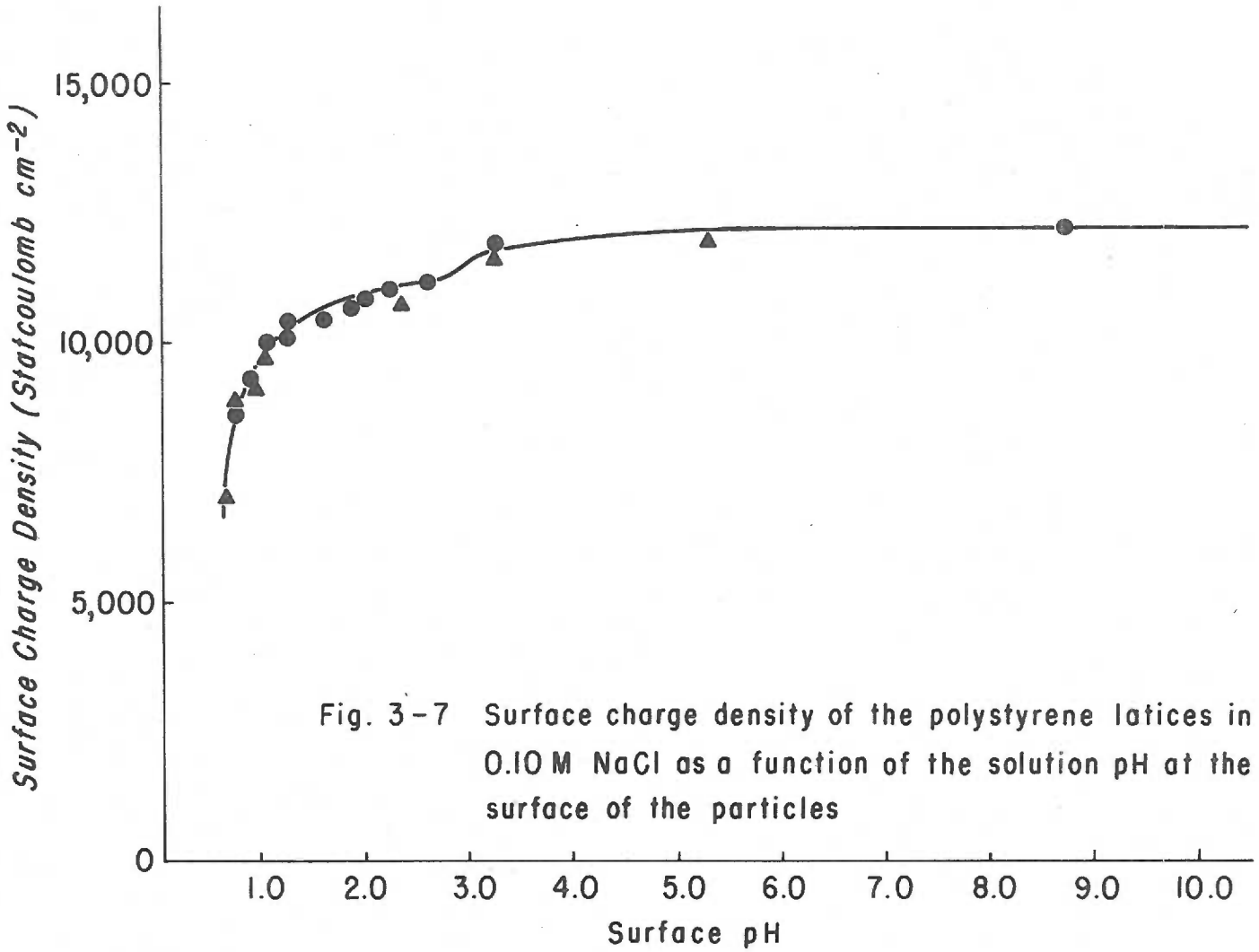

Fig. 3-7 Surface charge density of the polystyrene latices in 0.10 M NaCl as a function of the solution pH at the surface of the particles

constants for the individual experiments. The standard error of the correlation coefficients, K and 1/N(0), for each experiment was calculated according to the method described in section 2:4:1. The uncertainty in the individual rate constants were negligible in comparison to the scatter of the individual rate constants and were ignored when the standard deviation of the experimental rate constants were calculated. The large degree of scatter between replicate estimates of K is probably due to the inherent inaccuracy of diluting and counting particle suspensions with Coulter type counters.

Table 3-2. Rate constants for polystyrene latices in the presence of NaCl solutions of different concentrations.

NaCl Conc. (Molar)	$K \times 10^{12}$ $particle^{-1}\ cm^{3}\ sec^{-1}$	Number of Experiments	W	log W
2.00	3.00 ± 0.19	8	2.05	0.31 ± 0.02
1.00	2.98 ± 0.18	8	2.06	0.32 ± 0.02
0.70	2.68 ± 0.18	8	2.30	0.36 ± 0.02
0.35	2.79 ± 0.21	8	2.20	0.34 ± 0.03
0.20	2.72 ± 0.11	8	2.25	0.35 ± 0.01
0.10	1.12 ± 0.34	11	5.50	0.74 ± 0.23
0.08	0.39 ± 0.05	4	15.8	1.20 ± 0.15
0.04	0.08 ± 0.08	4	80	1.90 ± 0.16
0.02	0.05 ± 0.13	4	132	2.12 ± 0.28

The same data is presented (figure 3-8) in the form of a $\log_{10} W$ vs C_3 plot where C_3 represents the concentration of coagulating electrolyte. The point at the intersection of two line segments in the $\log_{10} W$ vs C_3 plot is called, C_c, the critical coagulation concentration of the salt. In theory, this salt concentration, 0.13 M,

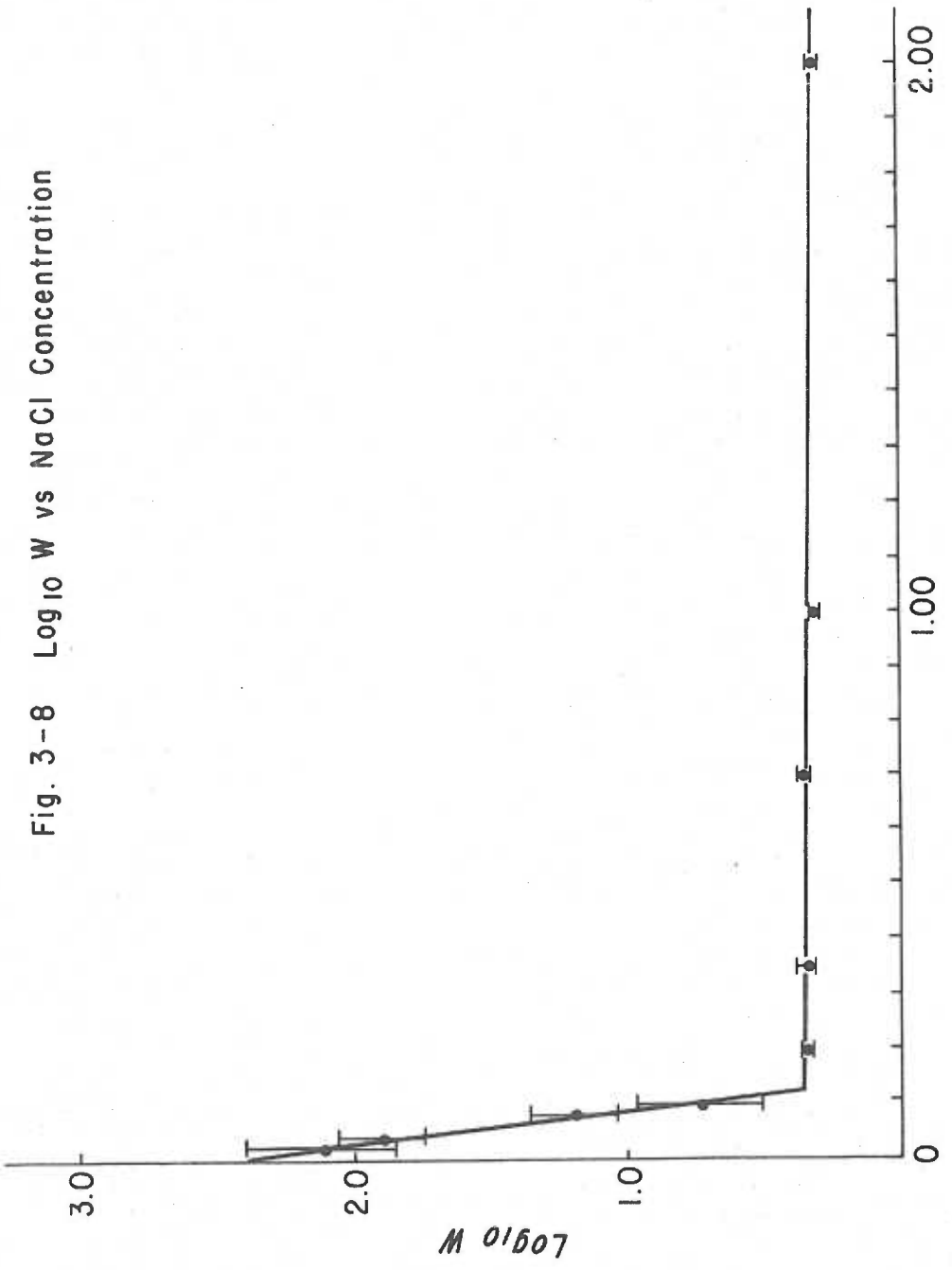

Fig. 3-8 Log_{10} W vs NaCl Concentration

produces a great enough reduction in electrostatic forces that $V_A > V_R$ at all distances between two colloidal particles. At salt concentrations higher than the critical coagulation concentration, the rate of coagulation is almost constant and is limited by diffusion alone. At lower salt concentrations, the rate of coagulation decreases exponentially because of rapidly increasing electrostatic forces. Thus, C_c is frequently used as a measure of an electrolyte's coagulating power.

3:5:4. Calculations of Hamaker's Constant

Hamaker's constant was determined by four different methods. The first three methods numerically solved equation 1-7 with different values of A, until the calculated value of W matched the experimental value. All evaluations of the integral in the equation were done with the trapezoidal rule to an accuracy of better than 1%. The calculations were done on a Hewlett Packard 9100B calculator. The programs used to calculate Hamaker's constant by each method are given in Appendix I.

The first method of calculating A used Verwey and Overbeek's (12) expression for V_R (equation 1-28). Honig et al.'s (8) correction factor for the viscous interactions between equal sized particles was also included. The values of A obtained by this method are slightly higher than those produced by the second method which used Honig and Mul's (18) equation for V_R between two spheres having a

fixed surface charge density. This was expected in that Honig and Mul's expression predicts slightly lower values for V_R than does Verwey and Overbeek's. Predicted values of V_R for two identical spheres are given for both equations in figure 3-9. The curves are only compared over the region $4.5\ \text{Å} < H \leq 180\ \text{Å}$ as Honig and Mul's approximation for V_R diverges rapidly from the true value of V_R at lower values of H and the two expressions are equivalent at larger H. This deficiency in their expression for V_R makes little difference when the value of Hamaker's constant is being calculated with their expression as $V_A \gg V_R$ when $H < 4.5\ \text{Å}$. The values selected for $\psi(0)$, κ and ϵ in figure 3-9 were those of the polystyrene latices in 0.10 M NaCl at 25°C. The second set of calculations also incorporated a correction factor for interparticle viscous interactions. The expression for V_R assumes that the surface charge of the sphere is constant. This assumption seemed reasonable in that charge groups on the surface of the polystyrene latices were covalently bound. Although this does not eliminate the possibility that some of the surface charges are bound by electrostatic forces, Frens et al. (24) have demonstrated that the concentration of adsorbed ions does not change appreciably during the course of a collision. Thus, models representing colloidal particles with a constant surface potential were not used to calculate V_R.

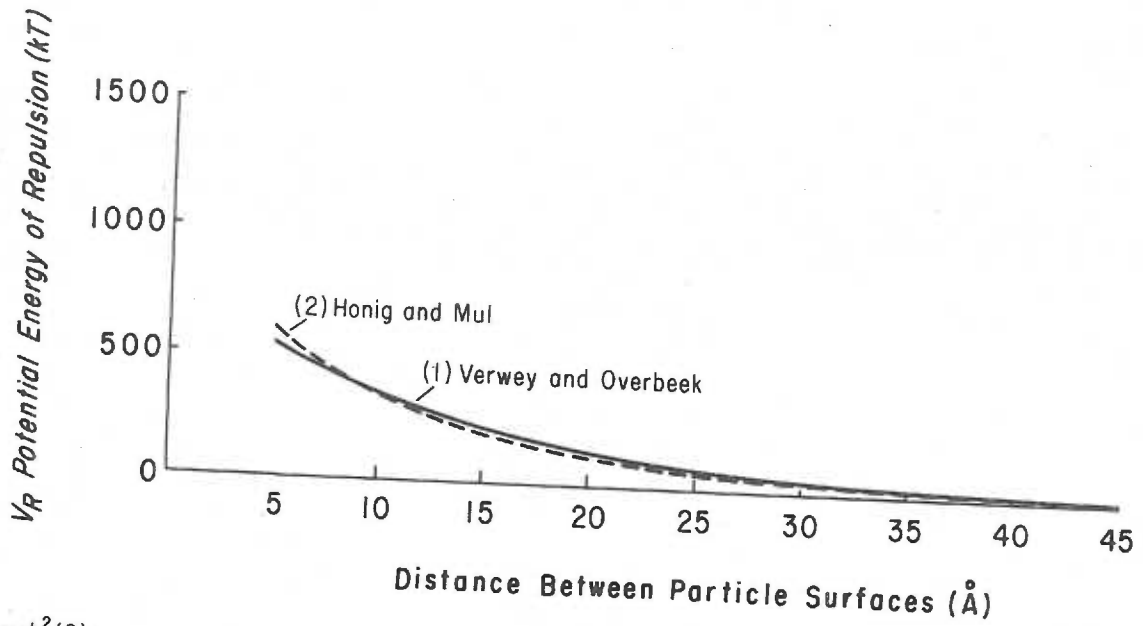

(1) $V_R = \frac{\epsilon a \psi^2(0)}{2kT} \ln(1+\exp(-\kappa a u))$

(2) $V_T = b\left\{\gamma^2 \exp(-\kappa a u)\left(\frac{2+\exp(-\kappa a u)}{2}\right) + \frac{\gamma^2 \exp(-2\kappa a u)}{2}\left(9+\frac{15}{(1+\gamma)^2}-2\kappa a u\right) - \frac{\gamma^2(2\ln(1-\exp(-\kappa a u)+\exp(-2\kappa a u)-2\exp(-\kappa a u)}{1+45\gamma^2+900\gamma^4}\right\}$

where $\gamma = \tanh\left(\frac{\epsilon\psi(0)}{4kT}\right)$; $b = \frac{1.21\times10^{23} a C_3}{\kappa^2}$

Fig 3-9 Potential energy of repulsion between two spheres as calculated by Verwey and Overbeek's expression (1) and Honig and Mul's expression (2) for polystyrene latices with a diameter of 0.90 microns and a surface potential of 163 microstatvolts in 0.10 M NaCl.

The third method was used to assess the effect of the Spielman correction term on the experimentally calculated value of A. Verwey and Overbeek's term for V_R was used and the calculations of the first method were repeated without the inclusion of the correction factor of Honig et al.

The last method of finding A was proposed by Ottewill and Shaw (93). It assumes that A does not change with salt concentration, and that at the critical coagulation concentration, the maximum of the V_T vs u curve equals zero. Thus, $V_T = 0$ when $\partial V_T/\partial u = 0$. To calculate V_T they use Reerink and Overbeek's (129) expression for V_R, which is taken from Verwey and Overbeek's work (12), and approximate V_A by $V_A = A/12u$. Differentiating V_T and setting it and V_T equal to zero they derive the Debye reciprocal radius, κ, at the critical coagulation concentration:

$$\kappa = 2.04 \times 10^{-5} \gamma^2 A^{-1} \qquad 3\text{-}5$$

where $\gamma = [e^z - 1]/[e^z + 1]$; $z = e\psi(0)/2kT$. Using this expression and the experimental value of the critical coagulation concentration 0.13 M, a value of 3.48×10^{-13} erg was calculated for Hamaker's constant.

Thus, the value of Hamaker's constant for the polystyrene latices in 0.10 M NaCl, as calculated by the first through the fourth methods respectively is $(3.76 \pm 0.01) \times 10^{-13}$, 3.68×10^{-13}, 3.67×10^{-13} and 3.48×10^{-13} ergs.

Hamaker's constant was also calculated at several ionic strengths from the rate of coagulation data described in section 3:5:3. All calculations were done by the method described in appendix I, using Verwey and Overbeek's expression for V_R. The calculated values for Hamaker's constant are plotted as a function of NaCl concentration in figure 3-10.

Since, the polystyrene latices in this experiment were not available to the scientific community at large, duplicate measurements of the size, surface charge density and types of surface charge groups are not available for comparison. However, Hamaker's constant is a frequently measured property of polystyrene and the value obtained can be compared with other values which have been published. A partial list of the various values of A, both theoretically and experimentally derived, are presented in table 3-3.

The information presented in table 3-3 shows that estimates of Hamaker's constant range over two orders of magnitude. This is largely due to the different assumptions and methods used to calculate A. Attempts to calculate Hamaker's constant on the basis of equation 1-31 and estimates of the intrinsic electronic frequency of polystyrene are the most inaccurate. This is primarily due to Hamaker's incorrect assumptions pertaining to the additivity of the attractive forces and his failure to account for the attractive contributions between particles in the infrared and microwave regions of the spectrum. Thus,

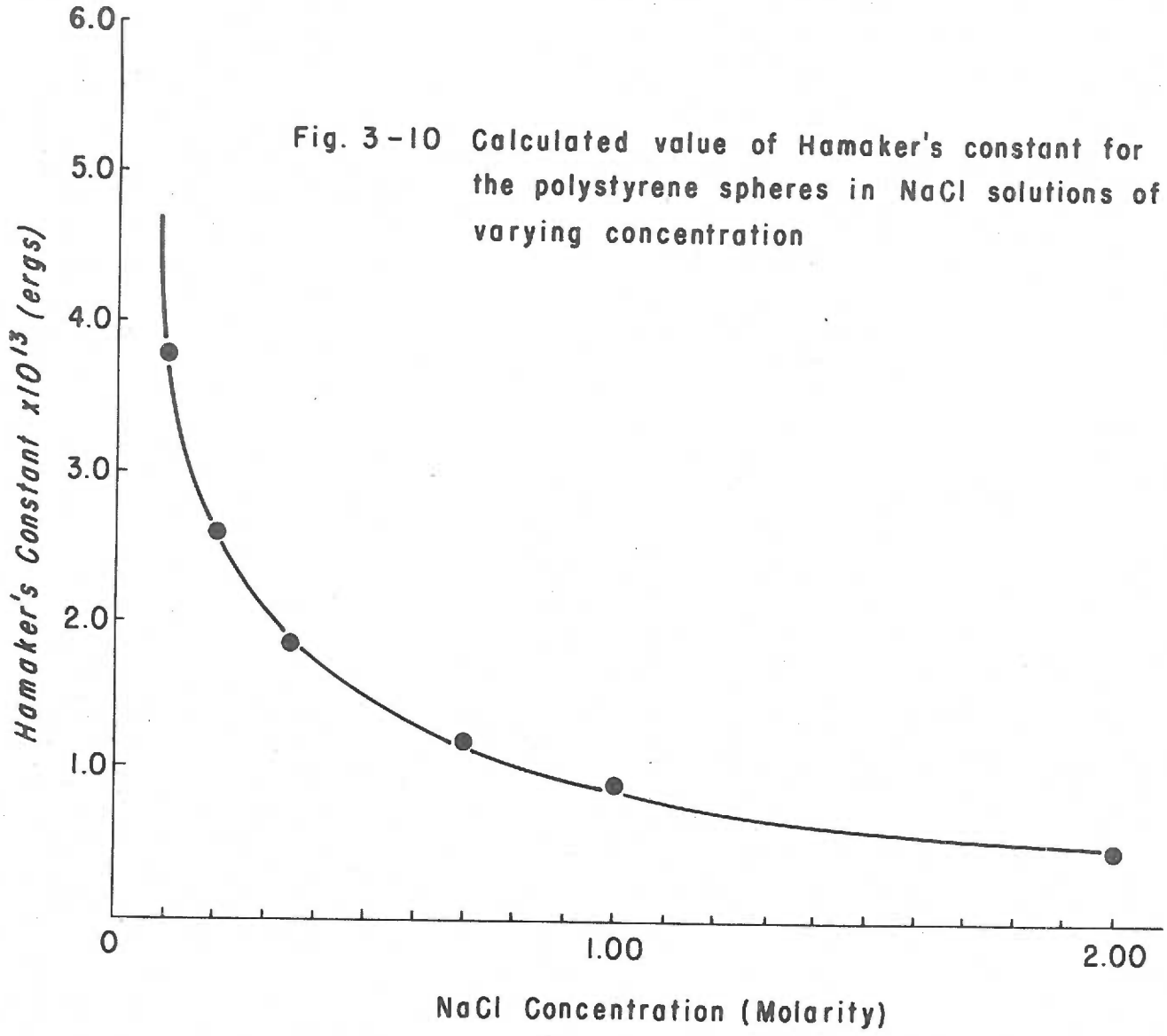

Fig. 3-10 Calculated value of Hamaker's constant for the polystyrene spheres in NaCl solutions of varying concentration

Table 3-3. Literature values of Hamaker's constant for polystyrene latices in water.

Range of Hamaker Constants (ergs)	Investigators	Reference
$(5.0\text{-}9.0) \times 10^{-13}$	Schenkel and Kitchener, 1960	(33)
0.5×10^{-13}	Fowkes, 1964	(130)
8.4×10^{-12}	Padday, 1966	(131)
$(0.5\text{-}1.5) \times 10^{-13}$	Watillon and Joseph-Petit, 1966	(94)
$(1.1\text{-}0.2) \times 10^{-13}$	Ottewill and Shaw, 1966	(93)
$(0.3\text{-}0.8) \times 10^{-13}$	Goldstein and Zimm, 1971	(132)
1.2×10^{-13}	Smith, Mitchell and Ninham, 1973	(35)
$(3.2\text{-}9.0) \times 10^{-14}$	Gingell and Parsegian, 1973	(133)
$(0.5\text{-}0.7) \times 10^{-13}$	Lichtenbelt et al., 1974	(92)
5.0×10^{-14}	Evans and Napper, 1975	(134)

these estimates are included parimarily as a historical note. The most recent and accurate methods of calculating A is based on the macroscopic field theory of Lifshitz and coworkers (37) which Parsegian and Ninham (38) have adapted to colloidal systems. Current estimates of A which have been made with this approach have assumed that the spheres were suspended in water. Smith, Mitchell and Ninham (35) have indicated that electrolytes damp the magnitude of interparticle attractive forces in the microwave region by a factor of $\exp(-\kappa H)$. Thus, the values of A listed in table 3-3 are probably too high. The classical method of calculating Hamaker's constant relies on the relationship between the rate of coagulation of a particle suspension and the potential energy of interaction between the aggregating particles. The validity of this method is limited by the accuracy of the experiments measuring the rate of coagulation data and particularly by the validity of the expressions for V_A and V_R. Thus, a partial list of reasons for the wide range of values obtained for A by the classical method will include:

1) The polystyrene spheres used in the different experiments had widely varying properties in terms of size, surface charge density and the amount and nature of surfactant adsorbed to the particles.
2) Different salts were often used to coagulate the polystyrene latices. The nature of the salt affects the magnitude of the

van der Waal's and electrostatic interactions between the particles.

3) Most of these calculations did not consider the viscous interactions between the particles, i.e., the "Spielman effect".

4) A variety of expressions for V_T were used. In particular expressions for the potential energy of repulsion were most frequently changed. Although most of the expressions for V_R provide a reasonable first approximation for monovalent salts whose concentration is less than 0.1 M, the precision of the expressions diminish at higher concentrations. This is due to their failure to account for:

   a) the finite size of the counterions in the double layer

   b) the "self-atmosphere" surrounding each ion

   c) the incompressibility of the suspending media

   d) the variations in the dielectric constant of the fluid in the double layer.

Although several investigators (120, 121) have developed methods of treating these problems in calculations of V_R, their treatments usually require a knowledge of parameters which have not yet been measured. Thus, in view of these discrepancies between the literature values and the limitations of the method, the values obtained for Hamaker's constant are in good agreement with those obtained by other investigators.

4. CHARACTERIZATION OF POLY(L-LYSINE)

The characteristics of poly(l-lysine) that are most needed to interpret its behavior at an interface are its number average (M_n) and weight average (M_w) molecular weights, degree of heterogeneity, configuration and degree of ionization at a given pH and ionic strength.

4:1. General Properties

Poly(l-lysine) is a linear polymer whose solubility is restricted to aqueous solutions with a pH of less than 12.3 (135). It was among the first poly(α-amino acids) to be synthesized and has served as a model protein for a variety of studies. Reviews on poly(α-amino acids) have dealt with their general characteristics (136), configuration (135), biological properties (137), chemical properties and methods of synthesis (138, 139).

Poly(l-lysine) is currently synthesized by a polymerization of the ε-carbobenzoxylated N-carboxy anhydride of lysine, as depicted below.

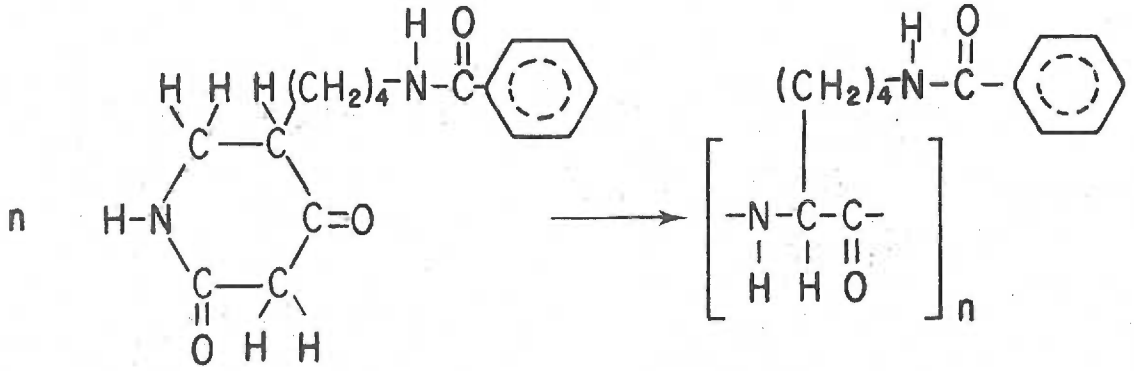

Following polymerization of the ϵ-carbobenzoxylated N-carboxy anhydride, the polymer is decarbobenzoxylated with PBr_3 or HBr to give poly(l-lysine · HBr) as below.

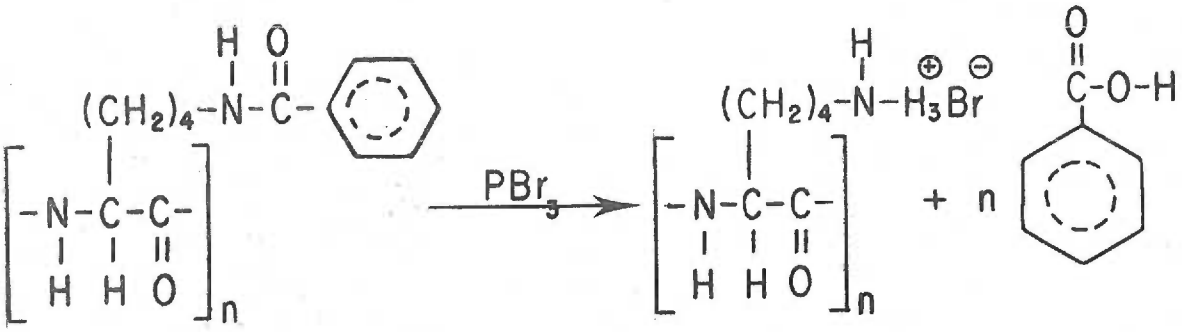

In theory, the range of polymer size can be controlled within narrow limits by selecting the appropriate solvent, temperature, initiator and monomer concentrations. However, in practice, poly(l-lysine) preparations are occasionally found to consist of two different molecular weight distributions (140, 141).

Poly(l-lysine) has been shown to adopt three and possibly four different configurations in solution. Depending on the extent of intramolecular electrostatic forces and solution temperature the polymer may adopt the configuration of a right handed α-helix, an antiparallel β-sheet, a random coil and possibly an extended α-helix. Since the intramolecular electrostatic forces are the dominant factor in determining polymer configuration, changes in solution pH can readily cause alterations in the configuration of the polymer. Applequist and Doty (142) demonstrated that the flow birefringence of poly(l-lysine)

solutions begins to decrease at pH 11.9 and disappears at pH 10.7. Their concurrent optical rotary dispersion (O.R.D.) studies showed a 10% decrease in helical content over the same pH range. Further decreases in pH to the pK of the polymer (143), 10.44, and beyond produce a rapid decrease in helical content as is evidenced by the N.M.R. studies of Bradbury and coworkers (144). The rapid decrease in helical content upon ionization of the polymer's ϵ-amino groups, is caused by a rapid increase in the intramolecular electrostatic forces which offset the stabilizing influence of the α-helix. The polymer is completely ionized at a pH of 9.0 and below (142).

Electrolytes reduce the effect of decreased pH by diminishing the magnitude of the intramolecular electrostatic forces. Potentiometric titration studies (145, 146) have demonstrated that a salt's effectiveness in reducing intramolecular repulsive forces is related to the ability of its anion to bind to poly(l-lysine). The stabilizing capabilities of anions are $F^- < Cl^- < CNS^-, ClO_4^-$.

The relationship between polymer size and configuration has been assessed by a number of investigators (147, 148). In aqueous solvents, the onset of helicity occurs with oligomers having a degree of polymerization of 13. Helicity is increased with an increasing size but even an oligomer of 22 segments does not exhibit complete helicity.

The transition between the polymer's α-helix and β-sheet configurations seems to be controlled by the temperature of the polymer

solution. Yu, Lippert and Peticolas (149) have shown a temperature dependent transition between the two structures using laser-Raman spectroscopy. They showed a rapid shift to the β-sheet between 20° and 33°C at pH 10.96 by monitoring the relative height of the amide III band at 1240 cm^{-1}. At pH 10.27, this shift was much more gradual, beginning at 30°C and reaching a maximum near 60°C. Circular dichroism, O.R.D. and infrared spectroscopy have been used to corroborate these findings (136).

Until recently, the fully ionized structure of poly(l-lysine) has been regarded as that of a random coil. However, Tiffany and Krimm (150) have detected similarities in the circular dichroism and O.R.D. spectra of poly(l-glutamic acid) and the poly(l-proline) II configurations. Krimm and Mark (151) have shown that if electrostatic forces alone control the conformation of a charged poly(amino acid), the most stable configuration of the polymer is a distorted left handed helix similar to the poly(l-proline) II structure. The more sophisticated calculations of Hiltner et al. (152) give further support to this proposal. However, Aebersold and Pysh's (153) calculations of the circular dichroism spectrum expected for the extended helix did not match the observed spectrum and as yet the strongest evidence in favor of the extended helix concept remains the similarity of the poly(l-glutamic acid) and poly(proline) II spectra.

Little is known about the configuration of the polymer at liquid-solid interfaces and the majority of investigations on the forces controlling polymer configuration at interfacial regions has been done at liquid-liquid or liquid-gas interfaces (154).

A number of the polymer's properties in aqueous solvents have been measured. These include its intrinsic viscosity (155), catalytic activity (156, 157), second virial coefficient (158), water of hydration (159), and surface tension (160).

4:2. Theory and Selection of Methods

4:2:1. Quantitation of Poly(l-lysine) Concentration

Although a number of methods for measuring poly(l-lysine) concentration exist, the most frequently used techniques rely on optical procedures. The obvious advantages of optical methods are rapidity, moderate sensitivity, accuracy, and availability of the necessary equipment. These advantages strongly suggested that the adaptation of one or more of the available optical techniques would provide the most suitable method of assaying poly(l-lysine) concentrations. Itzhaki (140) has developed a dye-binding assay, Sheth and Cohen (161) a fluorometric assay and Nevo et al. (1) a turbidimetric assay. Although each of these assays is capable of measuring poly(l-lysine) concentrations in the $\mu g\ ml^{-1}$ range, each must be calibrated by another means of measuring poly(l-lysine) concentration. This

requirement seemed prohibitive in view of the complexity of the assays developed by Itzhaki and Nevo et al. An attempt to use the assay of Sheth and Cohen was abandoned when sufficient precision could not be attained in establishing a calibration curve. Subsequently, a different method of assaying poly(l-lysine) concentration via the ninhydrin reaction was developed (162, 163). Collectively, these methods could measure poly(l-lysine) concentrations over a range of milligrams to nanograms ml^{-1}. An electrophoretic assay developed by Nevo et al. (1) was also used and is described in section 5:4:3.

4:2:2. Molecular Weight Distributions

Synthetic polymer preparations invarably exhibit a range of polymer molecular weights. A knowledge of the molecular weight distribution in a given polymer sample is particularly important when the polymer is of a low molecular weight, as many of the phenomena associated with polymer adsorption are molecular weight dependent. The best description of a molecular weight distribution gives the weight percentage of each molecular weight species present. In practice this is not attainable and a less comprehensive method of characterizing the range of molecular weights in a polymer sample is used. The most meaningful measures of molecular weight dispersion are given by the ratio of the weight to number average molecular weights, M_w and M_n respectively, and the standard deviation of the

molecular weight distribution, s, where (appendix II):

$$s = (M_n M_w - M_n^2)^{1/2} \qquad 4\text{-}1$$

Both the $M_w : M_n$ ratio and the standard deviation give adequate measures of the polymer's degree of dispersity when a unimodal distribution of molecular weights is present. However, bimodal molecular weight distributions have been observed for commercial samples of poly(l-lysine) (140, 141). Thus, adequate characterization of the molecular weight distribution requires a knowledge of the sample's modality, number average and weight average molecular weights.

Modality: The modality of a molecular weight distribution is most easily determined by molecular seiving procedures which provide semiquantitative, graphic measures of the distribution of molecular weights in a polymer sample. S.D.S. gel electrophoresis is frequently employed for neutral and globular proteins but does not work for strongly basic proteins which are precipitated by S.D.S. Conversely, Sephadex permeation chromatography provides a relatively quick and convenient means of assessing the breadth and modality of a molecular weight distribution. Under appropriate circumstances it can also provide an estimate of the distribution's average molecular weight. Empirical observations on the manner in which polymers elute through columns of Sephadex gels have indicated that polymers in a limited size range and of the same configuration will elute through the

column at a rate that is proportional to the size of polymer (164, 165). Thus, selection of a Sephadex which has the capability of fractionating polymers in the molecular weight range of interest enables an investigator to estimate the modality of polymer samples. The average molecular weight of the polymer can be estimated by comparing its order of elution with those of a series of suitable standards of known molecular weight. Standards should have narrow molecular weight distribution and the same degree or preferably lack of interaction with the Sephadex gel. These requirements pose little difficulty when working with neutral polymers or globular proteins, but polyelectrolytes whose size are quite sensitive to salt concentration and pH are much more difficult to find suitable standards for. The best calibration standard for a given polyelectrolyte is another sample of the same polymer with a very narrow, well characterized molecular weight distribution. In that suitable samples of poly(l-lysine) were not available for calibration of the Sephadex columns, only the modality and approximate measures of the size of the poly(l-lysine) molecules could be obtained.

Number Average Molecular Weights: Bonner et al.(166), Morawetz (167), and Andrews (165) have reviewed various methods of determining the number average molecular weight of a polymer. Of these methods, end group analysis, N.M.R. spectroscopy and osmometry seemed most promising.

Initial attempts at end group analysis, sought to titrate the carboxyl group at the end of the polymer by conductimetric and potentiometric means. These techniques were abandoned due to their lack of sensitivity. Other attempts at end group analysis included two methods wherein a readily identifiable group was bonded to the carboxyl group of the polymer and the ratio of lysine monomer to adduct determined. The first method took advantage of a reaction in which 1-ethyl-3(3-dimethyl-amino-propyl)-carbodiimide was used to attach alanine methyl ester (168). On completion of the reaction the excess alanine methyl ester was removed by dialysis. The average degree of polymerization was measured by hydrolyzing the polymer and determining the ratio of lysine to alanine on an amino acid analyzer. The erratic results achieved with the technique may have been due to a side reaction in which the carbodiimide-carboxyl intermediate, an o-acylisourea, cyclized with an ϵ-amino group on a poly(l-lysine) molecule. In the second technique the terminal carboxyl group was esterified with methanol and thionyl chloride and the degree of polymerization determined by N.M.R. spectroscopy. The polymer's degree of polymerization could be calculated by determining the ratio of the peak areas of the α-hydrogens on its peptide backbone to those of the methyl ester group. The technique failed as complete esterification could not be achieved when the polymer was in a solid state. Esterification of the polymer in solution was not feasible as poly(l-lysine) is soluble only in

predominantly aqueous solvents which react with thionyl chloride. Of the classical methods for determining molecular weight, only osmotic pressure measurements seemed sensitive enough to obtain an accurate molecular weight estimate.

The thermodynamic principles underlying the basis of osmotic pressure measurements state that when a solution is separated from a quantity of solvent by a semipermeable membrane capable of excluding the solute, solvent will pass through the membrane until the chemical potential of the solvent is the same on both sides of the membrane. If the solution is restricted to a fixed volume, solvent will diffuse into the solution until the pressure of solution alters the chemical potential of the solvent therein to that of the pure solvent. If μ_1 is the chemical potential of the solvent in the polymer solution and μ_1^o, the chemical potential of the pure solvent, the relationship between μ_1 and μ_1^o, at equilibrium, is given by the relationship:

$$\mu_1 = \mu_1^o + RT \ln a_1 + \int_{P_1}^{P} \overline{V}_1 dP = \mu_1^o \qquad 4\text{-}2$$

where a_1 is the activity of the solvent in the polymer solution, R is the gas constant, T the absolute temperature, and $\overline{V}_1$ the partial molar volume of the solvent. If it can be assumed that the partial molar volume of the solvent does not change with pressure, the osmotic pressure, Π, is given by:

$$\Pi = P - P_1 = \frac{RT \ln a_1}{\bar{V}_1} \qquad 4\text{-}3$$

where P_1 is the pressure of the solvent system and P, the pressure of the solution at equilibrium. If the polymer solution is sufficiently dilute, application of Raoult's law is justified. The activity of the solvent can be approximated by its mole fraction X_1. Thus $\ln a_1 = \ln X_1 \sim 1 - X_1$. For a multicomponent system obeying Raoult's law:

$$\Pi = \frac{RT}{\bar{V}_1} \Sigma X_i \qquad 4\text{-}4$$

where X_i is the mole fraction of each non-diffusable component.

The osmotic pressure of polymer solutions is described by equation 4-4 only at very low polymer concentrations, as interactions between the solute molecules cause large deviations from ideality at higher concentrations. At these concentrations the osmotic pressure of a two component polymer solution can be represented by the equation:

$$\Pi = RT[\frac{C_2}{M_n} + A_2C_2^2 + A_3C_2^3 + \ldots + A_nC_2^n] \qquad 4\text{-}5$$

where A_2, A_3 and A_n are the second, third and nth virial coefficients of the polymer respectively, and C_2 the polymer concentration in grams ml^{-1}. For uncharged polymers, A_2 is directly related to the excluded volume of the polymer, U_2.

Morawetz (167) has reported that the second virial coefficient of a spherical uncharged molecule is related to its volume, V_2, by:

$$A_2 = \frac{4V_2}{M_n^2} = \frac{U_2}{M_n^2} \qquad 4\text{-}6$$

The magnitude of a polyelectrolyte's second virial coefficient is very sensitive to the ionic strength of the solution and is generally an order to magnitude greater than that of an uncharged polymer. Polymers having no charge typically have A_2 values in the range of $1\text{-}5 \times 10^{-4}$ $cm^3 mole\ gm^{-2}$ (169).

The third virial coefficient is not frequently measured because of the difficulty of obtaining osmotic pressure measurements that are accurate enough to reduce the error associated with it to a fraction of its magnitude. When A_3 can be measured it serves as a useful measure of the degree to which polymer coils can interpenetrate one another. Extending the theory of Flory and Krigbaum (170, 171), Stockmayer and Casassa (172) and later Koyama (173) have shown the third virial coefficient, A_3, to be related to the second by the relationship:

$$A_3 = gA_2^2 M_n \qquad 4\text{-}7$$

where g is a function of temperature and the parameters which characterize the intermolecular potential energy of interaction (170, 171). For solutions of hard spheres, g attains a theoretical

maximum of 0.625, while nonionic polymer solutions exhibit a g value of about 0.25. Polyelectrolytes have values of g approaching 0.625 which implies that they act as impenetrable spheres with a radius roughly equal to (174) their radius of gyration.

When a polyelectrolyte is placed in a dialysis membrane permeable to all solution components but the polymer, electroneutrality requirements prevent the polyelectrolyte's counterions from diffusing across the membrane. Thus, the osmotic pressure of a polyelectrolyte solution is determined by the presence of the polymer and its counterions and as such does not reflect the molecular weight of the polymer. However, when large quantities of salt are present the equilibrium osmotic pressure contribution of the counterions is negligible. The extent of this swamping out effect can be calculated by the method outlined by Morawetz (175). Assume that a uni-univalent salt is added to a system in which a polyelectrolyte solution is separated from pure solvent by a semipermeable membrane. At equilibrium the chemical potential of the diffusable salt must be the same on both sides of the membrane. Thus:

$$\mu_3^o + RT \ln[m_b m_c (\gamma_\pm)^2] = \mu_2^o + RT \ln[m_b^1 m_c^1 (\gamma_\pm^1)^2] \qquad 4\text{-}8$$

where μ_3^o is the chemical potential of the salt in its reference state, m_b is the molality of by-ion on the polymer side, m_b^1 is the concentration of by-ion on the side containing only solvent, m_c is the

molality of counterion on the polymer side, m_c^1 is the molality of counterion on the other side, and $\gamma_\pm$ and $\gamma_\pm^1$ are the mean ionic activity coefficients of the salt ions on the polymer side and solvent side respectively. At equilibrium, the concentration of by-ion on the polymer side is equal to the concentration of added salt, m_s, present on that side $(m_b = m_s)$. The concentration of counterion, m_c, is equal to the molality of the added salt present, m_s, plus the molality of the polymer's counterions, m_p: $(m_c = m_s + m_p)$. On the other side of the membrane, the molality of by-ions, m_b^1, and counterions, m_c^1, equals the molality of the added salt present, m_s^1. Substituting the expressions for m_c and m_b into equation 4-8 and simplifying yields:

$$(m_p + m_s)(m_s)(\gamma_\pm)^2 = (m_s^1)^2(\gamma_\pm^1)^2 \qquad 4\text{-}9$$

Solving this equation for the concentration of added salt on the side of the membrane containing the polymer yields:

$$m_s = \left[\left(\frac{m_s^1\gamma_\pm^1}{\gamma_\pm}\right)^2 + \left(\frac{m_p}{2}\right)^2\right]^{1/2} - \frac{m_p}{2} \qquad 4\text{-}10$$

The difference in the concentration of added salt, Δm_s, on the two sides of the membrane is given by:

$$\Delta m_s = 2\left[\left(\frac{m_s^1\gamma_\pm^1}{\gamma_\pm}\right)^2 + \left(\frac{m_p}{2}\right)^2\right]^{1/2} - 2m_s^1 \qquad 4\text{-}11$$

As the amount of salt added to a polyelectrolyte solution increases, the osmotic pressure contribution of the excess salt ions approaches zero. Expanding equation 4-10 under the condition that $m_s^1 \gg m_p$, the difference in diffusable ion molarity on the two sides of the membrane is given by (see appendix III):

$$\Delta m_s \simeq \frac{m_p \gamma_\pm}{4 m_s^1 \gamma_\pm^1} \approx 0 \qquad 4\text{-}12$$

Okubo, Ise and Matsui (176) have investigated the relationship between polyelectrolyte concentration and the mean ionic activity coefficient of NaCl ions in NaCl-water-sodium poly(acrylate) systems. In systems having a NaCl concentration greater than 1.75 molal they found that $\gamma_\pm$ increased with polyelectrolyte concentration. When the NaCl concentration of the system was less than 0.5 molal, $\gamma_\pm$ decreased with sodium poly(acrylate) concentration up to approximately a polyelectrolyte concentration of 0.7 molal and then increased again. Several theories which have considered the free energy of polyelectrolyte solutions (177, 178) have provided semiquantitative explanations for the decrease in $\gamma_\pm$. Orofino and Flory (174) have suggested that decreases in $\gamma_\pm$ are due to the polyelectrolyte's ability to restrict the mobility of counterions in its vicinity and thereby decrease their activity. Even at high ionic strengths this trapping effect drastically reduces the activity of the counterions in the vicinity of the polyelectrolyte and osmotic contributions of a polyelectrolyte's counterions are

therefore greatly diminished. Thus, at high salt concentrations, where $4m_s^1\gamma_\pm^1 \gg m_p\gamma_\pm$, their contribution can be ignored.

Weight Average Molecular Weight: Analytical ultracentrifugation has become the standard method of determining weight average molecular weights for macromolecules. Alternative methods of determining M_w, such as dielectric dispersion, fluorescence depolarization, and light scattering, can often provide additional information about the shape of the molecule but are difficult to use and were not readily available.

Weight average molecular weights are usually determined by the technique of sedimentation equilibrium. The theoretical basis for the method is described by the following equation for an ideal two component system. It describes the equilibrium concentration, $C_2(x)$, of polymer or solute in the ultracentrifuge rotor as a function of distance, x, from the rotor's center of rotation:

$$\frac{d\ \ln[C_2(x)]}{dx^2} = \frac{M_w(1-\bar{\nu}\bar{\rho})\omega^2}{2RT} \qquad 4\text{-}13$$

where ω is the angular velocity of the rotor, R the gas constant, $\bar{\nu}$ the partial specific volume of the solute and $\bar{\rho}$ the density of the solution. When $C_2(x)$, $\bar{\nu}$, $\bar{\rho}$, and T and ω are known M_w can be calculated from the slope of a $\ln[C_2(x)]$ vs x^2 plot. However, until the recent development of the split-beam photoelectric scanner it has not been possible to directly determine solute

concentration at various points in the ultracentrifuge rotor. Since the photoelectric scanner is expensive, most laboratories continue to rely on the traditional Rayleigh interference optics. This type of an optical system is only capable of determining differences in solute concentration, and requires a separate determination of the absolute polymer concentration at one point in the rotor, if equation 4-13 is to be used. Yphantis (179) showed that when sedimentation equilibrium is established at sufficiently high rotor speeds, the meniscus of the solution is depleted of solute, and equation 4-13 can be used directly. Unfortunately, this technique is very sensitive to low molecular weight contaminants and is difficult to use with great precision. Richards et al. (180) have described a low speed method where absolute polymer concentrations could be determined by a second experiment using a synthetic boundary. Although this method allows the investigator to determine polymer molecular weights more accurately, the procedure is lengthy and demanding.

In 1968, Nazarian (181) published a method for calculating molecular weights from a knowledge of the changes in solute concentration alone. A simplified explanation of the theory behind his technique begins by integrating equation 4-13 from the center of rotation to give:

$$C_2(x) = C_2(0)\exp(cM_w x^2) \qquad 4\text{-}14$$

$$c = \frac{(1-\bar{\rho}\bar{\nu})\omega^2}{2RT}$$

where $C_2(0)$ equals the theoretical concentration of polymer at the center of rotation. The concentration of polymer, $C_2(x)$, is related to the absolute fringe number $J(x)$ at x by the equation:

$$J(x) = \frac{\lambda}{bn} C_2(x) \qquad 4\text{-}15$$

where b is the cell thickness, n the specific refractive increment of the solute and λ the wave length of light used by the interference optics. If equation 4-15 is substituted into equation 4-14, the absolute fringe number at x^2 is given by:

$$J(x) = \frac{\lambda}{bn} C_2(0)\exp(cM_w x^2) \qquad 4\text{-}16$$

The fringe shift $\Delta J(x)$ between points $x^2 = q$ and $x^2 = q + Q$ is given by:

$$\Delta J(x) = J(q+Q) - J(q) = \frac{\lambda}{bn}[C_2(Q) - C_2(0)]\exp(cM_w q) \qquad 4\text{-}17$$

The logarithm of this equation provides the working equation for Nazarian's method:

$$\ln[\Delta J(x)] = cM_w q + \ln\left(\frac{\lambda}{bn}[C_2(Q) - C_2(0)]\right) \qquad 4\text{-}18$$

Thus, if the logarithm of the fringe shift is plotted against the distance from the center of rotation squared, q, the molecular weight of the solute can be calculated from the slope of the plot. This

method requires the fringe shift to be measured at regular intervals of x^2 and the distribution of polymer concentrations to be at equilibrium. A knowledge of λ, b, n, $C_2(Q)$ or $C_2(0)$ is superfluous.

4:2:3. Determination of Polymer Size

The manner in which polymer size is characterized is usually dependent on the configuration of the polymer. When the polymer assumes a highly ordered configuration, its size is best given in terms of the number and geometric configuration of the smallest repeating unit in the polymer. Randon coil polymers are usually characterized in terms of the average distance between the two ends of the polymer or by the mean distance of the polymer's segments from their center of gravity. These two parameters are referred to as the polymer's root mean square end to end distance, $[r^2]^{1/2}$ and radius of gyration, $[r_g^2]^{1/2}$, respectively.

Early attempts to calculate $[r^2]^{1/2}$ from the number of segments in a polymer chain, b, equated the average dimensions of a polymer to those of a three dimensional random walk of b steps, each of length c where c corresponded to the distance between polymer segments. If no restrictions are placed on the location or direction of each step $[r^2]^{1/2}$ is given by:

$$[r^2]^{1/2} = [bc^2]^{1/2} \qquad 4\text{-}19$$

For linear polymers the radius of gyration is related to the root mean square end to end distance by:

$$[r_g^2]^{1/2} = \left(\frac{[r^2]}{6}\right)^{1/2} \qquad 4\text{-}20$$

Equations 4-19 and 4-20 usually do not satisfactorily describe the dimensions of actual macromolecules as they make no allowance for the properties of polymeric segments. Some of these properties are:

1) Polymer chains are not freely jointed and have a relatively constant angle, φ, between monomeric segments. Eyring (182) has calculated the effect of a fixed angle, φ, between the adjacent steps of a random walk, yielding:

$$[r^2]^{1/2} = [bc^2]^{1/2}\left[\frac{1-\cos(\varphi)}{1+\cos(\varphi)}\right]^{1/2} \qquad 4\text{-}21$$

2) The side groups of polymer chains often prohibit complete rotation of a given polymer segment about its axis. Benoit and Sadron (183) calculated the effect of restricting the rotation of each segment about its axis to Γ degrees. Estimation of Γ for all but the most simple of macromolecules is difficult and this parameter usually must be determined experimentally. Thus, for a random walk of b steps each of length c where the angle between adjacent steps is φ degrees and rotation about bond axis is limited to Γ degrees $[r^2]^{1/2}$ is given by:

$$[r^2]^{1/2} = bc^{1/2}\left[\frac{1-\cos(\varphi)}{1+\cos(\varphi)}\right]^{1/2}\left[\frac{1+\cos(\Gamma)}{1-\cos(\Gamma)}\right]^{1/2} = [r_o^2]^{1/2} \qquad 4\text{-}22$$

When the root mean square end to end distance of a polymer equals the value predicted by equation 4-22, the polymer is said to have adopted its unperturbed dimension. Under these conditions a polymer assumes the size it would have if its dimensions were controlled solely by bond lengths, bond angles, restrictions to rotation and the polymer's degree of polymerizations.

3) The finite size of each polymer segment makes a certain volume of space unavailable to other segments of the polymer whereas random walk calculations allow two or more steps to land on the same point at once. This excluded volume effect causes the dimensions of the polymer to be greater than the size predicted by equation 4-22 (44, 184).

4) The free energy of a given polymer configuration will depend on the heat of formation and the number of polymer segment-solvent contacts. Poor solvents, those in which the formation of polymer segment-solvent contacts is an endothermic process, cause segment-segment contacts to be favored. In these solvents polymers tend to adopt contracted configurations. When the solvent is poor enough that the tendency to form segment-segment contacts exactly balances the excluded

effects the polymer will adopt its unperturbed dimension. Solvents having this property are termed theta solvents. Good solvents are those which favor the formation of segment-solvent contacts and allow the polymer to adopt an expanded configuration. Thus, solvents which decrease the free energy of the polymer when polymer segment-solvent contacts are formed permit expanded polymer configurations and solvents which increase the free energy of the polymer on the formation of segment-solvent contacts cause contracted polymer configurations.

Since the majority of these properties cannot be readily determined, a priori calculation of polymer size, even in theta solvents, is difficult. Consequently, polymeric size must be determined experimentally for all but the most simple of macromolecules.

The size of a poly(l-lysine) molecule is best characterized by a measurement of its radius of gyration or root mean square end to end distance, as it exists as a random coil when in solution at a pH of less than 7.0. Light scattering techniques provide the best method of measuring a polymer's radius of gyration as they require no assumptions about the shape of the molecule. Unfortunately, the small size of the poly(l-lysine) molecule places it at the edge of the technique's resolving powers. In lieu of light scattering techniques, viscometry and Sephadex gel permeation chromatography were chosen for their

relative simplicity and ability to measure the hydrodynamic volume of the polymer, a parameter closely related to the polymer's radius of gyration.

The foundations for the viscometric determination of macromolecular configuration stem from Einstein's (185) calculations of the limiting viscosity number of a suspension of rigid uncharged spheres:

$$\lim_{\phi_2 \to 0} \frac{\eta/\eta_1 - 1}{\phi_2} = 2.5 \qquad 4\text{-}23$$

where η is the dynamic viscosity of the solution, η_1 is the dynamic viscosity of the solvent and ϕ_2 is the volume fraction occupied by the particles.

In 1940 Simha (186) calculated the limiting viscosity number of suspensions of rigid uncharged prolate and oblate ellipsoids:

$$\lim_{\phi_2 \to 0} \frac{\eta/\eta_1 - 1}{\phi_2} = (\eta) \qquad 4\text{-}24$$

where (η) will depend only on the axial ratio of the ellipsoid, in the limit of a zero rate of shear. Thus, if the general shape of an uncharged polymer is known, its limiting viscosity number can be used to interpret the hydrodynamic size in terms of an equivalent prolate or oblate ellipsoid. When polymer size is calculated this way, the actual size of the polymer, particularly polyelectrolytes, may differ greatly from their calculated size as:

1) The true volume fraction of the polymer is frequently unknown, and so limiting viscosity numbers are reported in terms of dl gm^{-1} or ml gm^{-1}. In 1935 Kraemer and Lansing (187) suggested that the volume fraction of the solute, ϕ_2, in the generalized Einstein equation be replaced with the concentration of the solute in grams dl^{-1}. In 1952 The Report on Nomenclature for the International Union of Pure and Applied Chemistry subsequently recommended that the units of concentration be changed to grams ml^{-1}. When the limiting viscosity number of a polymer is measured in terms of dl gm^{-1}, calculation of a polymer's size requires a reconversion to a dimensionless limiting viscosity number. This is most frequently done by means of the following relationship:

$$\phi_2 = C_2 \bar{\nu}_2 \qquad 4\text{-}25$$

where $\bar{\nu}_2$ is the partial specific volume of the polymer, at infinite dilution. This conversion equates the volume fraction of the polymer with the product of its mass and partial specific volume. Viscometric measurements of particle size measure the volume of the polymer, the water bound to it and entrapped by its coils. If the polymer is heavily hydrated, the use of this equation may result in serious errors (188, 189).

2) At higher rates of shear, ellipsoids and rigid polymers with large axial ratios will orient their major axis so that it lies in a plane of shear. This orientation decreases the extent to which the particles disrupt the laminar flow of the suspension and results in a decrease in the viscosity of the suspension. Suspensions or solutions whose viscosity decreases with increasing shear rate are said to be pseudoplastic. Polymer solutions which exhibit this type of behavior frequently consist of high molecular weight polyelectrolytes whose large axial ratio is created by the intramolecular repulsive forces between its charge groups. The smallest polyelectrolyte whose solution will be pseudoplastic, will depend on the ionic strength, pH of the solvent, and the charge density, extent of ionization and inherent stiffness of the polymer. Vink (190) has found that the smallest carboxymethylated cellulose ether whose solution was pseudoplastic at very low ionic strengths had a molecular weight of 90,000.

3) Suspensions of nondeformable charged particles frequently exhibit a greater viscosity than a suspension of geometrically equivalent particles with no charge. This phenomenon is termed an electroviscous effect and has two principle sources. The primary electroviscous effect is created by the shear induced distortion of the ionic atmosphere surrounding each

particle and is particularly noticeable at low ionic strengths. The secondary electroviscous effect is created by the interaction of the double layers of neighboring particles. The primary electroviscous effect becomes appreciable at ionic strengths less than 10^{-3} M (191) and the secondary electroviscous effect at particle concentrations which produce a solute volume fraction of greater than 1%. A general review of electroviscous effects has been given by Conway and Dobry-Duclaux (192).

In 1939 Debye and Beuche (193) and Kirkwood and Riseman (194) used the concept of a random coil to develop separate theories of the limiting viscosity number of a polymer. Kirkwood and Riseman envisaged polymers as a randomly coiled string of beads with a Gaussian distribution about their center of mass. If a polymer acted as a free draining coil, solvent velocity would be independent of position within the domain of a polymer's segments when the polymer moved through the solvent. The frictional coefficient and the limiting viscosity number of the polymer would then be proportional to the product of the frictional coefficient of a single segment and the number of segments in the polymer. Conversely, if solvent velocity were a function of segment density, the limiting viscosity number of the polymer would be related to the molecular weight of the polymer by:

$$[\eta] = b[M_v]^{\bar{a}} \qquad 4\text{-}26$$

where $\bar{a}$ is the Mark-Houwink parameter which has a value ranging from 0.5 to 1, M_v is the viscosity average molecular weight of the polymer and b is an experimentally determined constant that is a constant for a given polymer in a given solvent. Extending this work Flory (195) postulated that uncharged linear polymers in theta solvents would act as nondraining coils and that the root mean square end to end distance of the polymer would be related to its limiting viscosity number.

$$[\eta] = \frac{\Phi[r^2]^{3/2}}{M_v} = \frac{\Phi[r_o^2]^{3/2}\,\alpha^3}{M_v} \qquad 4\text{-}27$$

where Φ is a universal constant whose value is $2.1 \pm 0.2 \times 10^{-3}$ dl mole^{-1} Å^{-3} and α the chain expansion factor of the polymer, which give a measure of the polymer's expansion over its unperturbed dimension. The chain expansion factor, α, in any given configuration equals the ratio of the polymer's radius of gyration to the radius of gyration of the polymer in its unperturbed dimension. Alternatively, α may be calculated from the following equation, due to Orofino and Flory (169):

$$A_2 M_v = [\eta] 1.88 \ln(1+0.886(\alpha^2-1))$$

$$= \frac{\Phi[r_o^2]^{3/2}\alpha^3 1.88 \ln(1+0.886(\alpha^2-1))}{M_v} \qquad 4\text{-}28$$

Other expressions relating A_2 and $[\eta]$ have been reviewed by Kurata and Stockmayer (196).

Although equation 4-27 has been amply verified for most nonionic polymers and seems to hold for a variety of non-theta solvents, polyelectrolytes are not as well behaved and exhibit values of Φ (184) ranging from 0.9×10^{-3} to 6.6×10^{-3} dl mole^{-1} Å^{-3}. This enlarged range of Φ values reflects the effect of the polymer's charge groups on the configuration of the polymer. At low ionic strengths, intramolecular electrostatic forces between charge groups expand the conformation of the polyelectrolyte to the point that it may become a partially draining coil. Furthermore, the charge groups may produce electroviscous effects which increase the limiting viscosity number of the polymer in a manner that does not reflect its size. The magnitude of both of these effects will depend on the polyelectrolyte's degree of ionization and the ionic strength of the solvent. However, when the size of a polyelectrolyte does not greatly exceed its unperturbed dimensions and solvent ionic strengths are greater than ~ 0.01 M, equation 4-27 may be used.

Empirical determinations (197, 198) of the relationship between the limiting viscosity number of a polyelectrolyte and the ionic strength of its solvent have shown that in many polymer solvent systems the following expression holds:

$$[\eta] = \frac{c}{C_3^{1/2}} + b \qquad 4\text{-}29$$

where b and c are empirically determined constants and b is usually taken to represent the limiting viscosity number of the polymer at an infinite salt concentration. Although this relationship has not always been found to hold and has been shown to be too simplistic, it is often a good rule of thumb which holds for a variety of polyelectrolyte-solvent systems.

4:3. Materials and Equipment

Poly(l-lysine·HBr): lot number LY-164 poly(l-lysine·HBr) was purchased from the Miles Research Laboratories of Kankakee, Illinois. The listed weight average molecular weight, 33,000, was obtained by ultracentrifugation of the samples parent compound, poly(ε-carbobenzoxy-l-lysine), and corresponds to a degree of polymerization of 188. No measure of the samples heterodispersity was given.

Hydroxylysine·HCl: lot number 081873, d,l and allo-δ-hydroxylysine·HCl was obtained from the California Foundation for Biochemical Research of Los Angeles, California.

Dialysis tubing: 3/8 inch dialysis tubing was obtained from the Van Waters and Rogers Company of Seattle, Washington.

Membrane Osmometer: A Mechrolab model 502 membrane osmometer, manufactured by the Hewlett Packard Company of Avondale, Pennsylvania, was used.

Membranes: Selectron B-19 membranes were purchased from the Schleicher and Schuell Company of Keene, New Hampshire.

Uviscan Monitor: A Buchler uviscan III monitor was obtained from the Scientific Supplies Company of Portland, Oregon.

Viscometer: A modified Ubbelohde viscometer was constructed from the specifications listed in figure 4-1 by the glass blower for the Oregon Graduate Center, Alan Ryall. An Ubbelohde viscometer was used because it requires less polymer than other types of viscometers for the determination of limiting viscosity numbers and accurately reproduces a constant head of pressure with different amounts of solution in the viscometer. The all pyrex viscometer consists of a 55 ml mixing compartment attached to three parallel arms. A magnetic stirbar is kept and cleaned in situ in the mixing compartment. The timing arm of the viscometer, (A), consists of a 12 cm capillary tubing with an 0.28 ± 0.02 mm internal diameter which is fed by a 2.0 ± 0.1 ml bulb that provides a mean head of pressure of 13.6 ± 0.1 cm. The flow time for water at 25.00° is 190.70 seconds. The mean and maximum shear rate for water under these conditions is estimated at 440 ± 120 sec^{-1} and 650 ± 180 sec^{-1} respectively. The loading arm, (B), and cleaning arm, (C), of the viscometer have

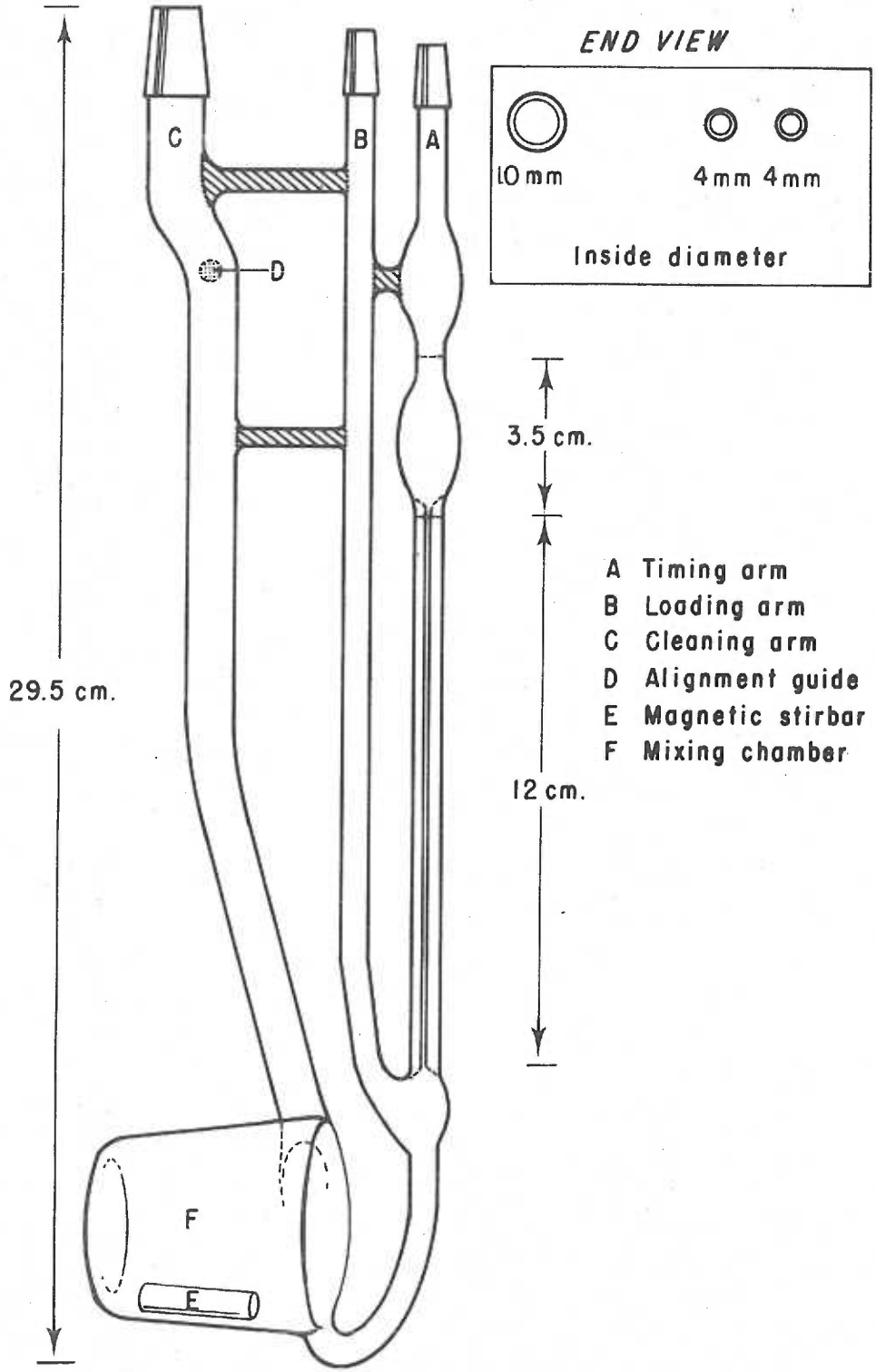

Fig 4-1 Diagram of an Ubbelohde viscometer

internal diameters of approximately 4.0 and 10.0 mm respectively. A piece of glass was fused to the sides of the loading arm to serve as an alignment guide when the viscometer was placed in the water bath.

Timers: A Hewlett Packard 524C electronic counter or a Heuer stopwatch was used to determine the flow times of polymer solutions in the viscometer. The counter and stopwatch could be read to the nearest 0.1 millisecond and 20 milliseconds respectively. The electronic timer was loaned by Dr. H.S. Mason of the University of Oregon Health Sciences Center, and the Heuer stopwatch purchased from the Van Waters and Rogers Company of Seattle, Washington.

Water bath: The water bath consisted of a 49 x 26 x 28 cm Lucite container holding 24 liters of water and was lagged on all sides with a 2 cm thick layer of polystyrene foam. Heating in the water bath was supplied by a single 80 watt showcase light bulb. Temperature gradients in the water bath were prevented by stirring the water bath with a circular paddle with a six inch diameter at a rate of 60 rpm. The water bath is pictured in figure 4-2. The temperature of the water bath was maintained to within ± 0.01°C by the toluene-mercury regulator diagrammed in figure 4-3. It consisted of a tubular grill containing approximately 280 ml of toluene which was connected to a glass side arm containing ten ml of mercury. The side arm narrowed down to a capillary tube with a radius of approximately 1.5 mm. The coefficient of cubic expansion for these amounts of toluene and mercury is

Fig. 4-2. Constant temperature bath

1) Stirring motor
2) Lagged tank
3) Toluene-Mercury regulator
4) Viscometer holder
5) Heating lamp
6) Stirring paddle

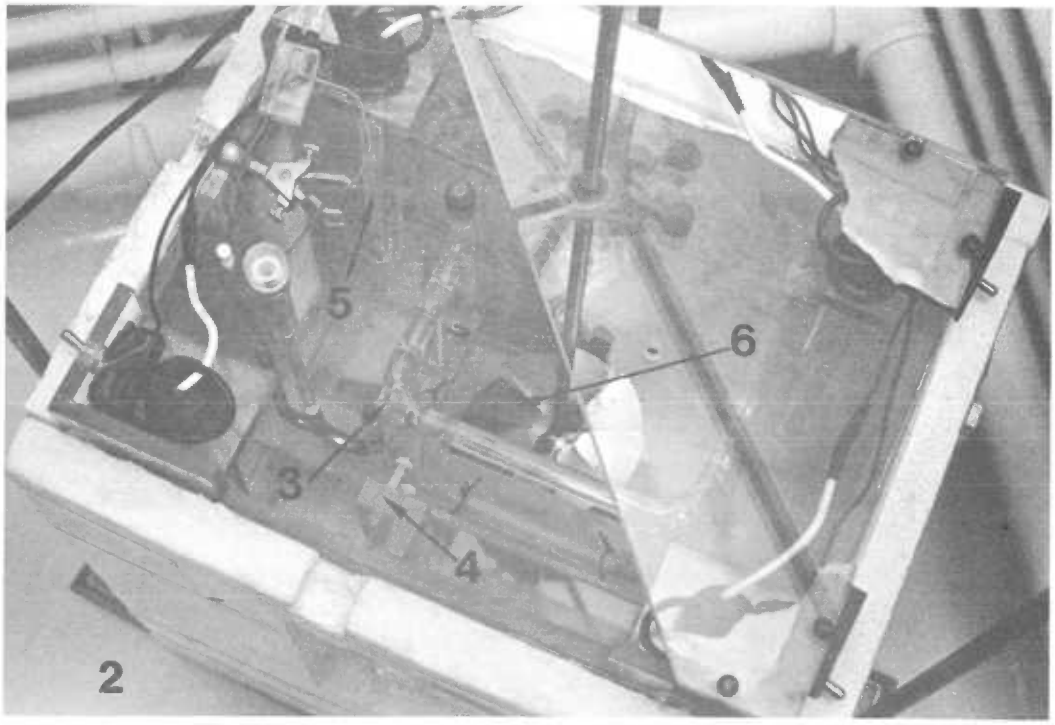
5
6
3
4
2

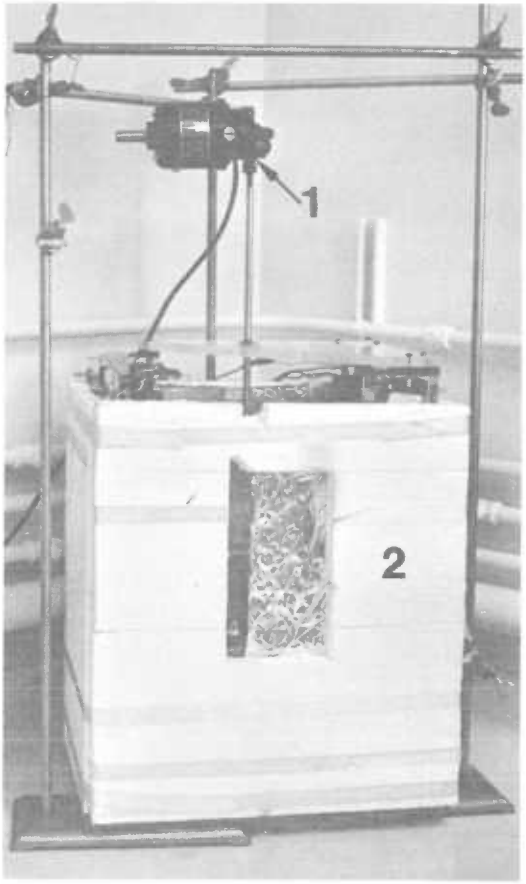
1
2

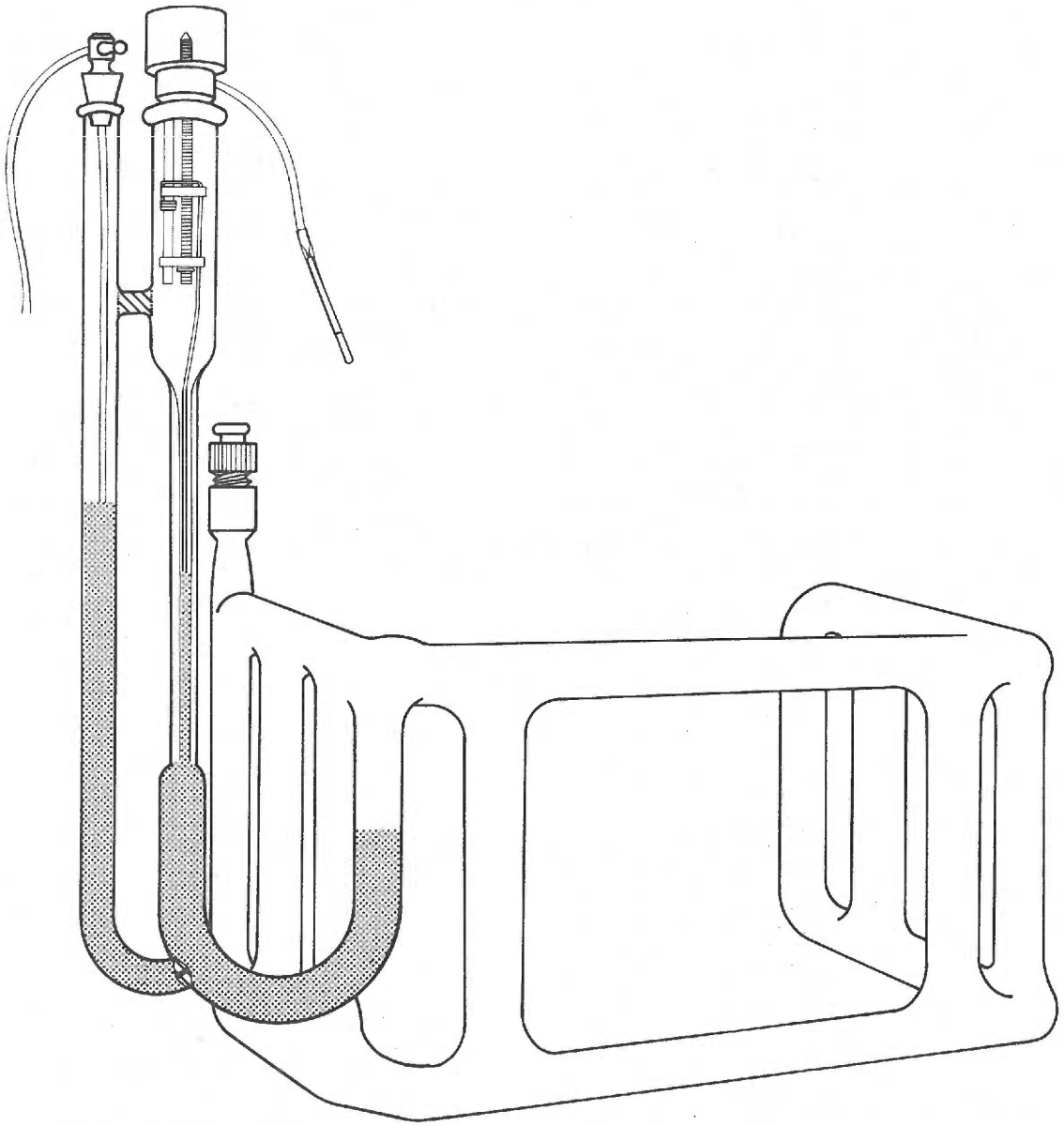

Fig 4-3 Diagram of the Toluene - Mercury Thermostat

0.31 ml deg^{-1} at 25° C. At this temperature the two fluids completely filled the grill and side arm of the regulator and the top of the mercury lies at about the midpoint of the capillary tube. A 0.01° increase in temperature causes the height of the mercury to rise by ~ 0.8 mm. The toluene-mercury regulator was calibrated with a Brooklyn bomb calorimeter thermometer. Viscometers were fastened to the wall of the water bath with a screw type viscometer holder which was permanently fused to the wall of the constant temperature bath.

Thermometer: A model 22552 bomb calorimeter thermometer was purchased from the Brooklyn Thermometer Company of Farmingdale, New York. The thermometer was calibrated and certified by the company and was divided into 0.01°C between the range of 22.00 and 28.00°C.

Amino Acid Analyzer: The amino acid analyzer was a Beckman Spinco model 120C modified with a long path photometer cell and a modified recorder where one millivolt gave a full scale deflection. These modifications produced a tenfold increase in the sensitivity of the instrument and have been described by Jones and Weiss (199). The column used for the separation of lysine and hydroxylysine was 0.9 x 13.0 cm column of Biorad-Aminex A-5. The pH 5.25 eluent buffer and ninhydrin reagent used by the machine has been described by Spackman (200). The analyzer was equipped with an automatic loading device whereby up to 20 samples could be given to the

machine to be processed automatically. Optimal performance of the machine seemed to be obtained when the separation column was cleaned often enough to keep the operating pressure of the buffer pump below 120 psi.

4:4. Methodology

4:4:1. Estimation of Poly(l-lysine) Concentration

Method I: The least sensitive and quickest method of detecting milligram and sub-milligram quantities of poly(l-lysine) is based on the ninhydrin reaction. In a typical assay a one to five ml aliquot of test fluid would be mixed with five ml of ninhydrin reagent (200) and the entire mixture heated in boiling water for 15 minutes. After cooling the mixture to room temperature, the presence of poly(l-lysine) could be estimated by determining the optical density of the solution at 570 mμ. This assay was used for analyzing the effluent of columns and in making initial estimates of poly(l-lysine) concentration when more accurate methods of measurement were needed.

Method II: A more accurate and sensitive means of analyzing poly(l-lysine) concentrations in the mg ml^{-1} to μg ml^{-1} region was achieved by hydrolyzing of the polymer with hydrochloric acid and measuring of the resultant lysine concentration on a calibrated automatic amino acid analyzer. When lysine concentration was measured

by this method a reproducibility of only 5% level could be obtained on duplicate samples.

Method III: A one percent degree of reproducibility was obtained with the amino acid analyzer by using an internal standard. Carnosine, histidine, ornithine, and arginine and hydroxylysine were tested as possible internal standards. All five were adequately resolved from lysine by the analyzer's short column, but only the hydroxylysine: lysine micromolar color yield ratio varied by less than 1% when measured over five duplicate samples. Furthermore, the lysine to hydroxylysine micromolar color yield ratio was not affected by any of the procedures in which poly(l-lysine) was hydrolyzed to lysine and suspended in the amino acid analyzer diluent buffer. The color yield of an amino acid is defined here in terms of the area under the elution profile that is printed out by the amino acid analyzer when the amino acid passes through it. The area of the elution profile is calculated by multiplying the number of optical density units between the peak and base line of the profile by the number of dots between the two points that mark the profile's half height. Thus, the micromolar color yield of an amino acid is defined as the elution profile area, in dot-O.D.'s, that would be produced by one micromole of the amino acid.

In a typical assay approximately 0.5 ml of a poly(l-lysine) solution was placed in a preweighed, acid cleaned hydrolysis tube. The exact amount of solution was then determined gravimetrically.

Hydroxylysine · HCl solution, 1.000 gm ml^{-1}, was added to the hydrolysis tube until roughly equimolar quantities of hydroxylysine and lysine were present. Concentrated HCl was added until a concentration of at least 6N HCl was attained, at which point the air in the tube was evacuated, and the tube flame sealed. The poly(l-lysine) was hydrolyzed by placing the tube in an oven for 12 hours at 105°C. The contents of the tube were then removed, flash evaporated, and suspended in and diluted with a pH 2.2 buffer (200) for the automatic amino acid analyzer, to a level of about 7 μg ml^{-1} of lysine. The sample would then be placed on an amino acid analyzer, along with a standard where the ratio of lysine to hydroxylysine was known. The concentration of poly(l-lysine) was calculated from the lysine to hydroxylysine micromolar color yield ratio and the amount of hydroxylysine placed in the poly(l-lysine) sample.

4:4:2. Preparation of the Polymer

Poly(l-lysine) solutions were usually prepared by simple dialysis of the polymer's hydrobromide salt against the solvent of interest. When the NaCl concentration of the desired poly(l-lysine) solution was equal to or greater than 0.10 M, an appropriate quantity of poly(l-lysine · HBr) was dissolved in 3 to 5 ml of that NaCl solution and dialyzed against 2 liters of the same for three days at room temperature. The dialysis fluid was changed every 24 hours. After dialysis

the polymer solution was diluted to the required strength. Poly(l-lysine) solutions with a NaCl concentration of less than 0.10 M were prepared by dissolving the polymer in 3 to 5 ml of 0.10 M NaCl and dialyzing it against 2 liters of 0.10 M NaCl as before. After the initial dialysis the dialyzing fluid was changed to the required NaCl concentration and the dialysis procedure carried out for another three days as previously mentioned.

The low molecular weight contaminant of the polymer sample could also be successfully removed by fractionating the polymer on a 95 x 5.0 cm Sephadex G-150 column, using 0.01 M NaCl as an eluent. Although the technique of fractionating the polymer allowed a greater amount of control on the width of the final molecular weight distribution, the polymer had to be concentrated and redialyzed against the solvent of interest after the initial fractionation. This procedure was not used as the advantages of using a molecular weight distribution which was sharper than could be obtained with dialysis were negligible.

4:4:3. Gel Permeation Chromatography

The modality and approximate size of the polymer sample were determined by fractionating it on columns of Sephadex G-10, G-75 and G-150. The Sephadex columns were prepared by placing the dehydrated Sephadex gels in boiling 0.01 M NaCl for the required number of hours, fineing the swollen beads and pouring the gel into a jacketless

column. The dimensions of the G-10, G-75, and G-150 beds were 2.5 x 95 cm, 2.5 x 39 cm, and 2.5 x 93 cm respectively. After the columns were poured a sample applicator was placed on top of the gel and the column was run for a minimum of 24 hours before a sample was placed on it. The flow rate of the Sephadex G-75 and G-150 columns were limited to a rate of approximately 11 ml $hour^{-1}$ by a peristaltic pump located near the eluate's point of efflux from the column. The Sephadex G-10 column was run under a head of pressure of approximately 100 cm of solvent.

All columns were loaded by removing the eluent from the top of the column until the nylon net of the sample applicator was no longer covered. Five to thirty mg of poly(l-lysine · HBr), which had been dissolved in 2-5 ml of eluent, were then layered on top of the sample applicator, and eluted into the column. When the net of the sample applicator was again dry 5 ml of eluent was layered on top of it and run into the column. After this chaser had been introduced into the bed of the column, more eluent was layered on top of the sample applicator net until the column was completely filled. The column was then sealed and connected to a reservoir of 0.01 M NaCl. Fluid from the column ran through a peristaltic pump and into a fraction collector which deposited approximately five ml aliquots of the effluent into preweighed tubes. The amount of fluid in each tube was determined gravimetrically. The approximate concentration of poly(l-lysine) in

each tube was determined by method I (section 4:4:1). No attempts were made to control the temperature of the column as room temperature usually remained within a five degree range.

Globular proteins were loaded and eluted through the column by the same procedures used for poly(l-lysine). Their relative concentration in the effluent was determined by a uviscan recording device which monitored the optical density of the effluent at 280 mμ.

4:4:4. Determination of Molecular Weights

Weight Average Molecular Weight: The polymer's weight average molecular weight, M_w, was determined by a low speed sedimentation equilibrium technique on a Beckman model E analytical ultracentrifuge. The polymer was prepared by dialyzing a poly(l-lysine) solution, with a polymer concentration of approximately 1 mg ml^{-1}, against three changes of 1.00 M NaCl over a three day period. After dialysis the polymer was placed in a two sector cell assembly and centrifuged at 20,407 RPM at 20.0 ± 0.1°C for 72 hours. Changes in polymer concentration in the cell were measured by interference optics, and recorded on photographic plates after 68 and 72 hours of centrifugation at full speed. Comparison of the interference fringe shifts with distance from the center of the rotor, x, in the photographs at 68 and 72 hours showed the polymer to be at equilibrium. The molecular weight of the polymer was determined by the method of

DiCamelli et al. (201). The partial specific volume of poly(l-lysine) was estimated by the method of Cohn and Edsall (202) to be 0.82 ml gm^{-1}. Measurements of the fringe shift at regular intervals of x^2 were accomplished with a Gaertner microcomparitor by averaging duplicate measurements on the shift of three adjacent fringes at each interval. Calculation of the polymer's weight average molecular weight was made with a program supplied by Dr. D. A. Rigas, of the University of Oregon Health Sciences Center.

Number Average Molecular Weight: The number average molecular weight of the polymer was determined by membrane osmometry with a Mechrolab 502 high speed membrane osmometer. The polymer was prepared by dialyzing 527 mg of poly(l-lysine · HBr) against 4 liters of saturated NaCl for two weeks. The dialysis fluid was changed every 48 hours. Analysis of the dialysate on Sephadex G-75 indicated that only the low molecular weight contaminant was removed from the sample. Preliminary testing of the membrane osmometer showed it to work poorly when saturated NaCl was used as a solvent, and so the poly(l-lysine) solution was dialyzed against 5.00 M NaCl for one month. The NaCl solution was changed at least four times during this period. Following dialysis, an aliquot of the 5.00 M NaCl was filtered through a medium grade sintered glass filter, to supply a reference solvent for the osmometer.

The dialyzed polymer solution was filtered through a medium grade sintered glass filter and diluted to a volume of 40 ml. An aliquot of this stock solution was removed and analyzed in triplicate for poly(l-lysine) concentration by method III (section 4:4:1). Aliquots of the stock solution were diluted to produce several poly(l-lysine) solutions with concentrations of approximately 0.2, 0.4, 0.6 and 0.8 that of the stock solution. The concentration of each poly(l-lysine) solution, relative to that of the stock solution, was determined gravimetrically.

The membrane osmometer's ability to measure osmotic pressures correctly was checked by determining the molecular weight of a dextran of known molecular weight. All osmotic pressure measurements were made with a Schleicher and Schuell B-19 Selectron membrane in a constant temperature room at 19.2 ± 0.1°C. Thermal equilibrium of the polymer solution was ensured by equilibrating them overnight in the constant temperature room. The osmotic pressure of a given polymer solution was determined by flushing and refilling the osmometer with one ml of the polymer solution and then allowing the osmometer to come to an equilibrium osmotic pressure. This procedure would then be repeated until consecutive osmotic pressure readings plateaued to within 0.01 gm cm^{-2}. This generally required four fillings, with each determination requiring an hour to reach equilibrium. After the osmotic pressure readings had reached a plateau the

procedure would be repeated with solvent to determine whether or not the reference pressure of the solvent had changed. If it had changed the measurement was repeated.

4:4:5. Viscometry

Determination of Flow Times: The initial steps in determining the flow times of a given fluid through a viscometer were of necessity involved with the preparation of the viscometer and the fluid. The viscometer had to be free of contamination, especially dust, and the fluid, homogeneous, free of contaminants and at thermal equilibrium.

The viscometer was cleaned by exposing its inner surfaces to a sulfuric acid and chromium trioxide cleaning solution for at least ten minutes before washing it with copious amounts of distilled water. After the viscometer had been rinsed with a minimum of five 50 ml washes of doubly distilled water it was rinsed with several washes of methanol and dried by aspirating filtered air through the viscometer. All air and cleaning fluids were passed through a Pyrex fine grade sintered glass filter directly into the viscometer. Repeated determinations of the flow times of distilled water indicated the heat evolved by this cleaning process did not induce hysteresis in the timing arm of the viscometer.

Fluids whose viscosity were to be determined were aspirated through a medium grade sintered glass filter into a tube which had

been cleaned by sulfuric acid-chromium trioxide cleaning solution. When the fluid had been aspirated into the tube the aspiration tube was clamped and removed from the vacuum source. When atmospheric pressure had been reached inside the tube, by diffusion of air through the filter, the filter was removed. This procedure minimized the risk of contamination by dust. Fluid was delivered into the loading or timing arm of the viscometer with a pipette or a syringe.

After the fluid had been placed in the large arm of the viscometer, all of the arms were covered with small beakers and the viscometer was placed in a constant temperature bath, at 25.00 ± 0.01°C, for at least 20 minutes to reach thermal equilibrium. The presence of the beakers kept the viscometer from being contaminated by atmospheric dust. The viscometer could be reproducibly positioned in the water bath by placing the glass alignment guide on the side of the loading arm in the alignment slot of the holding clamp. When thermal equilibrium had been attained, the beakers on the small arms of the viscometer were removed and the fluid aspirated into the timing arm of the viscometer. This was accomplished by placing a small rubber tubing on the timing arm and aspirating while the loading arm was sealed by a finger tip. When a sufficient amount of fluid had been pulled into the timing arm, suction was stopped and the seal on the loading arm broken. The rubber tubing was removed, the beakers replaced, and the length of time for the fluid to pass between the fiducial marks

determined. This procedure was repeated until three successive readings, whose values did not deviate by more than 0.1 percent of the mean from their mean were obtained. The average of these three readings were considered the flow time for that fluid.

Calibration of the Viscometer: Sucrose solutions were used as calibration standards as their viscosities are accurately known and their surface tensions are similar to those of aqueous poly(l-lysine) solutions (160). The low surface tension of benzene and other organic solvents made them unsuitable for calibration fluids, for in comparison with aqueous solvents, organic fluids dissipate a smaller percentage of their potential energy in changing the area of their liquid-solid interface when their flow time is determined. Thus, organic fluids pass through a capillary viscometer more quickly than would a solution with an equal viscosity but greater surface tension. All calibration solutions, 0.000, 5.000, 10.000 and 20.000 %(w/w) sucrose solutions were made up by weight and their flow times determined at 25.00 ± 0.01°C. Reagent grade sucrose was used and was stored from the day of purchase to the day of use in a vacuum desicator. The flow times of the sucrose solution were then fitted to the following equation with a linear regression analysis:

$$\frac{\nu}{t} = \frac{\bar{B}}{t^2} + \bar{A} \qquad 4\text{-}30$$

where ν and t are the kinematic viscosity, in centistrokes, and

average flow time of the sucrose solution. The constant $\bar{A}$ is a proportionality constant relating the flow time of a fluid in the viscometer to its kinematic viscosity and $\bar{B}$ is a correction term, primarily for the kinetic energy of the solution on its efflux from the timing arm of the viscometer. The values of $\bar{A}$ and $\bar{B}$ derived from the linear regression analysis are $(4.64876 \pm 0.00001) \times 10^{-3}$ cm^3 sec^{-2} and 1.2725 ± 0.0007 cm^2 respectively.

Determination of Limiting Viscosity Number: The determination of poly(l-lysine)'s limiting viscosity number at a given salt concentration was started by dissolving 35 to 200 mg of poly(l-lysine · HBr) in 3-5 ml of the appropriate solvent and dialyzing it by the procedure given in section 4:4:2. No attempt was made to buffer the poly(l-lysine) solution as the reduced viscosity of the polymer does not change with pH below a pH of 7 (142). After dialysis the polymer solution was filtered through a medium grade sintered glass filter which had been cleaned with a sulfuric acid-chromium trioxide mixture. The filtered polymer solution was then taken up in a disposable plastic syringe which had been thoroughly rinsed with filtered solvent. It was then deposited into the preweighed and dried viscometer, through the timing or cleaning arm. The quantity of solution deposited in the viscometer was determined gravimetrically. After the viscometer had been placed in the water bath for a minimum of twenty minutes to attain thermal equilibrium the flow time of the solution was determined.

The viscometer was then removed, dried and reweighed. An aliquot of the filtered solvent was placed in the viscometer by the same procedure used before. The quantity of solvent deposited in the viscometer was again determined gravimetrically. The solution and added solvent were mixed with a magnetic stirbar which was permanently kept in the mixing chamber of the viscometer. The flow time of the new polymer solution was determined as before and the procedure was repeated until the flow times of four different polymer concentrations had been determined. At the end of a run an aliquot of the solution was removed and the concentration of polymer determined by method III (section 4:4:1). pHydrion paper determinations of the pH of the poly(l-lysine) solution at this time always indicated a pH of less than 6.

When three or more experiments of this type had been determined, the average limiting viscosity number of the polymer solution was calculated by a linear regression analysis of the pooled reduced viscosity vs concentration data for that solvent.

4:5. Results

4:5:1. Gel Permeation Chromatography

Sephadex G-10: Figure 4-4 pictures the elution profile of poly(l-lysine · HBr) and alanine methyl ester on a 2.5 x 95 cm column of Sephadex G-10. The void volume of the column was 185 ± 5 ml. The larger peak in the figure represents the alanine methyl ester

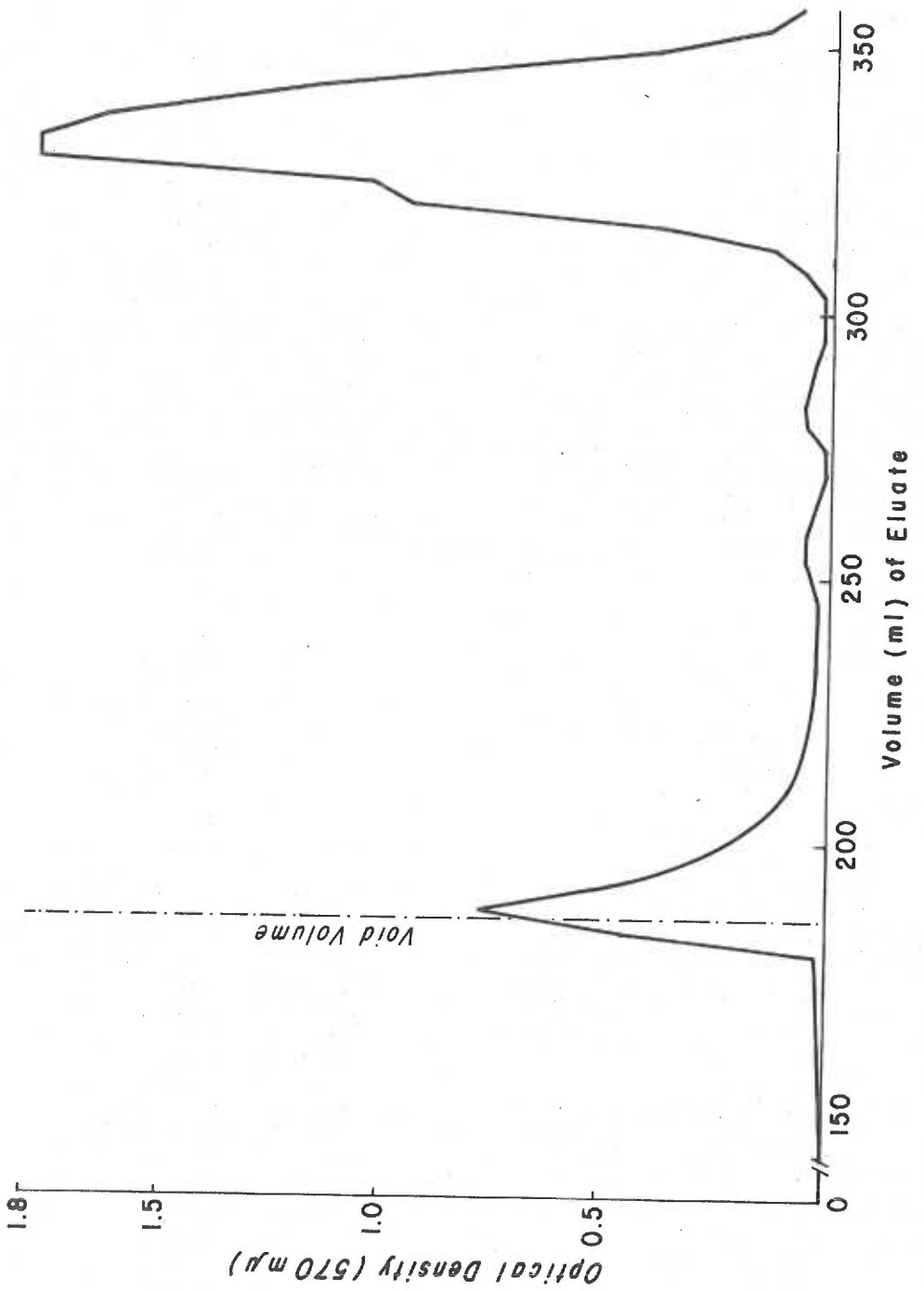

Fig 4-4 The elution profile of poly (l-lysine · HBr) (2.0 mg) and alanine methyl ester (1.0 mg) on a 2.5 x 95 cm column of Sephadex G-10. The solvent, 0.01 M NaCl, was eluted through the column under a head of pressure of 100 cm of solvent. The void volume of the column was 185± 5 ml.

sample and the smaller peak is the poly(l-lysine). The unimodal distribution of poly(l-lysine) in the column effluent indicates that both molecular weight components in the poly(l-lysine) sample have a molecular weight that exceeds 700, the size of the smallest molecule which is excluded from Sephadex G-10 beads.

Sephadex G-75: Figure 4-5 shows the elution profile of the globular proteins, aldolase, ovalbumin, chymotrypsin A and ribonuclease on a column of Sephadex G-75. The void volume of the column as determined by the half height of the leading edge of the aldolase peak was 70 ± 5 ml. A plot of $\log_{10}(M_n)$ vs the elution volume of the protein is plotted in figure 4-6 where the line drawn through the points represents the results of a linear regression analysis of the data. The elution volume of each protein was assumed to be given by the position of maximum optical density on the elution profile. The relationship between $\log_{10}(M_n)$ and elution profile as determined by linear regression analysis is:

$$\log_{10}(M_n) = (-1.1 \pm 0.2) \times 10^{-2} E_v + (5.89 \pm 0.22) \qquad 4\text{-}31$$

where E_v is the elution volume of the protein. The correlation coefficient of this analysis, -0.97, is a reflection of the column's ability to resolve the protein peaks.

The elution profile of the poly(l-lysine · HBr) sample on Sephadex G-75 is given in figure 4-7. The sample was well resolved into its

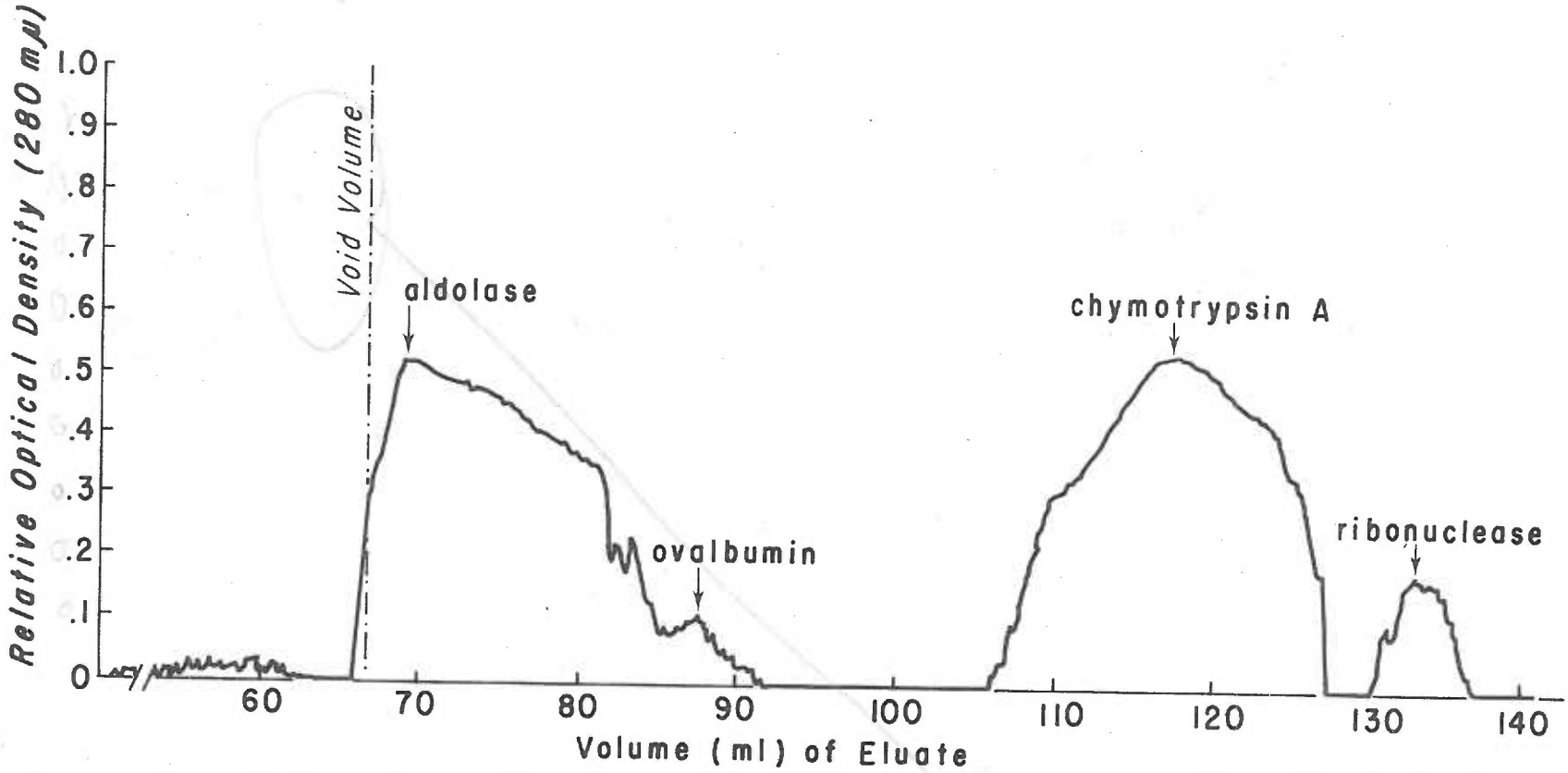

Fig 4-5 The elution profile of the globular proteins aldolase (12 mg), ovalbumin (5.2 mg), chymotrypsin A (6.7 mg) and ribonuclease (4.6 mg) on a 2.5 x 39 cm column of Sephadex G-75. The solvent, 0.01 M NaCl, was eluted through the column at a rate of 11.3 ml hr^{-1}. The void volume of the column was 70 ± 3 ml.

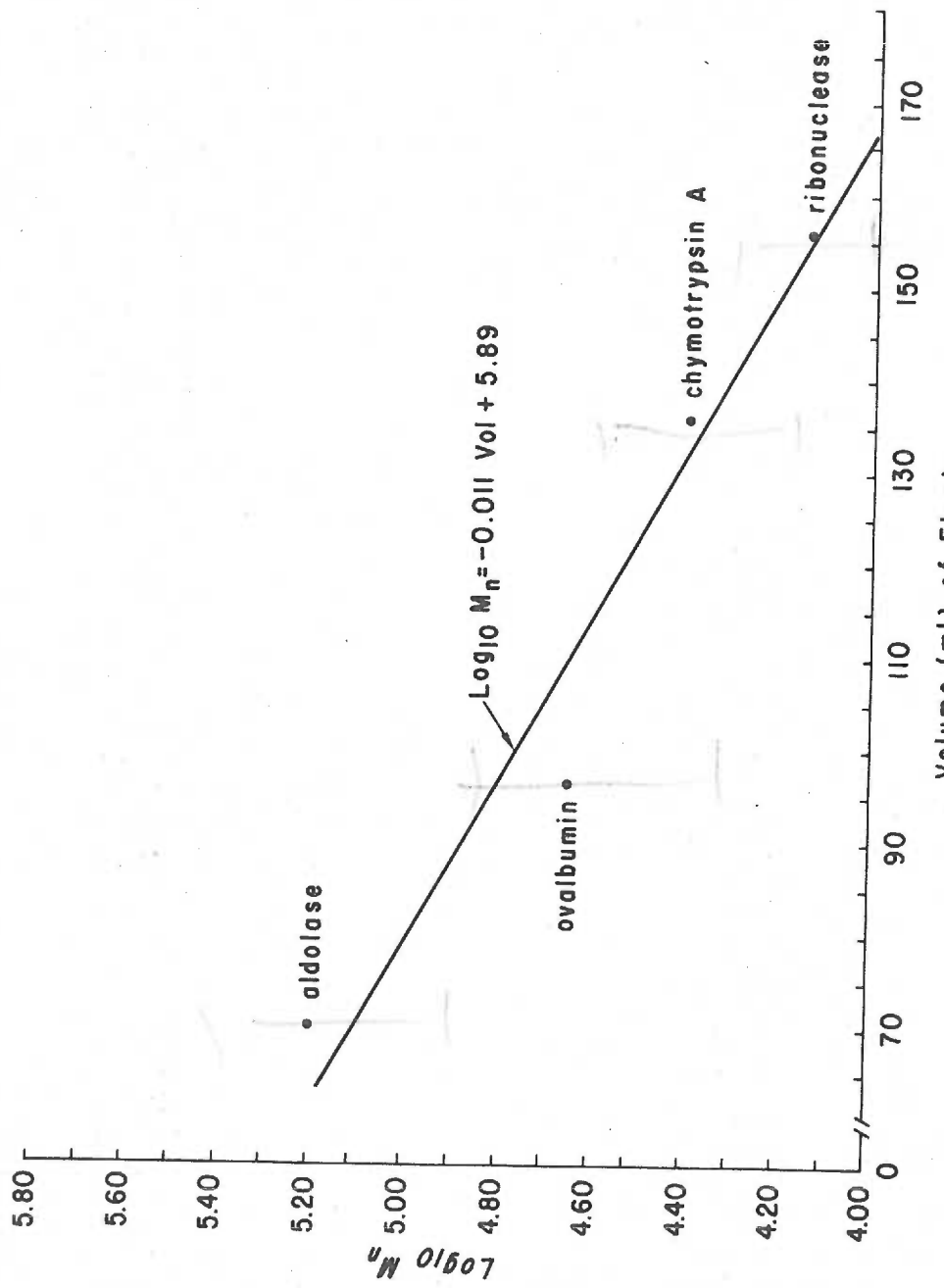

Fig 4-6 The relationship between the elution volume of a globular protein and $\log_{10}$ (M_n) on a 2.5 x 39 cm column of Sephadex G-75.

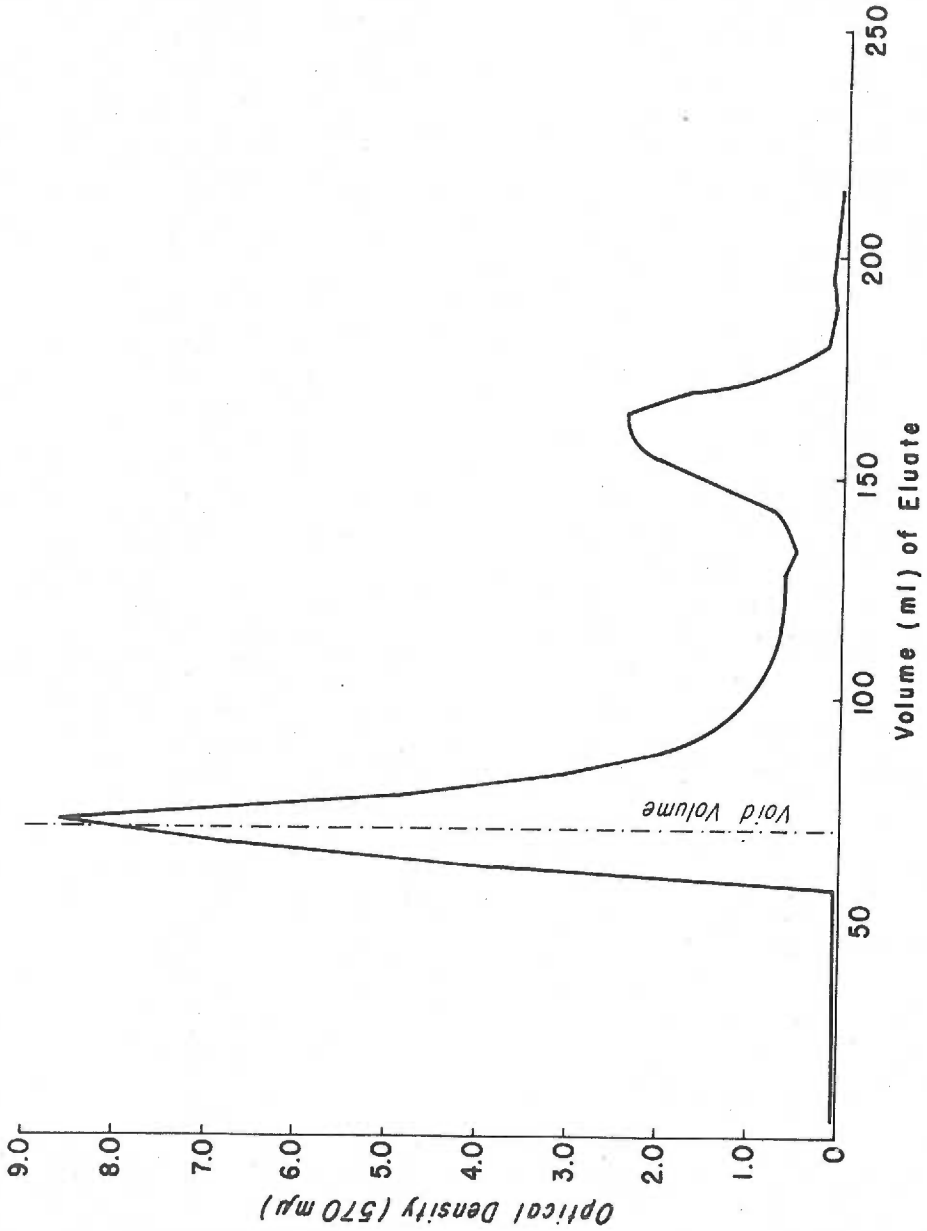

Fig 4-7 The elution profile of poly (l-lysine·HBr) (10.8 mg) on a 2.5 x 39 cm column of Sephadex G-75. The solvent, 0.10 M NaCl, was eluted through the column at a rate of 11.3 ml hr^{-1} . The void volume of the column was 70 ± 3 ml. Optical densities listed as being greater than 1.5 were obtained from the O. D. of the ninhydrin treated column effluent after it had been diluted by a factor of 10.

two component distributions with the large molecular weight component eluting in the void volume of the column. Thus, the radius of gyration of the larger component is greater than that of a dextran with a molecular weight of 50,000. Using the viscometric data of Wales et al. (203), and equation 4-27 with a value of 2×10^{-3} dl mole^{-1} Å^{-3} for Φ, $[r_g^2]^{1/2}$ for the larger component can be placed at ~ 75 Å or more. The smaller elution volume of the molecular weight component is slightly less than that of ribonuclease. Tanford (204) has reported that the hydrodynamic size of ribonuclease is approximately 20 Å. This estimate of the smaller component's size assumes that there is no attraction between the Sephadex gel and poly(l-lysine) or ribonuclease, and that the size of the ribonuclease molecule in 0.01 M NaCl is 20 Å.

Sephadex G-150: Figure 4-8 represents the elution profile of the poly(l-lysine) sample on the G-150 column. Both components of the polymer sample are fractionated by the column. Since G-150 fractionates dextrans in the molecular weight range of 1,000-200,000 Daltons, an upper limit of 135 Å can be placed on the polymer's radius of gyration, when it is in 0.01 M NaCl. This conclusion presupposes the absence of any attraction between the Sephadex gel and the poly(l-lysine) sample and that the size of dextran molecules can be calculated as before.

From the elution profiles of the polymer on the three different Sephadex gels it is apparent that the poly(l-lysine) sample had a

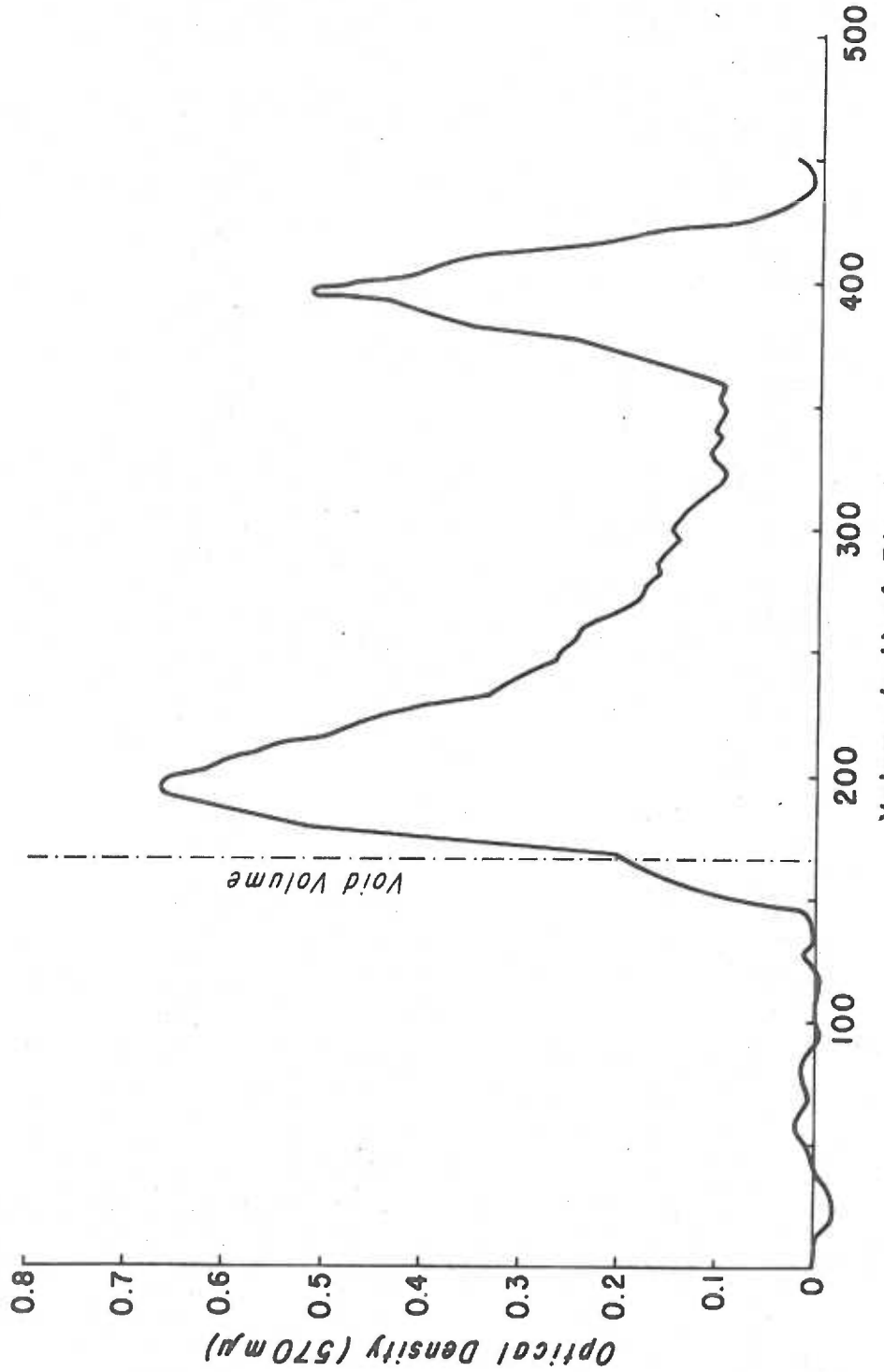

Fig 4-8 The elution profile of poly (l-lysine·HBr) (3.9 mg) on a 2.5 x 93 cm column of Sephadex G-150. The solvent, 0.01 M NaCl, was eluted through the column at a rate of 11.3 ml hr^{-1}. The void volume of the column was 167 ± 5 ml.

bimodal molecular weight distribution. If the polymer was not attracted to the Sephadex gels, the hydrodynamic radius of the smaller molecular weight component can be placed at less than 75 Å simply on the basis of the gels on which it was fractionated. The size of the smaller component can be more accurately estimated by comparing its elution volume with those of globular proteins of a known volume. This comparison was made on the Sephadex G-75 column and places the size of the smaller molecular weight component at about 20 Å. The radius of the gyration of the larger polymer can be placed between the limits of 75 Å and 135 Å on the basis of its elution properties on the Sephadex G-75 and G-150 columns.

4:5:2. Molecular Weight Averages

Number Average Molecular Weight: The reduced osmotic pressure of the poly(l-lysine) solutions are plotted against their concentration in figure 4-9. Linear regression analysis of the reduced osmotic pressure vs concentration data yields a y intercept and slope of 1.017 liter cm^{-2} and 3.62×10^{-2} liter^2 gm^{-1} cm^{-2} respectively. These coefficients correspond to a polymer molecular weight of $24,400 \pm 100$ gm $mole^{-1}$ and a second virial coefficient of $(1.46 \pm 0.04) \times 10^{-3}$ cm^3 moles gm^{-2}. The uncertainty terms correspond to the standard error of the linear regression coefficients as determined by the procedure listed in section 2:4:1. The Π/C_2 vs C_2

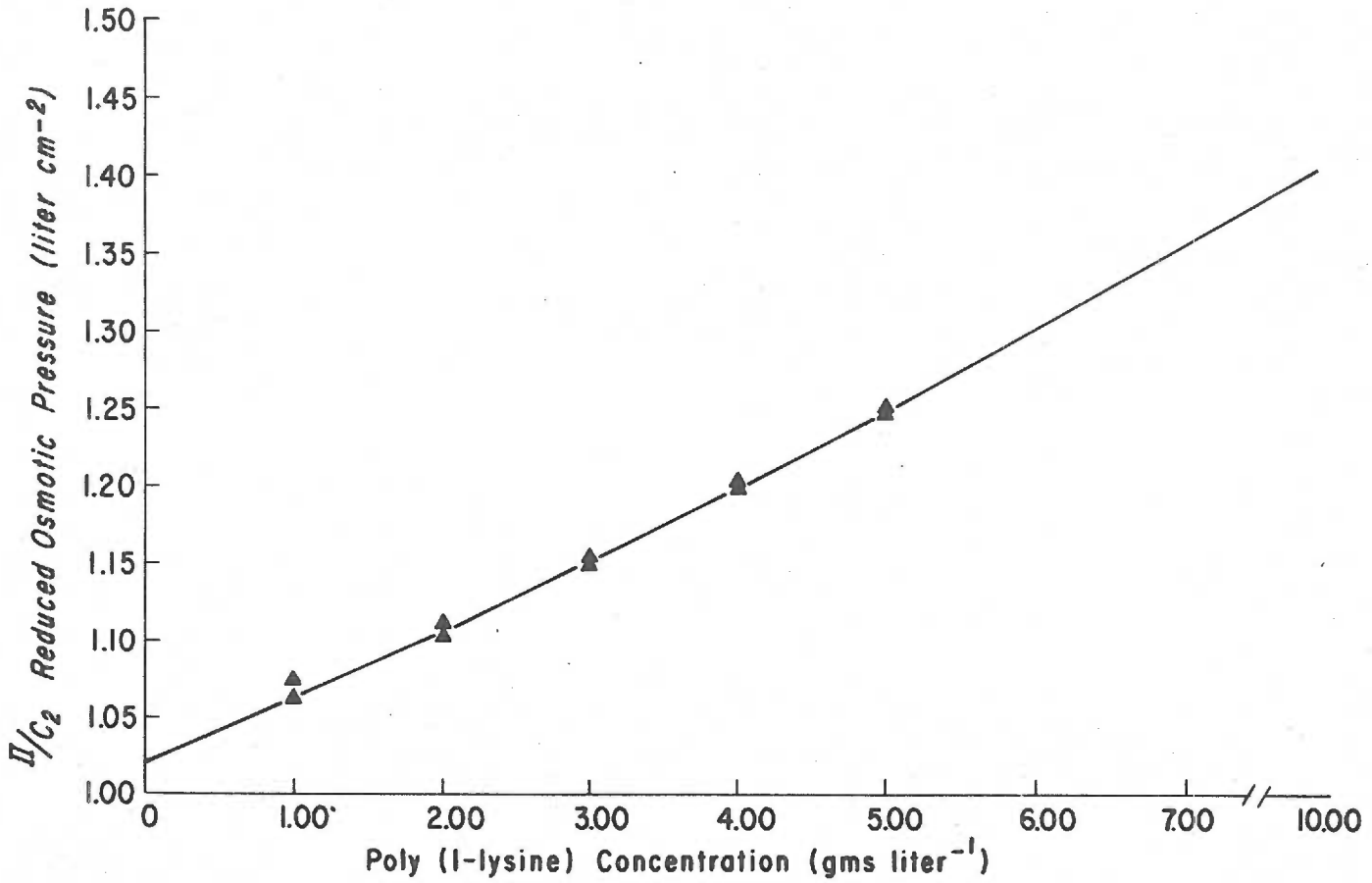

Fig 4-9 The reduced osmotic pressure of a poly (l-lysine) solution as a function of poly (l-lysine) concentration at 19.2 ± 0.1° C. The solid line represents a least squares fit of all the data but that of the lowest polymer concentration to the power series: $\Pi/C_2 = b_0 + b_1 C_2 + b_2 C_2^2$

data was also fitted to a second degree polynomial equation via the least squares analysis mentioned in section 2:4:1. The coefficients of the zero, first and second order terms of the power series, b_0, b_1 and b_2 were 1.031 ± 0.004, liter cm^{-2}, (2.70±0.28) x 10^{-2} $liter^2$ $cm^{-2}gm^{-1}$ and (1.2±4.7) x 10^{-3} liter $gm^{-2}cm^{-2}$ respectively. These coefficients were then used to calculate the g value of the polymer, from the relationship:

$$g = \frac{b_0 b_2}{b_1^2} = \frac{A_3}{A_2^2 M_n} \qquad 4\text{-}32$$

where A_2 and A_3 are the second and third virial coefficients of the polymer, respectively. The g value of a polymer can range from a value of 0 for polymers in theta solvents to theoretical maximum of 0.625 for solid spheres. The value of g can be regarded as a measure of the extent to which one polymer's center of gravity may approach anothers. For nonionic polymers g usually has a value of approximately 0.25. The value of g calculated from all the Π/C_2 vs C_2 data points is 1.73 ± 1.02. The reduced osmotic pressure of the poly(l-lysine) solution with the lowest polymer concentration was immediately suspect as the random errors associated with the determination of reduced osmotic pressures have their largest fractional value at low osmotic pressures. Thus, the value of the molecular weight, second and third virial coefficients of the polymer were recalculated from all of the reduced osmotic pressure-concentration

data but that of the solution with the lowest poly(l-lysine) concentration. The values of these parameters were 24,400 ± 200 gm $mole^{-1}$, (1.30±0.15) x 10^{-3} mole cm^3 gm^{-2} and (2.7±1.7) x 10^{-2} cm^6 mole gm^{-3} respectively. These parameters indicated that g had a value of 0.65 ± 0.44. This was taken as sufficient evidence for rejecting the data at the lowest poly(l-lysine) concentration and accepting the recalculated values of M_n, A_2 and A_3.

In that the number average molecular weight of this particular poly(l-lysine) has not been published, no comparison of M_n values is possible. However, Brandt and Flory (158) have published a value of 6.5 x 10^{-4} cm^3 mole gm^{-2} for the second virial coefficient of a poly(l-lysine) sample, with a number average molecular weight of 115,000. Although this value is nearly one-half that of the present study, their osmotic pressure measurements were done in 1.0 M NaBr at 37°C. Bianchi et al. (155) have investigated the relationship between the limiting viscosity number of a 150,000 Dalton poly(l-lysine) sample in 0.88 M KCl and KNO_3 solutions and temperature of the solution. Fitting their data to a linear regression analysis of $[\eta]$ vs T yields:

$$[\eta]_{KCl} = -5.3 \times 10^{-3} T + 1.03 \qquad 4\text{-}33$$

$$[\eta]_{KNO_3} = -2.4 \times 10^{-3} T + 0.77 \qquad 4\text{-}34$$

where $[\eta]_{KCl}$ and $[\eta]_{KNO_3}$ are the limiting viscosity numbers of the polymer in KCl and KNO_3 respectively, and T is the temperature

of the solution in degrees centigrade. From equations 4-27, 4-28, 4-33 and 4-34 it can be shown that in the presence of KCl and KNO_3 salts the second virial coefficient of poly(l-lysine) decreases by a factor of approximately 30 and 15 percent respectively when the temperature of the solution increases from 19.2 to 37° C. Thus, if bromide ions produce a similar change in the second virial coefficient with temperature, the observed value will still be approximately 20 percent greater than the value observed by Brandt and Flory. When the differences in polymer size and the unknown binding capacity of the bromide ions are considered this discrepancy is not unexpected.

No measurements of poly(l-lysine)'s third virial coefficient were found in the literature. However, the g value of a number of polyelectrolytes has been shown to be close to the maximum of 0.625. Thus, the observed value of 0.65 ± 0.44 is acceptable.

Weight Average Molecular Weight: M_w was calculated on the basis of the method developed by DiCamelli (201) with a program supplied by Dr. D.A. Rigas. The program calculated a weight average molecular weight of 31, 300 ± 100 for the polymer from measurements of the average fringe shift at regular intervals of x^2. A plot of the average fringe shift at regular intervals of x^2 after being sedimented for 72 hr in 1.00 M NaCl is given in figure 4-10. Examination of this plot shows it to curve upwards which is indicative of a deviation from thermodynamic ideality. In systems where non-ideality exists

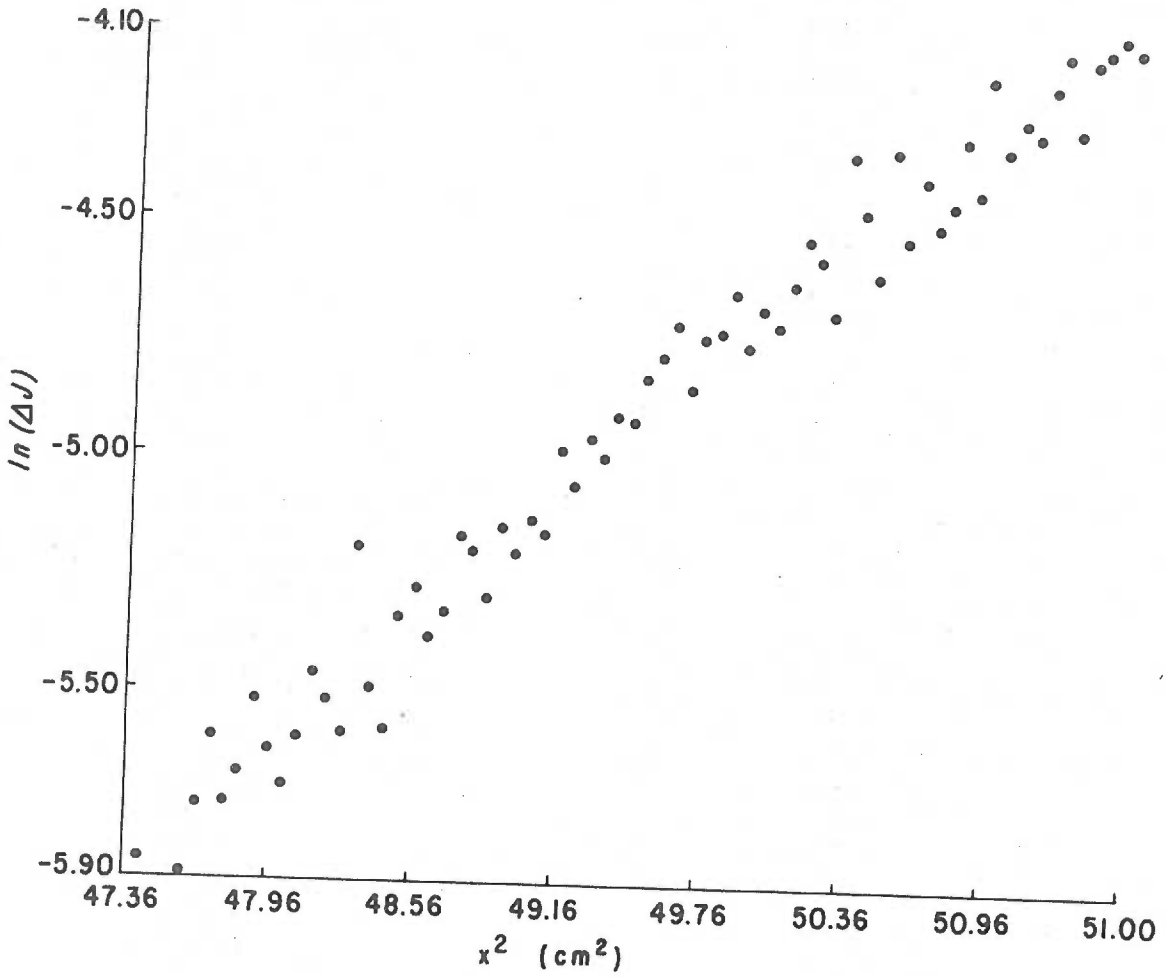

Fig 4-10 The logarithm of the fringe shift, Δ J, at regular intervals of x^2 for a dialyzed sample of poly (l-lysine) in 1.00 M NaCl at 20° C. The correlation coefficient, slope and y intercept of the least squares fit on a straight line through the data are 0.98, 0.187 and -11.4 respectively.

the apparent molecular weight of the solute will be dependent on its concentration in the centrifuge rotor, and estimates of the molecular weight of the solute will be less than their true value. Mijnlieff (205) has developed a complex theory relating the true molecular weight of a polymer to its observed value when the polymer solution is non-ideal. However, his theory cannot be readily applied as many of the parameters mentioned in it are not readily obtained and it is usually easier to experimentally alter the solvent until the polymer-solvent system exhibits thermodynamic ideality. For polyelectrolytes, this requires a reduction in their degree of ionization or an increase in the ionic strength of the solvent. Unfortunately uncharged poly(l-lysine) was not soluble in a variety of solvents and an attempt to determine the molecular weight of the polymer in 5.00 M NaCl proved unsuccessful as the density of the solvent kept the polymer from sedimenting at an acceptable rate. An alternative method for determining M_w for poly(l-lysine), involving the carbobenzoxylation of the polymer, has been outlined by Yaron and Berger (206), but because of limitations in time and material, measurement of the polymer's molecular weight in 1.00 M NaCl was used to obtain the present value of 31,300 for M_w. This estimate is reasonably close to the manufacturer's estimate of 33,000. However, it was not possible to determine whether or not the low molecular weight peak was present when the manufacturer estimated the molecular weight of the polymer. This was done by determining the molecular weight of the poly(l-lysine)'s parent compound

poly(ε-carbobenzoxy-l-lysine). In that typical polymerization techniques yield unimodal molecular weight distributions it is likely that the low molecular weight contaminant was created by a random cleavage of the polymer's peptide backbone when the parent compound was decarbobenzoxylated. Thus, it is unlikely that the manufacturer's estimate included the low molecular weight contaminant.

Estimates of the error involved in measuring M_w for a non ideal solute are difficult to make without applying Mijnlieff's theory. Since M_w was determined only to produce an estimate of the range of molecular weights in the polymer sample, the effort involved in this procedure is not warranted.

The spread of molecular weights in the polymer as estimated by the ratio of M_w to M_n is 1.3 and as estimated by s, 13,000. Since the most statistically probable polymer distributions have a $M_w:M_n$ ratio of 2, the fractionated polymer has, by comparison, a narrow molecular weight distribution.

4:5:3. Polymer Size

Figures 4-11 through 4-15 represent plots of the $\ln \eta_{sp}$ vs polymer concentration at the different NaCl concentration tests where η_{sp} is the reduced viscosity of the polymer solution. The reduced viscosity of the polymer was calculated from the kinematic viscosity of the polymer solution and solvent rather than their

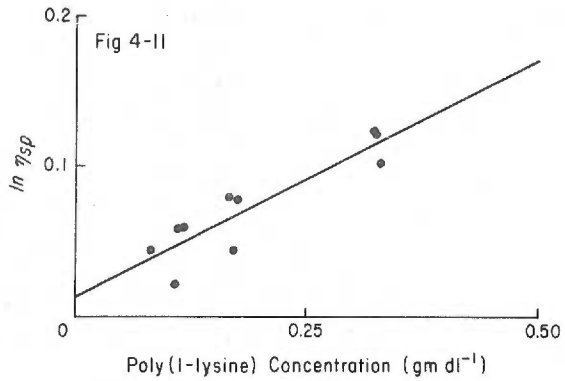
Fig 4-11
0.2
0.1
0
0.25
0.50
ln ηsp
Poly (l-lysine) Concentration (gm dl⁻¹)

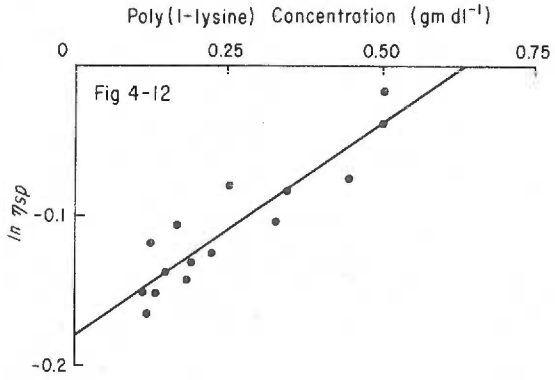
Poly (l-lysine) Concentration (gm dl⁻¹)
Fig 4-12
0
0.25
0.50
0.75
-0.1
-0.2
ln ηsp

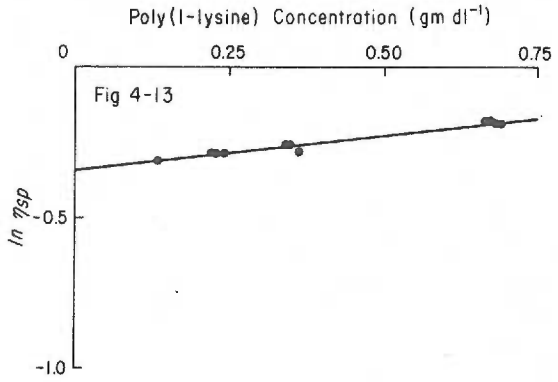
Poly (l-lysine) Concentration (gm dl⁻¹)
Fig 4-13
0
0.25
0.50
0.75
-0.5
-1.0
ln ηsp

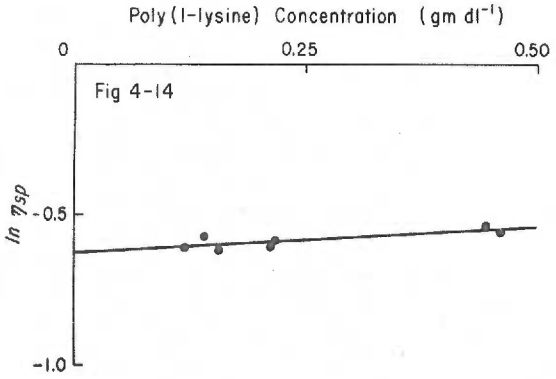
Poly (l-lysine) Concentration (gm dl⁻¹)
Fig 4-14
0
0.25
0.50
-0.5
-1.0
ln ηsp

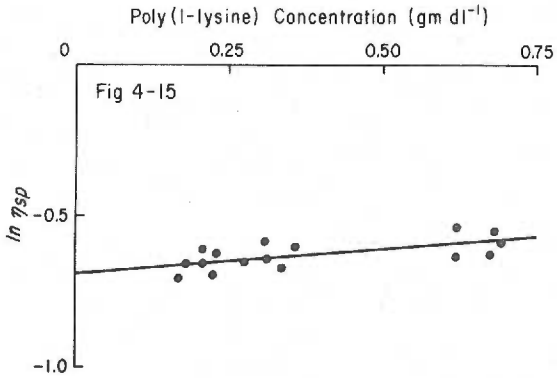
Poly (l-lysine) Concentration (gm dl⁻¹)
Fig 4-15
0
0.25
0.50
0.75
-0.5
-1.0
ln ηsp

dynamic viscosity as the difference between the density of the solvent and solution was negligible. Tanford (207) has demonstrated that this procedure is legitimate only in the case of linear polymers and should be avoided for globular proteins and other compact polymers. The limiting viscosity number was determined with a plot of $\ln \eta_{sp}$ vs C_2 rather than η_{sp} vs C_2 as Sakai (208) has shown this procedure to be the most reliable for polymers in good solvents. The concentration units of the polymer, gm dl^{-1}, are given in terms of the polymer and not in terms of its hydrobromide salt. In each figure the points represent the pooled data from 3 to 5 experiments performed at each ionic strength. The line drawn through them is the result of a linear regression analysis of the data. The error associated with the limiting viscosity number of the polymer and the slope of the reduced viscosity vs concentration curve were calculated by the procedure listed in section 2:4:1. The low correlation coefficients listed for the linear regression analyses are probably due to errors in the estimate of the polymer concentration in each run, as the correlation coefficients for individual determinations of limiting viscosity numbers always exceed 0.99. An alternative explanation for the low correlation coefficients is that particulate matter can lodge in the capillary tube of the viscometer at the start of an experiment and change its effective calibration constants. This would alter the apparent limiting viscosity number of the polymer and still yield a reduced viscosity vs concentration plot with a

high correlation coefficient. In view of the small variations in the flow times of the poly(l-lysine) solutions and the stringent procedures taken to clean the viscometer and keep it free from dust, this seems unlikely.

In figure 4-16 the limiting viscosity number of the polymer is plotted against the reciprocal of the square root of the salt concentration at which the limiting viscosity number was determined. The line drawn through the points was constructed from a linear regression analysis of the $[\eta]$ vs $C_3^{-1/2}$ data. The error associated with the slope and y intercept of this plot was calculated by the method given in section 2:4:1. Although, several investigators have noted that the relationship between $[\eta]$ and $C_3^{-1/2}$ which Pals and Hermans (198) propose is too simplistic and does not always hold, the correlation coefficient of the plot, 0.998, indicates the relationship is a good first approximation for this system. Thus, the relationship between $[\eta]$ and C_3 can be represented by:

$$[\eta] = (0.152 \pm 0.019) C_3^{-1/2} + (0.335 \pm 0.052) \qquad 4\text{-}35$$

where C_3 represents the molarity of the NaCl in the solution and $[\eta]$ is given in units of dl gm^{-1}.

The polymer's radius of gyration at 25°C in various concentrations of NaCl is given in figure 4-17, where the shaded area represents the range of values $[r_g^2]^{1/2}$ may assume. The value of $[r_g^2]^{1/2}$ at

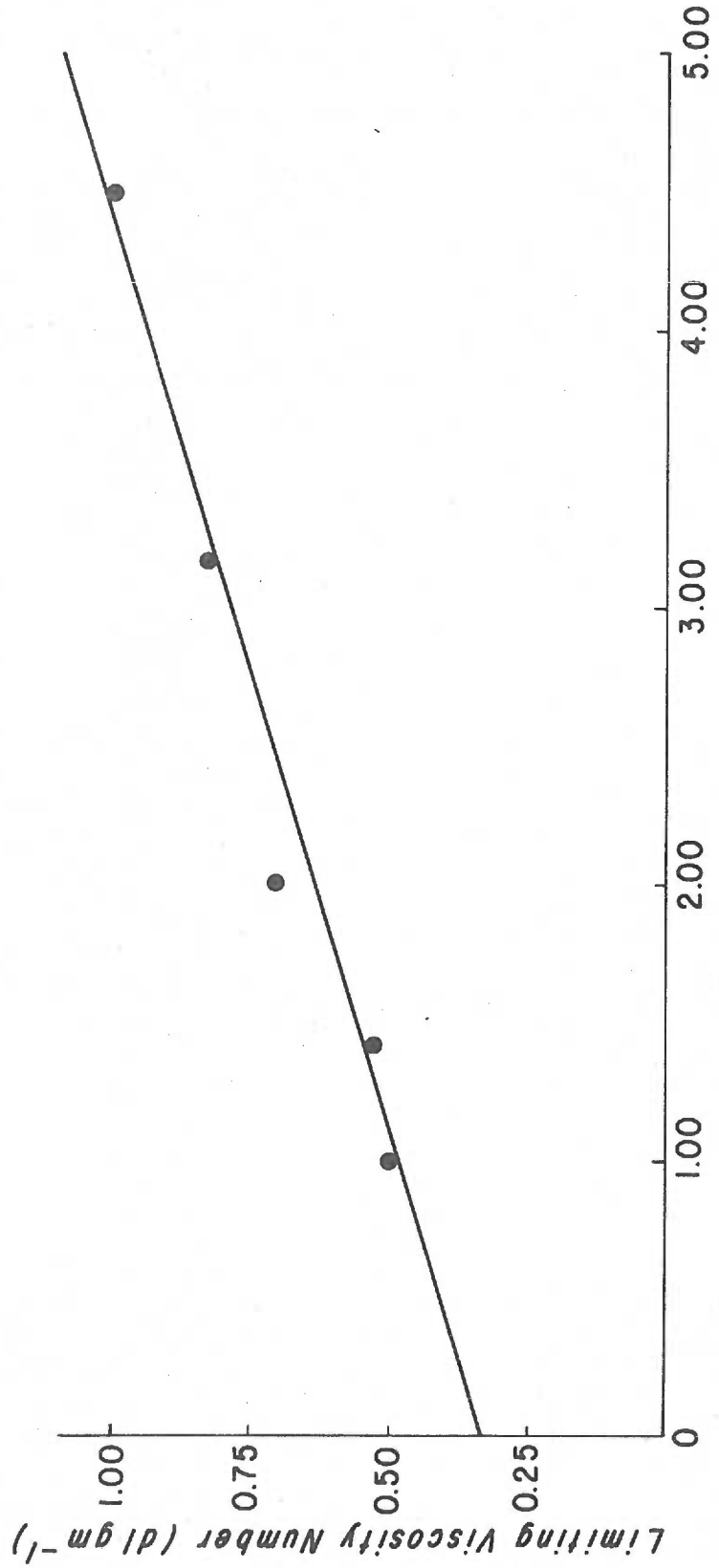

Fig 4-16 The limiting viscosity number of poly (l-lysine) at 25.00° C as a function of the inverse square root of the NaCl molarity.

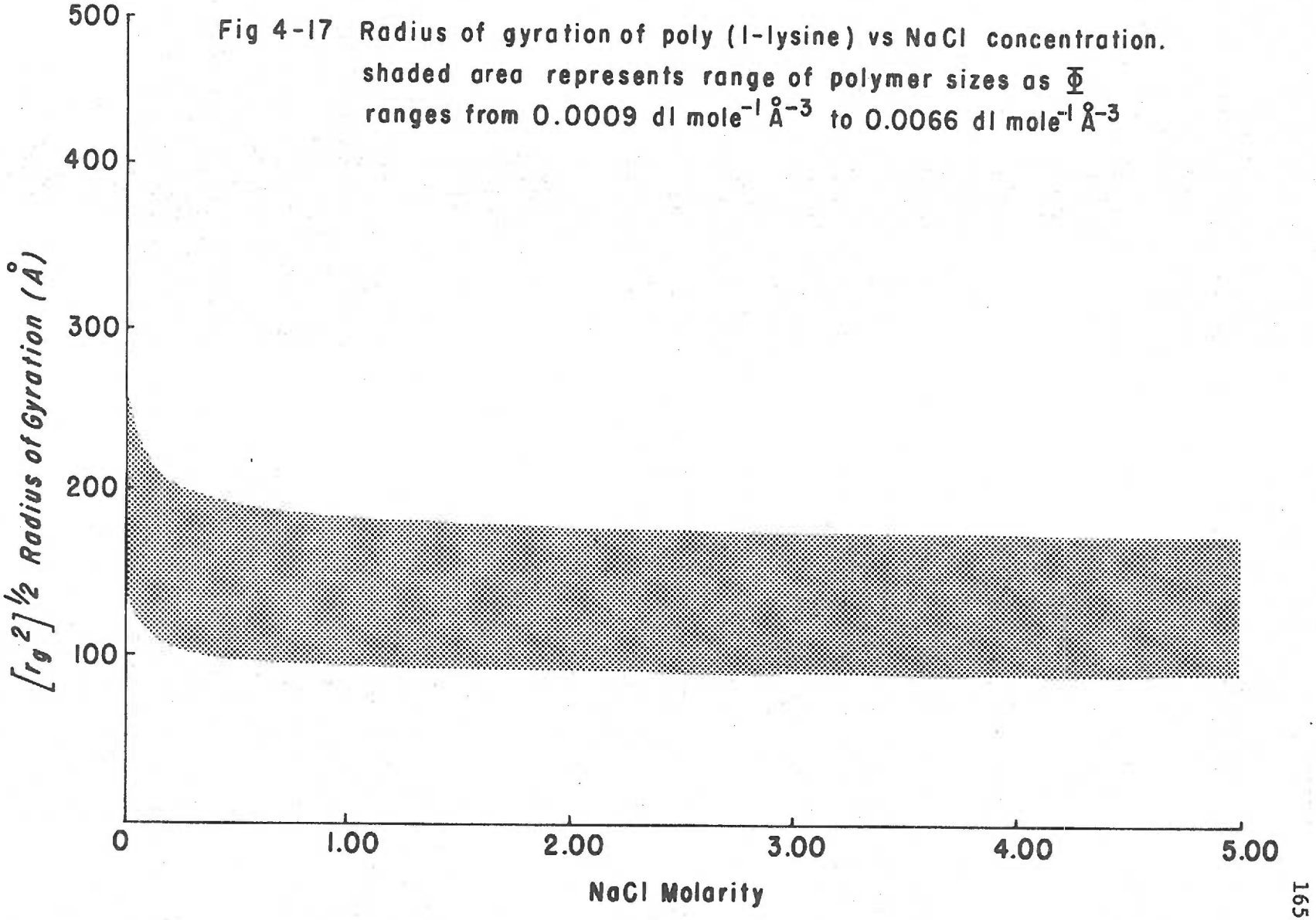

Fig 4-17 Radius of gyration of poly (l-lysine) vs NaCl concentration. shaded area represents range of polymer sizes as Φ ranges from 0.0009 dl mole^{-1} Å^{-3} to 0.0066 dl mole^{-1} Å^{-3}

various NaCl concentrations was calculated from equation 4-27, using equation 4-35 to calculate $[\eta]$ at the different salt concentrations. The shaded region in the figure represents the range of values $[r_g^2]^{1/2}$ may assume as Φ varies between its upper and lower limits of 6.6×10^{-3} to 0.9×10^{-3} dl mole^{-1} Å^{-3} (184).

5. ON THE INTERACTION OF POLY(L-LYSINE) AND POLYSTYRENE LATICES

The final portion of this work examines the rate at which a suspension of polystyrene latices aggregates when different amounts of poly(l-lysine) are adsorbed to the particles. From these data and measurements of the particle's electrophoretic mobilities, calculation of the free energy of interaction of two polymer covered particles will be made to reach a conclusion as to the mechanism by which a low molecular weight poly(l-lysine) aggregates a suspension of polystyrene latices.

5:1. General Properties

Polymer adsorption at liquid-solid interfaces has been studied extensively both theoretically (40-50, 209, 210) and experimentally (211, 212, 213). Reviews of the adsorption of polymers at liquid-solid interfaces have been given by Patat et al. (214), Ash (215), Kipling (216) and Rowland et al. (217). Much of the data concerning the adsorption properties of polymers, both in organic and aqueous solvents, has been generated by research on a vast range of medical and industrial problems concerned with the properties of polymer coated surfaces. The bulk of these studies have been made under conditions of relatively high surface coverage and despite the wide range of experimental conditions, polymers, solvents and adsorbent surfaces

the following generalizations can be made.

1) Polymers adsorb in a series of loops and trains. The average loop and train length is a function of the type of polymer, free energy of adsorption, solvent power and the regularity of binding sites.

2) Polymer adsorption is only slightly dependent on bulk polymer concentration. Adsorption isotherms rise very rapidly at low polymer concentrations and then tend to level off (64, 211).

3) On a weight basis, the amount of polymer adsorbed to an interface increases with the molecular weight of the polymer, up to a limiting molecular weight (212). Polymers having larger molecular weights are usually preferentially adsorbed at an interface, when in the presence of polymers of a lesser molecular weight (213, 218). Nestler (219) and Roe (97), however, have reported several systems where low molecular weight polymers are preferentially adsorbed.

4) Polymer adsorption may reach equilibrium in a period of time that may range from a few seconds to several weeks (220). Polymers with larger molecular weights usually require longer periods of time to reach equilibrium (213) and may never reach a configuration of lowest energy.

5) After a certain critical free energy of adsorption has been reached, usually a few tenths of a kT unit, the probability that

all the adsorbed segments of a large polymer will simultaneously detach is vanishingly small. Thus, strongly adsorbing high molecular weight polymers may irreversibly bind to a liquid-solid interface (1).

6) The temperature dependence of adsorption is small. Adsorption may be exothermic or endothermic and thus may increase or decrease with temperature (213).

The configuration of an adsorbed polymer layer has been treated theoretically by Silberberg (43), Hesselink (46), Hoeve (40) and a variety of other investigators who have used statistical mechanics to calculate the equilibrium configuration of the adsorbed polymer. Clayfield and Lumb (209, 210, 221, 222) and Lax (223, 224) have used computers to make Monte Carlo calculations of the most probable configurations of an adsorbed polymer. This technique does not demand that the polymer be at equilibrium and avoids a difficult mathematical treatment of the polymer's excluded volume. The configuration of several types of adsorbed polymer layers have been assessed by a number of techniques including ellipsometry (225), infrared spectroscopy (67) and viscometry (64). These techniques are difficult and as yet, the adsorbed configurations of only a few polymers have been characterized. Thus many of the current concepts of the configuration of adsorbed polymer layers are derived from a consensus of theoretical treatments which have only been partially verified. Some of the

common features of theoretical predictions concerning the equilibrium configuration of a single macromolecule adsorbed to a liquid-solid interface are:

1) There is a wide distribution of train and loop sizes available to the polymer.

2) The average loop and train length is controlled by the free energy of adsorption to the interface, when all sites on the adsorbent surface are capable of binding the polymer. Small adsorption energies favor larger loops and smaller trains while larger adsorption energies favor larger trains and smaller loops.

3) The percentage of polymer loops adsorbed to a surface increases rapidly with adsorption energy until a certain critical adsorption energy is reached. The percentage of polymer segments in a train configuration then increases very little with increasing adsorption energy.

4) The configuration of a polymer loop is controlled by the solvent-polymer interactions. In poor solvents the layer collapses and in better solvents it expands. The configuration of a polyelectrolyte loop is determined by a combination of electrostatic and polymer solvent interactions. At low and moderate salt concentrations the electrostatic interactions control the configuration of the polymer.

5) At high adsorption energies the bulk of the polymer is adsorbed and the thickness of the adsorbed layer is independent of the molecular weight of the polymer. At very low adsorption energies, where only a few segments of the polymer are adsorbed the thickness of the adsorbed polymer layer will be close to the dimensions of the polymer in free solution and therefore roughly proportional to the square root of the polymer's molecular weight.

When a polymer is added to a colloidal suspension the stability of the suspension is frequently altered. Since the stability of colloidal suspensions are determined by interfacial free energies, the effect of the polymer is a manifestation of the dominant free energies which lie in the adsorbed polymer layer. The various free energies associated with polymer layers were discussed in the introduction. The effect of certain types or combinations of interfacial free energies are readily apparent on examination of the mechanisms by which polymers alter the stability of colloidal suspensions.

When the interfacial free energies of an adsorbed polymer layer are large enough to decrease the total free energy of a two particle system, when the polymer layers of the particles overlap, the polymer acts as an aggregating agent. Reviews on the properties of polymeric flocculating agents have been given by LaMer and Healy (226) and Vincent (227). Although a number of interfacial free energies originate

in the polymer layer, aggregation may only be produced by one or more of the following:

1) Bridging: Large molecular weight polymers may simultaneously adsorb to two or more particles. This phenomenon was first proposed by Ruehrwein and Ward (228) and was later characterized by LaMer and coworkers (229, 230, 231, 232, 233). Bridging represents the primary mechanism by which neutral polymers aggregate particle suspensions. However, polyelectrolytes are also capable of flocculating particles by a bridging mechanism, regardless of the sign of the charges on the polyelectrolyte and particle (68).

2) Charge Reduction: Polyelectrolytes, having a charge whose sign is opposite that of the particle to which it adsorbs, will decrease the electrostatic repulsion between particles when adsorbed in small quantities. In theory, polyelectrolytes can be viewed as multivalent ions which rapidly supress the double layer and thereby cause aggregation by a reduction of the repulsive forces between the particles. However, simple charge neutralization due to the formation of ionic bonds must also account for much of the decrease in the electrostatic potential of the particle.

3) Enthalpic Destabilization: Napper and coworkers (234, 235) have noted that for at least 60 sterically stabilized dispersions,

the point of incipient instability for the dispersion occurs when the suspending medium becomes a theta solvent for the adsorbed polymer. At this point the second, and therefore the third virial coefficients of the polymer are zero. As the solvent becomes progressively poorer, the second virial coefficient turns negative and the polymer sheaths on the particles are rendered self attracting.

The free energies which are responsible for aggregating particles are dependent on polymer concentration and usually predominate only when moderate amounts of polymer are adsorbed. LaMer and Healy (226) postulated that neutral polymers were most effective in aggregating slimes when 50 percent of the binding sites on an unaggregated particle were used to bind polymer and the other 50 percent to bind polymers adsorbed to other particles. Polyelectrolytes also display a range of concentrations in which they reduce the electrostatic repulsion between particles to a level that a maximum aggregation rate is observed (64).

When the amount of polymer adsorbed to a particle exceeds a certain limit, the free energies which denote repulsive forces between the particles increase rapidly with greater polymer adsorption. When these free energies are large enough the polymer acts as a dispersant and stabilizes colloidal suspensions. The free energies which allow polymers to stabilize suspensions are:

1) Enthalpic Stabilization: When polymers are in the presence of good solvents, the heat of mixing two polymer layers is positive. Under these conditions, particles are stabilized by adsorbed polymers as large osmotic pressures are generated when the polymer layers of colliding particles overlap (62,66).
2) Entropic Stabilization: When the volume available to a polymer is decreased by the presence of another polymer or an impenetrable surface, the entropy of the polymer is decreased (59,61,221). When a large number of polymers are adsorbed to the surface of a particle, their collective decrease in entropy, on the collision of two particles, is often enough to prevent aggregation.
3) Electrostatic Stabilization: If the absolute value of the potential of a particle increases on the adsorption of a polymer, it will be electrostatically stabilized. Polyelectrolytes are very effective agents for stabilizing particle suspensions by this mechanism. However, neutral polymers may also increase the electrostatic potential of a particle by the Brooks' effect (55).

5:2. Theory and Selection of Methods

The only procedures which have not been previously discussed are those for mixing poly(l-lysine) solutions and polystyrene latex

suspensions and assaying ng ml^{-1} concentrations of poly(l-lysine).

5:2:1. Mixing

Fleer (64), Gregory (3) and other investigators have noted that the rate of polymer induced particle aggregation is dependent on the manner in which the polymer is mixed with the particles. When the polymer is mixed in a fashion that allows some particles to adsorb more polymer than others the rate of particle aggregation will be more rapid and variable from suspension to suspension, than particle dispersions which are uniformly coated with polymer.

The requirements for dispersing particles in a polymer solution are stringent, as the fluids must be mixed rapidly and in a manner that coats each particle with the same amount of polymer. Thus, the particles cannot be dispersed by methods which cause the particles to move through a zone of fluid containing the polymer or vice versa, as a nonuniform distribution of particle coatings will result. Low molecular weight polyelectrolytes which adsorb strongly and essentially irreversibly to particles are especially likely to coat particles in a nonuniform fashion. Thus, an optimal method of mixing polymer solutions and particle dispersions would produce a homogeneous suspension of polymer and particles before the polymer was allowed to adsorb onto the particles. After a homogeneous suspension had been achieved, adsorption would be initiated. This procedure should produce the most

uniformly coated particle suspension as it exposes each particle to the same amount of polymer.

Continuous flow mixing devices approach this optimal method as they sequentially expose the majority of the particles to the same amount of polymer. A number of these mixing devices have been developed for studies of the kinetics of rapid reactions (236). The simplest of the continuous flow mixers are made of glass Y joints or plastic blocks, which have a Y or T shaped channel drilled in them. Fluids are mixed when they are pushed into two arms of the Y shape channel at a high enough velocity to create turbulent flow of the liquids. In circular pipes, fluids exhibit several different types of flow patterns which can be characterized by a dimensionless number, R_e, the Reynold's number. When $R_e < 2100$ fluid flow is laminar and when $R_e > 10,000$, fluid flow is completely turbulent. When $2100 < R_e < 10,000$ the flow properties of the fluid are in a state of transition. The Reynold's number of a fluid can be calculated from the equation:

$$R_e = \frac{2a\bar{\rho}v_f}{\eta} \qquad 5\text{-}1$$

where a is the radius of the pipe, $\bar{\rho}$ the density of the fluid, and v_f its velocity in the pipe. Although Y type mixing chambers are adequate for a variety of mixing procedures, better mixing can be obtained with the more sophisticated jet type of mixers. These devices

are usually constructed from plastic blocks which have a cylindrical cavity drilled in them, where two fluids are mixed. The fluids are simultaneously injected into the cylindrical cavity from a series of holes or jets in the wall of the cavity that direct the fluids into the cavity at an angle that is almost tangential to the wall. This creates a swirling to the fluids and thereby mixes them. This type of mixer is capable of completely mixing two fluids within a period of several milliseconds. Thus, they are well suited to the present problem of combining two fluids which must be mixed rapidly and homogeneously but in a manner that exposes each particle to the same amount of polymer solution.

5:2:2. Adsorption Isotherms

The adsorption isotherm of poly(l-lysine) could be determined in a straight forward manner with the assays for poly(l-lysine) described in section 4:4:1. However, a determination of the free energy of interaction between two polymer coated particles requires a knowledge of the electrostatic potential of the particle and the amount of polymer adsorbed to the particle. Thus, a simple determination of poly(l-lysine)'s adsorption isotherm was complicated by the necessity of determining the electrophoretic mobility of the polystyrene latices after the amount of polymer adsorbed to the particles was known. The most sensitive assay of poly(l-lysine) described in section 4:4:1 could

measure only $\mu g\ ml^{-1}$ quantities of poly(l-lysine). Saturating quantities of poly(l-lysine) are in the range of ~0.1 $\mu g\ cm^{-2}$ (1). If the adsorption isotherm was to be determined with bulk poly(l-lysine) concentrations in the range of 0-10 $\mu g\ ml^{-1}$, particle concentrations would have to be on the order of 10^9 particles ml^{-1}. At these concentrations it seemed unlikely that a uniform coating of polymer would be obtained by the mixing method described in the previous section. Furthermore, particle aggregation at these concentrations would be rapid enough to interfere with electrophoretic mobility measurements. The only means meeting the requirements of the adsorption isotherm was to work at particle concentrations near 5×10^{-7} particles ml^{-1}. Radiochemical procedures or the electrophoretic assay described by Nevo and coworkers (1) were the only methods which seemed suitable for determining the poly(l-lysine) concentrations which would be used at these particle concentrations.

The operating principles of both methods are quite simple. The amount of radiolabeled poly(l-lysine) which adsorbs to a surface is determined from a knowledge of the polymer's specific activity and a measurement of the activity of the particles which have adsorbed the polymer. The electrophoretic assay, simply characterizes the electrophoretic mobility of an aliquot of a stock solution of polystyrene latices in 0.10 M NaCl after it has been mixed with an equal volume of 0.10 M NaCl having a known poly(l-lysine) concentration. The poly(l-lysine)

concentration of the calibration solutions are assessed by quantitatively diluting a poly(l-lysine) solution of known concentration. After the calibration curve has been established, the poly(l-lysine) concentration of an unknown 0.10 M NaCl solution may be determined by mixing it with an equal volume of the stock polystyrene latices and determining their electrophoretic mobility. The assay can only be used when the poly(l-lysine) is dissolved in 0.10 M NaCl at a pH of less than 8. Furthermore, the surfaces of all glassware or objects which come into contact with the unknown polymer solution, or the suspension of poly-(l-lysine) coated polystyrene latices must be scrupulously clean and saturated with an irreversibly adsorbed coat of poly(l-lysine).

5:3. Materials and Equipment

Harvard Syringe Drive: A Harvard dual infusion/withdrawal pump was manufactured by the Harvard Apparatus Company of Cover, Mass. and loaned by Dr. H.S. Mason.

Four Jet Mixer: A Lucite four jet mixer pictured in figure 5-1 was loaned by Dr. H.S. Mason.

Corex Centrifuge Tubes: 150 ml Corex centrifuge tubes were purchased from Corning Glassworks of Sunnyvale, California.

Tritiated Poly(l-lysine · HBr): A 200 mg sample of the poly(l-lysine · HBr) used in this study was tritiated by the Amersham-Searle Company of Arlington Heights, Illinois.

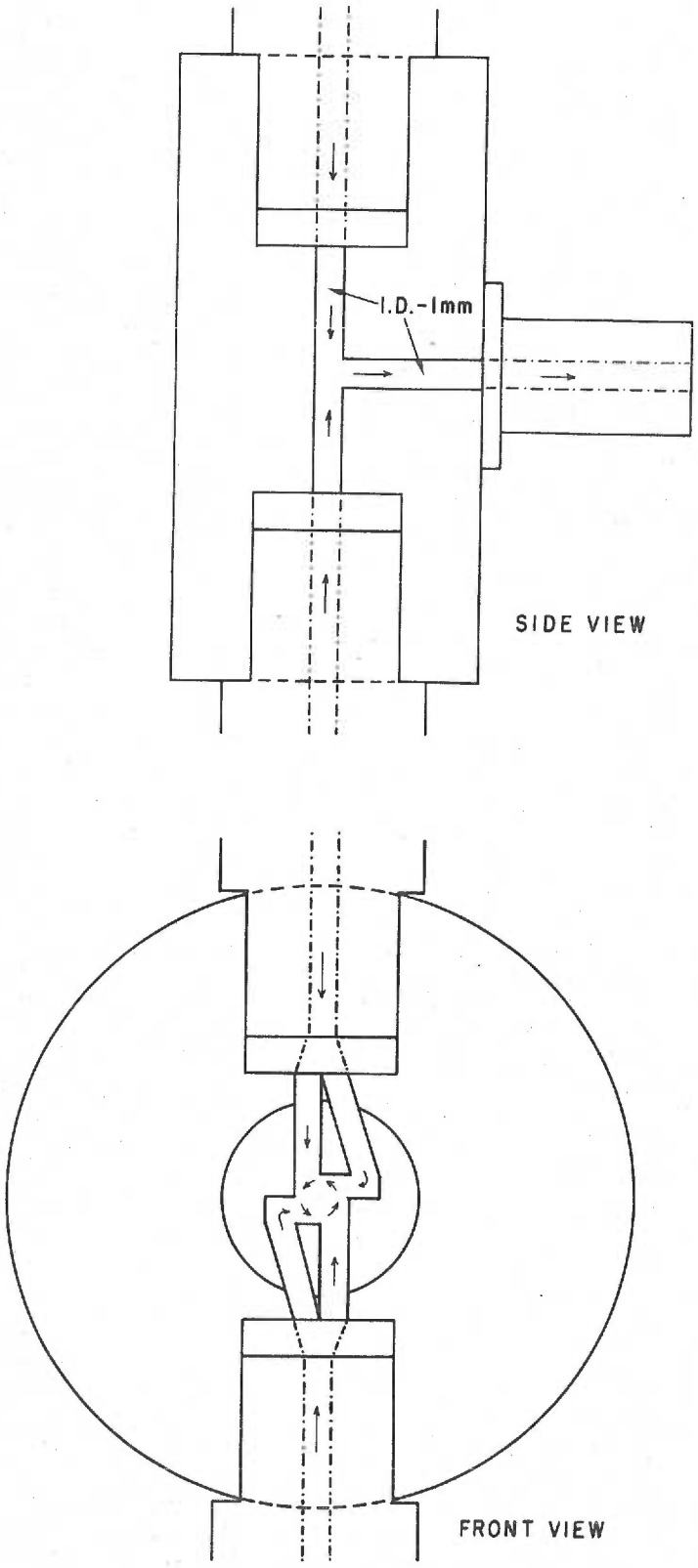

Fig 5-1 Diagram of a Four Jet Mixer

5:4. Methodology

5:4:1. Measurement of Aggregation Rate

A poly(l-lysine) solution was prepared by dialyzing a poly(l-lysine · HBr) sample against 0.10 M NaCl and then distilled H_2O as described in section 4:4:2. After dialysis the poly(l-lysine) solution was diluted and the concentration of this stock solution was determined, by method III of section 4:4:1, to be 56.6 ± 1.5 μg ml^{-1}. Six liters of a stock polystyrene latex suspension, suspension A, was prepared by the method described in section 3:4:1. After preparation the particles were kept in solution by continuous stirring. The particle concentration was measured at (1.05±0.03) x 10^8 particle ml^{-1}.

Typical aggregation experiments were initiated by making up a liter of 0.20 M NaCl containing between 0 and 3000 microliters of stock poly(l-lysine) solution. The poly(l-lysine) solution and an equal amount of polystyrene latex stock solution A were mixed by the method described in the following section (5:4:2) and the rate of aggregation determined by the method described in section 3:4:4. At the end of the aggregation experiment the electrophoretic mobility of the polystyrene latices was determined in a poly(l-lysine) coated electrophoresis chamber by the method described in section 3:4:5.

Two experiments were also performed to test whether or not the adsorbed poly(l-lysine) had reached an equilibrium configuration in the

standard aggregation experiments. In these experiments equal volumes of a poly(l-lysine) solution and a polystyrene latex suspension, with a concentration ~ 2×10^8 particle ml^{-1}, were mixed by the standard method (section 5:4:2) and allowed to equilibrate overnight. The poly(l-lysine)-polystyrene latex suspension was then mixed with an equal volume of 0.20 M NaCl and the rate of aggregation determined. The particles aggregated at the same rate as other suspensions whose particles had an equivalent electrophoretic mobility but had been mixed with poly(l-lysine) and NaCl by the standard method.

5:4:2. Mixing of Polystyrene Latices and Poly(l-lysine) Solutions

Two types of mixing devices were tested for their ability to uniformly coat the particles of a polystyrene latex suspension with poly(l-lysine). The effectiveness of the mixing devices was assessed by mixing equal volumes of a standard poly(l-lysine) solution and polystyrene latex suspension A and determining the coefficient of variation of the polymer coated particle's electrophoretic mobility. The standard poly(l-lysine) solutions (49.9 ng ml^{-1}) consisted of 60 ml of 0.2 M NaCl containing 50 microliters of the stock poly(l-lysine) solution.

The first mixing device used the throw of a drill press, to simultaneously depress the plungers of two 12 ml syringes containing the test fluids. Both fluids were driven into the arms polyethylene Y joint with an internal diameter of 0.2 cm. Fluid exiting from the

mixing device had a Reynold's number of approximately 500 which was not sufficient to produce turbulence. The coefficient of variation of the electrophoretic mobilities of the particles in the standard test mixture was 0.16 ± 0.04.

The second mixing device used a Harvard dual syringe drive to expell the polystyrene latex suspension and poly(l-lysine) solution from two 60 ml plastic syringes into a four jet mixing chamber. The syringe drive was run at a maximum rate of 1.1 cm sec^{-1} which caused the poly(l-lysine)-polystyrene latex suspension to exit from the mixing chamber at a rate of ~12 ml sec^{-1}. This mixing device reduced the aforementioned coefficient of variation to 0.05 ± 0.01.

5:4:3. Adsorption Isotherms

Poly(l-lysine) Adsorption vs Time: The time dependence of poly(l-lysine) adsorption was determined by mixing an aliquot of a polystyrene latex suspension A with an equal volume of a 0.20 M NaCl poly(l-lysine) solution by the method described in section 5:4:2 and determining the electrophoretic mobility of the particles at various times after mixing. The time dependence of polymer adsorption was tested at three different polymer concentrations. All adsorption isotherms were determined at room temperature, 23 ± 2° C.

Poly(l-lysine) Adsorption vs Bulk Solution Polymer Concentration. The first phase of the adsorption isotherm was concerned with the

development of an assay for detecting poly(l-lysine) concentrations in the range of 0-100 ng ml^{-1}. In an attempt to develop a radiochemical assay a sample of poly(l-lysine·HBr) was sent to the Amersham-Searle Company for tritium labeling. The tritiated polymer was received with a specific activity of approximately 0.1 millicuries mg^{-1}, a low but acceptable level for the detection of poly(l-lysine) in the ng ml^{-1} range. Unfortunately, the polymer had been degraded by radioautolysis and the technique had to be abandoned. An alternative assay was developed by a modification of the method used by Nevo and coworkers (1).

The calibration curve of the assay was established by determining the electrophoretic mobility of a stock polystyrene latex suspension after it had been mixed with an equal volume of a poly(l-lysine) solution of known concentration. Six liters of a stock polystyrene latex suspension, suspension B, were made up to a concentration of $(5.45\pm0.16) \times 10^{7}$ particle ml^{-1} by the procedure listed in section 3:4:2. The poly(l-lysine) solutions were made by placing 50 ml of 2.00 M NaCl and between 10 and 3000 microliters of the stock poly(l-lysine) solution (see section 5:4:1) in a 1 liter volumetric flask, and filling the flask to volume with distilled water. While the poly(l-lysine) solution was being stirred, equal volumes of polystyrene latex suspension B and 0.20 M NaCl were mixed with the four jet mixer and the Harvard syringe drive. Immediately thereafter this suspension and the

freshly prepared poly(l-lysine) solution were mixed by the same procedure. After the polystyrene latices had been exposed to the poly(l-lysine) solution for a minimum of 30 minutes at room temperature (23 ± 2° C), the electrophoretic mobility of the polystyrene latices was determined. This procedure was repeated at seven different poly(l-lysine) concentrations to establish the relationship between poly(l-lysine) concentration and the electrophoretic mobility of the polystyrene latices.

The adsorption isotherm was established by mixing equal volumes of a polystyrene latex suspension A and an 0.20 M NaCl solution with a known concentration of poly(l-lysine) in it. The two fluids were mixed at room temperature by the method described in section 5:4:2 and deposited into 150 ml ethanolic-KOH cleaned poly(l-lysine) coated Corex centrifuge tube. After a 30 minute incubation period the electrophoretic mobility of an aliquot of the polystyrene latices was determined. The remainder of the particles were removed from suspension by centrifugation at 14,000 x g for 20 minutes. The supernatant was used to rinse and partially fill a 35 ml plastic syringe. Another 35 ml plastic syringe was rinsed and filled with the polystyrene latex suspension B after it had been diluted with an equal volume of 0.20 M NaCl. When both syringes were connected to the four jet mixer, the contents of the two syringes were mixed with the Harvard syringe drive and the electrophoretic mobility of the resultant

suspension determined. From this electrophoretic mobility determination, the amount of polymer adsorbed to the particles of suspension A, and hence the adsorption isotherm could be established.

5:4:4. Cleaning of Glassware

All glassware and other objects which were to come into contact with the polystyrene latex suspension or the poly(l-lysine) solution were cleaned with the ethanolic-KOH procedure (section 2:3). Any materials which were to be in contact with the poly(l-lysine) solution were also equilibrated for a minimum of 10 minutes in a bath of the stock poly(l-lysine) solution which had been diluted tenfold with distilled water. The plastic disposable syringes, tubing and mixing device were exceptions to this procedure in that they were only exposed to the poly(l-lysine) solution. After exposure to the poly(l-lysine) solution, all materials were rinsed a minimum of ten times with distilled water. This procedure has been shown to leave a saturated, irreversibly adsorbed layer of poly(l-lysine) on glass (1).

5:5. Results

5:5:1. Adsorption Isotherms

Figures 5-2 through 5-5 present the various relationships between total poly(l-lysine) concentration, the extent of polymer adsorption and the electrophoretic mobility and zeta potential of each particle.

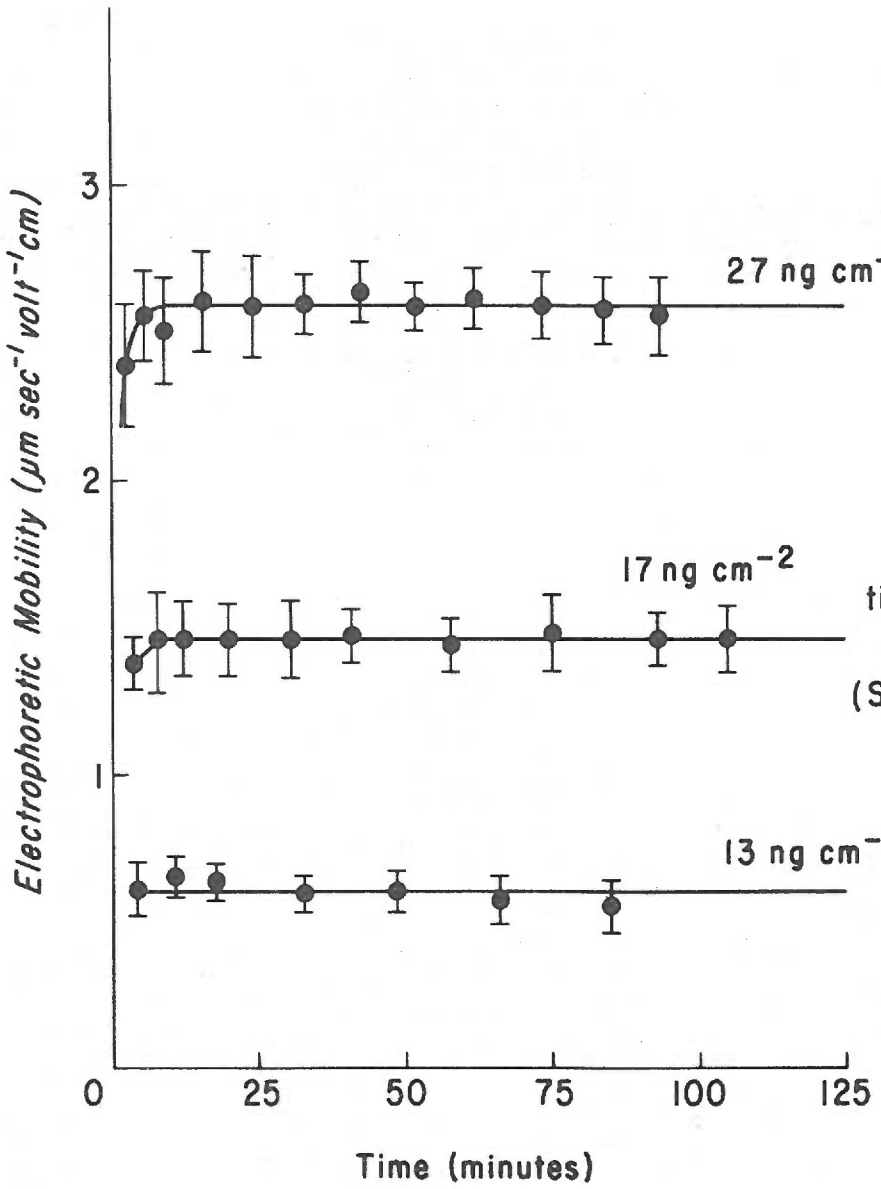

Fig 5-2
Electrophoretic mobility of
polystyrene latices
vs
time of exposure to poly(l-lysine) solutions
of different concentrations
(Surface Poly (l-lysine) Concentrations
of 27, 17 and 13 ng cm^{-2})

The relationship between the electrophoretic mobility of a particle and the length of time it has been exposed to a poly(l-lysine) solution is given in figure 5-2. The error bars represent the standard deviation of the electrophoretic mobilities of ten particles. The data presented in this figure indicates that polymer adsorption is essentially complete after the polymer and particles have been mixed for five minutes. The electrophoretic mobility of the particles does not decrease with time as is observed in the case of polyelectrolytes of a higher molecular weight (58, 91). This suggests that the polymer has reached an equilibrium configuration as it may be demonstrated that the zeta potential of a particle will depend on the distribution of charges in the adsorbed polymer layer (appendix IV). Furthermore low molecular weight polymers typically reach an equilibrium configuration in a rather short period of time.

Figures 5-3 and 5-4 depict the manner in which the electrophoretic mobility of polystyrene latices vary with total polymer concentration. The total concentration of a polymer in a suspension refers to the amount of polymer in solution plus the amount of particle bound polymer per unit volume of suspension. Bulk solution polymer concentration refers only to the amount of polymer in solution per unit volume of the suspending medium. Error bars in both figures represent the standard deviation of the electrophoretic mobilities of at least 20 particles. The polystyrene latex particle concentration in the

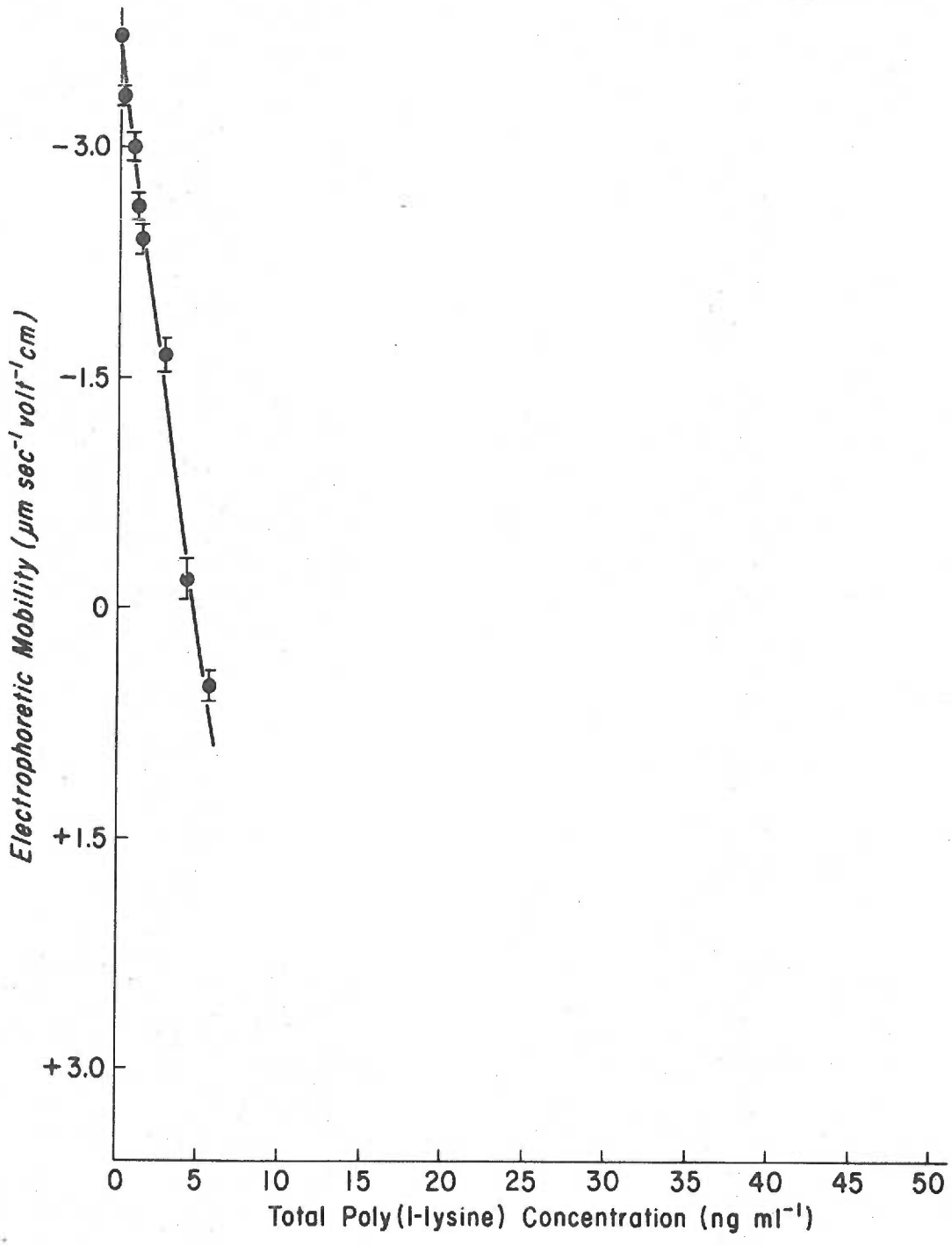

Fig 5-3 Electrophoretic mobility of polystyrene latices vs total poly (l-lysine) concentration. Polystyrene latex particle concentration is $(1.36 \pm 0.04) \times 10^7$ particles ml^{-1}.

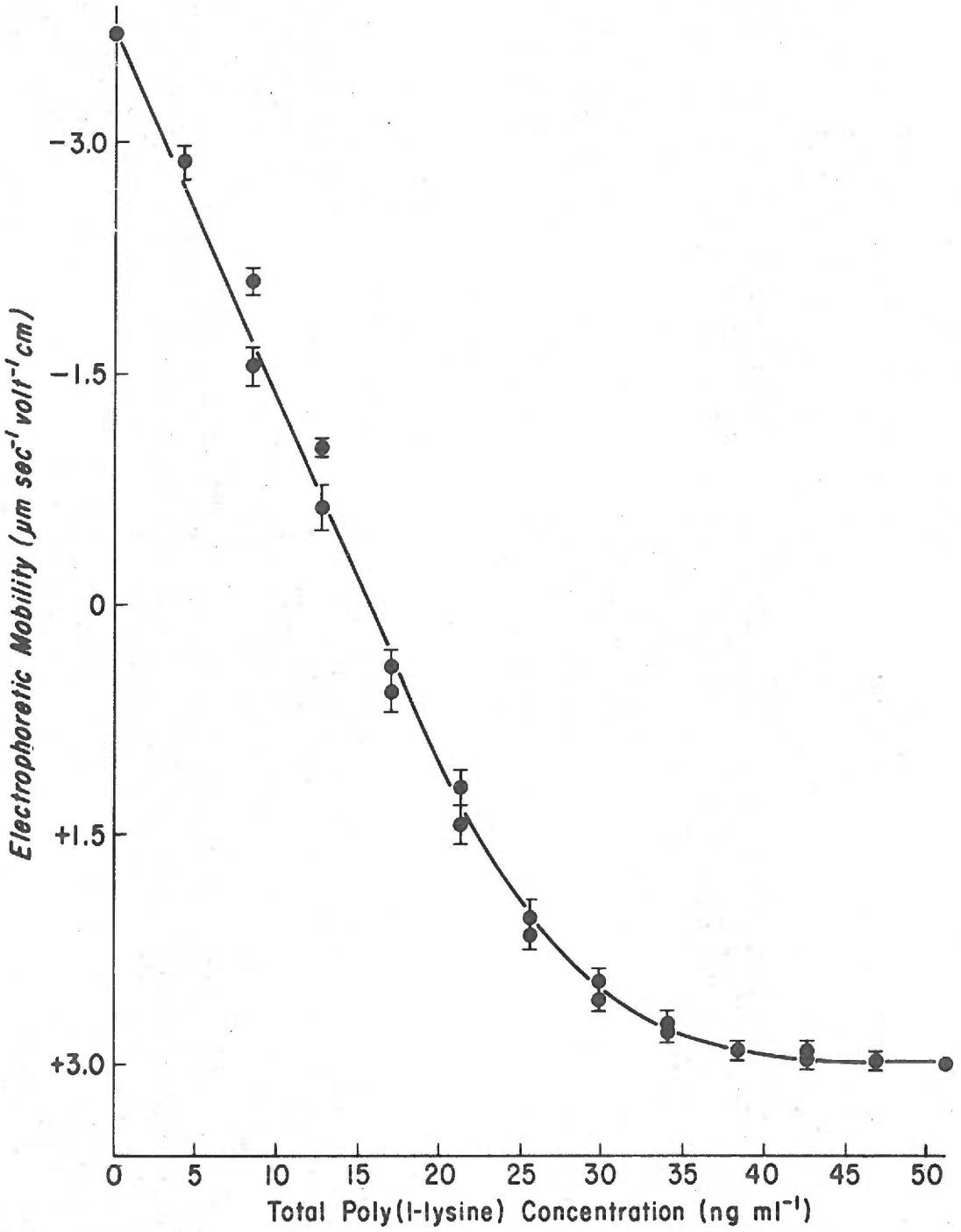

Fig 5-4 Electrophoretic mobility of polystyrene latices vs total poly (l-lysine) concentration. Polystyrene latex particle concentration is $(5.74 \pm 0.17) \times 10^7$ particles ml^{-1}.

solutions depicted by figures 5-3 and 5-4 are $(1.36\pm0.03) \times 10^7$ particles ml^{-1} and $(5.74\pm0.17) \times 10^7$ particles ml^{-1} respectively.

The data, presented in figure 5-3, was used to construct the calibration curve for the electrophoretic assay. Linear regression analysis of the data points indicated that when stock polystyrene solution B was mixed with an equal volume of 0.20 M NaCl and this suspension mixed with an equal volume of a 0.10 M NaCl-poly(l-lysine) solution, the electrophoretic mobility of the polymer coated particles was related to the total polymer concentration of the suspension by:

$$C_2 = (1.332\pm0.060)u_e + (4.810\pm0.151)$$

where the dimensions of C_2 are ng ml^{-1} and u_e, $\mu m\ sec^{-1} volt^{-1}$ cm.

The adsorption isotherm of poly(l-lysine) is presented in figure 5-5, where the amount of poly(l-lysine) adsorbed per cm^2 of the polystyrene-0.10 M NaCl interface is plotted as a function of total polymer concentration. A 12% error is associated with the adsorption isotherm. This uncertainty reflects the errors involved in estimating the total and solution polymer concentrations and particularly the surface area of the polystyrene latex suspension. As in the experiments of Nevo and coworkers (1), the polymer exhibits complete adsorption at low polymer concentrations. Total adsorption of the polymer ceases when the surface concentration of polymer reaches a level of $0.02\ \mu g\ cm^{-2}$. If the area of a lysine monomer is assumed to be

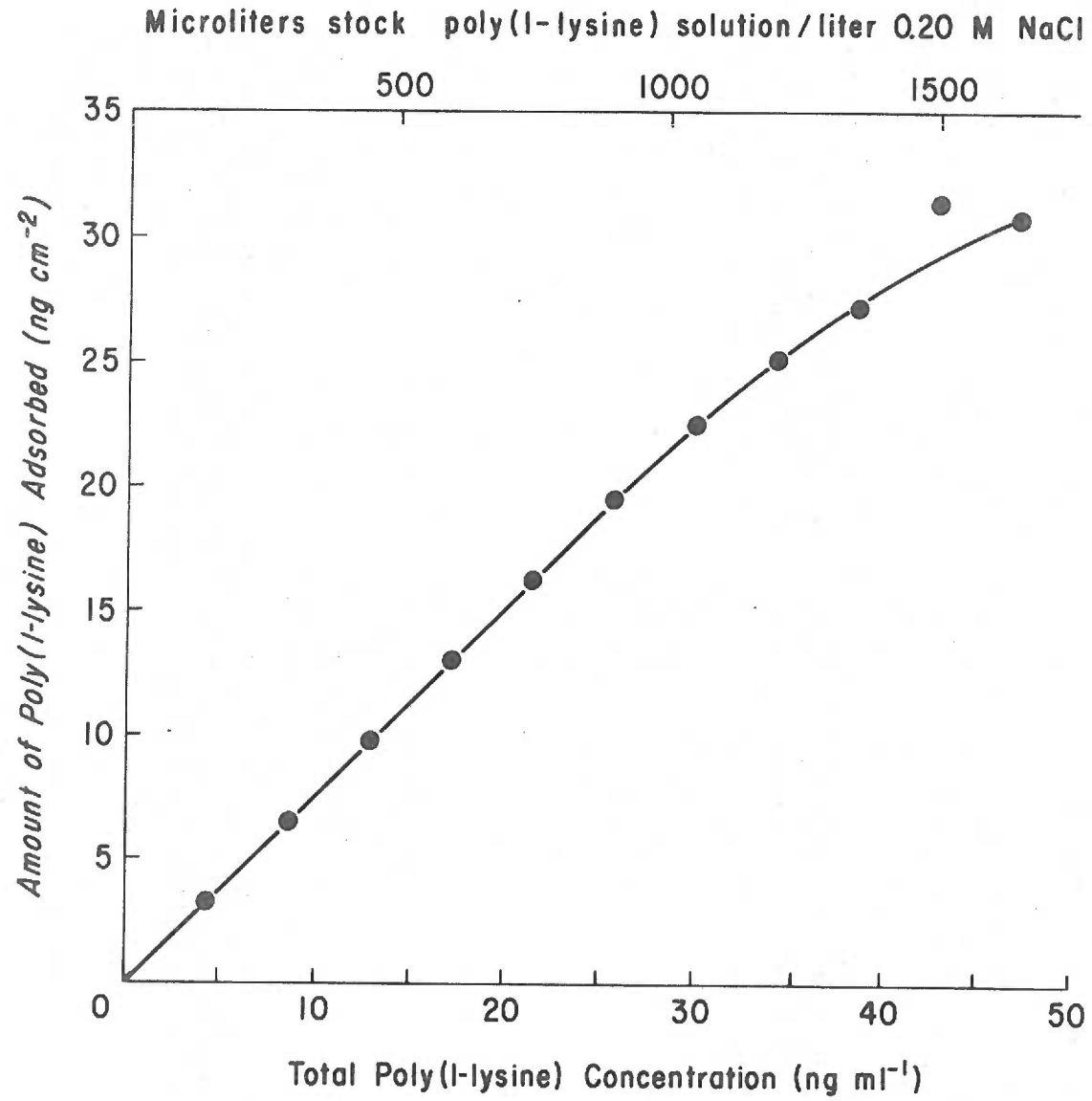

Fig 5-5 Poly (l-lysine) adsorption at the polystyrene – 0.10 M NaCl interface vs total poly (l-lysine) concentration.

approximately 60 $\mathring{A}^2$, as postulated by Nevo et al. (1), complete adsorption of the polymer from solution ceases when an amount of polymer that is sufficient to cover 50 percent of each particle's surface is present.

5:5:2. Aggregation Rate

The rate of polystyrene latex aggregation is plotted in figures 5-6 and 5-7 as a function of the electrophoretic mobility and zeta potential of the particles respectively. The error bars on the data points, equal the standard error of the rate constants, and the standard deviation of the electrophoretic mobility of the polymer covered particles. All rate constants in figures 5-6 and 5-7 have been adjusted to the value they would have at 20°C by the use of equations 1-3 and 1-4.

5:5:3. Theoretical Rate Constants

Calculations of the theoretical rate constants pictured in figure 5-8 show that the predicted rate of aggregation is always greater than the observed rate constant. An uncertainty of approximately 20% is associated with the theoretical value of W. According to the definitions of flocculation, coagulation and stabilization given in the introduction, this data shows that while poly(l-lysine) has reduced the charge on the particles it has not only failed to increase the rate of aggregation past the predicted rate, by a bridging mechanism but has stabilized the particle

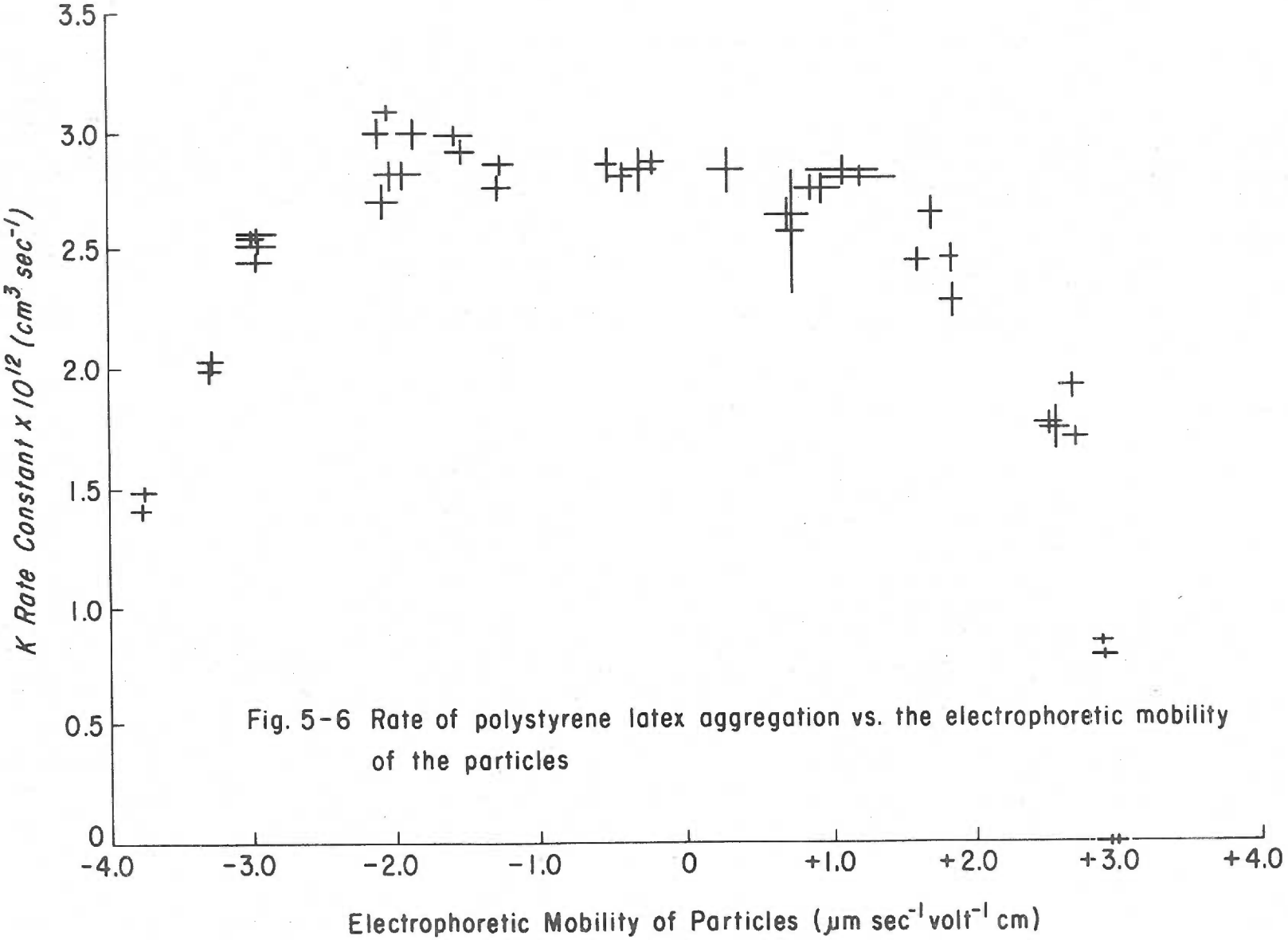

Fig. 5-6 Rate of polystyrene latex aggregation vs. the electrophoretic mobility of the particles

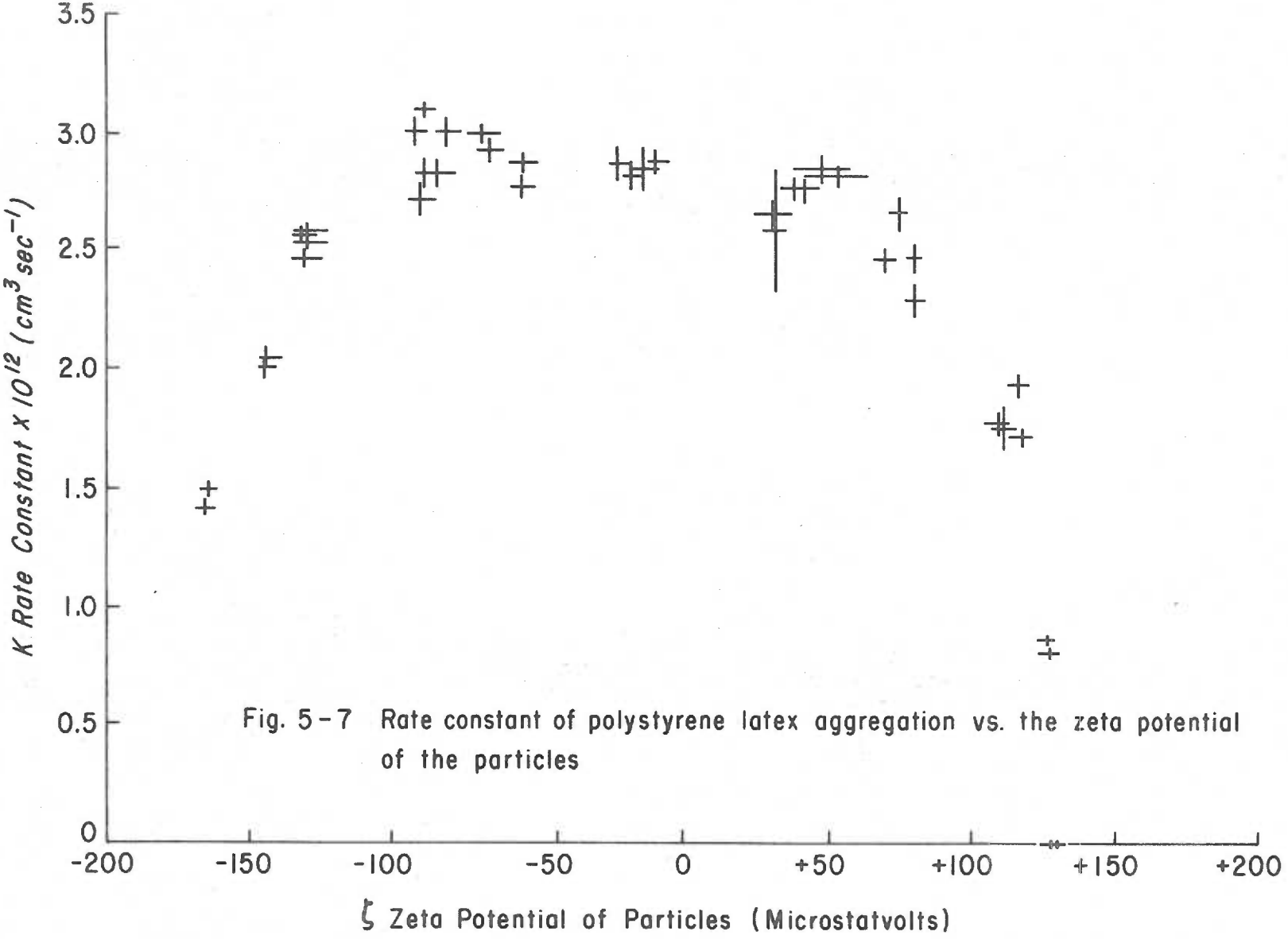

Fig. 5-7 Rate constant of polystyrene latex aggregation vs. the zeta potential of the particles

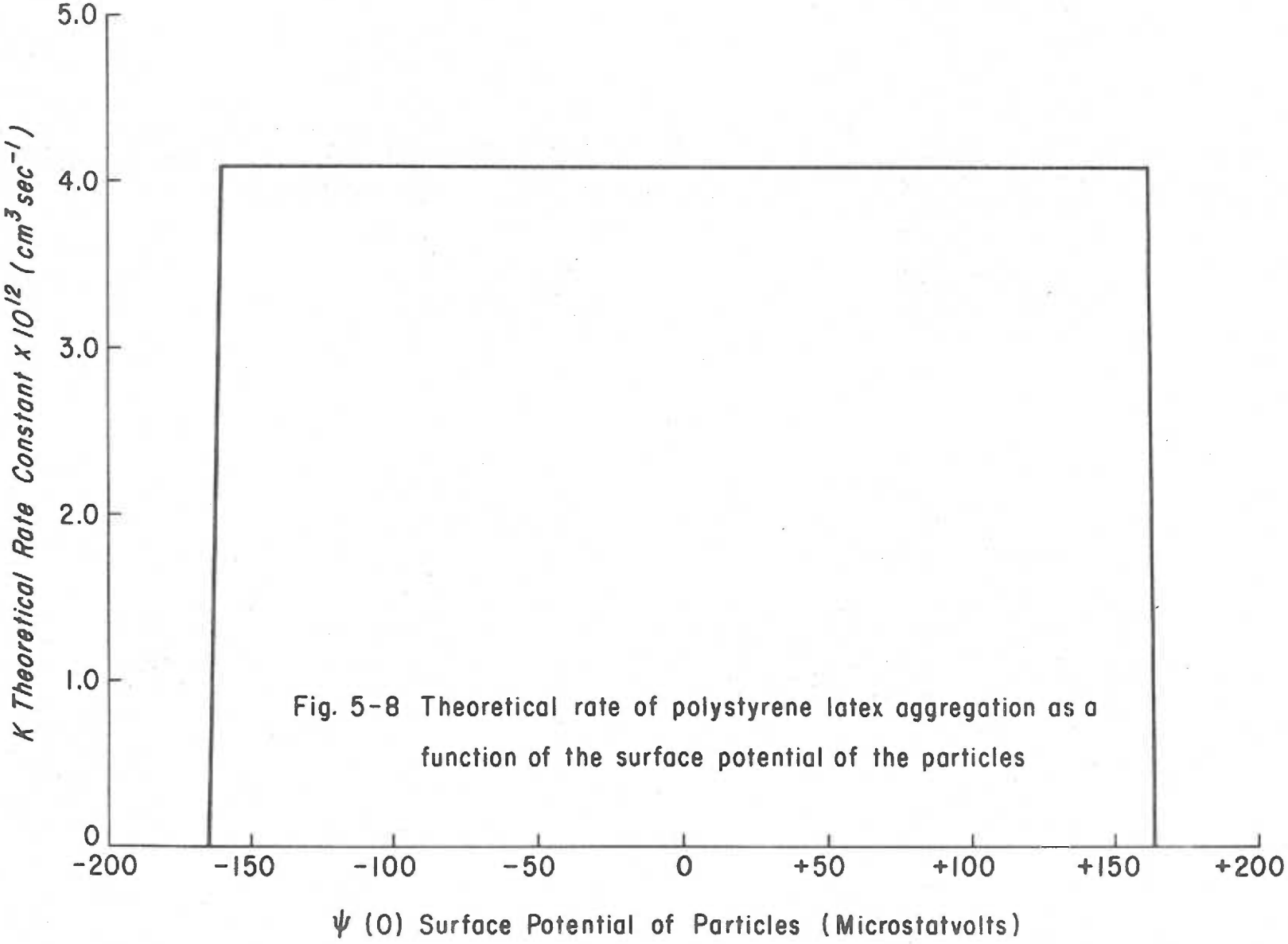

Fig. 5-8 Theoretical rate of polystyrene latex aggregation as a function of the surface potential of the particles

suspension. Thus, the polymer's mechanism of aggregation must be considered to be one of coagulation. While supporting evidence for this conclusion will be discussed it is opportune to examine the accuracy of the prediction concerning the polymer's ability to act as a stabilizing agent.

Stabilizing agents are compounds which adsorb to the surface of particles and produce large increases in the free energy of a two particle system when the adsorbed layers on two particles begin to overlap. Polyelectrolytes have frequently been used as stabilizing agents as they can readily increase the free energy of a two particle system by electrostatic, osmotic and entropic mechanisms. Thus, the conclusion that the polymer acts as a stabilizing agent was fully anticipated when most of the polystyrene particle's surface was covered with poly(l-lysine). The reason for this expectation can be readily seen in figure 5-9 where the potential energy of interaction between two polymer covered particles is plotted as a function of the distance between them when electrostatic, osmotic and van der Waal's forces are taken into account. However, when the surfaces of the polystyrene latex particles are not completely covered with polymer, the extent to which the osmotic forces generated by an adsorbed polymer layer contribute to the repulsive forces between two particles is difficult to calculate. This is because the adsorbed polymers no longer behave as a layer of material and begin to act as isolated macromolecules. Ash (215) has

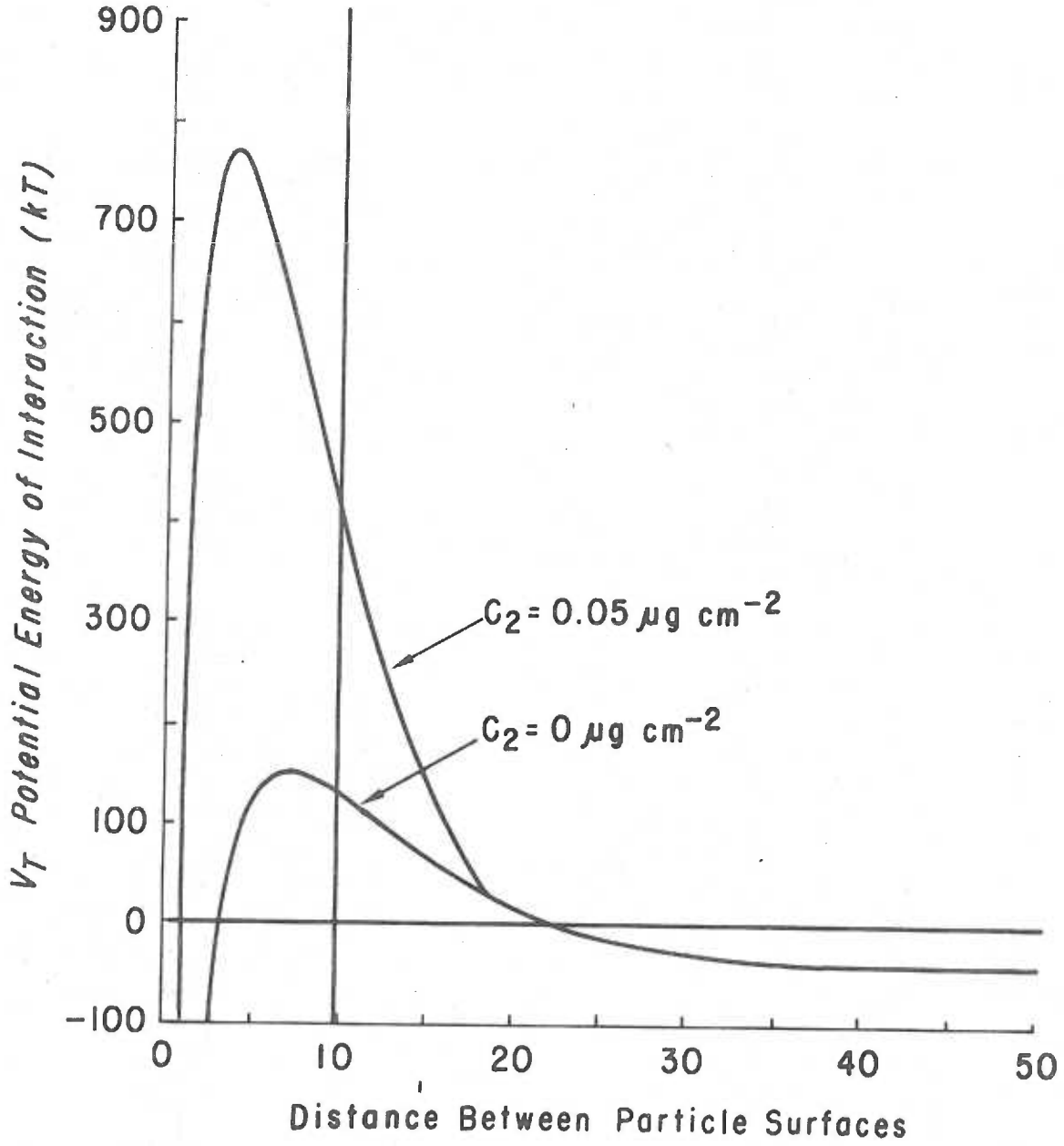

Fig 5-9 The effect of an adsorbed layer of neutral polymer on the potential energy of interaction between two particles. Parameters relevant to the potential energy of interaction between the particles are: polymer concentration 0.05 $\mu g\ cm^{-2}$ and 0 $\mu g\ cm^{-2}$, $\epsilon a\ \psi^2(0)/2kT = 1225$, $A/6kT = 1.500$, $A_2 = 1.3 \times 10^{-3}$ mole $cm^3\ gm^{-2}$, $\kappa a = 500$, $a = 4500$ Å, $\delta = 10$ Å

pointed out that the properties of a single macromolecule at an interface are quite different from the properties of a layer of macromolecules, as many of the properties of the continuous layer are the result of the interactions between the segments of the adsorbed macromolecules. Thus, in the absence of detailed knowledge about the configuration and properties of isolated macromolecules it is difficult to calculate the extent to which they contribute to the potential energy of repulsion between colliding particles and useless to speculate about the point at which polymer based repulsive forces become negligible. However, it is evident that the discrepancy between the rate constants of the experimental and calculated data cannot be attributed to polymer generated repulsive forces at all levels of polymer adsorption. An examination of the rapid rate at which the difference between the observed and calculated rate constants increases when the surface potential of the particles is between -163 and -160 microstatvolts, leads to the following conclusion. If the rate at which the observed discrepancy increases were proportional to the amount or the square of the amount of polymer adsorbed, the plateau region observed in the experimental data would never have been seen. Since entropic forces between particles are proportional to the amount of polymer adsorbed and osmotic forces proportional to the square of the amount of polymer adsorbed this conclusions suggests that part of the discrepancy between the theoretical and observed rate constants must arise from the models

used to calculate V_A and V_R. Parsegian and Ninham (38) have frequently mentioned the fundamental defects in Hamaker's method of calculating V_A and have noted that in aqueous solutions this approach should only be considered a first approximation. Similarly, Verwey and Overbeek's (12) and Honig and Mul's (18) formulations for V_R are only first approximations whose limitations have been frequently cited (120-122). More precise descriptions of V_A and V_R have been proposed but are quite unwieldy and require extensive computer facilities. The improbable prediction that low levels of polymer adsorption generate sizable repulsive forces is therefore attributable to the limitations of the models used and it is likely that with the advent of better models for predicting V_A and V_R much better quantification of a polymer's stabilizing effect on particle suspensions will be obtained. Thus in view of the rather crude approximations used to predict V_T, the successful prediction of polymeric stabilization at high levels of polymer adsorption is a surprisingly good result.

The second and most important prediction of the theoretical calculations is that the low molecular weight poly(l-lysine) molecules used aggregated the polystyrene latex suspensions by a coagulative mechanism. The following support for this conclusion comes from the available literature on the subject and predictions of the polymer's mode of action, based on its probable configuration at the time of an interparticle collision.

When the particles of a suspension collide, the configuration of an adsorbed polymer can range from the configuration it adopts in solution to its equilibrium configuration at the surface of the particle. Viscometric studies presented in section 4:5:3 have shown that the poly(l-lysine) molecules used in this study have a radius of gyration that is approximately 95 Å in 0.10 M NaCl. The shape of the molecule should be approximately spherical as the dimensions of the polymer have only expanded by a factor of 1.3 from its dimensions in 1.00 M NaCl. At equilibrium the configuration of the adsorbed isolated poly(l-lysine) molecule at the polystyrene-0.10 M NaCl interface is unknown but an analysis of the forces which control its configuration suggest that it is tightly adsorbed to the surface of the polystyrene latices. The major forces which control the configuration of the adsorbed polymer are:

1) Electrostatic Forces: These forces are the major factor in determining the configuration of a polyelectrolyte in solution or at an interface. For poly(l-lysine), the predominant electrostatic forces are intramolecular forces which produce expanded polymer configurations and the attractive forces between the ϵ-amino groups of the polymer and the sulfate groups on the polystyrene latices. Katchalsky, Lifson and Mazur's (177) calculations of the free energy of a homologous polyelectrolyte have shown that in aqueous solutions of low and moderate ionic strength most of the free energy of any given polymeric

configuration may be attributed to intramolecular electrostatic interactions. The importance of these interactions can be readily deduced from the rapid rise in the limiting viscosity number of polyelectrolyte as the ionic strength of its suspending medium decreases. At the interface these intramolecular electrostatic forces also act to keep the polyelectrolyte from adopting a contracted configuration. However, the concentration of salt used in the present experiment was large enough that intramolecular forces were minimal, as an order of magnitude increase in the concentration of NaCl in the solvent reduced the polymer's radius of gyration by only 14%. The attractive force between the sulfate groups on groups on the polystyrene latices and the ϵ-amino groups on the poly(l-lysine) molecules is the major factor in binding the poly(l-lysine) molecules to the polystyrene latices. This electrostatic attraction not only binds the polymer to the surface of the particle but reduces image forces, the extent of intramolecular repulsive forces and allows van der Waal's forces to bind the aliphatic side chains of the electrostatically bond lysine segments to the surface of the polystyrene latices. The importance of electrostatic bond formation has been demonstrated in Connor and Ottewill's (69) investigation of the adsorption of a series of homologous N-alkyltrimethylammonium ions onto the surface of polystyrene latices. Measurement of the surfactants' adsorption isotherms and infrared spectroscopic studies showed that the surfactants were initially bound to the surface of the

polystyrene latices by an electrostatic interaction between their quaternary ammonium ions and the carboxyl groups on the surface of the polystyrene latices. The strength of the electrostatic bond caused the percentage of carboxyl groups electrostatically associated with a surfactant to rise very rapidly with the equilibrium concentration of adsorbed polymer. When all of the carboxyl groups were bound to a surfactant molecule, additional increases in the amount of surfactant adsorbed to the polystyrene latices came only with much larger increases in the concentration of surfactant in bulk solution. Thus the high affinity adsorption isotherm poly(l-lysine) exhibits at the polystyrene-0.10 M NaCl interface is probably due to the strength of the electrostatic bond between its ϵ-amino group and the sulfate groups on the surface of the particles.

2) Image Forces: Loeb (25) has discussed these forces and indicated that they are an alternative way of viewing the effect of an ion's surroundings on the free energy of the ion. When an ion is transferred from one medium to another of lower dielectric constant or ionic strength, the free energy of the ion will increase. Thus, ions are negatively adsorbed from interfacial regions which have a lower dielectric constant than that of their solvent. The effect of image forces and intramolecular repulsive forces on polyelectrolytes has been demonstrated by Davies' (154) measurements of the surface potential of films of poly(l-lysine) and other proteins at the air-water and oil-water

interface. When the ϵ-amino groups of the lysine segments were unionized, van der Waal's forces would concentrate the side chains and backbone of the polymers into the air-water interface. Conversely, measurements on films of partially ionized proteins demonstrated that the ionized ϵ-amino groups did not reside in the interfacial region but remained in bulk solution. Thus, image forces tend to keep ionized ϵ-amino groups out of the polystyrene-0.10 M NaCl interfacial region unless they are electrostatically bound to a sulfate group. However, like electrostatic forces, image forces also decay exponentially with increased ionic strength and so it is doubtful that they are of great significance in 0.10 M NaCl.

3) van der Waal's Forces: For the isolated macromolecules at a liquid-solid interface three different van der Waal's interactions must be considered. These are the interactions of the polymer's segments with the solvent molecules, the molecules that constitute the solid phase of the interface and other segments of the same polymer. At higher levels of polymer coverage interpolymeric van der Waal's forces must also be accounted for. A qualitative description of the role of solvent-segment interactions is that contracted polymer configurations with more segment-segment contacts are favored in poor solvents while segment-solvent contacts and expanded polymer configurations are favored in good solvents. Water must be considered a poor solvent for poly(l-lysine) in that the polymer is soluble only when its ϵ-amino

groups are ionized. Thus, lysine segments whose ϵ-amino groups are neutralized by ion bonds or other means would be expected to favor intrasegmental contacts rather than solvent-segment contacts. This has also been demonstrated by Davies' (154) measurements of the surface potential of poly(l-lysine) films at the air-water and oil-water interface. At the air-water interface the unionized side chains of the poly(l-lysine) molecules remained in the interfacial region unless the layer was compressed enough to push the chains into a vertical position where the aliphatic chains of the lysine segments could associate with one another in the air. At the oil and water interface, van der Waal's forces between the oil and the unionized lysine groups kept the lysine segments predominately in the oil phase. Therefore at a liquid-solid interface, van der Waal's forces between the poly(l-lysine) molecules and the polystyrene molecules should bind the lysine side chains to the solid phase of the interface when the ϵ-amino groups of the segments are electrostatically bound to sulfate groups. This prediction is supported by Connor and Ottewill's (69) study of the adsorption of cationic surfactants. They noted that with each additional methylene group in the alkyl group of the surfactant the equilibrium concentration of surfactant required to reverse the charge on the polystyrene decreased by a regular increment. They concluded that this effect was a manifestation of the contribution each methylene group makes to the surfactant's heat of adsorption at the interface. Since this regular

incremental decrease would only be observed if all of the methylene groups of the aliphatic chain were bound to the interface, they concluded that the surfactant molecules lay flat in the interfacial region of the particles to which they were bound. As higher levels of surfactant were adsorbed to the particles, measurements of the area occupied by one surfactant molecule indicated that they were standing on end, presumably with their unbound quaternary ammonium ions extending into the aqueous phase. This finding agrees with Davies' (154) measurements which show that when the lysine side chains of molecules adsorbed to the air-water or oil-water interface were ionized, they did not remain in the interface but stayed in bulk solution. Thus, the van der Waal's forces which keep a surfactant or the aliphatic side chains of a lysine segment in an interfacial region are not as large as the image and intramolecular electrostatic repulsive forces which repel unbound charge groups from the interface. However, if the charge group of a lysine segment is electrostatically bound to another charge group in the interface, van der Waal's forces will bind the methylene groups of the segment to the interface.

4) Entropic Factors: Fleer (64) has divided the total entropy of a polymer into two different categories, the entropy of the individual polymer segments and the configurational entropy of the polymer as a whole. The loss of entropy a segment experiences on adsorption depends on what percentage of its contact sites it loses in the process.

Fleer has suggested that the entropy loss a polymer segment, with a coordination number of 6, experiences on adsorption increases the free energy of the polymer by about 0.3 kT. The adsorption of the polymer segments also decreases the total number of configurations available to the polymer as a whole. This also increases the free energy of the polymer. However, the observations of Davies (154) and Connor and Ottewill (69) indicate that the decrease in the entropy a polymer experiences at an interface causes an increase in the free energy of the polymer that is minor when compared to the effect of van der Waal's and electrostatic forces.

Thus, the forces which cause poly(l-lysine) to adopt a configuration in which its segments lie predominately in the interface are the electrostatic attractive forces between the polymer's ϵ-amino groups and the ionized sulfate groups of the polystyrene latices, the van der Waal's attraction between the polystyrene molecules and lysine segments and the polymer's preference for segment-segment contacts rather than solvent-segment contacts when the ϵ-amino groups of the polymer are not ionized. Factors which cause the polymer to stay in bulk 0.10 M NaCl are the decrease in entropy the polymer experiences when it adsorbs to the interface and the reduced dielectric constant of the interfacial region which increases the free energy of unbound ions and the extent of intramolecular electrostatic repulsive forces. However the reduced dielectric constant of the interfacial region is

partially offset by the high concentration of ions found at the interface (0.10 M-0.70 M). Therefore, the equilibrium configuration of a poly(l-lysine) molecule adsorbed to the polystyrene-0.10 M NaCl interface should not be available for bridging.

The length of time a polymer requires to establish an equilibrium configuration may range from many hours to a few tenths of a second. Polymers of low molecular weight generally require less time to establish an equilibrium configuration than a large polymer. However, the time required to establish an equilibrium configuration is not determined by the size of the polymer alone, as a polymer of given molecular weight adsorbing to a set surface may establish its final configuration virtually instantaneously or require several hours depending on the quality of the solvent (220). Thus, the time a polymer requires to reach an equilibrium configuration will be determined by the specific polymer, its molecular weight, the solvent and interface being considered. At present the length of time a polymer requires to reach its equilibrium configuration cannot be predicted and must be determined experimentally.

The few studies which have shown that low molecular weight polyelectrolytes act as flocculating agents have employed high concentrations of suspended particle and stirred the polymer-particle mixture thereby achieving a large interparticle collision rate. This procedure involves a significant number of the adsorbed polymer

molecules in an interparticle collision before they have reached an equilibrium configuration. Alnice and Robertson (58) placed 50 Å x 1,000 Å microcrystalline cellulose fibers in suspension at a concentration of 10^{12} particles ml^{-1} and aggregated them with several samples of polyethylenimine of differing molecular weight. Simple calculations show that Brownian motion alone causes the interparticle collision rate to be 3×10^{13} sec^{-1} in these fiber suspensions. This is at least five orders of magnitude greater than the collision rate of the present study. After the cellulose fibers had sedimented they noted that the volume of the sediment in the suspension aggregated by a 30,000 Dalton polymer was larger than the volume of a suspension aggregated by an 1,800 Dalton polymer. This is classic evidence for the existence of interparticle bridging. When the two sediments were redispersed and the polymer given time to rearrange its configuration the volume of the two sediments were approximately equal. The "contraction reaction" has been observed by a number of investigators (237, 238, 239) and has been attributed to a rearrangement of the configuration of the adsorbed polymer to one in which the bulk of the polymer segments are unavailable for bridging. In another study, Dixon and coworkers (240) also used low molecular weight polyethylenimines as flocculating agents. In their study a suspension of silica particles was mixed with a polymer solution, mechanically stirred and vacuum filtered. The filtered fluid was then refiltered through the packed bed

of particles to determine the length of time required to collect a given volume of fluid. Their findings indicated that a polymer with a molecular weight of 32,000 Daltons could act as a flocculating agent. However, the concentration of particles employed in their study was approximately one order of magnitude greater than the present work and the polymer was mixed with the particles during stirring over a five minute period. A calculation of the time required to halve the number of particles in the unstirred suspension, when each collision results in an aggregate, is six minutes. The stirring undoubtedly decreased this time.. Thus it is probable that their method of mixing the polymer and particles resulted in a significant number of collisions between particles when adsorbed polymers had not reached an equilibrium configuration. Unfortunately no experiments were done in which the concentrations of particles were varied or the filter beds redispersed, and it is not possible to determine whether the polymer had reached an equilibrium configuration. Thus, there is no experimental evidence where a low molecular weight polyelectrolyte has been shown to act as a flocculating agent after it has reached an equilibrium configuration.

These studies of Dixon et al. (240) and Alnice and Robertson (58) differ from the present study in which low particle concentrations were employed and after the initial mixing of polymer and particle no stirring of the system occurred. Under these conditions, the time required to

halve the number of particles in the suspension under conditions of rapid coagulation is approximately 60 minutes. Conversely, the electrophoretic mobility of the poly(l-lysine) coated polystyrene latices reached a constant value within five minutes. Since the electrophoretic mobility of a polymer covered particle has been shown to be a function of polymer configuration (appendix IV), these measurements and the available data on the length of time low molecular weight polyelectrolytes require to reach equilibrium suggest that the poly(l-lysine) molecules reached an equilibrium configuration within five minutes. The segments of the adsorbed poly(l-lysine) molecules were therefore very likely to be in a train configuration for most of the interparticle collisions and therefore unavailable for bridging. This suggests that the poly(l-lysine) sample used acted as a coagulating agent when aggregating the polystyrene latices, which is the same conclusion which had been reached by a comparison of the theoretical and measured rate constants. Thus, the experimental data from this work, other experiments in the literature and the predictions of current theories of polymer configuration at an interface are in full agreement and demonstrate that the mechanism by which a polyelectrolyte aggregates a particle suspension may be deduced from a comparison of the observed rate of polymer induced particle aggregation and the theoretical rate at an uncoated particle suspension with the same zeta potential.

6. CONCLUSIONS

The major conclusion of this work is that the theories of classical colloidal chemistry may be successfully combined with the criteria set forth in section 1:2 to establish a kinetic basis for determining the mechanism by which a polymer aggregates a suspension of particles. Although current methods of assessing the potential energy on interaction between particles are in need of considerable refinement, the results of this investigation indicate they are serviceable. In addition to this conclusion, this thesis has produced a number of smaller findings concerning the solution properties of poly(l-lysine), the physical properties of polystyrene latices, the nature of their interactions, and effect of poly(l-lysine) on the properties of polystyrene latex particle suspensions.

6:1. Poly(l-lysine)-Polystyrene Latex Interactions

1) When a low molecular weight poly(l-lysine) molecule has had time to establish an equilibrium configuration on the surface of a polystyrene latex particle, it induces aggregation of the particles by a coagulative mechanism.
2) Poly(l-lysine) adsorption is very rapid and essentially irreversible when a small percentage of the surface area of a

suspension of polystyrene latex particles is covered by the polymer.

3) Dispersions of polystyrene latices with uniform coatings of poly(l-lysine) can only be attained when the particles and polymer are mixed by a method which exposes particles to the same amount of poly(l-lysine), or more accurately to the same concentration of poly(l-lysine).

4) When approximately 50 percent of the particle's surface is covered with polymer, adsorption is no longer irreversible and the adsorbed polymer is in equilibrium with a polymer in solution. On a statistical basis, adsorption is no longer irreversible when less than ~ 35% of the polymer's ϵ-amino groups are electrostatically bound to sulfate groups.

5) Poly(l-lysine) reaches a state, within five minutes, where further changes in its configuration does not affect the electrophoretic mobility of the particles to which it adsorbs. The polymer is therefore assumed to have reached an equilibrium configuration within five minutes.

6) The equilibrium configuration of the polymer permits interparticle bridging only after two particles have formed a stable aggregate.

7) The equilibrium configuration of the isolated polymer lies predominately in the polystyrene-0.10 M NaCl interfacial region.

8) At high levels of poly(l-lysine) adsorption, the adsorbed polymer layer stabilizes the polystyrene latices by a mechanism that cannot be attributed to electrostatic forces alone. This implies that the polymer is no longer adsorbed primarily in the interfacial region of the particle.

9) It is possible to measure surface concentrations of poly(l-lysine) in the range of 10^{-10} gm cm^{-2} with an electrophoretic assay.

6:2. Poly(l-lysine) Properties

1) The commercial sample had a bimodal molecular weight distribution. The major peak of the molecular weight distribution had a number average molecular weight of 24,000 ± 200 and a weight average molecular weight of 31,300 ± 100.

2) In comparison to typical polymer molecular weight distributions, which have a $M_w:M_n$ ratio of 2, this molecular weight distribution was relatively narrow with a $M_w:M_n$ ratio of 1.28.

3) The charge on the ϵ-amino groups of the poly(l-lysine) molecules cause them to behave as nonideal solutes even in the

limit of infinite dilution. This effect is reduced by the presence of an electrolyte but is still detectable in 1.00 M NaCl.

4) The polymer's radius of gyration decreased linearly with increases in the square root of the solution's NaCl concentration as predicted by Pals and Hermans (198).

5) The limiting viscosity number of the polymer increased from a theoretical value of 0.33 ± 0.05 dl gm^{-1}, in a NaCl solution of an infinite concentration to a value of 1.01 ± 0.01 dl gm^{-1} in 0.05 M NaCl at 25°C. At 0.10 M NaCl, 25°C, the limiting viscosity number of the polymer has a value of 0.83 ± 0.03 dl gm^{-1}.

6) The radius of gyration of the poly(l-lysine) molecules increases by a factor of 1.45 when the NaCl concentration of the polymer's solvent changes from a theoretical NaCl solution of infinite concentration to 0.05 M NaCl. Twenty percent of this increase occurs as the NaCl concentration changes from 0.10 M to 0.05 M.

7) The second virial coefficient of the polymer in 5.00 M NaCl at 19.2°C is $(1.30 \pm 0.15) \times 10^{-3}$ mole $cm^3 gm^{-2}$.

8) The third virial coefficient of the polymer in 5.00 M NaCl at 19.2°C is $(2.7 \pm 1.7) \times 10^{-2}$ cm^6 mole gm^{-3}.

9) Measurement of the polymer's g value, 0.65 ± 0.44, indicates that it behaves like an impenetrable sphere with a radius equivalent to its radius of gyration.

6:3. Polystyrene Latex Properties

1) The polystyrene latices had a mean diameter of 0.90 ± 0.05 μm with a standard deviation of 0.01 μm.
2) The surface charge density of the fully ionized particles was approximately 1.22×10^{4} statcoulombs cm^{-2}. This indicates that the average distance between anionic sites on the particle was approximately 20 Å.
3) Analysis of the variation of the particle's electrophoretic mobility with solution pH indicated that 90% of the surface charge groups were due to sulfate ions, while the remaining 10% had a pK (3.6) close to that of a carboxyl group (~ 3.9).
4) The decrease in the electrophoretic mobility of the particles at low pH was not due to the hydrolysis of the surface charge groups.
5) The critical coagulation concentration of the particles in NaCl is 0.13 M.
6) The maximal rate of coagulation attained by the particles was only 49% of the rate predicted by von Smoluchowski for rapid coagulation. This discrepancy has been explained by

Spielman (7) and Honig et al. (8) in terms of the viscous interaction between colliding particles.

7) The calculated value of Hamaker's constant decreased steadily from its maximum value, 3.8×10^{-13} ergs in 0.10 M NaCl to its minimum value in 2.00 M NaCl of 0.5×10^{-13} ergs. This decreasing value of Hamaker's constant with increasing ionic strength is in agreement with the predictions of Smith et al. (35). However, it is probably much larger than the actual decrease in A as the electromagnetic fluctuations which can be damped by salt ions constitute no more than 70% the attractive forces between particles in aqueous solutions.

8) Polystyrene latices do not fall into an infinitely deep primary minimum when aggregated by high salt concentrations as their aggregates are readily dispersed by the high rates of shear encountered at the orifice of the Electrozone-celloscope.

APPENDIX I

CALCULATION OF HAMAKER'S CONSTANT

This appendix documents the method which was used to establish the manner in which the potential energy of attraction, V_A, varies with the distance between two polystyrene spheres immersed in 0.10 M NaCl. Two methods of calculating V_A as a function of distance were available. The more recent and accurate method stems from Lifshitz' theory (37) of van der Waal's forces in condensed media. It has been developed and extended to colloidal systems by the work of Ninham (35), Parsegian (38, 133), Napper (134) and their respective coworkers. However, this method was not used as it requires extensive computer facilities and predicts values of V_A which differ by no more than 5% of the other theory over the range of particle separations of interest (< 200 Å). The classical theory of the attractive forces between particles differs from the Lifshitz theory by assuming that the forces between two particles are additive and can be viewed as an electromagnetic fluctuation of a single wavelength in the ultraviolet region. The concept of additivity maintains that the total force between two particles is equal to the sum of the attractive forces between every atom in one particle and every other atom in the other particle. For two atoms, in vacuo, separated by a distance R, the potential energy of attraction between them, V_A, is given by:

$$V_A = - \frac{T}{R^6} \qquad 1\text{-}29$$

where T is a constant whose magnitude is a function of the wavelength of the electromagnetic fluctuations of the attractive forces between the atoms. A theory of the potential energy of attraction between two particles was developed by Hamaker (32) who assumed that the forces between the atoms in the two particles were additive and that their potential energy of attraction was given by equation 1-29. He showed that the potential energy of attraction of two spherical particles of material 2 in a vacuum was given by:

$$V_A = \frac{A_{22}}{6} \left[\frac{2}{(u+2)^2 - 4} + \frac{2}{(u+2)^2} + \ln\left[\frac{(u+2)^2 - 4}{(u+2)^2} \right] \right] \qquad 1\text{-}30$$

where u is the reduced separation distance between the spheres which is defined as the ratio of the distance between the surface of the spheres, to their radii a. A_{22} is defined as Hamaker's constant for material 2 in a vacuum. Hamaker's constant is therefore a measure of the intrinsic attraction between the atoms of material 2. When particles of material 2 are suspended in a condensed medium with a Hamaker's constant, A_{11}, it is necessary to account for the effect of displacing the volume of suspending fluid in which the particles of material 2 are suspended. Hamaker has taken this into consideration and shown that the effective Hamaker's constant, A, of particles of material 2, suspended in material 1 is given by:

$$A = (A_{22}^{1/2} - A_{11}^{1/2})^2 \qquad 1\text{-}32$$

Thus, the task of calculating the manner in which the potential energy of attraction between two spheres of polystyrene latex in 0.10 M NaCl varies with distance requires only that the magnitude of the particle's Hamaker constant, A, be evaluated.

The classical procedure for evaluating A is to experimentally measure some property of the material of interest which can be expressed as a mathematical function of experimentally accessible parameters and Hamaker's constant. From this information the value of A which would give rise to the experimentally measured parameters can be calculated. Some properties of particles and particle suspensions which have been used to evaluate Hamaker's constant are interfacial tensions (130), the sedimentation coefficient of particles (132) and the critical coagulation concentration (93) of a particle suspension. The Hamaker's constant of the particles in a suspension has also been related to the rate at which the particles coagulate. A function expressing this relationship will be used to evaluate Hamaker's constant for polystyrene latices suspended in 0.10 M NaCl in this appendix.

The rate at which a particle suspension coagulates, K, was first related to the potential energy of interaction between particles, V_T, by Fuch's (9) work with aerosols in the equation:

$$W = \frac{K_o}{K} = 2\int_0^{\infty} \frac{\exp(\frac{V_T}{kT})du}{(u+2)^2} \qquad \text{A1-1}$$

where V_T is the sum of the potential energy of attraction, V_A, and the potential energy of repulsion, V_R between the particles. K_o is von Smoluchowski's (4) estimate of the rate at which particles aggregate when every collision results in an aggregate. For a suspension of particles suspended in a fluid of viscosity, η, K_o is given by:

$$K_o = \frac{4kT}{3\eta} \qquad \text{A1-2}$$

According to the D.L.V.O. (11, 12) theory of colloidal stability, the potential energy of repulsion, between colloidal particles whose radius a is much smaller than the Debye-Hückel reciprocal length of their suspending medium, κ, is given by:

$$V_R = \frac{\epsilon a \psi^2(0)}{2} \ln[1+\exp(-\kappa a u)] \qquad \text{1-28}$$

where ϵ is the dielectric constant of the suspending medium and $\psi(0)$ is the surface potential of the particles.

Fuch's theory has subsequently been improved by Spielman (7) and Honig et al. (8) who corrected its failure to account for the viscous interactions between colliding spheres. With the inclusion of the correction factor published by Honig et al., the rate of coagulation of a particle suspension is related to the potential energy of interaction of

the spheres and hence, Hamaker's constant by:

$$W = \frac{K_o}{K} = 2\int_0^{\infty} \frac{(6u^2+13u+2)du}{(6u^2+4u)(u+2)^2} \exp\left[\frac{V_T}{kT}\right] \qquad \text{A1-3}$$

where

$$V_T = \frac{\epsilon a \psi^2(0)}{2} \ln[1+\exp(-\kappa a u)] - \frac{A}{6}\left[\frac{2}{(u+2)^2-4} + \frac{2}{(u+2)^2} + \ln\frac{(u+2)^2-4}{(u+2)^2}\right] \qquad \text{1-34}$$

The equation, A1-3, is the primary expression used to evaluate Hamaker's constant in this thesis. The remaining portion of this appendix demonstrates the manner in which this expression was evaluated to obtain a value of A when the values of W, a, ϵ, $\psi(0)$, T and κ were known.

The general procedure for evaluating the magnitude of A was to evaluate the integral in equation A1-3 with different values of A until the value of the integral matched the experimentally derived value of W. This procedure was complicated by the difficulty of analytical solution for A by direct integration of equation A1-3 and the unfeasibility of using numerical methods of an integral with an infinite upper limit. The integral was therefore evaluated by rewriting it as the sum of three separate integrals and solving these integrals by a combination of numerical and analytical procedures. The three integrals used to express equation A1-3 are written as:

$$W \equiv W_0^{\infty} = W_{20}^{\infty} + W_{0.5}^{20} + W_0^{0.5} \qquad \text{A1-4}$$

where,

$$W_b^c = 2\int_b^c \frac{6u^2+13u\ 2}{(6u^2+4u)(u+2)^2}\exp[\frac{V_T}{kT}]du \qquad \text{A1-5}$$

The first integral to be evaluated was W_{20}^{∞} which could be assessed by straight forward integration. This was possible as the potential energy of interaction between two particles is vanishingly small when the distance between the particle surfaces is more than a few particle diameters apart. When the distance between the particles is ten times the diameter of the particles the potential energy of interaction between them is approximately 10^{-8} kT units. The exponential term in the integral can be replaced by the first term of its power series under these circumstances yielding:

$$W_{20}^{\infty} = 2\int_{20}^{\infty} \frac{(6u^2+13u+2)du}{(6u^2+4u)(u+2)^2} \qquad \text{A1-6}$$

This equation may be integrated by rewriting equation A1-6 in its simplest form to yield:

$$W_{20}^{\infty} = 2\int_{20}^{\infty} \frac{du}{8u} + 2\int_{20}^{\infty} \frac{27du}{8(6u+4)} - 2\int_{20}^{\infty} \frac{11du}{16(u+2)} \qquad \text{A1-7}$$

Each integral may be integrated to give:

$$W_{20}^{\infty} = \frac{\ln u}{4}\Big]_{20}^{\infty} + \frac{27\ln(6u+2)}{24}\Big]_{20}^{\infty} - \frac{11\ln(u+2)}{8}\Big]_{20}^{\infty} \qquad \text{A1-8}$$

or, equivalently

$$W_{20}^{\infty} = \ln \left. \frac{u^{1/4}(6u+4)^{27/24}}{(u+2)^{11/8}} \right]_{20}^{\infty} \qquad \text{A1-9}$$

$$= \frac{\ln(\infty)^{1/4}(6(\infty)+4)^{27/24}}{(\infty+2)^{11/8}} - \frac{\ln(20)^{1/4}(6(20)+4)^{27/24}}{(20+2)^{11/8}}$$

The value of the indeterminate term in equation A1-9 cannot be solved by repeated application of L'Hopital's rule and reduction of the numerator and denominator to their respective series approximations is exceedingly cumbersome. The indeterminate term was therefore evaluated by using increasing values of u to show that it asymptotically approached the limit of 2.0157 as u approached infinity. Thus:

$$W_{20}^{\infty} = \frac{\ln(7.0562)(20+2)^{11/8}}{(20)^{1/4}(6(20+4)^{27/24}} = 0.09416 \qquad \text{A1-10}$$

If V_T is assumed equal to zero for all values of u, the colloidal suspension becomes absolutely stable, as $W_0^{\infty} = \infty$. This conclusion clashes with classical thinking which predicts the onset of rapid coagulation at $V_T = 0$, and reflects the influence of the viscous interactions between the particles.

When the distance between the particles is small enough ($u < 20$) that the $\exp(V_T)$ term must be considered, equation A1-5 was evaluated by the trapezoidal rule. This rule describes a numerical method of estimating the value of integrals and states:

$$\int_b^c \xi(s)dx = \lim_{(\Delta s \to 0)} ([\xi(b+\Delta s)+\xi(b+2\Delta s)+\ldots+\xi(c-\Delta s)] + \frac{1}{2}[\xi(b)-\xi(c)])\Delta s \qquad \text{A1-11}$$

Since the trapezoidal rule gives the exact value of the integral only in the limit of infinitely small Δs, it is necessary to know how accurately the trapezoidal rule predicts the value of the integral when Δs is finite. Limits of the integral's accuracy can be made by the use of the following theorem:

$$\int_b^c \xi(s)dx = \gamma - \frac{c-b}{12}\xi''(f)\Delta s^2 \qquad \text{A1-12}$$

where γ is the value of the integral obtained by the application of the trapezoidal rule and $\xi''(f)$ is the value of the second derivative of $\xi(s)$ at f where $b < f < c$. Although f is usually unknown, it is possible to maximize $\xi''(s)$ and thereby place an upper limit on the error produced when the trapezoidal rule is applied with a finite value of Δs.

When $0.5 \leq u \leq 20$, V_R is vanishingly small for the polystyrene latices in 0.10 M NaCl and $W_{0.5}^{20}$ can be written as:

$$W_{0.5}^{20} = \int_{0.5}^{20} \frac{6u^2+13u+2}{(6u^2+4u)(u+2)^2} \exp[\frac{-V_A}{kT}] \qquad \text{A1-13}$$

This integral cannot be solved by direct integration and the trapezoidal rule must be used to find it. Since computational time for the evaluation of this integral on a Hewlett Packard 9100B calculator

is on the order of five years for a Δs of 10^{-7}, it was necessary to calculate the maximum value of Δs which would give a sufficient level of accuracy. This was done by rewriting equation A1-12 as the sum of three integrals, deriving an expression for the error involved in solving each of the integrals by the trapezoidal rule and finding the value of the independent variable which maximizes the sum of the three error terms.

Substituting $s = u + 2$, equation A1-13 can be rewritten as:

$$W_{0.5}^{20} = \begin{cases} \frac{1}{4}\int_{2.5}^{22} \frac{\exp(\bar{b}Z(s))ds}{s-2} & \text{A1-14} \\ + \frac{27}{4}\int_{2.5}^{20} \frac{\exp(\bar{b}Z(s))ds}{6s-8} & \text{A1-15} \\ - \frac{11}{8}\int_{2.5}^{22} \frac{\exp(\bar{b}Z(s))ds}{s} & \text{A1-16} \end{cases}$$

where

$$V_A = \bar{b}Z(s), \quad \bar{b} = -\frac{A}{6kT} \quad \text{and} \quad Z(s) = \frac{2}{s^2-4} + \frac{2}{s^2} + \ln\frac{s^2-4}{s^2}$$

To calculate the error that might be incurred in numerically evaluating each of these integrals by the trapezoidal rule, it was necessary to find the second derivative of equations A1-14, A1-15 and A1-16, and apply the theorem given in equation A1-12. Thus for equation A1-14, let:

$$\xi(s) = \frac{\exp(\bar{b}Z(s))}{4(s-2)} \qquad \text{A1-17}$$

differentiating $\xi(s)$ with respect to s yields;

$$4\xi'(s) = \frac{\bar{b}Z'(s)\exp(\bar{b}Z(s))}{(s-2)} - \frac{\exp(\bar{b}Z(s))}{(s-2)^2} \qquad \text{A1-18}$$

and differentiating a second time with respect to s yields,

$$4\xi''(s) = \frac{(\bar{b}Z'(s))^2\exp(\bar{b}Z(s))}{(s-2)} + \frac{\bar{b}\exp(\bar{b}Z(s))Z''(s)}{(s-2)} - \frac{\bar{b}Z'(s)\exp(\bar{b}Z(s))}{(s-2)^2} - \frac{\bar{b}Z'(s)\exp(\bar{b}Z(s))}{(s-2)^2} + \frac{2\exp(\bar{b}Z(s))}{(s-2)^3} \qquad \text{A1-19}$$

or equivalently,

$$4\xi''(s) = \exp(\bar{b}Z(s))\left[\frac{(\bar{b}Z'(s))^2}{(s-2)} - \frac{2\bar{b}Z'(s)}{(s-2)^2} + \frac{\bar{b}Z''(s)}{(s-2)} + \frac{2}{(s-2)^3}\right] \qquad \text{A1-20}$$

thus, the error term for equation A1-14 is

$$\frac{c-b}{12}\xi''(s)\Delta s^2 = \left(\frac{19.5}{12}\right)\exp(\bar{b}Z(s))\left[\frac{(\bar{b}Z'(s))^2}{(s-2)} - \frac{2\bar{b}Z'(s)}{(s-2)^2} + \frac{\bar{b}Z''(s)}{(s-2)} + \frac{2}{(s-2)^3}\right]\Delta s^2 \qquad \text{A1-21}$$

From equation A1-15 let

$$\xi(s) = \frac{27\exp(\bar{b}Z(s))}{4(6s-8)} \qquad \text{A1-22}$$

and following the same procedure as before, $\xi(s)$ is differentiated with respect to s to yield:

$$\frac{4}{27}\xi'(s) = \frac{\bar{b}Z'(s)\exp(\bar{b}Z(s))}{(6s-8)} - \frac{6\exp(\bar{b}Z(s))}{(6s-8)^2} \qquad \text{A1-23}$$

the second derivative of A1-22 is therefore,

$$\frac{4}{27}\xi''(s) = \exp(\bar{b}Z(s))\left[\frac{(\bar{b}Z'(s))^2}{(6s-8)} - \frac{12\bar{b}Z'(s)}{(6s-8)^2} + \frac{\bar{b}Z''(s)}{(6s-8)} + \frac{72}{(6s-8)^3}\right] \quad \text{A1-24}$$

thus, the error term for equation A1-15 is

$$\frac{c-b}{12}\xi''(s)\Delta s^2 = \left(\frac{19.5}{12}\right)\frac{27\exp(\bar{b}Z(s))}{4}\left[\frac{(\bar{b}Z'(s))^2}{(6s-8)} - \frac{12\bar{b}Z'(s)}{(6s-8)^2} + \frac{\bar{b}Z''(s)}{(6s-8)} + \frac{72}{(6s-8)^3}\right]\Delta s^2 \quad \text{A1-25}$$

For equation A1-16 let

$$\xi(s) = \frac{11}{8}\,\frac{\exp(\bar{b}Z(s))}{s} \quad \text{A1-26}$$

and again,

$$\frac{8}{11}\xi'(s) = \frac{\bar{b}Z'(s)\exp(\bar{b}Z(s))}{s} - \frac{\exp(\bar{b}Z(s))}{s^2} \quad \text{A1-27}$$

$$\frac{8}{11}\xi''(s) = \exp(\bar{b}Z(s))\left[\frac{(\bar{b}Z'(s))^2}{s} - \frac{2Z'(s)}{s^2} + \frac{\bar{b}Z''(s)}{s} + \frac{2}{s^3}\right] \quad \text{A1-28}$$

thus, the error term for equation A1-16

$$\frac{c-b}{12}\xi''(s)\Delta s^2 = \left(\frac{19.5}{12}\right)\frac{11\exp(\bar{b}Z(s))}{8}\left[\frac{(\bar{b}Z'(s))^2}{s} - \frac{2Z'(s)}{s^2} + \frac{\bar{b}Z''(s)}{s} + \frac{2}{s^3}\right]\Delta s^2$$

To maximize the sum of equations A1-21, A1-25 and A1-29 requires a knowledge of the behavior of $\exp[\bar{b}Z(s)]$, $Z(s)$, $Z'(s)$ and $Z''(s)$ when s increases. Thus, differentiating $Z(s)$ with respect to s yields:

$$Z'(s) = -\frac{4s}{(s^2-4)^2} - \frac{4}{s^3} + \frac{8}{s(s^2-4)} = \frac{-64}{(s^2-4)^2 s^3} \qquad \text{A1-30}$$

the second derivative is therefore,

$$Z'' \qquad Z''(s) = \frac{64(7s^6-40s^4+48s^2)}{s^6(s^2-4)^4} = \frac{64(7-(40/s^2)+(48/s^4))}{(s^2-4)^4} \qquad \text{A1-31}$$

Inspection of equations A1-30 and A1-31 indicates that the absolute values of $Z'(s)$ and $Z''(s)$ decrease with increasing values of s. Furthermore, the term $\exp[\bar{b}Z(s)]$ asymptotically approaches 1 as s increases and can be eliminated from equations A1-21, A1-25 and A1-29 without fear of underestimating the maximum potential error involved in estimating equation A1-13 by the trapezoidal rule. Thus, after the $\exp[\bar{b}Z(s)]$ term has been eliminated from equations A1-21, A1-25 and A1-29, a value greater than the maximum potential error term is found by summing these equations when s has a value of 2.5. This procedure yielded:

$$\frac{c-b}{12}\xi''(f)\Delta s^2 < \Delta s^2[2.1427\bar{b}^2+20.330\bar{b}+13.947] \qquad \text{A1-32}$$

For $\bar{b} = A/6kT < 10$ evaluation of $W_{0.5}^{20}$ with a $\Delta s = 10^{-3}$ produces an error of less than 2.5×10^{-4}. Since the value of $W_{0.5}^{\infty}$ is greater than 1 for $A/6kT < 5$, an error of less than 0.01% is produced by this particular trapezoidal rule approximation.

$W_{0.5}^{\infty}$ was expressed as a function of $\bar{b}$ by calculating $W_{0.5}^{20}$ at different values of $\bar{b}$, adding the value of W_{20}^{∞} to it and fitting

the resultant $W_{0.5}^{\infty}$ vs $\bar{b}$ data to a power series via a least squares analysis to yield:

$$W_{0.5}^{\infty} = 1.2602 - 0.03506\bar{b} + 0.00159\bar{b}^2 \qquad \text{A1-33}$$

$W_0^{0.5}$ was calculated by the same method used to calculate $W_{0.5}^{20}$ but with a different Δs. Again, the choice of Δs was determined by applying the theorem presented in equation A1-12 to the integral for $W_0^{0.5}$, which can be written as:

$$W_0^{0.5} = \begin{cases} \frac{1}{4}\int_{2.0}^{2.5} \frac{\exp(\theta(s))ds}{s-2} & \text{A1-34} \\ + \frac{27}{4}\int_{2.0}^{2.5} \frac{\exp(\theta(s))ds}{6s-8} & \text{A1-35} \\ - \frac{11}{8}\int_{2.0}^{2.5} \frac{\exp(\theta(s))ds}{s} & \text{A1-36} \end{cases}$$

where $\theta(s) = V_T/kT$ and V_T has been rewritten as a function of s by making the substitution $s = u+2$.

The error involved in using the trapezoidal rule to calculate the value of integral A1-34, A1-35 and A1-36 can be immediately written as:

$$\frac{c-b}{12}\xi''(s)\Delta s^2 = \begin{cases} \left(\frac{0.5}{12}\right)\frac{\exp(\theta(s))}{4}\left[\frac{(\theta'(s))^2}{(s-2)} - \frac{2\theta'(s)}{(s-2)^2} + \frac{\theta''(s)}{(s-2)} + \frac{2}{(s-2)^3}\right]\Delta s^2 & \text{A1-37} \\ + \left(\frac{0.5}{12}\right)\frac{27\exp(\theta(s))}{4}\left[\frac{(\theta'(s))^2}{(6s-8)} - \frac{2\theta'(s)}{(6s-8)^2} + \frac{\theta''(s)}{(6s-8)} + \frac{2}{(6s-8)^3}\right]\Delta s^2 & \text{A1-39} \\ - \left(\frac{0.5}{12}\right)\frac{11\exp(\theta(s))}{8}\left[\frac{(\theta'(s))^2}{s} - \frac{2\theta'(s)}{s^2} + \frac{\theta''(s)}{s} + \frac{2}{s^3}\right]\Delta s^2 & \text{A1-39} \end{cases}$$

Maximizing the sum of expressions A1-37, A1-38 and A1-39 requires an evaluation of the behavior of $\exp[\theta(s)]$, $\theta'(s)$ and $\theta''(s)$. Using equation 1-28 to represent V_R:

$$\theta(s) = \bar{c}\ln(1+\exp[-\tau(s-2)]) + \bar{b}\frac{2}{s^2-4} + \frac{2}{s^2} + \ln\frac{s^2-4}{s^2} \qquad \text{A1-40}$$

where $\bar{c}$ equals $\epsilon a\psi^2(0)/2kT$ and $\tau = \kappa a$. Thus,

$$\theta'(s) = \frac{-\bar{c}\tau}{(\exp[\tau(s-2)]+1)} - \frac{64\bar{b}}{(s^2-4)^2(s)^3} \qquad \text{A1-41}$$

and $\theta''(s)$ equals

$$\theta''(s) = \frac{\bar{c}\tau^2\exp(\tau[s-2])}{[1+\exp(\tau[s-2])]} + \frac{64\bar{b}(7-(40/s^2)+(48/s^4))}{(s^2-4)^4} \qquad \text{A1-42}$$

Since $\theta(s)$, $\theta'(s)$ and $\theta''(s)$ are complex functions which do not change regularly with s, the maximum of the sum of expressions A1-37, A1-38 and A1-39 cannot be found by inspection. Furthermore, equating the first derivative of their sum with zero to find the maximum

yields an expression which is not readily soluble.

Consequently, numerical analysis was used to determine the manner in which the values of τ, $\epsilon a\psi^2(0)/2kT$ and $A/6kT$ effected the position and magnitude of the maximum in the $\xi''(s)$ function. This was done on a PDP-8/m computer in a Focal 8 language. The figures in the following discussion of this work were however drawn with a Hewlett Packard 7200A graphic plotted which was attached to a PDP 11/20 computer. The values of $\epsilon a\psi^2(0)/2kT$, $A/6kT$ and τ used to construct the figures in the following discussion were chosen so that they were similar to the values actually used in the calculations of $W_0^{0.5}$. However, the PDP 11/20 computer and its accompanying language Focal 11 would not accept numbers larger than 10^{39} and the values of τ, $\epsilon a\psi^2(0)/2kT$ and $A/6kT$ often had to be changed to keep the values of $(c-b)\xi''(s)/12$ less than 10^{39}.

The effect of varying τ can be observed in figures A1-1 and A1-2 which present two families of $\xi''(s)$ vs s curves that have been generated by varying τ. Figure A1-1 shows that when the quantities of $\epsilon a\psi^2(0)/2kT$ and $A/6kT$ are invariant, changes in τ, $\tau < 300$, do not effect the magnitude of $\xi''(s)$ when $2.01 < s < 2.50$. Furthermore, the values $\xi''(s)$ assumed in this region are negligible in comparison to the values it assumes when $2.00 < s < 2.01$. The variation in $\log_{10}[(c-b)\xi''(s)/12]$ when $2.00 < s < 2.01$ are presented in figure A1-2 where a family of curves have again been

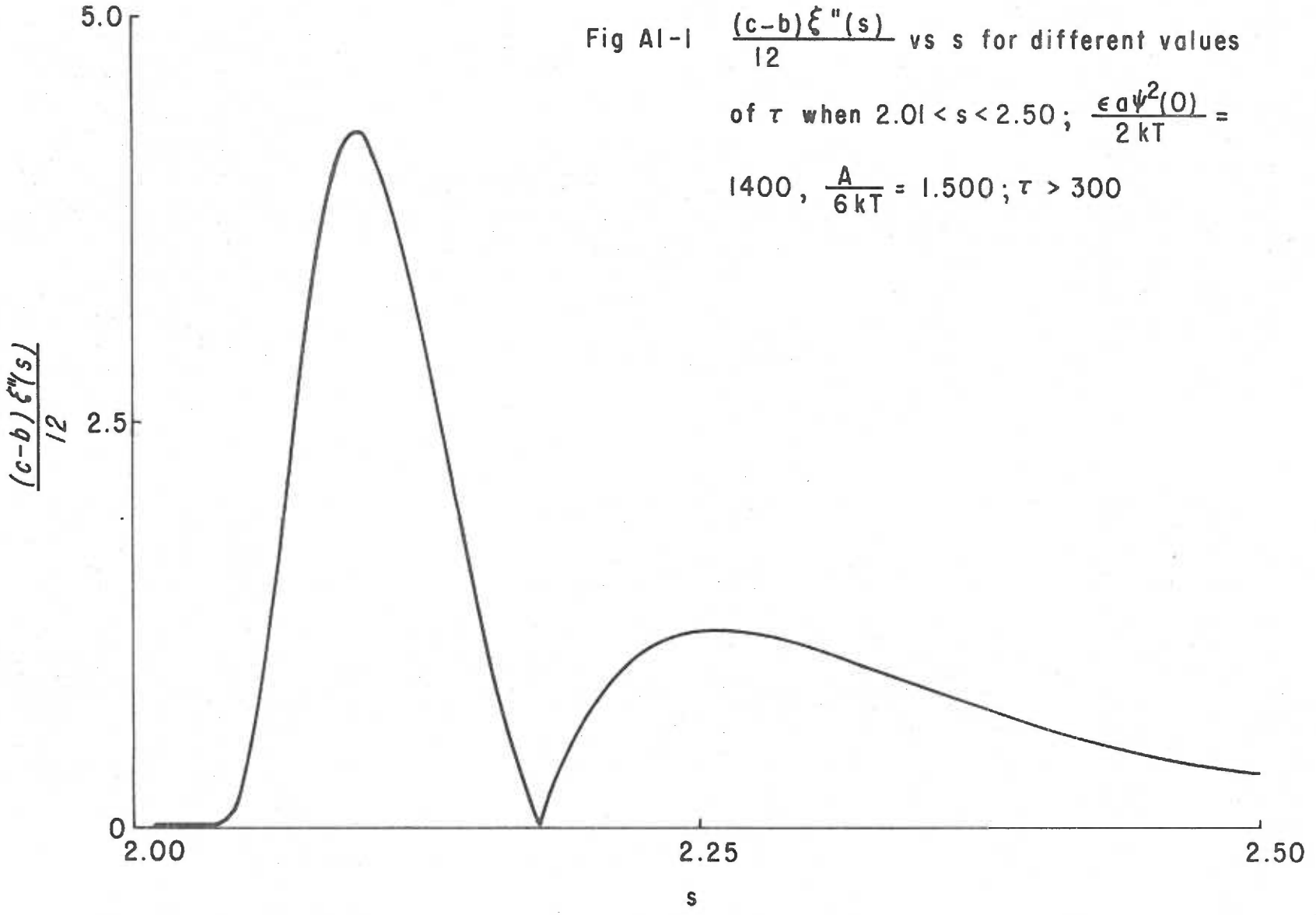

Fig A1-1 $\frac{(c-b)\xi''(s)}{12}$ vs s for different values of τ when $2.01 < s < 2.50$; $\frac{\epsilon a \psi^2(0)}{2kT} = 1400$, $\frac{A}{6kT} = 1.500$; $\tau > 300$

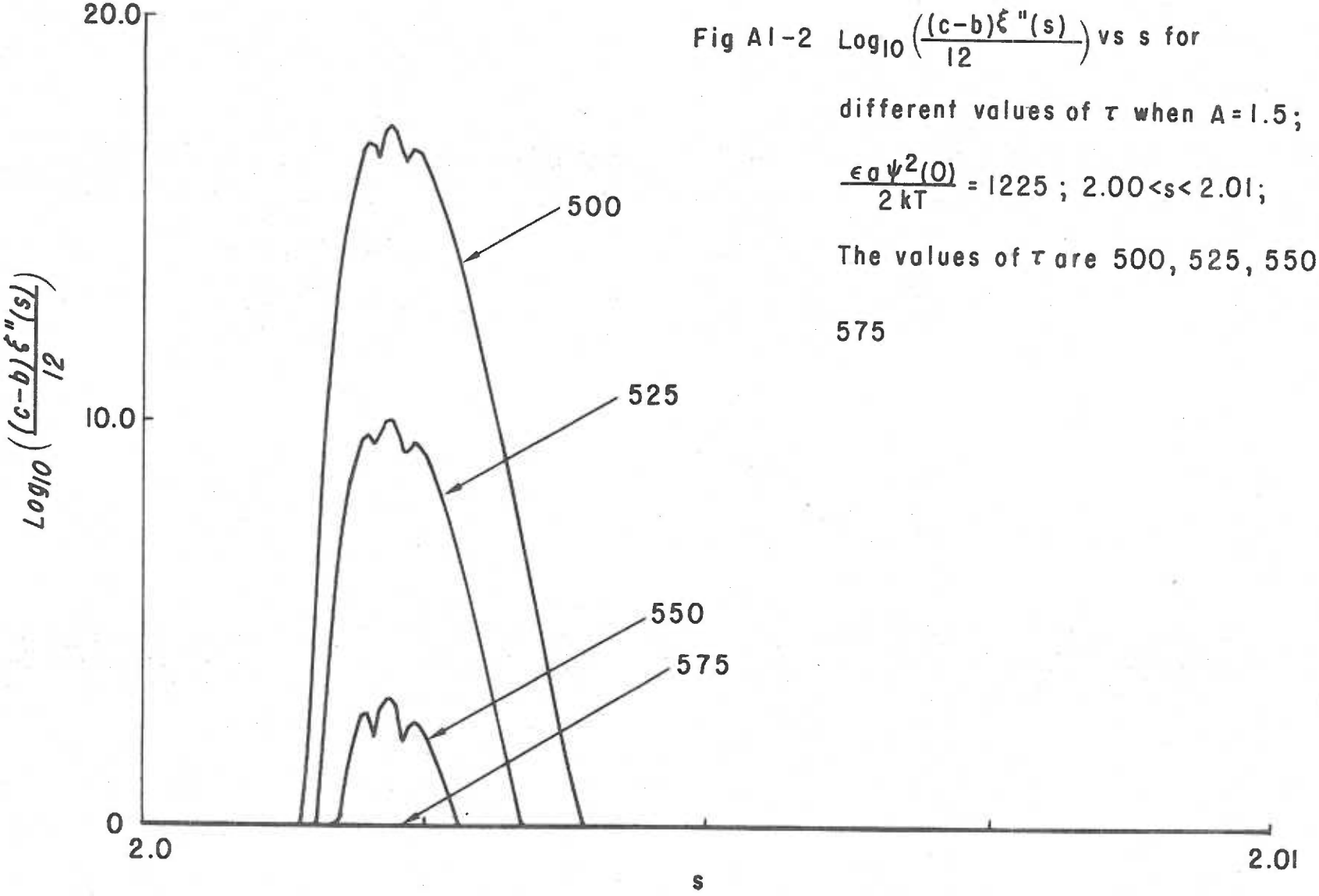

Fig A1-2 $\log_{10}\left(\frac{(c-b)\xi''(s)}{12}\right)$ vs s for different values of τ when A = 1.5; $\frac{\epsilon a \psi^2(0)}{2kT} = 1225$; $2.00 < s < 2.01$; The values of τ are 500, 525, 550, 575

generated by varying τ. From this figure it is apparent that the maximum value of $\xi''(s)$ is quite sensitive to τ and can easily attain values in excess of 10^{100} as τ approaches 300. This reflects the dependence of the $\theta(s)$ term on the value of τ and the dominance of the $\exp[\theta(s)]$ term in controlling the value of $\xi''(s)$.

Figures A1-3 and A1-4 present two families of curves which demonstrate the effect of varying $\epsilon a\psi^2(0)/2kT$ when the values of $A/6kT$ and τ are held constant. Figure A1-3 shows that when $s > 2.01$, variations in $\epsilon a\psi^2(0)/2kT$ do not change the value of $\xi''(s)$, which is quite small in comparison to its magnitude when $2.00 < s < 2.01$. In this region small changes in $\epsilon a\psi^2(0)/2kT$ exponentially increase $\xi''(s)$ due to the $\exp[\theta(s)]$ term. This effect is demonstrated in figure A1-4, where $\log_{10}[(c-b)\xi''(s)/12]$ is plotted against s. Again the maximum values of $\xi''(s)$ become very large as the potential energy of repulsion term becomes larger than the potential energy of attraction term at a given value of s.

Figures A1-5 and A1-6 show the manner in which variations in the value of $A/6kT$ affect $\xi''(s)$. In figure A1-5, where $\log_{10}[(c-b)\xi''(s)/12]$ is calculated when $2.01 < s < 2.50$, it is evident that the value of A causes the maximum of $\xi''(s)$ in this region to change. However, the maximum value of $\xi''(s)$ is still negligible in comparison to its maximum value when $2.00 < s < 2.01$. This is demonstrated by figure A1-6 which presents a family of

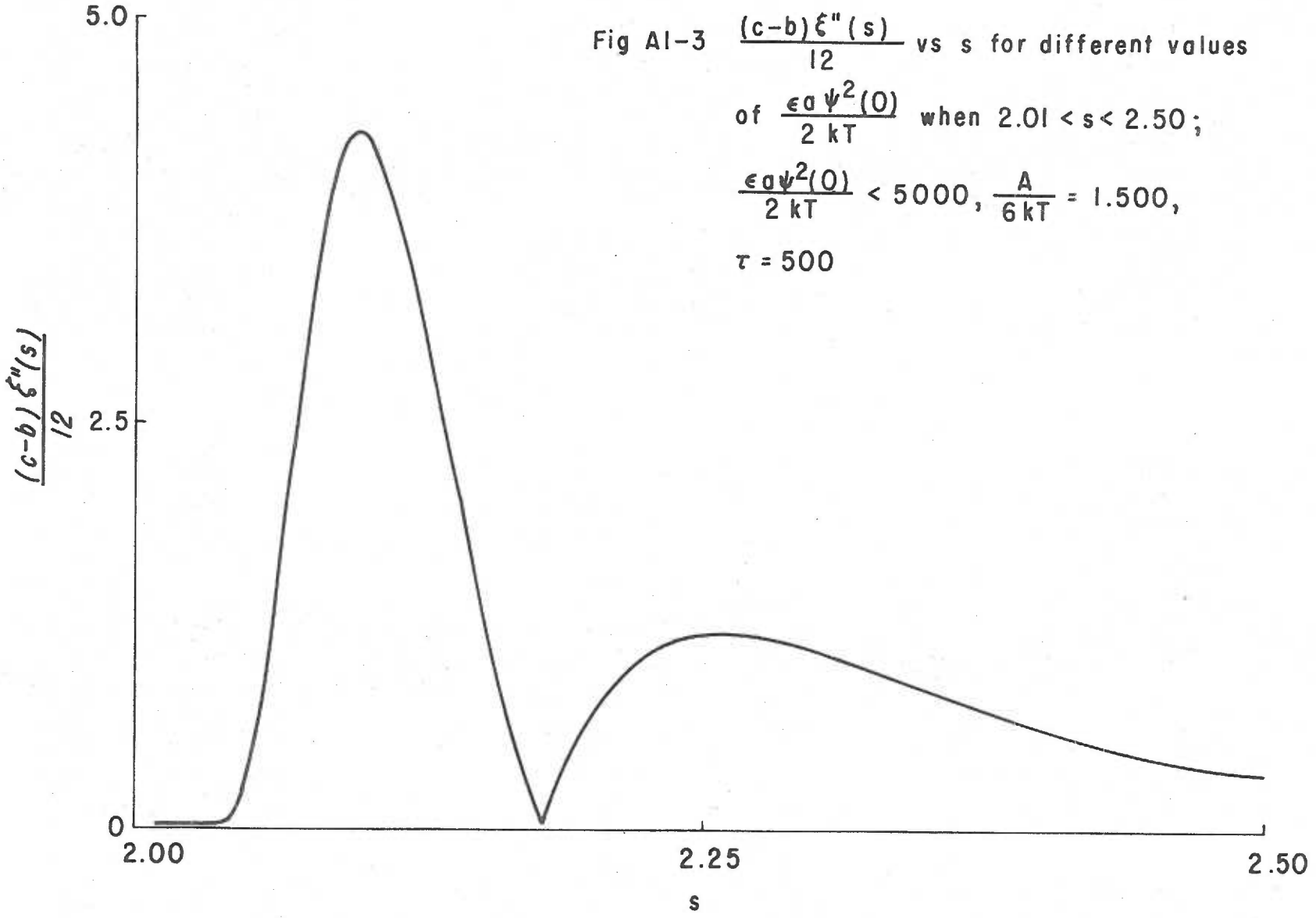

Fig AI-3 $\frac{(c-b)\xi''(s)}{12}$ vs s for different values of $\frac{\epsilon a \psi^2(0)}{2\,kT}$ when $2.01 < s < 2.50$; $\frac{\epsilon a \psi^2(0)}{2\,kT} < 5000$, $\frac{A}{6\,kT} = 1.500$, $\tau = 500$

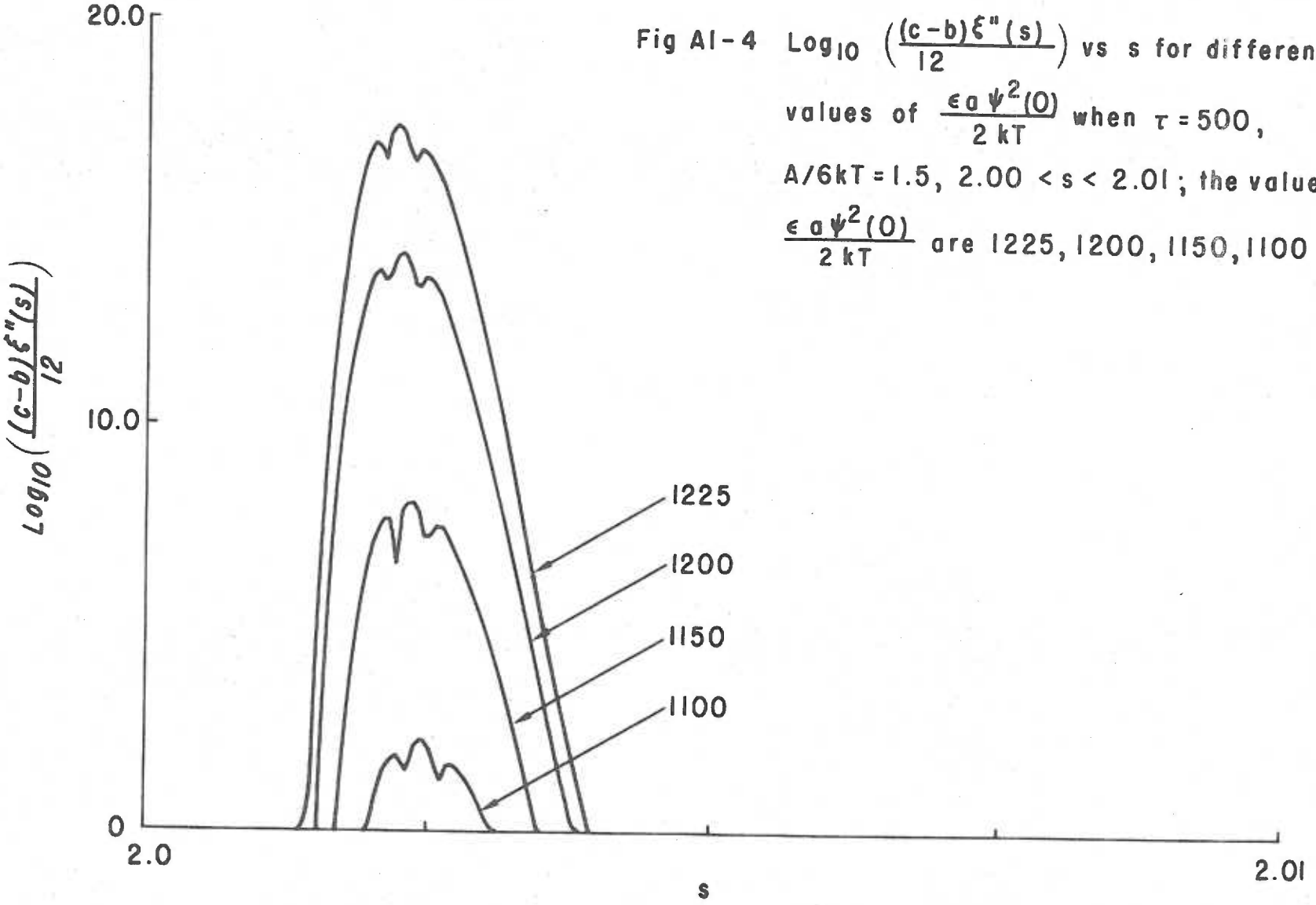

Fig A1-4 $Log_{10}\left(\frac{(c-b)\xi''(s)}{12}\right)$ vs s for different values of $\frac{\epsilon a \psi^2(0)}{2kT}$ when $\tau = 500$, $A/6kT = 1.5$, $2.00 < s < 2.01$; the values $\frac{\epsilon a \psi^2(0)}{2kT}$ are 1225, 1200, 1150, 1100

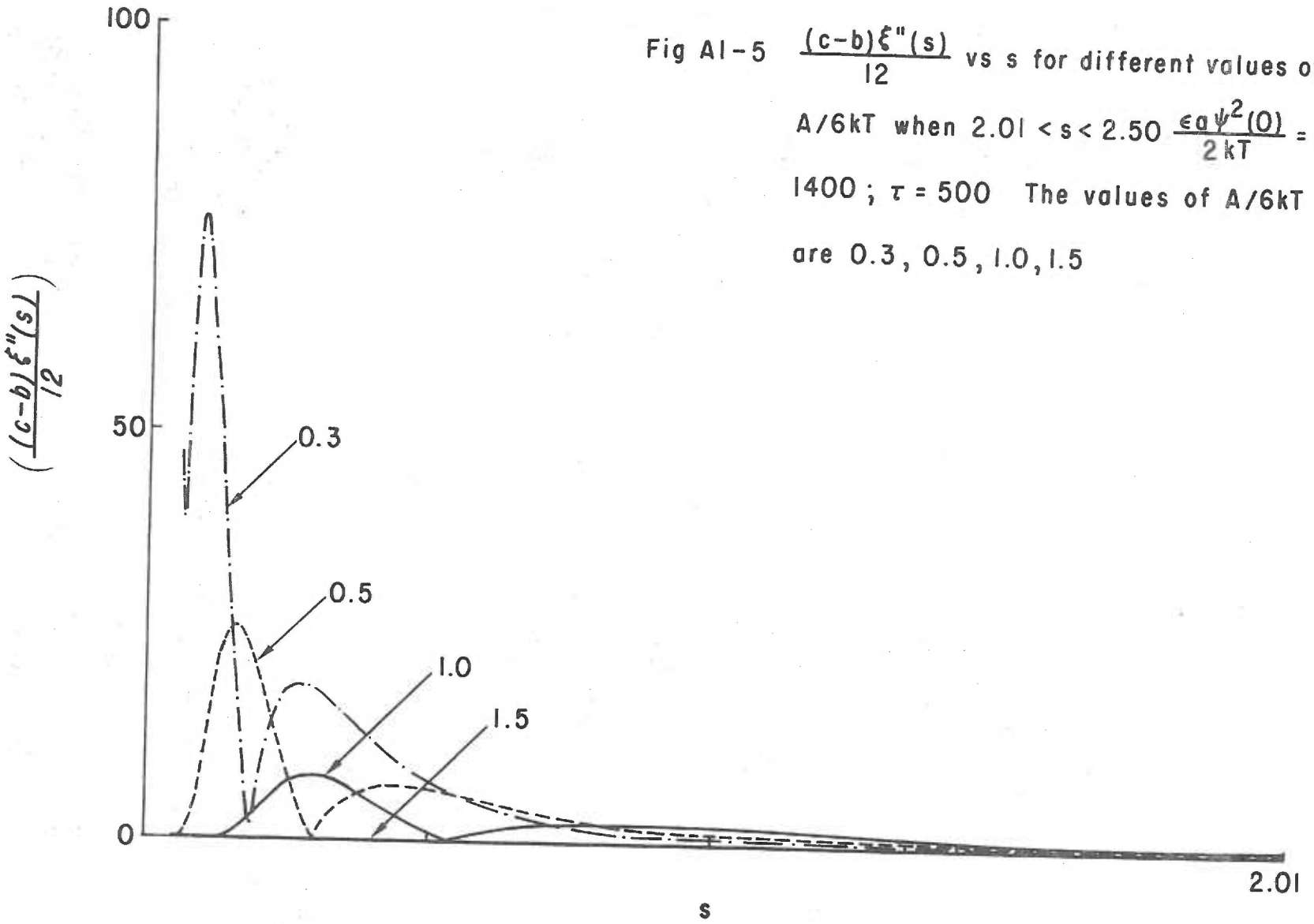

Fig A1-5 $\frac{(c-b)\xi''(s)}{12}$ vs s for different values of A/6kT when $2.01 < s < 2.50$ $\frac{\epsilon a \psi^2(0)}{2kT} = 1400$; $\tau = 500$ The values of A/6kT are 0.3, 0.5, 1.0, 1.5

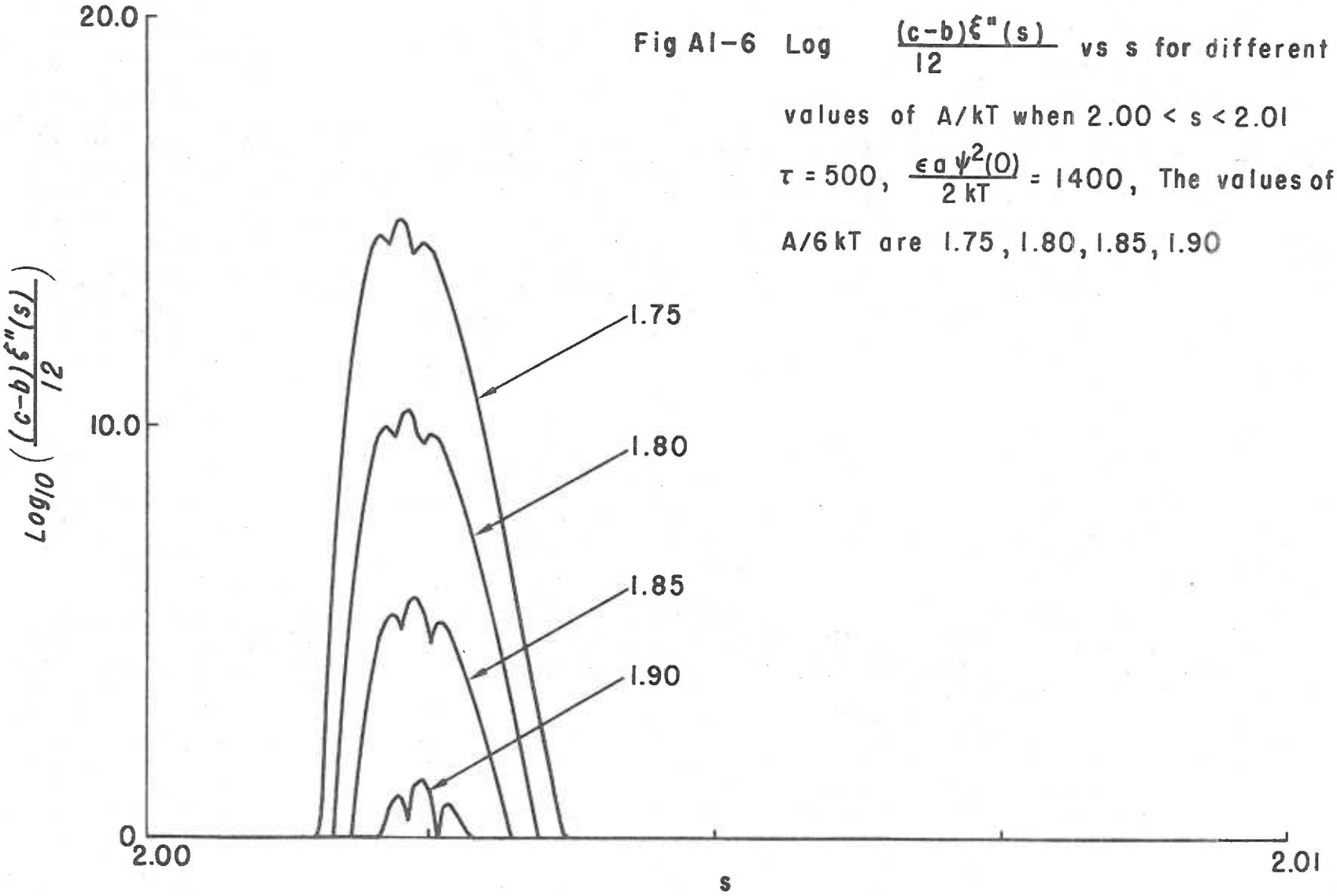

Fig AI-6 Log $\frac{(c-b)\xi''(s)}{12}$ vs s for different values of A/kT when $2.00 < s < 2.01$ $\tau = 500$, $\frac{\epsilon a \psi^2(0)}{2\,kT} = 1400$, The values of A/6 kT are 1.75, 1.80, 1.85, 1.90

$\log_{10}[(c-b)\xi''(s)/12]$ vs s curves which have been generated by varying the value of $A/6kT$. Again the role of the $\exp[\theta(s)]$ term in controlling the value of $\xi''(s)$ is evident as is the effect of $A/6kT$ on $\theta(s)$.

Figures A1-2, A1-4 and A1-6 show that the maximum value of the expression $((c-b)\xi''(s)/12)\Delta s^2$ may easily exceed $10^{100}\ \Delta s^2$. Thus, it was not possible to use the maximum value of $(c-b)\xi''(s)/12$ as a means of estimating the value of Δs to be used in calculating $W_0^{0.5}$ and an empirical approach was selected. This entailed calculating the value of $W_0^{0.5}$ by the trapezoidal rule using ever decreasing values of Δs until the value of $W_0^{0.5}$ did not change by more than 0.01% when the value of Δs was decreased by an order of magnitude. By this procedure a value of 10^{-5} was chosen as an appropriate size for Δs.

The program used to calculate $(c-b)\xi''(s)/12$ is given in table A1-1. The programs used to calculate W_b^c using Verwey and Overbeek's (12) and Honig and Mul's (18) expression for V_R are given in tables A1-2 and A1-3 respectively.

Table A1-1. The program used to calculate $\log_{10}[(c-b)\xi''(s)/12]$ on the PDP 11/20 computer.

```
 W
C:FOCAL-11,LFOCA-A

  1.10 SET T=500; T "PLTL",!
  1.20 SET A=0
  1.30 SET E=500
  1.40 FOR S=2.01,0.01,2.5; DO 2

  2.30 SET VA=A*<(2/(S↑2-4))+(2/S↑2)+FSBR(15,(S↑2-4)/S↑2)>
  2.31 SET Q=1/FSBR(14,T*(S-2));SET VR=E*FSBR(15,1+Q)
  2.33 SET GS=FSBR(14,VR-VA)
  2.40 SET G1=(A*64/(S↑2-4)↑2*S↑3)-E*T/(FSBR(14,T*(S-2))+1)
  2.50 SET M=E*T↑2/(2+FSBR(14,1/T*(S-2))+FSBR(14,T*(S-2)))
  2.51 SET N=A*64*(7-(40/S↑2)+(48/S↑4))/(S↑2-4)↑4
  2.52 SET G2=M-N
  2.60 SET X=G1↑2/(S-2)-(2*G1/(S-2)↑2)+G2/(S-2)+2/(S-2)↑3
  2.61 SET Y=G1↑2/(6S-8)-2*G1/(6*S-8)↑2+G2/(6*S-8)+2/(6*S-8)↑3
  2.62 SET Z=(G1↑2/S-2*G1/S↑2+G2/S+2/S↑3)*11/192
  2.63 SET P=FABS(GS*<X/96+27*Y/96+Z>);IF (P-1)2.64,2.65,2.65
  2.64 SET P=1
  2.65 SET TEST=FSBR(15,P)/2.3026
  2.66 T %4 FITR((S-2)*20000), FITR(TEST*100), !

 14.01 C EXP: FSBR(14,ARG)
 14.03 I (&-88)14.05;SET &=10↑38; R
 14.05 I (88+&)14.07,14.10,14.10
 14.07 SET &=0; R
 14.10 I (&↑2-.01)14.2;S &=&/2;D 14;S &=&↑2;R
 14.20 S &=1+&+&↑2/2+&↑3/6+&↑4/24+&↑5/120+&↑6/720

 15.01 C LOG: FSBR(15,ARG)
 15.05 I (&-10↑19)15.10;SET &=43; R
 15.10 I (&↑2-2.04*&+1)15.2;S &=FSQT(&);D 15;S &=2*&;R
 15.20 S &=(&-1)/(&+1);S &=2*(&+&↑3/3+&↑5/5+&↑7/7)
*
```

Table A1-2. The program used to calculate W_b^c from equation A1-5 with Verwey and Overbeek's (12) expression for V_R on a Hewlett Packard 9100B calculator. Column A refers to an address in the calculator's memory and column B refers to the instruction that is placed in it. Values which must be placed in storage registers are A = u; B = A/6kT; C = $\epsilon a \psi^2(0)/2kT$; D = $-\kappa a$.

A	B	A	B	A	B	A	B	A	B
0.0	20	2.0	33	4.0	17	6.0	05	8.0	27
0.1	13	2.1	25	4.1	27	6.1	33	8.1	26
0.2	27	2.2	35	4.2	13	6.2	40	8.2	32
0.3	36	2.3	35	4.3	36	6.3	13	8.3	05
0.4	06	2.4	40	4.4	25	6.4	21	8.4	36
0.5	36	2.5	34	4.5	74	6.5	05	8.5	23
0.6	13	2.6	13	4.6	27	6.6	53	8.6	13
0.7	27	2.7	27	4.7	01	6.7	00	8.7	25
0.8	01	2.8	36	4.8	33	6.8	01	8.8	33
0.9	03	2.9	27	4.9	25	6.9	67	8.9	14
0.a	36	2.a	25	4.a	65	6.a	34	8.a	45
0.b	02	2.b	04	4.b	27	6.b	16	8.b	27
0.c	33	2.c	34	4.c	16	6.c	27	8.c	01
0.d	25	2.d	02	4.d	36	6.d	14	8.d	25
1.0	33	3.0	30	5.0	25	7.0	36	9.0	32
1.1	13	3.1	35	5.1	30	7.1	36	9.1	01
1.2	27	3.2	22	5.2	34	7.2	27	9.2	33
1.3	06	3.3	35	5.3	25	7.3	67	9.3	40
1.4	36	3.4	31	5.4	74	7.4	34	9.4	14
1.5	04	3.5	65	5.5	24	7.5	14	9.5	44
1.6	33	3.6	33	5.6	34	7.6	36	9.6	00
1.7	13	3.7	02	5.7	13	7.7	67	9.7	00
1.8	36	3.8	22	5.8	36	7.8	34		
1.9	25	3.9	35	5.9	60	7.9	17		
1.a	35	3.a	25	5.a	13	7.a	33		
1.b	13	3.b	33	5.b	27	7.b	25		
1.c	27	3.c	14	5.c	25	7.c	33		
1.d	02	3.d	36	5.d	32	7.d	12		

Table A1-3. The program used to calculate W_b^c from equation A1-5 with Honig and Mul's (18) expression for V_R on a Hewlett Packard 9100 B calculator. Column A refers to an address in the calculator's memory and column B refers to the instruction that is places in it. Values which must be placed in storate registers are $A = 0.32/\kappa a$; $B = A/6kT$; $C = \tanh(\psi(0)/4kT)$; $D = -\kappa a = \tau$; $-D = 1.134 \times 10^{25}\, a^3 M/(\kappa a)^2$.

A	B	A	B	A	B	A	B	A	B
0.0	20	2.0	33	4.0	40	6.0	25	8.0	16
0.1	13	2.1	25	4.1	34	6.1	36	8.1	27
0.2	27	2.2	35	4.2	16	6.2	40	8.2	36
0.3	36	2.3	35	4.3	13	6.3	34	8.3	01
0.4	06	2.4	40	4.4	27	6.4	14	8.4	33
0.5	36	2.5	34	4.5	17	6.5	27	8.5	01
0.6	13	2.6	13	4.6	36	6.6	27	8.6	05
0.7	27	2.7	27	4.7	25	6.7	36	8.7	30
0.8	01	2.8	36	4.8	27	6.8	11	8.8	35
0.9	03	2.9	27	4.9	74	6.9	00	8.9	11
0.a	36	2.a	25	4.a	27	6.a	00	8.a	30
0.b	02	2.b	04	4.b	36	6.b	36	8.b	34
0.c	33	2.c	34	4.c	27	6.c	04	8.c	17
0.d	25	2.d	02	4.d	01	6.d	05	8.d	27
1.0	33	3.0	30	5.0	30	7.0	22	9.0	13
1.1	13	3.1	35	5.1	34	7.1	36	9.1	36
1.2	27	3.2	22	5.2	30	7.2	01	9.2	02
1.3	06	3.3	35	5.3	65	7.3	33	9.3	36
1.4	36	3.4	31	5.4	33	7.4	25	9.4	25
1.5	04	3.5	65	5.5	02	7.5	33	9.5	33
1.6	33	3.6	33	5.6	22	7.6	67	9.6	74
1.7	13	3.7	02	5.7	30	7.7	34	9.7	36
1.8	36	3.8	22	5.8	35	7.8	14	9.8	02
1.9	25	3.9	35	5.9	25	7.9	30	9.9	35
1.a	35	3.a	25	5.a	33	7.a	35	9.a	44
1.b	13	3.b	33	5.b	16	7.b	40	9.b	34
1.c	27	3.c	14	5.c	27	7.c	34	9.c	00
1.d	02	3.d	36	5.d	36	7.d	14	9.d	00

Table A1-3. Continued.

A	B	A	B	A	B	A	B
-0.0	16	-2.0	67	-4.0	13	-6.0	33
-0.1	36	-2.1	34	-4.1	33	-6.1	4-
-0.2	36	-2.2	14	-4.2	40	-6.2	14
-0.3	36	-2.3	33	-4.3	13	-6.3	26
-0.4	36	-2.4	67	-4.4	25	-6.4	32
-0.5	67	-2.5	34	-4.5	37	-6.5	04
-0.6	34	-2.6	17	-4.6	30	-6.6	23
-0.7	14	-2.7	36	-4.7	60	-6.7	13
-0.8	34	-2.8	67	-4.8	27	-6.8	44
-0.9	40	-2.9	34	-4.9	15	-6.9	33
-0.a	34	-2.a	16	-4.a	35	-6.a	00
-0.b	14	-2.b	34	-4.b	26	-6.b	00
-0.c	17	-2.c	25	-4.c	32		
-0.d	27	-2.d	74	-4.d	06		
-1.0	13	-3.0	24	-5.0	52		
-1.1	36	-3.1	34	-5.1	33		
-1.2	25	-3.2	13	-5.2	00		
-1.3	74	-3.3	36	-5.3	01		
-1.4	27	-3.4	37	-5.4	61		
-1.5	36	-3.5	60	-5.5	27		
-1.6	27	-3.6	24	-.56	14		
-1.7	02	-3.7	12	-5.7	45		
-1.8	35	-3.8	01	-5.8	45		
-1.9	25	-3.9	26	-5.9	27		
-1.a	33	-3.a	32	-5.a	01		
-1.b	16	-3.b	04	-5.b	26		
-1.c	36	-3.c	36	-5.c	32		
-1.d	36	-3.d	27	-5.d	02		

APPENDIX II

DERIVATION OF THE RELATIONSHIP BETWEEN THE STANDARD DEVIATION OF A DISTRIBUTION OF MOLECULAR WEIGHTS AND THE WEIGHT AND NUMBER AVERAGE MOLECULAR WEIGHTS OF THE DISTRIBUTION

Some of the moments of the distribution of a random variable b are defined as follows:

$$1^{st} \text{ moment} \equiv \text{MEAN} \equiv \sum_i p_i b_i \equiv \bar{b}_1 \qquad \text{A2-1}$$

$$2^{nd} \text{ moment} \equiv \sum_i p_i b_i^2 = \bar{b}_2 \qquad \text{A2-2}$$

$$2^{nd} \text{ moment about the mean} \equiv \text{variance} \equiv \sum_i p_i (b_i - \bar{b}_1)^2 = (\bar{b}_2 - \bar{b}_1^2) \equiv \sigma^2 \qquad \text{A2-3}$$

$p_i \equiv$ the probability of b_i

For molecular weight distributions where M_i is the molecular weight of the i^{th} species, N_i is the number of molecules of the i^{th} type in the distribution and p_i is the probability or fraction of molecules of the i^{th} type:

$$M_n \equiv \frac{\sum_i N_i M_i}{\sum_i N_i} = \sum_i p_i M_i = \bar{b}_1 \qquad \text{A2-4}$$

$$M_w \equiv \frac{\sum_i N_i M_i^2}{\sum_i N_i M_i} = \frac{\dfrac{\sum_i N_i M_i^2}{\sum_i N_i}}{\dfrac{\sum_i N_i M_i}{\sum_i N_i}} = \frac{\bar{b}_2}{\bar{b}_1} \qquad \text{A2-5}$$

thus,

$$\bar{b}_2 = M_n M_w \qquad \text{A2-6}$$

and substituting A2-6 and A2-4 into A2-3, the standard deviation of a molecular weight distribution, σ, is

$$\sigma = (M_n M_w - M_n^2)^{1/2}$$

APPENDIX III

THE OSMOTIC CONTRIBUTION OF A POLYELECTROLYTE'S COUNTERIONS IN THE PRESENCE OF A LARGE CONCENTRATION OF INDIFFERENT ELECTROLYTE

The purpose of this appendix is to calculate the concentration of osmotically active salt ions in a salt-polyelectrolyte solution which is separated from a salt solution by a membrane that is impermeable to the polymer alone. When the system is at equilibrium the concentration of salt on the side of the membrane exposed to the salt-polyelectrolyte solution, m_s, is given by:

$$m_s = \left[\left(\frac{m_s^1 \gamma_\pm^1}{\gamma_\pm}\right)^2 + \left(\frac{m_p}{2}\right)^2\right]^{1/2} - \frac{m_p}{2} \qquad 4\text{-}10$$

where m_s^1 and $\gamma_\pm^1$ are the concentration and mean ionic activity coefficient of the salt ions on the side of the membrane not exposed to the polyelectrolyte. m_p and $\gamma_\pm$ are the concentration of the polyelectrolyte's counterions and the mean ionic activity coefficient of the salt ions in the presence of the polyelectrolyte. Equation 4-10 can be rewritten as

$$m_s = \frac{-m_p}{2} + \frac{m_s^1 \gamma_\pm^1}{\gamma_\pm}\left[1 + \left(\frac{\frac{m_p}{2}}{\frac{m_s^1 \gamma_\pm^1}{\gamma_\pm}}\right)^2\right]^{1/2} \qquad A3\text{-}1$$

or

$$m_s = \frac{-m_p}{2} + \frac{m_s^1 \gamma_\pm^1}{\gamma_\pm} \left[1 + \left(\frac{m_p \gamma_\pm}{2 m_s^1 \gamma_\pm^1} \right)^2 \right]^{1/2} \qquad \text{A3-2}$$

when $m_s^1 \gg m_p$, equation A3-2 can be rewritten by use of the following series expansion:

$$(b+1)^{1/2} = 1 + \frac{b}{2} - \frac{b^2}{8} + \frac{b^3}{16} - \frac{5b^4}{128} + \ldots \quad (-1 < b < 1) \qquad \text{A3-3}$$

Thus, when $m_s^1 \gg m_p$, let

$$b = \left(\frac{m_p \gamma_\pm}{2 m_s^1 \gamma_\pm^1} \right) \qquad \text{A3-4}$$

and substituting the square root term in equation A3-2 for its series expansion yields:

$$m_s = -\frac{m_p}{2} + \frac{m_s^1 \gamma_\pm^1}{\gamma_\pm} \left[1 + \frac{b}{2} - \frac{b^2}{8} + \frac{b^3}{16} - \frac{5b^4}{128} + \ldots \right] \qquad \text{A3-5}$$

since $b \ll 1$,

$$m_s \simeq \frac{-m_p}{2} + \frac{m_s^1 \gamma_\pm^1}{\gamma_\pm} \left[1 + \frac{b}{2} \right] \qquad \text{A3-6}$$

or, substituting back the original value for b,

$$m_s \simeq \frac{m_s^1 \gamma_\pm^1}{\gamma_\pm} - \frac{m_p}{2} + \frac{m_p^2 \gamma_\pm}{8 m_s^1 \gamma_\pm^1} \qquad \text{A3-7}$$

The difference in the concentration of ions on the two sides of the membrane, Δm_s, is:

$$\Delta m_s = m_p + 2m_s - 2m_s^1 \qquad \text{A3-8}$$

where m_s' is the concentration of salt on the side of the membrane not exposed to the polyelectrolyte. When m_s, for expression A3-7, is substituted into equation A3-8 the result is:

$$\Delta m_s \simeq m_p + \frac{2m_s^1\gamma_\pm^1}{\gamma_\pm} - m_p + \frac{2m_p^2\gamma_\pm}{8m_s^1\gamma_\pm^1} - 2m_s^1 \qquad \text{A3-9}$$

$$\simeq \frac{m_1^2\gamma_\pm}{4m_s^1\gamma_\pm^1} + 2m_s^1\left(\frac{\gamma_\pm^1}{\gamma_\pm} - 1\right)$$

or, at very high ionic strengths where $m_s^1 \gg m_p$, $\frac{\gamma_\pm^1}{\gamma_\pm} \simeq 1$

$$\Delta m_s \simeq \frac{m_p^2}{4m_s^1} \sim 0 \qquad \text{4-12}$$

APPENDIX IV

A MODEL FOR THE ELECTROSTATIC POTENTIAL OF A PARTICLE WITH AN ADSORBED POLYELECTROLYTE

A major factor influencing the interation of colloidal particles is the electrostatic potential of the particles. When polyelectrolytes adsorb to the surface of the particle the electrostatic potential will be altered in a manner that depends primarily on the configuration, degree of ionization and extent of binding. The following calculations are an attempt to estimate the manner in which the potential of the particle-polymer system varies with the configuration of the adsorbed polymer and distance from the surface of the particle.

The configuration of a large molecular weight polymer adsorbed to a flat surface has been predicted by Silberberg (43), Rubin (39), Hesselink (46) and Motomura and Matuura (47-50). The adsorbed polymer is usually pictured in terms of alternating loops of varying numbers of polymer segments adsorbed to the surface and then extending into the liquid phase. Most of these models assume that polymeric configuration in solution can be analyzed in terms of a three dimensional random walk by a totally flexible molecule. A serious limitation of this model is that it usually leads to an underestimation of the average configuration by the creation of an excluded volume effect. However, this is usually treated by the inclusion of an expansion factor

or by restricting the application of the predictions to work with theta solvents. In a theta solvent the interactions between segments of the same molecule are eliminated. Silberberg (44) has attempted a mathematical treatment of this problem, while Clayfield and Lumb (209, 210) and Lax (223, 224) used Monte Carlo techniques with the aid of computers to treat it. A second problem with most of the aforementioned formulations of polymeric configuration is that all polymeric conformations are treated as being equally probable with no weighting of the probability of the various configurations on the basis of their free energies. This is a hazardous approximation to make with polyelectrolytes where the electrostatic contribution to the configurational free energy of the polymer is usually quite large. Finally, the polymers to be used in the following experiment are of a relatively low molecular weight and as such a considerable portion of the polymeric segments extending into the solution may be attached only at an end, thereby forming a tail. These end effects undoubtedly affect the distribution of polymer segments about the adsorbent surface. However, if the portion of polymeric segments in loop and tail configurations were known the overall distribution of the segments could be estimated as Hesselink (46) has derived an expression for the distribution of segments in the loop and tail configurations. Unfortunately, few predictions and little information exist on the distribution of segments for low molecular weight polyelectrolytes. Thus, as a first

approximation, it will be assumed that the distribution of polymer segments about the adsorbent surface will be described by a uniform probability density. This distribution has been selected on the assumption that the average configuration for loops and tails of the adsorbed polymer is a maximal extension from the surface to which they are anchored. Under these conditions, a fairly uniform distribution of segments throughout the polymer layer would result. An obvious shortcoming of this model is the tacit assumption that the loops and tails are of a uniform size. In actuality, an exponentially decaying distribution of neutral polymer segments is more probable (46). However, as a first attempt, the distribution of segments in the polymer layer will be assumed uniform.

In this derivation the level of polymer adsorption will be assumed large enough to be uniform. The probability density for the distribution of polymer segments is given by equations A4-1 and A4-2, where δ is the thickness of the adsorbed polymer layer.

$$p(x) = \frac{1}{\delta} \qquad 0 < x < \delta \qquad \text{A4-1}$$

$$p(x) = 0 \qquad 0 > x > \delta \qquad \text{A4-2}$$

$p(x)$ is the probability of finding a charge group of the polymeric chain at a distance x from the plane's surface. Further assumptions include:

1) The polymer can be treated as if it were adsorbed to an infinite plane of surface potential, $\psi(0)$.
2) The distribution of charge groups on the surface are uniformly smeared.
3) The charges of the polyelectrolyte can be treated as point charges.
4) The potential of the system, $\psi(x)$, is small enough that $\frac{e\psi(x)}{kT} \ll 1$ at all points.
5) The distribution of mobile ions with respect to a charged surface is described by the Boltzmann distribution.
6) The dielectric constant in the adsorbed polymer layer is equivalent to that of the bulk solution.

The model described is represented in figure A4-1.

Region 1 encompasses the adsorbed polymer layer and extends from the surface of the plane to the end of the polymer layer, a distance δ away. Region II extends from the edge of the polymer layer to infinity. The variation of potential in either region is given by Poisson's equation:

$$\frac{d^2\psi(x)}{dx^2} = \frac{-4\pi}{\epsilon}\rho(x) \qquad \text{A4-3}$$

where ϵ is the dielectric constant of the region and $\rho(x)$ is defined as:

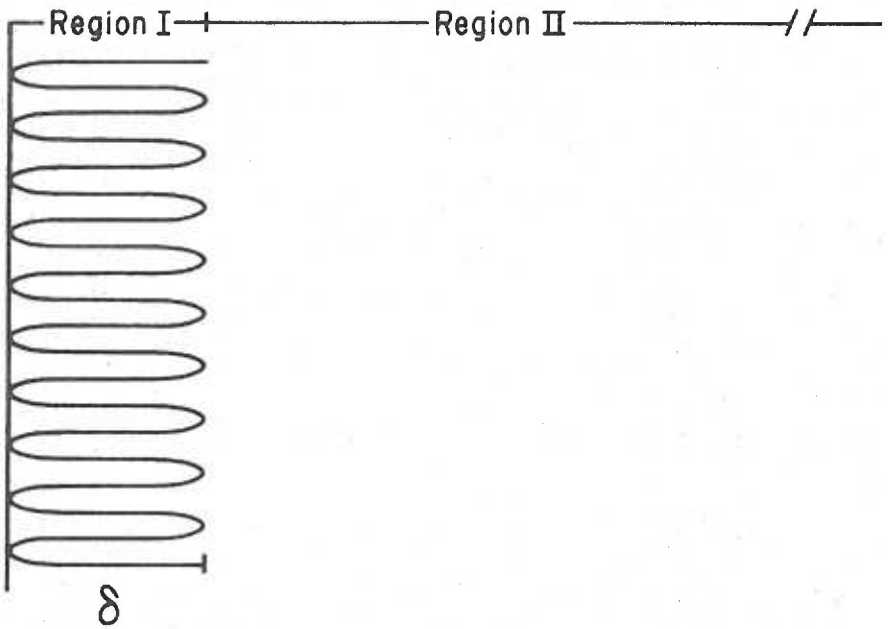

Fig A4-1 Polymer layer of uniform thickness adsorbed to an infinite plane

$$\rho(x) = \sum zen_i(x) \qquad \text{A4-4}$$

where z = the valence of the ion; $n_i(x)$ is the number of ions per cm^3 of the i^{th} species at a given point, and e is the electronic charge unit. To solve for the variation of potential in Region I let:

$\psi_1(x)$ = the potential of the system at a distance x from the surface of the plane in Region I.

$\psi_1(0)$ = the system potential at the surface of the adsorbing plane.

$\psi_1(\delta)$ = the system potential at the far edge of the polymer layer.

$n_i(x) = n_i(\infty)\exp[\frac{-ze\psi(x)}{kT}]$ = the concentration of mobile ions. This is a function of distance from the plane, as predicted by the Boltzmann equation.

n_p = the concentration of polymeric charge groups in Region I. There is no dependence on distance from the adsorbent surface.

Solving for $\rho(x)$ and substituting into equation A4-3 gives:

$$\frac{d^2\psi(x)}{dx^2} = \frac{-4\pi ze}{\epsilon}[n_i(\infty)\exp(\frac{-ze\psi(x)}{kT}) + n_p - n_i(\infty)\exp(\frac{ze\psi(x)}{kT})] \qquad \text{A4-5}$$

$$\frac{d^2\psi(x)}{dx^2} = \frac{8\pi zen_i(\infty)}{\epsilon}[\sinh(\frac{ze\psi(x)}{kT}) - \frac{n_p}{2n_i(\infty)}] \qquad \text{A4-6}$$

Expanding the sinh term and using only the linear portion (assumes $\frac{ze\psi(x)}{kT} \ll 1$):

$$\frac{d^2\psi(x)}{dx^2} = \frac{8\pi z e n_i(\infty)}{\epsilon}\left[\frac{ze\psi(x)}{kT} - \frac{n_p}{2n_i(\infty)}\right] \qquad \text{A4-7}$$

On substituting:

$$\kappa = \left[\frac{8\pi z^2 e^2 n_i(\infty)}{\epsilon kT}\right]^{1/2} \qquad \text{A4-8}$$

$$\gamma = \frac{4\pi z e n_p}{\epsilon} \qquad \text{A4-9}$$

Equation A4-7 reduces to:

$$\psi''(x) - \kappa^2\psi(x) = -\gamma \qquad \text{A4-11}$$

where

$$\psi''(x) = \frac{d^2\psi(x)}{dx^2} \qquad \text{A4-11}$$

To solve this equation the complimentary homogeneous equation $\psi''(x) - \kappa^2\psi(x) = 0$ is solved first. It has a general solution of:

$$\psi(x) = d\exp(-\kappa x) + f\exp(\kappa x) \qquad \text{A4-12}$$

where d and f are constants determined by boundary conditions.

In solving the non homogeneous equation by the method of undetermined multipliers, the first trial solution, $\psi_t(x)$, is:

$$\psi_t(x) = d\exp(-\kappa x) + f\exp(\kappa x) + c \qquad \text{A4-13}$$

where c is a constant. To evaluate c it is required:

$$\psi_t''(x) - \kappa^2\psi_t(x) + \gamma = 0 \qquad \text{A4-14}$$

To solve for $\psi_t''(x)$:

$$\psi_t'(x) = -d\kappa \exp(-\kappa x) + f\kappa \exp(\kappa x) \qquad \text{A4-15}$$

$$\psi_t''(x) = d\kappa^2 \exp(-\kappa x) + f\kappa^2 \exp(\kappa x) \qquad \text{A4-16}$$

Substituting A4-16 and A4-13 into A4-14:

$$d\kappa^2 \exp(-\kappa x) + f\kappa^2 \exp(\kappa x) - d\kappa^2 \exp(-\kappa x)$$

$$- f\kappa^2 \exp(\kappa x) - \kappa^2 c + \gamma = 0 \qquad \text{A4-17}$$

Thus,

$$c = \frac{\gamma}{\kappa^2} \qquad \text{A4-18}$$

Substituting A4-18 into A4-13 yields the general solution for the potential in Region I:

$$\psi_1(x) = d \exp(-\kappa x) + f \exp(\kappa x) + \frac{\gamma}{\kappa^2} \qquad \text{A4-19}$$

In Region II, the potential is computed by solving equation A4-6 when $n_p = 0$. If the sinh term is again linearized the solution $\psi_2(x)$ is:

$$\psi_2(x) = \bar{d} \exp(-\kappa x) + \bar{f} \exp(\kappa x) \qquad \text{A4-20}$$

where $\bar{d}$ and $\bar{f}$ are constants whose values are determined by the boundary conditions. The following boundary conditions are to be used:

$$\psi_2(\infty) = 0 \qquad \text{A4-21}$$

$$\psi_2(\delta) = \psi_1(\delta) \qquad \text{A4-22}$$

$$\psi_2'(\delta) = \psi_1'(\delta) \qquad \text{A4-23}$$

$$\psi_1(0) = \psi_1(0) \qquad \text{A4-24}$$

Applying the boundary conditions in A4-21 requires the constant $\bar{f}$ in equation A4-20 to be zero. Thus,

$$\psi_2(x) = \bar{d}\ \exp(-\kappa x) \qquad \text{A4-25}$$

Applying the other boundary conditions to the appropriate equations yields:

$$\bar{d}\ \exp(-\kappa\delta) = d\ \exp(-\kappa\delta) + f\ \exp(\kappa\delta) + \frac{\gamma}{\kappa^2} \qquad \text{A4-26}$$

$$-\bar{d}\kappa\ \exp(-\kappa\delta) = -d\kappa\ \exp(-\kappa\delta) + f\kappa\ \exp(\kappa\delta) \qquad \text{A4-27}$$

$$\psi_1(0) = d + f + \frac{\gamma}{\kappa^2} \qquad \text{A4-28}$$

Rearranging A4-26:

$$(\bar{d}-d)\exp(-\kappa\delta) = f\ \exp(\kappa\delta) + \frac{\gamma}{\kappa^2} \qquad \text{A4-29}$$

Rearranging A4-27:

$$(\bar{d}-d)\exp(-\kappa\delta) = -f\ \exp(\kappa\delta) \qquad \text{A4-30}$$

Thus

$$\frac{\gamma}{\kappa^2} = -2f\ \exp(\kappa\delta) \quad \text{or} \quad f = -\frac{\gamma}{2\kappa^2}\exp(-\kappa\delta) \qquad \text{A4-31}$$

Substituting A4-31 into A4-28

$$d = \psi_1(0) + \frac{\gamma\ \exp(-\kappa\delta)}{2\kappa^2} - \frac{\gamma}{\kappa^2} = \psi_1(0) + \frac{\gamma}{\kappa^2}\left[\frac{\exp(-\kappa\delta)-2}{2}\right] \qquad \text{A4-32}$$

Substituting A4-31 and A4-32 into A4-26:

$$\bar{d}\ \exp(-\kappa\delta) = \left[\psi_1(0) + \frac{\gamma}{\kappa^2}\left[\frac{\exp(-\kappa\delta)-2}{2}\right]\right]$$

$$\exp(-\kappa\delta) - \frac{\gamma}{2\kappa^2}\exp(-\kappa\delta)\exp(\kappa\delta) + \frac{\gamma}{\kappa^2} \qquad \text{A4-33}$$

$$\bar{d} = \psi_1(0) + \frac{\gamma}{2\kappa^2}\exp(-\kappa\delta) - \frac{\gamma}{\kappa^2} - \frac{\gamma}{2\kappa^2}\exp(\kappa\delta) + \frac{\gamma}{\kappa^2}\exp(\kappa\delta) \qquad \text{A4-34}$$

$$\bar{d} = \psi_1(0) - \frac{\gamma}{\kappa^2}\sinh(\kappa\delta) + \frac{\gamma}{\kappa^2}[\exp(\kappa\delta)-1] \qquad \text{A4-35}$$

Thus the potential in Region II, $\psi_2(x)$ is:

$$\psi_2(x) = [\psi_1(0) - \frac{\gamma}{\kappa^2}\sinh(\kappa\delta) + \frac{\gamma}{\kappa^2}[\exp(\kappa\delta)-1]]\exp(-\kappa x) \qquad \text{A4-36}$$

or, equivalently:

$$\psi_2(x) = [\psi_1(0) + \frac{\gamma}{\kappa^2}[\cosh(\kappa\delta)-1]]\exp(-\kappa x) \qquad \text{A4-37}$$

The potential in Region I is:

$$\psi_1(x) = [\psi_1(0) + \frac{\gamma}{\kappa^2}(\frac{\exp(-\kappa\delta)-1}{2})]\exp(-\kappa x) - [\frac{\gamma}{2\kappa^2}\exp(-\kappa\delta)]\exp(\kappa x) + \frac{\gamma}{\kappa^2} \qquad \text{A4-38}$$

$$\psi_1(x) = \psi_1(0)\exp(-\kappa x) - \frac{\gamma\exp(-\kappa\delta)\sinh(\kappa x)}{\kappa^2} + \frac{\gamma}{\kappa^2}[1-\exp(-\kappa x)] \qquad \text{A4-39}$$

The relationship between polymer configuration and the distribution of potential from a flat surface is presented in figures A4-2, A4-3, A4-4 and A4-5. These figures demonstrate the manner in which the distribution of potential in the region near the flat surface changes as the configuration of the polymer collapses into one in which the segments of the polymer lie predominately in or near the surface-solvent interface. From these figures some predictions can be made:

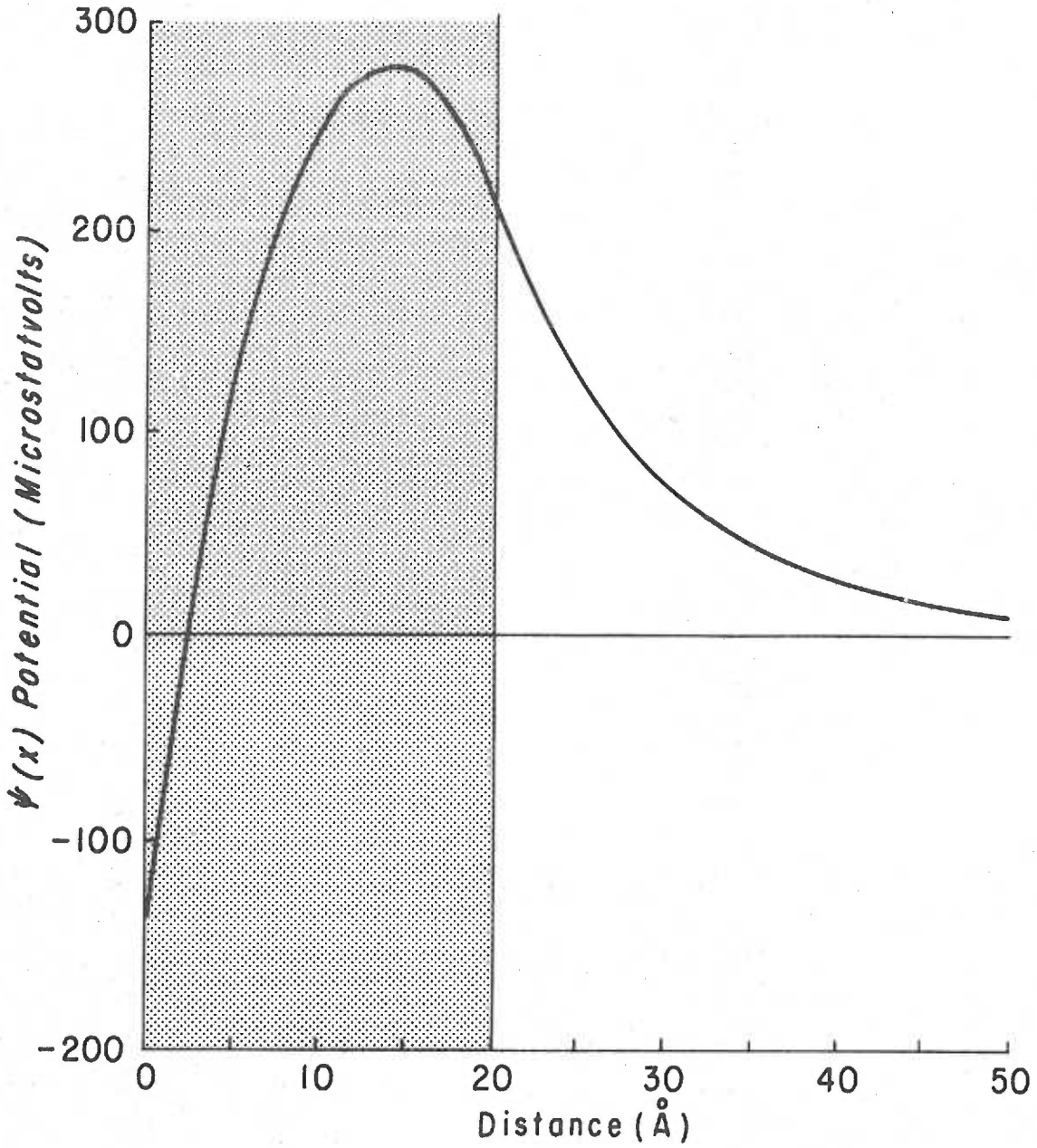

Fig A4-2 The distribution of potential from a surface which has adsorbed a layer of cationic polyelectrolyte 20 Å thick. Properties of the system which affect the distribution of potential are: $\psi(0) = -163$ microstatvolts, $\kappa = 0.1049$, $C_2 = 60$ Å^2 per segment, $T = 298.2$, $\epsilon = 77.26$.

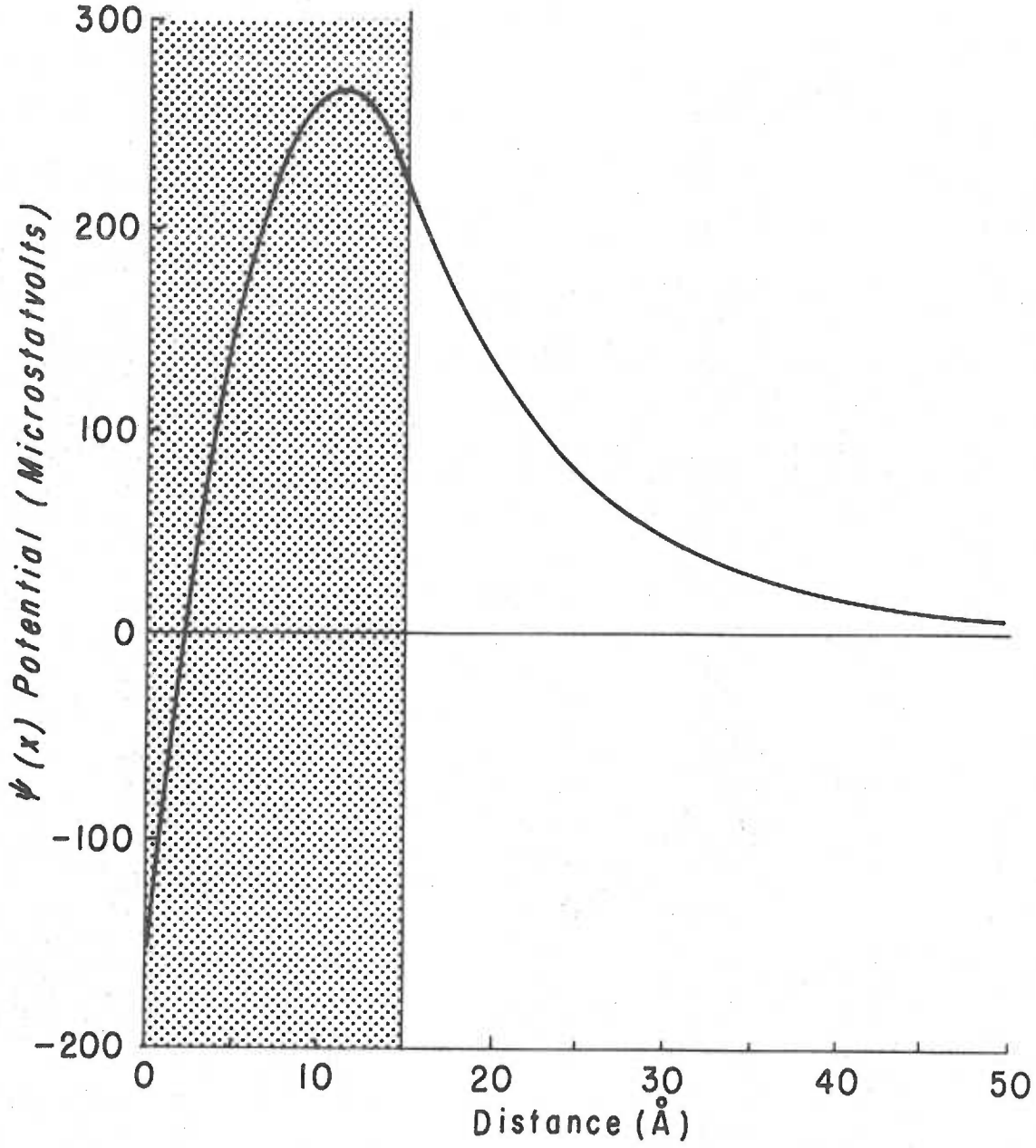

Fig A4-3 The distribution of potential from a surface which has adsorbed a layer of cationic polyelectrolyte 15 Å thick. Properties of the system which affect the distribution of potential are: ψ (0) = -163 microstatvolts, κ = 0.1049, C_2 = 60 Å^2 per segment, T = 298.2, ϵ = 77.26.

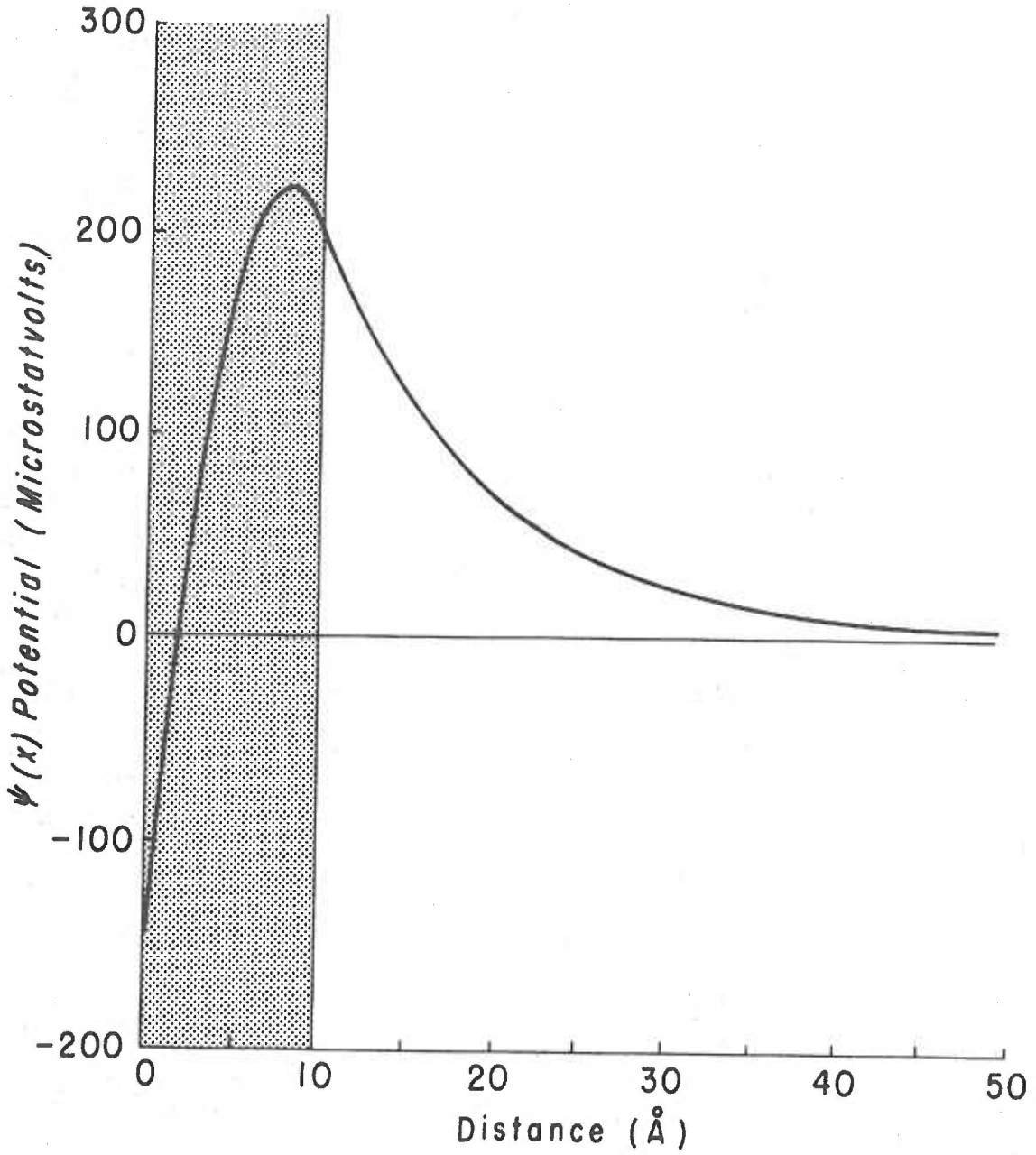

Fig A4-4 The distribution of potential from a surface which has adsorbed a layer of cationic polyelectrolyte 10 Å thick. Properties of the system which affect the distribution of potential are: ψ (0) = -163 microstatvolts, κ = 0.1049, C_2 = 60 Å^2 per segment, T = 298.2, ϵ = 77.26.

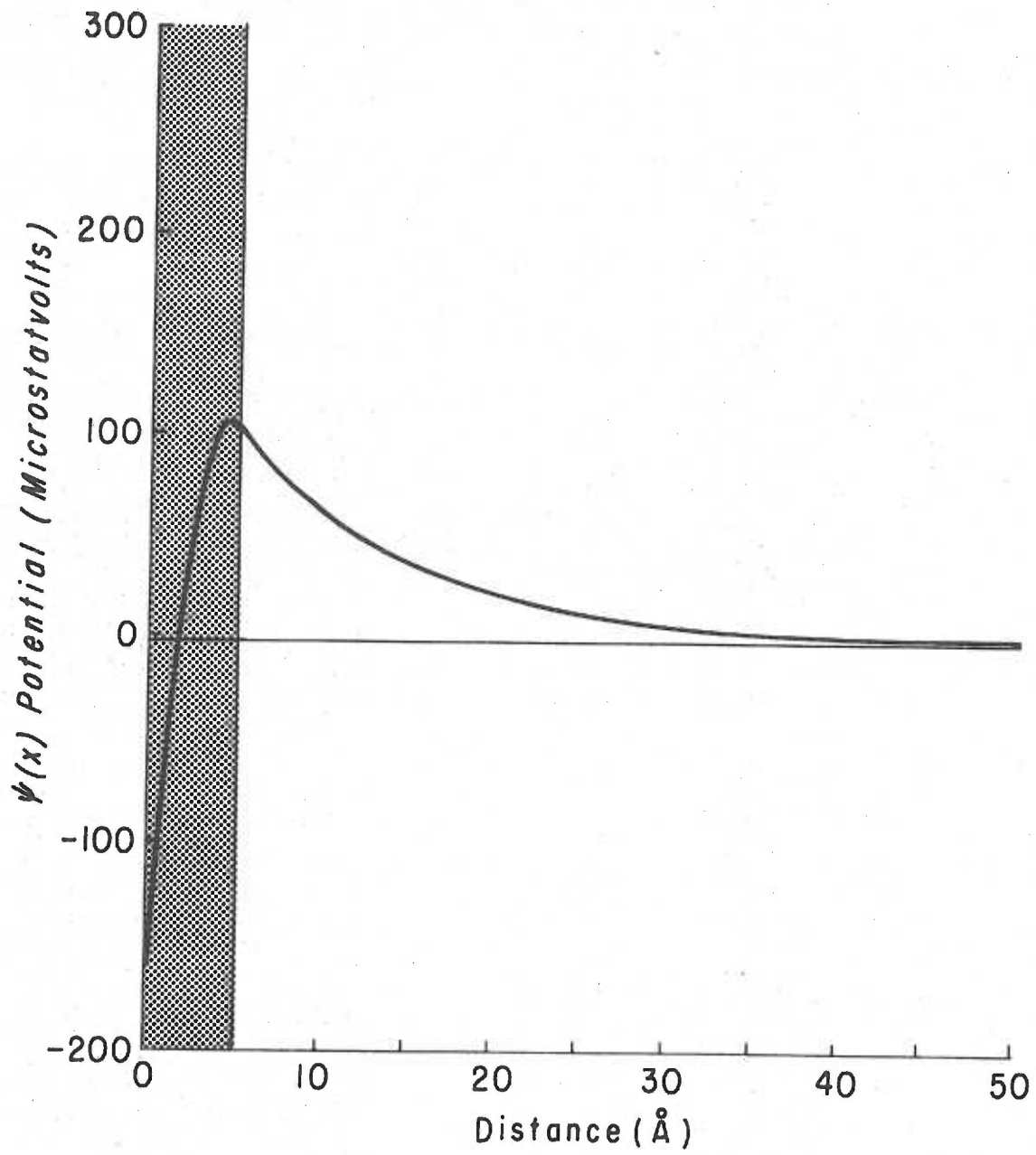

Fig A4-5 The distribution of potential from a surface which has adsorbed a layer of cationic polyelectrolyte 5 Å thick. Properties of the system which affect the distribution of potential are: $\psi(0) = -163$ microstatvolts, $\kappa = 0.1049$, $C_2 = 60$ Å^2 per segment, $T = 298.2$, $\epsilon = 77.26$.

1) For a given amount of adsorbed polymer, the potential at a given distance x away from the adsorbent surface increases with increasing layer thickness. This is if the distance x is greater than the layer thickness.

2) At a distance x from the adsorbent surface, where $x \ll \delta$, the potential at x decreases with increasing layer thickness.

3) A polymer is maximally effective in reducing the potential of the surface when it has first adsorbed to it and is least tightly bound. At this point the polymer segment distribution may well be uniform, especially if the polymer is adsorbed only at a few points.

Values of constants to be used in calculations:

$\epsilon = 77.26$ (0.100 M)

$k = 1.380 \times 10^{-16}$ erg K^{-1}

$T = 298.2°K$

$N = 6.022 \times 10^{23}$

$$\kappa = \frac{1}{0.343}\left(\frac{I}{\epsilon}\right)^{1/2} \text{Å}^{-1} = \left[\frac{8\pi z^2 e^2 n_i(\infty)}{\epsilon k T}\right]^{1/2} = 0.1049 \text{ Å}^{-1} \text{ (0.100 M)}$$

$$\gamma = \frac{4\pi z e n_p}{\epsilon}$$

$$n_p = \frac{\#\text{Particles}/\text{Å}^2}{\delta}$$

δ = layer thickness Å

$e = 4.803 \times 10^{-10}$ esu-statcoulomb

$$\frac{\gamma}{\kappa^2} = \frac{1.202 \times 10^{-2}}{\delta} \text{ (0.100 M NaCl); 1 segment/59 Å}^2$$

BIBLIOGRAPHY

1. Nevo, A., DeVries, A., & Katchalsky, A. Interaction of basic polyamino acids with the red blood cell. I. Combination of polylysine with single cells. Biochim. Biophy. Acta, 1955. 17, 536-547.

2. Katchalsky, A., Danon, D., Nevo, A., & DeVries, A. Interactions of basic polyelectrolytes with the red blood cell. II. Agglutination of red blood cells by polymeric bases. Biochim. Biophys. Acta, 1959. 33, 120-138.

3. Gregory, J. Rates of flocculation of latex particles by cationic polymers. J. Colloid & Interface Sci., 1973. 42, 448-456.

4. von Smoluchowski, M. Versuch einer mathematischen Theorie der Koagulations - Kinetik kolloider Lösungen. Z. Phys. Chem., 1917. 92, 129-168.

5. Hatton, W., McFadyen, P., & Smith, A.L. Rapid flocculation rates of polystyrene latex dispersions. J. Chem. Soc., Faraday Trans. I, 1974. 70, 655-660.

6. Matthews, B.A., & Rhodes, C.T. Some studies of flocculation phenomena in pharameutical suspensions. J. Pharm. Sci., 1968. 57, 570-573.

7. Spielman, L.A. Viscous interactions in Brownian coagulation. J. Colloid & Interface Sci., 1970. 33, 562-571.

8. Honig, E.P., Roebersen, G.J., & Wiersema, P.H. Effect of hydrodynamic interaction on the coagulation rate of hydrophobic colloids. J. Colloid & Interface Sci., 1971. 36, 97-109.

9. Fuks, N. Effect of the charge of aerosols on their stability. Z. Phys., 1934. 89, 736-742.

10. Deryaguin, B.V. Repulsive forces between charged colloid particles and the theory of slow coagulation and stability of lyophobe sols. Trans. Faraday Soc., 1940. 36, 203-215.

11. Derjaguin, B.V., & Landau, L.D. Theory of the stability of strongly charged lyophobic sols and the adhesion of strongly charged particles in solutions of electrolytes. Acta Phys. Chim. URSS, 1941. 14, 633-662.

12. Verwey, E.J.W., & Overbeek, J.Th.G. Theory of the stability of lyophobic colloids. Amsterdam: Elsevier, 1948.

13. Parfitt, G.D. Fundamental aspects of dispersion. In G.D. Parfitt (Ed.) Dispersions of powders in liquids. New York: Elsevier, 1969. (pages 81-121)

14. Vold, M.J. The effect of adsorption on the van der Waal's interaction of spherical colloidal particles. J. Colloid Sci., 1961. 16, 1-12.

15. Gouy, G.L. Constitution of the electric charge at the surface of an electrolyte. J. Phys., 1910. 9, 457-467.

16. Chapman, D.L. A contribution to the theory of electrocapillarity. Phil. Mag., 1913. 25, 475-481.

17. Devereux, O.F., & deBruyn, P.L. Interaction of plane parallel double layers. Cambridge, Mass.: M.I.T. Press, 1963. (pages 1-361)

18. Honig, E.P., & Mul, P.M. Tables and equations of the diffuse double layer repulsion at constant potential and constant charge. J. Colloid & Interface Sci., 1971. 36, 258-272.

19. Deryagin, B.V. A theory of interaction of particles in presence of electric double layers and the stability of lyophobe colloids and disperse systems. Acta Phys. Chim. URSS, 1939. 10, 333-346.

20. Kirkwood, J.G., & Schumaker, J.B. Forces between protein molecules in solution arising from fluctuations in proton charge and configuration. Proc. Natn. Acad. Sci., U.S.A., 1952. 38, 863-871.

21. Pethica, B.A. The physical chemistry of cell adhesion. Expl. Cell Res., 1971. Suppl. 8, 123-140.

22. Bierman, A. Electrostatic forces between nonidentical colloidal particles. J. Colloid Sci., 1955. 10, 231-245.

23. Parsegian, V.A., & Gingell, D. On the electrostatic interaction across a salt solution between two bodies bearing unequal charges. Biophys. J., 1972. 12, 1192-1204.

24. Frens, G., Engel, D.J.C., & Overbeek, J.Th.G. Non-equilibrium methods for the direct determination of potentials of zero charge. Trans. Faraday Soc., 1967. 63, 418-423.

25. Loeb, A.L. An interionic attraction theory applied to the diffuse layer around colloidal particles. I. J. Colloid Sci., 1951. 6, 75-91.

26. Debye, P. Van der Waal's cohesive forces. Phys. Z., 1920. 21, 178-187.

27. Debye, P. Molecular forces and their electrical interpretation. Phys. Z., 1921. 22, 302-308.

28. Keesom, W.H. The second virial coefficient for rigid spherical molecules whose mutual attraction is equivalent to that of a quadruplet placed over its center. Proc. Akad. Wentenschappen, 1916. 18, 636-646.

29. London, F. Theory and systematics of molecular forces. Z Phys., 1930. 63, 245-279.

30. Slater, J.C., & Kirkwood, J.G. The van der Waal's forces in gases. Phys. Rev., 1931. 37, 682-697.

31. Moelwyn-Hughes, E.A. Physical chemistry. (2nd Ed.) London: Pergamon, 1961.

32. Hamaker, H.C. The London-van der Waal's attraction between spherical particles. Physica, Eindhoven, 1937. 4, 1058-1072.

33. Schenkel, J.H., & Kitchener, J.A. A test of the Derjaguin-Verwey-Overbeek theory with a colloidal suspension. Trans. Faraday Soc., 1960. 56, 161-173.

34. Ottewill, R.H., & Walker, T. The influence of non-ionic surface active agents on the stability of polystyrene latex dispersions. Kolloid-Z. Z. Polym., 1968. 227, 108-116.

35. Smith, E.R., Mitchell, D.J., & Ninham, B.W. Deviations of the van der Waal's energy for two interacting spheres from the predictions of Hamaker theory. J. Colloid & Interface Sci., 1973. 45, 55-68.

36. Casimir, H.B.G., & Polder, D. The influence of retardation on the London-van der Waal's forces. Phys. Rev., 1948. 73, 360-372.

37. Dzyaloshinskii, I.E., Lifshitz, E.M., & Pitaevskii, L.P. The general theory of van der Waal's forces. Adv. Phys., 1961. 10, 165-209.

38. Parsegian, V.A., & Ninham, B.W. Toward the correct calculation of van der Waal's interactions between lyophobic colloids in an aqueous medium. J. Colloid & Interface Sci., 1971. 37, 332-341.

39. Rubin, R.J. Random-walk model of chain-polymer adsorption at a surface. J. Chem. Phys., 1965. 43, 2392-2407.

40. Hoeve, C.A.J. Density distribution of polymer segments in the vicinity of an adsorbing surface. J. Chem. Phys., 1965. 43, 3007-3008.

41. Roe, R.J. Conformation of an isolated polymer molecule at an interface. II. Dependence on molecular weight. J. Chem. Phys., 1965. 43, 1591-1598.

42. Silberberg, A. The adsorption of flexible macromolecules. Part I. The isolated macromolecule at a plane interface. J. Phys. Chem., 1962. 66, 1872-1884.

43. Silberberg, A. The adsorption of flexible macromolecules. Part II. The shape of the adsorbed molecule; the adsorption isotherm surface tension and pressure. J. Phys. Chem., 1962. 66, 1884-1907.

44. Silberberg, A. Adsorption of flexible macromolecules. III. Generalized treatment of the isolated macromolecule; the effect of self-exclusion. J. Chem. Phys., 1967. 46, 1105-1114.

45. Silberberg, A. Adsorption of flexible macromolecules. IV. Effect of solvent-solute interactions, solute concentration, and molecular weight. J. Chem. Phys., 1968. 48, 2835-2851.

46. Hesselink, F.Th. On the density distribution of segments of a terminally adsorbed molecule. J. Phys. Chem., 1969. 73, 3488-3490.

47. Motomura, K., & Matuura, R. Conformation of absorbed polymeric chain. I. Mem. Fac. Sci. Kyushu, Univ. Ser. C Chemistry. 6, 97-107.

48. Motomura, K., & Matuura, R. Conformation of adsorbed polymeric chain. II. J. Chem. Phys., 1969. 50, 1281-1287.

49. Motomura, K., Sekita, K., & Matuura, R. Conformation of adsorbed polymeric chain. III. Bull. Chem. Soc. Japan, 1971. 44, 1243-1248.

50. Motomura, K., Moroi, Y., & Matuura, R. Conformation of adsorbed polymeric chain. IV. Bull. Chem. Soc. Japan, 1971. 44, 1248-1252.

51. Johnson, G.A., Lecchini, S.M.A., Smith, E.G., Clifford, J., & Pethica, B.A. Role of water structure in the interpretation of colloidal stability. Discuss. Faraday. Soc., 1966. 42, 120-133.

52. Osmond, D.W.J., Vincent, B., & Waite, F.A. The van der Waal's attraction between colloid particles having adsorbed layers. I. A reappraisal of the "Vold effect". J. Colloid & Interface Sci., 1973. 42, 262-269.

53. Vincent, B. The van der Waal's attraction between colloid particles having adsorbed layers. II. Calculation of interaction curves. J. Colloid & Interface Sci., 1973. 42, 270-285.

54. Kiefer, J.E., Parsegian, V.A., & Weiss, G.H. Model for van der Waal's attraction between spherical particles with nonuniform adsorbed polymer. J. Colloid & Interface Sci., 1975. 51, 543-546.

55. Brooks, D.E. Theoretical and experimental studies on the interaction of neutral polymers with cell surfaces. Thesis, University of Oregon Medical School, 1971.

56. Black, A.P., Birkner, F.B., & Morgan, J.J. The effect of polymer adsorption on the electrokinetic stability of dilute clay suspensions. J. Colloid & Interface Sci., 1966. 21, 626-648.

57. Gregory, J. Flocculation of polystyrene particles with cationic polyelectrolytes. Trans. Faraday Soc., 1969. 65, 2260-2268.

58. Alnice, G.B., & Robertson, A.A. Aggregation of microcrystalline cellulose with polyethylenimine. J. Colloid & Interface Sci., 1974. 252, 920-927.

59. Bagchi, P., & Vold, R.D. Entropic repulsion between two identical spherical particles coated with a polymeric adsorption layer in a theta solvent. J. Colloid & Interface. Sci., 1972. 38, 652-653.

60. Hesselink, F.Th. On the theory of the stabilization of dispersions by adsorbed macromolecules. I. Statistics of the change of some configurational properties of adsorbed macromolecules on the approach of an impenetrable interface. J. Phys. Chem., 1971. 75, 65-71.

61. Hesselink, F.Th., Vrij, A., & Overbeek, J.Th.G. On the theory of the stabilization of dispersions by adsorbed macromolecules. II. Interaction between the two flat particles. J. Phys. Chem., 1971. 75, 2094-2103.

62. Bagchi, P. Theory of stabilization of spherical colloidal particles by nonionic polymers. J. Colloid & Interface Sci., 1974. 47, 86-99.

63. Meier, D.J. Theory of polymeric dispersants. Statistics of constrained polymer chains. J. Phys. Chem., 1967. 71, 1861-1868.

64. Fleer, G.J. Polymer adsorption and its effect on colloidal stability: A theoretical and experimental study on the polyvinyl alcohol-silver iodide system. Thesis: Agricultural University, Wageningen, The Netherlands, 1971.

65. Flory, P.J. Principles of polymer chemistry. Ithaca: Cornell University Press, 1953. (pages 497-514)

66. Fischer, E.W. Electronenmikroskopische Untersuchungen zur Stabilität von Suspensionen in makromolekularen Lösungen. Kolloid-Z., 1958. 160, 120-141.

67. Fontana, B.J., & Thomas, J.R. The configuration of adsorbed alkyl methacrylate polymers by infrared and sedimentation studies. J. Phys. Chem., 1961. 65, 480-487.

68. LaMer, V.K. Filtration of colloid dispersions flocculated by anionic and cationic polyelectrolytes. Trans. Faraday Soc., 1966. 42, 248-254.

69. Connor, P., & Ottewill, R.H. The adsorption of cationic surface active agents on polystyrene surfaces. J. Colloid & Interface Sci., 1971. 37, 642-651.

70. Saunders, F.L. Adsorption of methylcellulose on polystyrene latexes. J. Colloid & Interface Sci., 1968. 28, 475-480.

71. Hickman, K., White, I., & Stark, E. A distilling system for purer water. Science, 1973. 180, 15-25.

72. Kay, M., & McClure, D.W. A simple surface and interfacial tension experiment. J. Chem. Ed., 1970. 47, 540-541.

73. Weast, R.C. (Ed.) Handbook of chemistry and physics. (52nd Ed.) Cleveland, Ohio: Chem. Rubber Pub. Co., 1971. (page F30)

74. Shinodo, K., Nakagawa, T., Tamamushi, B., & Iseumura, T. Colloidal surfactants. New York, Academic Press, 1963. (pages 181-187)

75. Joos, P. The action of electrolytes on the foam stability of a non-ionic surface active agent. In J.Th.G. Overbeek (Ed.) Internatn. Cong. Surf. Active Substances, IV., Brussels. New York: Gordon and Breach, 1964. (pages 1161-1166)

76. Kitchener, J.A., & Cooper, C.F. Current concepts in the theory of foaming. Q. Rev. Chem. Soc., 1959. 13, 71-97.

77. Hughes, R.C., Mŭrau, P.C., & Gunderson, G. Ultra-pure water. Analyt. Chem., 1971. 43, 691-696.

78. Bangham, A.D., & Hill, M.W. Distillation and storage of water. Nature, London, 1972. 237, 408.

79. Snedecor, G.W., & Cochran, W.G. Statistical methods. (6th Ed.) Ames, Iowa: Iowa State Univ. Press, 1967. (page 147)

80. Topping, J. Errors of observation and their treatment. London, England: Chapman & Hall, Ltd., 1961. (pages 96-112)

81. Freund, J.E. Mathematical statistics. (2nd Ed.) Englewood Cliffs, New Jersey: Prentice-Hall Inc., 1971. (page 220)

82. Topping, J. Loc Cit., (page 82)

83. Wright, M.H., & James, A.M. The surface conductivity at the polystyrene latex particle/electrolyte interface. Kolloid-Z. Z. Polym., 1973. 251, 745-751.

84. James, A.M., & Carter, M.N.A. Surface conductance studies of model particles. I. Determination of the formation factor. J. Colloid & Interface Sci., 1969. 29, 696-701.

85. Chan, F.S., & Goring, D.A.I. The primary electroviscous effect in a sulfonated polystyrene latex. J. Colloid & Interface Sci., 1966. 22, 371-377.

86. Chan, F.S., Blachford, J., & Goring, D.A.I. The secondary electroviscous effect in a charged spherical colloid. J. Colloid & Interface Sci., 1966. 22, 378-385.

87. Stone-Masui, J., & Watillon, A. Electroviscous effects in dispersions of monodisperse polystyrene latices. J. Colloid & Interface Sci., 1968. 28, 187-201.

88. Alfrey, T., Bradford, E.B., Vanderhoff, J.W., & Oster, G. Optical properties of uniform particle-sized latices. J. Opt. Soc. Am., 1954. 44, 603-609.

89. Tabibian, R.M., Heller, W., & Epel, J.N. Experimental investigation on the light scattering of colloidal spheres. I. Specific turbidity. J. Colloid Sci., 1956. 11, 195-213.

90. Wallace, T.P., Cembrola, R.J., Migliore, A.J., & DeCann, D.E. Size distribution analysis of polymer latex systems via combination of light scattering and ultracentrifugation techniques. J. Colloid & Interface Sci., 1975. 51, 283-291.

91. Birkner, F.B., & Morgan, J.J. Polymer flocculation kinetics of dilute colloidal suspensions. J. Am. Wat. Wks. Assn., 1928. 60, 175-191.

92. Lichtenbelt, J.W.Th., Pathmamanoharan, C., & Wiersema, P.H. Rapid coagulation of polystyrene latex in a stopped-flow spectrophotometer. J. Colloid & Interface Sci., 1974. 49, 281-285.

93. Ottewill, R.H., & Shaw, J.N. Stability of monodisperse polystyrene latex dispersions of various sizes. Discuss. Faraday Soc., 1966. 42, 154-174.

94. Watillon, A., & Joseph-Petit, A.M. Interactions between spherical particles of monodisperse polystyrene latices. Discuss. Faraday Soc., 1966. 42, 143-153.

95. Corrin, M.L., Lind, E.L., Roginsky, A., & Harkins, W.D. Adsorption of long-chain electrolytes from aqueous solution on graphite of known area and on polystyrene. J. Colloid Sci., 1949. 4, 485-495.

96. Vanderhoff, J.W., & van den Hul, H.J. Well-characterized monodisperse latexes as model colloids. J. Macromol. Sci., 1973. A7, 677-707.

97. Roe, C.P. Emulsion polymerization with a surface active polyelectrolyte as the sole emulsifier. J. Colloid & Interface Sci., 1971. 37, 93-101.

98. Ottewill, R.H., & Shaw, J.N. Studies on the preparation and characterization of monodisperse polystyrene latices. Kolloid-Z. Z. Polym., 1967. 215, 161-166.

99. Vanderhoff, J.W., & Bradford, E.B. An investigation of the mechanism and kinetics of emulsion polymerization by electron microscopy. Tech. Pap. Addr. Tech. Ass. Pulp. Pap. Ind., 1956. 39, 650-655.

100. Koteras, A., Furusawa, K., & Takeda, Y. Colloid chemical studies of polystyrene latexes polymerized without surface-active agents. I. Method for preparing monodisperse latexes and their characterization. Kolloid-Z. Z. Polym., 1970. 239, 677-681.

101. Pugh, T.L., & Heller, W. Density of polystyrene and polyvinyl-toluene latex particles. J. Colloid Sci., 1957. 12, 173-180.

102. van den Hul, H.J., & Vanderhoff, J.W. The characterization of latex particle surfaces by ion exchange and conductometric titration. J. Electroanal. Chem., 1972. 37, 161-182.

103. Filippusson, H., & Hornby, W.E. The preparation and properties of yeast β-fructofuranosidase chemically attached to polystyrene. Biochem. J., 1970. 120, 215-219.

104. Groves, M.J., & Freshwater, D.C. Particle-size analysis of emulsion systems. J. Pharm. Sci., 1968. 57, 1273-1291.

105. Bradford, E.B., & Vanderhoff, J.W. Electron microscopy of monodisperse latices. J. Appl. Phys., 1955. 26, 864-871.

106. Heide, H.G. The prevention of contamination without beam damage to the specimen. In S.S. Breeze (Ed.) Electron Microscopy, 5th International Congress for Electron Microscopy, Philadelphia, Vol. 1. New York: Academic Press, 1962. art. A-4.

107. Davidson, J.A., & Haller, H.S. Latex particle size analysis V. Analysis of errors in electron microscopy. J. Colloid & Interface Sci., 1973. 47, 459-472.

108. Harvey, R.J. Measurement of cell volumes by electric sensing zone devices. In D.M. Prescott (Ed.) Methods in cell physiology. Vol. 3. New York: Academic Press, 1968. (pages 1-23)

109. Grover, N.B., Naaman, J., Ben-Sasson, S., & Doljanski, F. Electrical sizing of particles in suspensions I. Theory. Biophys. J., 1969. 9, 1398-1414.

110. Kachel, V., Metzger, H., & Ruhenstroth-Bauer, G. Der Einfluβ der Partikeldurchtrittsbahn auf die Volumenverteilungskurven nach dem Coulter-Verfahren. Z. Ges. Exp. Med., 1970. 153, 331-347.

111. Princen, L.H., & Kwolek, W.F. Coincidence corrections for particle size determinations with the Coulter counter. Rev. Scient. Inst., 1965. 36, 646-653.

112. Edmundson, I.C. Coincidence error in Coulter counter particle size analysis. Nature, London, 1966. 212, 1450-1452.

113. von Smoluchowski, M. Handbuch der Elektrizitat und des Magnetismus. B. Graetz (Ed.) Leipzig: Barth, 1914. 2, (page 366).

114. Booth, F. The cataphoresis of spherical solid nonconducting particles in a symmetrical electrolyte. Proc. Roy. Soc., 1950. A203, 514-533.

115. Overbeek, J.Th.G. Quantitative interpretation of the electrophoretic velocity of colloids. Adv. Colloid Sci., 1950. 3, 97-135.

116. Henry, D.C. The cataphoresis of suspended particles. I. The equation of cataphoresis. Proc. Roy. Soc., 1931. A133, 106-129.

117. Wiersema, P.H., Loeb, A.L., & Overbeek, J.Th.G. Calculation of the electrophoretic mobility of a spherical colloid particle. J. Colloid & Interface Sci., 1966. 22, 78-99.

118. Haydon, D.A. A study of the relation between electrokinetic potential and surface charge density. Proc. Roy. Soc., 1960. A258, 319-328.

119. Haydon, D.A. The surface charge of cells and some other small particles as indicated by electrophoresis I. The zeta potential-surface charge relationships. Biochim. Biophys. Acta, 1961. 50, 450-457.

120. Bell, G.M., & Levine, S. A modified Poisson-Boltzmann equation in electric double layer theory. In B.E. Conway and R.G. Barradas (Eds.) Chemical physics of ionic solutions. New York: John Wiley & Sons, 1966. (pages 406-461)

121. Hurwitz, H.D., Sanfeld, A., & Steinchen-Sandfeld, A. Equilibrium properties of polarized systems. The case of the diffuse part of the double electrochemical layer. Electrochim. Acta, 1964. 9, 929-961.

122. Sanfeld, A., Devillez, E., & Terlinck, P.J. A local thermodynamic approach of the repulsive energy between colloidal particles. J. Colloid & Interface Sci., 1970. 32, 33-40.

123. Roe, J.W., & Hartley, G.S. Ionic concentrations at interfaces. Trans. Faraday Soc., 1940. 36, 101-109.

124. Seaman, G.V.F. Electrokinetic behavior of red cells. In D. MacN. Surgenor (Ed.) The red blood cell. Vol. 2. (2nd Ed.) New York: Academic Press, 1975. (pages 1135-1229)

125. Matthews, B.A., & Rhodes, C.T. Some observations on the use of the Coulter counter model B in coagulation studies. J. Colloid & Interface Chem., 1970. 32, 339-348.

126. Bangs, L. Personal Communication, 1975.

127. Cooper, W.D., & Parfitt, G.D. Comparison of particle size distributions of "monodisperse" particles from 0.8 to 3.5 μ in diameter using a Coulter counter and electron microscopy. Kolloid-Z. Z. Polym., 1968. 223, 160-166.

128. Watillon, A. (No title) Discuss. Faraday Soc., 1966. 42, 170-171.

129. Reerink, H., & Overbeek, J.Th.G. The rate of coagulation as a measure of the stability of silver iodide sols. Discuss. Faraday Soc., 1954. 18, 74-84.

130. Fowkes, F.M. Attractive forces at interfaces. Ind. Engng. Chem., 1964. 56, 40-52.

131. Padday, J.F. (No title) Discuss. Faraday Soc., 1966. 42, 164-166.

132. Goldstein, B., & Zimm, B.H. Effect of concentration and intermolecular forces on the sedimentation of polystyrene spheres. J. Chem. Phys., 1971. 54, 4408-4413.

133. Gingell, D., & Parsegian, V.A. Prediction of van der Waals interactions between plastics in water using the Lifshitz theory. J. Colloid & Interface Sci., 1973. 44, 456-463.

134. Evans, R., & Napper, D.H. On the calculation of the van der Waals attraction between latex particles. J. Colloid & Interface Soc., 1973. 45, 138-147.

135. Lotan, N., Berger, A., & Katchalsky, E. Conformation and conformational transitions of poly-α-amino acids in solution. A. Rev. Biochem., 1972. 41, 869-902.

136. Fasman, G.D., (Ed.) Poly-α-amino acids. New York: Marcel Dekker, Inc., 1967.

137. Sela, M., & Katchalski, E. Biological properties of poly-α-amino acids. Adv. Protein Chem., 1959. 14, 392-478.

138. Katchalski, E. Poly-α-amino acids. Adv. Protein Chem., 1951. 6, 123-185.

139. Katchalski, E., & Sela, M. Synthesis and chemical properties of poly-α-amino acids. Adv. Protein Chem., 1958. 13, 243-492.

140. Itzhaki, R.F. Colorimetric method for estimating polylysine and polyarginine. Analyt. Biochem., 1972. 50, 569-575.

141. Stewart, J.W., & Stahmann, M.A. Chromatographic analysis of polylysine with carboxymethylcellulose. In M.A. Stahmann (Ed.) Polyamino acids, polypeptides and proteins. Madison, Wisc.: U. of Wisc. Press, 1962. (pages 95-104)

142. Applequist, J., & Doty, P. α-Helix formation in poly-ε-carbobenzoxy-l-lysine and poly-l-lysine. In M.A. Stahmann (Ed.) Polyamino acids, polypeptides and proteins. Madison, Wisc.: U. of Wisc. Press, 1962. (pages 161-179)

143. Katchalsky, A., Shavit, N., & Eisenberg, H. Dissociation of weak polymeric acids and bases. J. Polym. Sci., 1954. 13, 69-84.

144. Bradbury, E.M., Crane-Robinson, C., Goldman, H., & Rattle, H.W.E. Proton magnetic resonance and optical spectroscopic studies of water-soluble polypeptides, poly-l-lysine HBr, poly(l-glutamic acid), and copoly(l-glutamic acid^{42}, l-lysine HBr^{28}, l-alanine^{30}). Biopolymers, 1968. 6, 851-862.

145. Ciferri, A., Puett, D., Rajagh, L., & Hermans, J. Potentiometric titrations and the helix-coil transition of poly(l-glutamic acid) and poly-l-lysine in aqueous salt solutions. Biopolymers, 1968. 6, 1019-1036.

146. Peggion, E., Cosani, A., Terbojevich, M., & Borin, G. Conformation studies on polypeptides. The effect of sodium perchlorate on the conformation of poly-l-lysine and of random copolymers of l-lysine and l-phenylalanine in aqueous solution. Biopolymers, 1972. 11, 633-643.

147. Becker, R.R., & Stahmann, M.A. The synthesis of high molecular weight lysine polypeptides. J. Am. Chem. Soc., 1952. 74, 38-41.

148. Yaron, A., Katchalski, E., Berger, A., Fasman, G.D., & Sober, H.A. The chain length dependence of the conformation for oligomers of l-lysine in aqueous solution: optical rotary dispersion studies. Biopolymers, 1971. 10, 1109-1120.

149. Yu, T.J., Lippert, J.L., & Peticolas, W.L. Laser Raman studies of conformational variations of poly-l-lysine. Biopolymers, 1973. 12, 2161-2176.

150. Tiffany, M.L., & Krimm, S. New chain conformations for poly(glutamic acid) and polylysine. Biopolymers, 1968. 6, 1379-1382.

151. Krimm, S., & Mark, J.E. Conformations of polypeptides with ionized side chains of equal length. Proc. Natn. Acad. Sci. U.S.A., 1968. 60, 1122-1129.

152. Hiltner, W.A., Hopfinger, A.J., & Walton, A.G. Helix-coil controversy for polyamino acids. J. Am. Chem. Soc., 1972. 94, 4324-4327.

153. Aebersold, D., & Pysh, E.S. Optical properties of amorphous polypeptides. I. One state solutions. J. Chem. Phys., 1970. 53, 2156-2163.

154. Davies, J.T. Some factors influencing the orientation of ϵ-amino groups in monolayers of proteins and amino acid polymers. Biochemistry, N.Y., 1954. 56, 509-513.

155. Bianchi, E., Bicchi, A., Conio, G., & Ciferri, A. Intrinsic viscosity of the coiled forms of poly-l-glutamic acid and poly-l-lysine in salt solutions. J. Macromol. Sci., 1967. A1, (5), 909-915.

156. Nozawa, T., Akimoto, Y., & Hatano, M. The asymmetrically selective hydrolysis of phenylalanine esters catalyzed by poly-l-lysine/copper (II) complexes. Makromolek. Chem., 1972. 158, 21-26.

157. Nozawa, T., Akimoto, Y., & Hatano, M. On the mechanism of the stereo-selective hydrolysis of phenylalanine esters catalyzed by poly(l-lysine)-copper(II) complexes. Makromolek. Chem., 1972. 161, 289-291.

158. Brandt, D.A., Flory, P.J. The configuration of random polypeptide chains. I. Experimental results. J. Am. Chem. Soc., 1965. 87, 2788-2791.

159. Glasel, J.A. Participation of water in conformational changes of biopolymers as studied by deuteron magnetic relaxation. J. Am. Chem. Soc., 1970. 92, 375-381.

160. Neumann, A.W., Moscarello, M.A., & Epand, R.M. The application of surface tension measurements to the study of conformational transitions in aqueous solutions of poly-l-lysine. Biopolymers, 1973. 12, 1945-1957.

161. Sheth, K., & Cohen, L.H. A fluorometric protein assay suitable for histones based on lysine content. Analyt. Chem., 1970. 37, 142-148.

162. Davies, R.L. The determination of lysine and ornithine using acid ninhydrin. J. Chromat., 1972. 71, 564-566.

163. Yemm, E.W., & Cocking, E.C. The determination of amino-acids with ninhydrin. Analyst, London, 1955. 80, 209-213.

164. Granath, K.A., & Kvist, B.E. Molecular weight distribution analysis by gel chromatography on Sephadex. J. Chromat., 1967. 28, 69-81.

165. Andrews, P. Estimation of molecular size and molecular weights of biological compounds by gel filtration. Meth. Biochem. Analysis, 1970. 18, 1-53.

166. Bonnar, R.U., Dimbat, M., & Stross, F.H. Number-average molecular weights. New York: Interscience Publishers, Inc., 1958.

167. Morawetz, H. High polymers. In Macromolecules in solution. Vol. XXI. New York, Interscience Publishers: 1965. (pages 161-181)

168. Hoare, D.G., & Koshland, D.E. A method for the quantitative modification and estimation of carboxylic acid groups in proteins. J. Biol. Chem., 1967. 242, 2447-2453.

169. Orofino, T.A., & Flory, P.J. Relationship of the second virial coefficient to polymer chain dimensions and interactions parameters. J. Chem. Phys., 1957. 26, 1067-1076.

170. Flory, P.J., & Krigbaum, W.R. Statistical mechanics of dilute polymer solutions II. J. Chem. Phys., 1950. 18, 1086-1094.

171. Flory, P.J. Statistical mechanics of dilute polymer solutions. J. Chem. Phys., 1949. 17, 1347-1348.

172. Stockmayer, W.H., Casassa, E.F. The third virial coefficient in polymer solutions. J. Chem. Phys., 1952. 20, 1560-1566.

173. Koyama, R. Theory of dilute polymer solutions. J. Chem. Phys., 1957. 27, 234-239.

174. Orofino, T.A., & Flory, P.J. The second virial coefficient for polyelectrolytes. Theory and experiment. J. Phys. Chem., 1959. 63, 283-290.

175. Morawetz, H. Loc. cit. (pages 340-348)

176. Okubo, T., Ise, N., & Matsui, F. Mean activity coefficient of polyelectrolytes in the ternary system water - sodium polyacrylate - sodium chloride. J. Am. Chem. Soc., 1967. 89, 3697-3703.

177. Katchalsky, A., Lifson, S., & Mazur, J. The electrostatic free energy of polyelectrolyte solutions. I. Randomly kinked macromolecules. J. Polym. Sci., 1953. 11, 409-423.

178. Rice, S.A., & Nagasawa, M. Polyelectrolyte solutions. New York: Academic Press, 1961.

179. Yphantis, D.A. Equilibrium ultracentrifugation of dilute solutions. Biochemistry, N.Y., 1964. 3, 297-317.

180. Richards, E.G. Ultracentrifuge studies with Rayleigh interference optics. II. Low speed sedimentation equilibrium of homogeneous systems. Biochemistry, N.Y., 1968. 7, 1054-1076.

181. Nazarian, G.M. Determination of molecular weight from the interference pattern of sedimentation equilibrium in the ultracentrifuge. Analyt. Chem., 1968. 40, 1766-1769.

182. Eyring, H. The resultant electric moment of complex molecules. Phys. Rev., 1932. 39, 746-748.

183. Benoit, H., & Sandron, C. Complements à l'étude de la statistique des chaines moléculaires en solution diluee. J. Polym. Sci., 1949. 4, 473-482.

184. Raziel, A. Excluded volume study of polyelectrolyte solutions potassium polystyrenesulfonate. Ph.D. Thesis. Rehovot, Israel: Weizmann Inst. Sci., 1971.

185. Einstein, A. Eine neue Bestimmung der Moleküldimensionen. Ann. Physik., 1906. 19, 298-306.

186. Simha, R. The influence of Brownian movement on the viscosity of solutions. J. Phys. Chem., Ithaca, 1940. 44, 25-34.

187. Kraemer, E.O., & Lansing, W.D. Molecular weights of cellulose and cellulose derivatives. J. Phys. Chem., Ithaca, 1935. 39, 153-168.

188. Wang, J.H. The hydration of desoxyribonucleic acid. J. Am. Chem. Soc., 1955. 77, 258-260.

189. Oncley, J.L. Evidence from physical chemistry regarding the size and shape of protein molecules from ultracentrifugation, diffusion, viscosity, dielectric dispersion and double refraction of flow. Ann. N.Y. Acad. Sci., 1941. 41, 121-150.

190. Vink, H. Viscosity of polyelectrolyte solutions. Makromolek. Chem., 1970. 131, 133-145.

191. Booth, F. The electroviscous effect for suspensions of solid spherical particles. Proc. Roy. Soc., 1950. A123, 533-551.

192. Conway, B.E., & Dobry-Duclaux, A. Viscosity of suspensions of electrically charged particles and solutions of polymeric electrolytes. In F.R. Eirich (Ed.) Rheology, theory and application. Vol. 3. New York: Academic Press, 1969. (pages 83-120)

193. Debye, P., & Beuche, A.M. Intrinsic viscosity, diffusion and sedimentation rate of polymers in solution. J. Chem. Phys., 1948. 16, 573-579.

194. Kirkwood, J.G., & Riseman, J. Intrinsic viscosities and constants of flexible macromolecules in solution. J. Chem. Phys., 1948. 16, 565-573.

195. Flory, P.J. (1953) Loc. cit. (pages 602-639)

196. Kurata, M., & Stockmayer, W.N. Intrinsic viscosities and unperturbed dimensions of long chain molecules. Fortschr. Hochpolymer. Forsch., 1963. 3, 196-312.

197. Strauss, U.P., Woodside, D., & Wineman, P. Counterion binding by polyelectrolytes. I. Exploratory electrophoresis, solubility and viscosity studies of the interaction between polyphosphates and several univalent cations. J. Phys. Chem., 1957. 61, 1353-1356.

198. Pals, D.T.F., & Hermans, J.J. Sodium salts of pectin and carboxymethyl cellulose in aqueous sodium chloride. I. Viscosities. Rec. Trav. Chim., 1952. 71, 433-457.

199. Jones, R.T., & Weiss, G. Long-path flow cells for automatic amino acid analyzers. Analyt. Biochem., 1964. 9, 377-382.

200. Spackman, D.H. Instruction manual and handbook for Beckman/Spinco model 120 amino acid analyzer. Palo Alto, 1960.

201. DiCamelli, R.F., Holohan, P.D., Basinger, S.F., & Lebowitz, J. Molecular weight determinations by low-speed sedimentation equilibrium. Combined use of the Nazarian equation and the Griffith rapid equilibrium technique. Analyt. Biochem., 1970. 36, 470-494.

202. Cohn, E.J., & Edsall, J.T. Proteins, amino acids and peptides as ions and dipolar ions. New York: Reinhold, 1943. (pages 370-381)

203. Wales, M., Marshall, P.A. & Weissberg, S.G. Intrinsic viscosity-molecular weight relationships for dextran. J. Polym. Sci., 1953. 10, 229-240.

204. Tanford, C. Physical chemistry of macromolecules. (5th Ed.) New York: John Wiley & Sons, Inc., 1967. (page 395)

205. Mijnlieff, P.J. Effects of charge on the sedimentation, the diffusion and the sedimentation equilibrium of colloidal electrolytes. In J.W. Williams (Ed.) Ultracentrifugal analysis in theory and practice. New York: Academic Press, 1963. (pages 88-102)

206. Yaron, A., & Berger, A. The determination of the molecular weight of poly-l-lysine. Biochim. Biophys. Acta, 1963. 69, 397-399.

207. Tanford, C. Intrinsic viscosity and kinematic viscosity. J. Phys. Chem., 1955. 59, 798-799.

208. Sakai, T. Extrapolation procedures for intrinsic viscosity and for Huggins constant K'. J. Polym. Sci., 1968. A2(6), 1659-1672.

209. Clayfield, E.J., & Lumb, E.C. The simulation of random copolymer adsorption. II. Loop formation and segment density distribution. J. Colloid & Interface Sci., 1974. 217, 16-26.

210. Clayfield, E.J., & Lumb, E.C. The simulation of random adsorption. I. Lattice model using a computer. J. Colloid & Interface Sci., 1974. 47, 6-15.

211. Dunn, V.K., & Vold, R.D. Adsorption of polystyrene on Graphon from toluene. In K.L. Mittal (Ed.) A.C.S. Symposium Series 8, Adsorption at interfaces. Washington, D.C.: American Chemical Soc., 1975.

212. Brooks, M.C., & Badger, R.M. An adsorption system for the fractionation of nitrocellulose with respect to molecular weight. J. Am. Chem. Soc., 1950. 50, 4384-4388.

213. Kolthoff, I.M., & Kahn, A. The sorption of GR-S type rubber by carbon block. I. Sorption from benzene solution by Graphon. J. Phys. & Colloid Chem., 1950. 54, 251-256.

214. Patat, F., Killmann, E., & Schliebener, C. Die Adsorption von Macromolekülen aus Lösung. Fortschr. Hochpolym. Forsch., 1964. 3, 332-393.

215. Ash, S.G. Polymer adsorption at the solid/liquid interface. Colloid Sci., 1973. 1, 103-122.

216. Kipling, J.J. Adsorption from solutions of non-electrolytes. New York: Academic Press, 1965.

217. Rowland, F., Bulas, R., Rothstein, E., & Eirich, F.R. Structure of macromolecules at liquid-solid interfaces. Ind. Engng. Chem., 1965. 57, 46-52.

218. Felter, R.E., & Ray, L.N., Jr. Polymer adsorption studies at the solid liquid interface using gel permeation chromatography I. Molecular weight distribution among the adsorption isotherm. J. Colloid & Interface Sci., 1970. 32, 349-360.

219. Nestler, C.H. Adsorption and electrophoretic studies of poly(acrylic acid) on calcium sulfate. J. Colloid & Interface Sci., 1968. 26, 10-18.

220. Greene, B.W. The effect of added salt on the adsorbability of a synthetic polyelectrolyte. J. Colloid & Interface Sci., 1971. 37, 144-153.

221. Clayfield, E.J., & Lumb, E.C. A theoretical approach for polymeric dispersant action. I. Calculation of entropic repulsion exerted by random polymer chains terminally adsorbed on plane surfaces and spherical particles. J. Colloid & Interface Sci., 1966. 22, 269-284.

222. Clayfield, E.J., & Lumb, E.C. A theoretical approach for polymeric dispersant action. II. Calculation of the dimensions of terminally adsorbed macromolecules. J. Colloid & Interface Sci., 1966. 22, 285-293.

223. Lax, M. Configuration of an adsorbed polymer molecule: solvent effect. J. Chem. Phys., 1974. 60, 1931-1936.

224. Lax, M. Configuratioal properties of self-avoiding walks generated in the presence of an interacting solid barrier. J. Chem. Phys., 1974. 60, 2245-2249.

225. Stromberg, R.R. Passaglia, E., & Grant, W.H. Rates of adsorption and desorption of polystyrene on a chrome surface. J. Natn. Bur. Res. Stands., 1963. 67 A, 431-440.

226. LaMer, V.K., & Healy, T.W. Adsorption-flocculation reactions of macromolecules at the solid-liquid interface. Rev. Pure. Appl. Chem., 1963. 13, 112-133.

227. Vincent, B. Effect of adsorbed polymers on dispersion stability. Adv. Colloid & Interface Sci., 1974. 4, 193-277.

228. Ruehrwein, R.A., & Ward, D.W. Mechanism of clay aggregations by polyelectrolytes. Soil Sci., 1952. 73, 485-492.

229. LaMer, V.K., & Smellie, R.H., Jr. Flocculation, subsidence and filtration of phosphate slimes. I. General. J. Colloid Sci., 1956. 11, 704-709.

230. LaMer, V.K., & Smellie, R.H., Jr. Flocculation, subsidence, and filtration of phosphate slimes. II. Starches as agents for improving flocculation, subsidence and filtration of phosphate slimes. J. Colloid Sci., 1956. 11, 710-719.

231. Smellie, R.H., Jr., & LaMer, V.K. Flocculation, subsidence and filtration of phosphate slimes. III. Subsidence behavior. J. Colloid Sci., 1956. 11, 720-731.

232. LaMer, V.K., Smellie, R.H., Jr., & Lee, P.K. Flocculation, subsidence and filtration of phosphate slimes. IV. Flocculation by gums, and polyelectrolytes and their influence on filtration rate. J. Colloid Sci., 1957. 12, 230-239.

233. LaMer, V.K., Smellie, R.H., Jr., & Lee, P.K. Flocculation, subsidence and filtration of phosphate slimes. V. The optimum filtration rate as a function of solid content and specific area. J. Colloid Sci., 1957. 12, 566-574.

234. Napper, D.H., & Netschey, A. Studies of the steric stabilization of colloidal particles. J. Colloid & Interface Sci., 1971. 37, 528-535.

235. Dobbie, J.W., Evans, R., Gibson, D.V., & Smitham, J.B. Enhanced steric stabilization. J. Colloid & Interface Sci., 1973. 45, 557-565.

236. Berger, R.L. A ten jet mixer. In B. Chance, R.H. Eisenhart, Q.H. Gibson, & K.K. Lonberg-holn (Eds.) Rapid mixing and sampling techniques in biochemistry. New York: Academic Press, 1964. (pages 33-37)

237. Kragh, A.M., & Lanston, W.B. The flocculation of quartz and other suspensions with gelatine. J. Colloid Sci., 1962. 17, 101-123.

238. Peterson, C., & Kwei, T.W. The kinetics of polymer adsorption onto solid surfaces. J. Phys. Chem., 1961. 65, 1330-1333.

239. Healy, T.W., & LaMer, V.K. The adsorption-flocculation reactions of a polymer with an aqueous colloidal dispersion. J. Phys. Chem., 1962. 66, 1835-1838.

240. Dixon, J. K., LaMer, V. K., Li, C., Messinger, S., & Linford, H. B. Effect of the structure of cationic polymers on the flocculation and the electrophoretic mobility of crystalline silica. J. Colloid & Interface Sci., 1967. 23, 465-473.